SCALING-UP AND FUTURE PERSPECTIVES OF BIOELECTROCHEMICAL SYSTEMS FOR WASTEWATER TREATMENT AND HYDROGEN PRODUCTION

Óscar Guerrero Sodric

Universitat Autònoma de Barcelona

SCALING-UP AND FUTURE PERSPECTIVES OF BIOELECTROCHEMICAL SYSTEMS FOR WASTEWATER TREATMENT AND HYDROGEN PRODUCTION

— PhD Thesis —

Óscar Guerrero Sodric

Supervisors: Dr. Juan Antonio Baeza Labat

Dr. Albert Guisasola i Canudas

Academic tutor: Dr. Albert Guisasola i Canudas

A thesis submitted in fulfilment of the requirements for the Doctoral degree in Environmental Science and Technology

GENOCOV research group

Departament d'Enginyeria Química, Biològica i Ambiental

Escola d'Enginyeria

Universitat Autònoma de Barcelona

Bellaterra, February 2024

GENOCOV
Departament d'Enginyeria Química,
Biològica i Ambiental
Escola d'Enginyeria
Universitat Autònoma de Barcelona
Barcelona · Spain
info@genocov.com

Research Group on Biological Treatment and Valorisation of Liquid and Gaseous Effluents
GENOCOV

UAB
Universitat Autònoma de Barcelona

ALBERT GUISASOLA I CANUDAS i **JUAN ANTONIO BAEZA LABAT**, Catedràtics Laborals del Departament d'Enginyeria Química, Biològica i Ambiental de la Universitat Autònoma de Barcelona,

CERTIFIQUEM:

Que l'enginyer ÓSCAR GUERRERO SODRIC ha realitzat sota la nostra direcció, el treball que amb títol "SCALING-UP AND FUTURE PERSPECTIVES OF BIOELECTROCHEMICAL SYSTEMS FOR WASTEWATER TREATMENT AND HYDROGEN PRODUCTION" es presenta en aquesta memòria, i que constitueix la seva Tesi per optar al Grau de Doctor per la Universitat Autònoma de Barcelona.

I per a què se'n prengui coneixement i consti als efectes oportuns, presentem a l'Escola d'Enginyeria de la Universitat Autònoma de Barcelona l'esmentada Tesi, signant el present certificat.

Bellatera, 13 de febrer de 2024

Dr. Albert Guisasola i Canudas

Dr. Juan Antonio Baeza Labat

To my parents Elena & Toni,

to my brother Toni,

to my wife Irene and our son Guim.

"Our posturing, our imagined self-importance, the delusion that we have some privilege position in the Universe, are challenged by this point of pale light. Our planet is a lonely speck in the great enveloping cosmic dark. In our obscurity, in all this vastness, there is no hint that help will come from elsewhere to save us from ourselves."

Carl Sagan, Pale Blue Dot, 1994

Acknowledgments

As I stand here on the precipice of this grand achievement, the culmination of countless hours spent hunched over papers, scribbling furiously on notebooks, and staring blankly at computer screens, I find myself compelled to express my heartfelt gratitude to the collective force of support, encouragement, and laughter that has been my constant companion throughout this journey. From the early days of my academic pursuits to the culmination of this thesis, I have been blessed with an extraordinary network of individuals who have made my path not just intellectually stimulating but also genuinely enjoyable.

First, I am filled with immense gratitude for the exceptional guidance and support provided by my supervisors, Albert and Juan. Their dedication to my intellectual growth has been instrumental in shaping my research journey. Their enthusiasm and belief in my abilities have been a source of immense motivation, pushing me to reach beyond my perceived limits and strive for excellence. I extend my heartfelt gratitude for their invaluable contributions to my academic and personal growth. Without their guidance, support, and friendship, this thesis would not have been possible. I am deeply indebted to their unwavering belief in my potential, and I cherish the memories we have created along this path. Thank you for being my mentors and my anchors in the stormy seas of academia.

I would also like to extend my heartfelt gratitude to the entire Department of Chemical, Biological, and Environmental Engineering, encompassing the dedicated teachers, supportive administration, skilled technicians, diligent cleaning staff, and motivated students. Their collective efforts have created a vibrant environment that has enriched my academic journey in countless ways.

Then I feel extremely lucky to have such good workmates in pilot plant who have shared immeasurable knowledge and support during my stay.

- Lluc, the N_2O boy, a true gem of person. Brilliant, hard-working, and resourceful, he has been one of the most constant companions throughout my doctoral journey. I feel incredibly fortunate to have crossed paths with him. I am deeply grateful for his unwavering presence, and I have no doubt that he is destined for a life brimming with success and happiness.

- CongCong, the phosphorus master, the first neighbour of my reactor and the most peaceful mind. I am so happy to know you. For the first time that we met, I knew that you were someone special. I feel in debt with you for all the things that you have taught me during this journey. Thanks for making my stay so much better. I have no doubt that you will reach everything you want.

- Mengqi, the phosphorus girl, the current neighbour of my reactor and the most charming person. It is an honour to know you. You are an inspiration to me, always creating a positive and supportive atmosphere that makes everyone feel good. I am so glad I have you around. Thanks for every second that you have spent with me. I am convinced that your future is bright with promise and prosperity.

- Ana, the VFAs girl, our analytical queen, and my office mate. You have taught me so much about hard work and dedication. As an engineer fellow, we had the chance to share lots of chemical engineering conversations. Thanks for all the support that you gave me. I firmly believe that you will lead a life filled with remarkable achievements and unwavering happiness.

- Javi, the ammonia boy, a detail perfectionist. It was a pleasure to work with you. I am in debt with you for always being there to listen, giving advice, and lending a helping hand. I wish you nothing but the best in all your endeavours and a future filled with happiness, success, and love.

- Marina, the vivianite girl. Thanks for bringing so much laughter and positivity into our workplace. Your sense of humour has helped lighten our days and made our work environment more enjoyable. I really appreciate your presence and the moments we have shared.

I am so grateful to have five wonderful bioelectrochemistry workmates who have not only shared their passion for science with me but have also generously supported me on many occasions, lending a helping hand with various tasks throughout my work.

- Zainab, beyond your exceptional skills and knowledge, you are a wonderful person, consistently demonstrating support and encouragement both in my professional and personal life. Your presence has been a source of immense inspiration and strength, and I am deeply grateful for your unwavering kindness and friendship.

- Mariella, our coffee breaks spent discussing the technical problems of our reactors were among the most cherished moments of my doctoral journey. You are an incredible person, someone who radiates an infectious positive energy that fills the room with vitality. I am deeply grateful for the wealth of knowledge you shared with me and for the support you showed for my well-being throughout my thesis.

- Pilar, the veteran bioelectrochemistry girl. You have been an invaluable asset and an exemplary role mode. I have learned so much from your vast knowledge and experience, and I am grateful for the many opportunities we have had to collaborate and share ideas.

- Mira, your presence in the group has been a constant source of inspiration and encouragement, and I am deeply indebted to you for your guidance. Our late-night conversations in Greece were a lifeline for my pre-show jitters. I will forever cherish those moments of shared anxiety and the kind support you provided.

- David, although we met later in our journey, I already consider you a valuable and inspiring colleague. Working with you has been a true enrichment, and I am grateful for your insights, support, and friendship. I hope we can continue collaborating in the future.

I am immensely grateful to the other members of GENOCOV for their support and fostering a vibrant and collaborative environment. To Alex, my sincere thanks for your constant encouragement and willingness to offer guidance whenever needed. Manu, your positive energy, and unwavering support throughout this hard journey is invaluable. Dani, I express my deepest gratitude for your mentorship, guidance and the wealth of knowledge you shared with me. Eric, your great sense of humour brought joy to this process, reminding me to celebrate the journey alongside pursuing my objectives. Franc, I am indebted to your exceptional expertise in electrochemistry, and your willingness to explain complex concepts and answer my numerous questions. Many thanks to Lorena, Laura, Carolina, Serena, Pietro, Francesco, Alex R., and the early birds, Xikai, Yizhen, Liwen and Guanxiong, for their contributions to my progress.

Then, I would also like to express my sincere gratitude to my colleagues in the office – Ana, Kike, Edu, Shamim, David, Elena, Marta and Michel – for their support and patience during my time here. You are incredible people with amazing talent, and I am sure you will successfully achieve every single purpose you have in mind. Your warm hospitality, kindness and friendship made my stay really enjoyable and your willingness

to tolerate my occasional frustrations was truly commendable. Wish you nothing but the best!

Beyond those already mentioned, I am grateful to several other members of the department who enriched my experience and contributed to my progress: Jesica, for your friendship and willingness to lend a hand; Xènia, for your enthusiasm and constant encouragement; Aina, for your expertise; Sales, for your kindness and friendship; and Arnau, Dani S., Marina T., Derya, Dino, Diana, Esther, María, Nathaly, Rafa, Matías, Golafarin, Carlos, Jose, Javier, Pol, Roberto, Nico and Anna, whose collaborative spirit and contributions favoured a supportive research environment.

Outside the UAB, my deepest gratitude extends to my family. To my parents, whose unwavering support has been essential for all my achievements. Their love and encouragement have fuelled my pursuit of knowledge and ambition throughout every stage of my life. Their presence embodies an extraordinary strength and wisdom, which they have generously shared with me, guiding me through challenges and celebrating success. I am eternally grateful for their unwavering belief in me and the sacrifices they have made to ensure my education. Then, my special gratitude goes for my amazing wife Irene, the queen of patience and understanding, who has filled my life with joy and laughter, even during the most challenging moments. Her optimism, sharp intellect, and gentle spirit have been a constant source of inspiration for me. Words cannot express how grateful I am for her sacrifices and support. This achievement would not have been possible without her, and I am deeply grateful for her love and her belief in me. Then, my thanks to my lovely relatives for their love and support, which have been my guiding light throughout this journey: Iaia Cande, Toni, Elena, Lucas, Lourdes, Miquel, Oriol, Helena, Mar, Rut, Dunya, Laura, Jorge, Alberto, Lola, Carme, Uri and Ramon. I am incredibly lucky to have them by my side. Lastly, to my dearest friends, who have become my chosen family. Thanks to Xavi, Ignasi, Adri, Stephanie, Abel, Aitor and Jordi for always being my rocks. Whether it is celebrating my achievements or offering a supportive ear during tough times, they know how to manage my emotions with humour and kindness. I'm incredibly lucky to have friends like them who understand me so well.

The person I am today, brimming with passion for life, would not exist without these people.

Financial support

This work was supported by the LIFE+ NIMBUS project (LIFE19 ENV/ES/000191) (www.life-nimbus.eu). The author is a member of the GENOCOV research group (Grup de Recerca Consolidat de la Generalitat de Catalunya, 2021 SGR 515, www.genocov.com).

Thesis summary

Sustainable wastewater treatment presents a critical challenge within the context of climate change. While conventional methods are effective, they are energy-intensive, prompting the need for innovative solutions. In this context, environmental engineering is undergoing a paradigm shift towards viewing wastewater as a resource rather than merely waste.

Among the plethora of opportunities to recover resources from wastewater, microbial electrolysis cells (MECs) offer a promising approach, simultaneously treating wastewater and producing hydrogen, a renewable energy source. MECs have reported promising results at lab-scale, but its practical relevance is less explored. In fact, most of the research about MECs focuses on fundamental aspects of bioelectrochemical hydrogen production under controlled conditions, low reactors volumes, and employing easily biodegradable substrates. With this view, this thesis focuses into the critical factors influencing the pilot-scale performance of MECs for wastewater treatment.

Initially, a 135 L double-chamber MEC was operated under a wide range of operational conditions (chemical oxygen demand (COD) concentration, temperature, hydraulic residence time and applied potential) to determine how hydrogen yield and energy efficiency can be improved by modifying the operational parameters. The experimental outcomes were used to evaluate the treatment of 1 m^3 of urban wastewater by an MEC and the results were compared with two existing technologies reported in the literature: conventional activated sludge (CAS) and high-rate activated sludge (HRAS). The MEC pilot plant achieved the best results with synthetic wastewater, yielding a high current density (1.23 A m^{-2}) and hydrogen production (13.40 L d^{-1}, 0.10 m^3 m^{-3} d^{-1} and 10 L m^{-2} d^{-1}). However, the low COD concentration of urban wastewater limited the plant performance, and the MEC yielded a maximum average hydrogen production of 5.1 ± 0.2 L d^{-1} (0.038 m^3 m^{-3} d^{-1} or 3.9 L m^{-2} d^{-1}). These are much better results than similar MEC pilot plants treating domestic wastewater. The comparison between MECs and CAS/HRAS indicated that MECs have the potential to become an alternative to conventional wastewater treatment in terms of energy recovery, but the limited volumetric treatment capacity hinders its full-scale implementation.

Furthermore, the effect of nickel (Ni) foam in current generation and hydrogen production was studied for the first time at pilot-scale, developing a novel cathode configuration

based on two interconnected Ni-foam sheets. The performance of Ni-foam was compared to a cassette operating with stainless-steel (SS) wool cathode. The MEC was successfully run with real industrial wastewater from the confectionery industry with good hydrogen production results (19.07 L m^{-2} d^{-1} and 0.21 m^3 m^{-3} d^{-1}), high current densities (>2 A m^{-2}), and considerable organic matter removal efficiencies (>40 %). The high COD concentration of industrial wastewater allowed high current densities, but the coulombic efficiencies (CEs) (around 20 %) indicated that other simultaneous organic matter removal processes occur, possibly related to heterotrophic oxidation in the upper layers of the reactor and methanogenesis in the lower part due to anaerobic conditions. The novel cassette configuration with a double Ni-foam sheet cathode offered the highest current density and hydrogen production rates observed so far at this scale. The improvement with the novel configuration is 202% over the SS-wool cathode. However, the higher performance trade-off is the higher cost of Ni-foam.

Building upon the pilot-scale knowledge, a 1 m^3 MEC pilot reactor was scaled up within a real wastewater treatment plant to assess its performance under real-conditions. The experimental outcomes were used to evaluate the techno-economic viability of the process and the results were compared to CAS. The operation with synthetic wastewater yielded significant hydrogen production rates under a wide range of applied potentials, with higher applied potentials leading to increased current densities and hydrogen production rates. Under these conditions, the minimum applied potential requirement to drive the hydrogen evolution reaction (0.35 L H_2 m^{-2} d^{-1}) was 0.4 V, demonstrating that hydrogen production can be produced in a large-scale MEC at a low energy input. On the other hand, a maximum hydrogen production of 8.59 L H_2 m^{-2} d^{-1} was achieved at 1.4 V. The operation of the pilot plant with urban wastewater demonstrated the ability to establish functional biofilms directly from urban wastewater, eliminating the need for external substrates and simplifying the inoculation process. Furthermore, continuous hydrogen production was achieved in all cases, demonstrating robust operation and stability, even in the face of temperature variations and changes in influent characteristics. An average total COD removal of 34 ± 5 % and 51 ± 4 % was achieved at a hydraulic residence time of 1 and 2 days, respectively. When comparing SS-wool and Ni-foam cathodes, the maximum specific hydrogen production rates observed with urban wastewater were 2.12 L m^{-2} d^{-1} and 3.45 L m^{-2} d^{-1}, respectively. This represents a lower rate of improvement than in the case of using Ni-foam with high-strength wastewaters.

Based on the hydrogen sales revenue and the electricity consumption costs, the pilot plant could be profitable under very specific conditions. Furthermore, a significant reduction in the treatment cost per unit of COD removed is achieved compared to CAS. However, the high capital expenses associated with MEC components hinder commercial viability, emphasizing the need for cost-effective materials and manufacturing techniques. Material costs represent a 99% of the net present value, overshadowing the benefits of lower electricity costs and the hydrogen revenue.

Overall, this thesis places MECs in the current context of wastewater treatment, providing valuable insights for bridging the gap between lab-scale research and real-world applications. While challenges remain, further development and cost reduction hold promise for large-scale implementation and sustainable wastewater management.

Resumen de la tesis

El tratamiento sostenible de las aguas residuales plantea un reto crítico en el contexto del cambio climático. Aunque los métodos convencionales son eficaces, consumen mucha energía, lo que obliga a buscar soluciones innovadoras. En este contexto, la ingeniería medioambiental está experimentando un cambio de paradigma, considerando las aguas residuales como un recurso y no como un mero residuo.

Entre la multitud de oportunidades para recuperar recursos de las aguas residuales, las celdas de electrólisis microbianas (MECs) ofrecen un enfoque prometedor, ya que tratan simultáneamente las aguas residuales y producen hidrógeno, una fuente de energía renovable. Las MECs han obtenido resultados prometedores a escala laboratorio, pero su relevancia práctica está mucho menos estudiada. De hecho, la mayor parte de la investigación sobre las MECs se centra en los aspectos fundamentales de la producción bioelectroquímica de hidrógeno en condiciones controladas, con reactores de bajo volumen y empleando sustratos fácilmente biodegradables. Con esta visión, esta tesis se centra en los factores críticos que influyen en el rendimiento a escala piloto de las MECs para el tratamiento de aguas residuales.

En primer lugar, se evaluó el funcionamiento de una MEC de doble cámara de 135 L en una amplia gama de condiciones operacionales (concentración de demanda química de oxígeno (DQO), temperatura, tiempo de residencia hidráulico y potencial aplicado) para determinar cómo se puede mejorar la producción de hidrógeno y la eficiencia energética modificando los parámetros operativos. Los resultados experimentales se utilizaron para evaluar el tratamiento de 1 m^3 de aguas residuales urbanas mediante una MEC y los resultados se compararon con dos tecnologías existentes reportadas en la bibliografía: lodos activos convencionales (CAS) y lodos activos de alta velocidad (HRAS). La planta piloto obtuvo los mejores resultados con aguas residuales sintéticas, obteniendo una elevada densidad de corriente (1,23 A m^{-2}) y producción de hidrógeno (13,40 L d^{-1}, 0,10 m^3 m-^{3} d^{-1} y 10 L m^{-2} d^{-1}). Sin embargo, la baja concentración de DQO de las aguas residuales urbanas limitó el rendimiento de la planta, y la MEC alcanzó una producción media máxima de hidrógeno de 5,1 ± 0,2 L d^{-1} (0,038 m^3 m^{-3} d^{-1} o 3,9 L m^{-2} d^{-1}). Estos resultados son significativamente mejores que los reportados en plantas piloto MEC similares con aguas residuales domésticas. La comparación entre las MECs y el CAS/HRAS indica que las MECs tienen potencial para convertirse en una alternativa al

tratamiento convencional de aguas residuales en términos de recuperación de energía, pero la limitada capacidad de tratamiento volumétrico dificulta su aplicación a gran escala.

Por otra parte, se estudió por primera vez a escala piloto el efecto de la espuma de níquel (Ni) en la generación de corriente y la producción de hidrógeno, desarrollando una novedosa configuración de cátodo basada en dos láminas de espuma de Ni interconectadas. El rendimiento de la espuma de Ni se comparó con un cátodo de lana de acero inoxidable (SS). La MEC operó satisfactoriamente con aguas residuales industriales reales procedentes de la industria alimentaria con buenos resultados de producción de hidrógeno (19,07 L m^{-2} d^{-1} y 0,21 m^3 m^{-3} d^{-1}), altas densidades de corriente (>2 A m^{-2}) y considerables eficiencias de eliminación de materia orgánica (>40 %). La elevada concentración de DQO de las aguas residuales industriales permitió altas densidades de corriente, pero las eficiencias coulómbicas (en torno al 20 %) indicaron que también se producían otros procesos simultáneos de eliminación de materia orgánica, posiblemente relacionados con la oxidación heterótrofa en las capas superiores del reactor y la metanogénesis en la parte inferior debido a las condiciones anaeróbicas. La novedosa configuración de cátodo con doble lámina de espuma de Ni ofreció las mayores densidades de corriente y tasas de producción de hidrógeno observadas hasta la fecha a esta escala. La mejora con la nueva configuración es del 202% respecto al cátodo de lana de SS. Sin embargo, el aumento de rendimiento tiene la contrapartida del mayor coste de la espuma de Ni.

En base a los conocimientos adquiridos a escala piloto, se escaló y construyó una MEC de 1 m^3 para evaluar su rendimiento en condiciones reales de una planta de tratamiento de aguas residuales urbanas. Los resultados experimentales se utilizaron para estudiar la viabilidad tecnoeconómica del proceso y se compararon con los del CAS. El funcionamiento con aguas residuales sintéticas dio lugar a importantes tasas de producción de hidrógeno en una amplia gama de potenciales aplicados, siendo los potenciales aplicados más elevados los que dieron lugar a mayores densidades de corriente y tasas de producción de hidrógeno. En estas condiciones, el mínimo potencial aplicado necesario para llevar a cabo la reacción de evolución del hidrógeno (0,35 L H_2 m^{-2} d^{-1}) fue de 0,4 V, lo que demuestra que se puede producir hidrógeno en una MEC a gran escala con un bajo aporte energético. Por otro lado, se alcanzó una producción máxima de hidrógeno de 8,59 L H_2 m^{-2} d^{-1} a 1,4 V. La operación de la planta

piloto con aguas residuales urbanas demostró la capacidad de establecer biopelículas funcionales utilizando directamente estas aguas, eliminando la necesidad de sustratos externos y simplificando el proceso de inoculación. Además, se logró una producción continua de hidrógeno en todos los casos, lo que demuestra un funcionamiento robusto y estable, incluso frente a variaciones de temperatura y cambios en las características del influente. Se alcanzó una eliminación total media de DQO del 34 ± 5 % y del 51 ± 4 % con un tiempo de residencia hidráulico de 1 y 2 días, respectivamente. Al comparar los cátodos de lana de SS y espuma de Ni, las tasas máximas de producción específica de hidrógeno observadas con aguas residuales urbanas fueron de 2,12 L m^{-2} d^{-1} y 3,45 L m^{-2} d^{-1}, respectivamente. Esto representa una tasa de mejora menor que en el caso de utilizar espuma de Ni con aguas residuales más concentradas. Teniendo en cuenta los beneficios por la venta de hidrógeno y los costes de consumo eléctrico, la planta piloto podría ser rentable en condiciones muy concretas. Además, se consigue una reducción significativa del coste de tratamiento por unidad de DQO eliminada en comparación con el CAS. Sin embargo, los elevados costes de capital asociados a los componentes de la MEC dificultan actualmente su viabilidad comercial, lo que destaca la necesidad de utilizar materiales y técnicas de fabricación rentables. De hecho, los costes de los materiales representan el 99% del valor actual neto, lo que eclipsa los beneficios derivados de la reducción de los costes de electricidad y de los ingresos por hidrógeno.

En conjunto, esta tesis sitúa a las MECs en el contexto actual del tratamiento de aguas residuales, aportando ideas valiosas para reducir la distancia entre la investigación a escala laboratorio y su aplicación práctica. Aunque todavía existen retos por superar, el desarrollo y la reducción de costes son la esperanza de cara a su aplicación a gran escala y a la gestión sostenible de las aguas residuales.

Resum de la tesi

El tractament sostenible de les aigües residuals planteja un repte crític en el context del canvi climàtic. Encara que els mètodes convencionals són eficaços, consumeixen molta energia, la qual cosa obliga a buscar solucions innovadores. En aquest context, l'enginyeria mediambiental està experimentant un canvi de paradigma, considerant les aigües residuals com un recurs i no només com un residu.

Entre la multitud d'oportunitats per a recuperar recursos de les aigües residuals, les cel·les d'electròlisi microbianes (MECs) ofereixen un enfocament prometedor, ja que tracten simultàniament les aigües residuals i produeixen hidrogen, una font d'energia renovable. Les MECs han obtingut resultats prometedors a escala laboratori, però la seva rellevància pràctica està molt menys estudiada. De fet, la major part de la recerca sobre les MECs es centra en els aspectes fonamentals de la producció bioelectroquímica d'hidrogen en condicions controlades, amb reactors de baix volum i emprant substrats fàcilment biodegradables. Amb aquesta visió, aquesta tesi es centra en els factors crítics que influeixen en el rendiment a escala pilot de les MECs per al tractament d'aigües residuals.

En primer lloc, es va avaluar el funcionament d'una MEC de doble cambra de 135 L sota diferents condicions operacionals (concentració de demanda química d'oxigen (DQO), temperatura, temps de residència hidràulic i potencial aplicat) per a determinar com es pot millorar la producció d'hidrogen i l'eficiència energètica modificant els paràmetres operatius. Els resultats experimentals es van utilitzar per a avaluar el tractament d'1 m^3 d'aigües residuals urbanes mitjançant una MEC i els resultats es van comparar amb dues tecnologies existents reportades a la bibliografia: llots actius convencionals (CAS) i llots actius d'alta velocitat (HRAS). La planta pilot va obtenir els millors resultats amb aigües residuals sintètiques, amb una elevada densitat de corrent (1,23 A m^{-2}) i producció d'hidrogen (13,40 L d^{-1}, 0,10 m^3 m^{-3} d^{-1} i 10 L m^{-2} d^{-1}). Per una altra banda, la baixa concentració de DQO de les aigües residuals urbanes va limitar el rendiment de la planta, i la MEC va obtenir una producció mitjana màxima d'hidrogen de 5,1 ± 0,2 L d^{-1} (0,038 m^3 m^{-3} d^{-1} o 3,9 L m^{-2} d^{-1}). Aquests resultats són considerablement millors que els de plantes pilot MEC similars que tracten aigües residuals domèstiques. La comparació entre les MECs i el CAS/HRAS suggereix que les MECs tenen potencial per a convertir-se en una alternativa al tractament convencional d'aigües residuals, en termes de recuperació

d'energia, però la limitada capacitat de tractament volumètric dificulta la seva aplicació a gran escala.

D'altra banda, es va estudiar per primera vegada a escala pilot, l'efecte de l'escuma de níquel (Ni) en la generació de corrent i la producció d'hidrogen, desenvolupant una nova configuració de càtode basada en dues làmines d'escuma de Ni interconnectades. El rendiment de l'escuma es va comparar amb un càtode de llana d'acer inoxidable (SS). La MEC es va operar satisfactòriament amb aigües residuals industrials reals procedents de la indústria alimentària amb bons resultats de producció d'hidrogen (19,07 L m^{-2} d^{-1} i 0,21 m^3 m^{-3} d^{-1}), altes densitats de corrent (>2 A m^{-2}) i considerables eficiències d'eliminació de matèria orgànica (>40 %). L'elevada concentració de DQO de les aigües residuals industrials va permetre altes densitats de corrent, però les eficiències coulòmbiques (entorn al 20%) indicaven que també es produïen altres processos simultanis d'eliminació de matèria orgànica, possiblement relacionats amb l'oxidació heteròtrofa a les capes superiors del reactor i la metanogènesi a la part inferior degut a les condicions anaeròbiques. La nova configuració de càtode amb doble làmina d'escuma de Ni va oferir les majors densitats de corrent i taxes de producció d'hidrogen observades fins a la data a aquesta escala. La millora amb la nova configuració és del 202% respecte al càtode de llana d'SS. No obstant això, l'augment de rendiment té la contrapartida del major cost de l'escuma de Ni.

En base als coneixements adquirits a escala pilot, es va escalar i construir una MEC d'1 m^3 dins per a avaluar el seu rendiment en condicions reals d'una planta de tractament d'aigües residuals. Els resultats experimentals es van utilitzar per a estudiar la viabilitat tecnoeconòmica del procés i es va comparar amb la del CAS. El funcionament amb aigües residuals sintètiques va donar lloc a importants taxes de producció d'hidrogen en un ampli rang de potencials aplicats, essent els potencials aplicats més elevats els que van donar lloc a majors densitats de corrent i taxes de producció d'hidrogen. En aquestes condicions, el mínim potencial aplicat necessari per a dur a terme la reacció d'evolució de l'hidrogen (0,35 L H_2 m^{-2} d^{-1}) va ser de 0,4 V, la qual cosa demostra que es pot produir hidrogen en una MEC a gran escala amb una baixa aportació energètica. D'altra banda, es va aconseguir una producció màxima d'hidrogen de 8,59 L H_2 m^{-2} d^{-1} a 1,4 V. L'operació de la planta pilot amb aigües residuals urbanes va demostrar la capacitat d'establir biopel·lícules funcionals utilitzant directament aquestes aigües, eliminant la necessitat de substrats externs i simplificant el procés d'inoculació. A més a més, es va aconseguir una

producció contínua d'hidrogen en tots els casos, la qual cosa demostra un funcionament robust i estable, fins i tot enfront de variacions de temperatura i canvis en les característiques de l'influent. Es va aconseguir una eliminació total mitjana de DQO del 34 ± 5% i del 51 ± 4% amb un temps de residència hidràulic d'1 i 2 dies, respectivament. En comparar els càtodes de llana d'SS i escuma de Ni, les taxes màximes de producció específica d'hidrogen observades amb aigües residuals urbanes van ser de 2,12 L m^{-2} d^{-1} i 3,45 L m^{-2} d^{-1}, respectivament. Això representa una taxa de millora menor que en el cas d'utilitzar escuma de Ni amb aigües residuals més concentrades. Tenint en compte els beneficis per la venda d'hidrogen i els costos de consum elèctric, la planta pilot podria ser rendible en condicions molt concretes. A més a més, s'aconsegueix una reducció significativa del cost de tractament per unitat de DQO eliminada en comparació amb el CAS. No obstant això, els elevats costos de capital associats als components de la MEC dificulten actualment la viabilitat comercial, destacant la necessitat d'utilitzar materials i tècniques de fabricació rendibles. De fet, els costos dels materials representen el 99% del valor actual net, la qual cosa eclipsa els beneficis derivats de la reducció dels costos d'electricitat i dels ingressos de l'hidrogen.

En conjunt, aquesta tesi situa les MEC en el context actual del tractament d'aigües residuals, aportant idees valuoses per a reduir la distància entre la recerca a escala laboratori i l'aplicació pràctica. Si bé encara existeixen reptes per superar, el desenvolupament i la reducció de costos són l'esperança de cara a la seva aplicació a gran escala i a la gestió sostenible de les aigües residuals.

Contents

Acknowledgments i
Financial support v
Thesis summary vii
Resumen de la tesis xi
Resum de la tesi xv
Contents xix
Chapter I 1
1. General introduction 3
1.1. Wastewater treatment: From waste to resource 3
1.2. Hydrogen: A clean and versatile energy-carrier 4
1.3. Fundamentals of Bioelectrochemical Systems 6
1.3.1. Exoelectrogenic microorganisms 9
1.3.2. Thermodynamics and electromotive force 10
1.3.2.1. Microbial Fuel Cells 12
1.3.2.2. Microbial Electrolysis Cells 13
1.3.2.3. Voltage losses 14
1.3.3. Single-chamber vs double-chamber MECs 15
1.4. Unleashing the power of MECs 17
1.5. Critical parameters affecting MEC performance 18
1.6. Hydrogen production in MECs 18
1.7. Current challenges facing MEC development 20
1.8. The LIFE+ NIMBUS project 21
1.8.1. Environmental problem targeted 21
1.8.2. Project objectives 22
Chapter II 25
2. Objectives and research questions 27
2.1. Objectives 27
2.2. Research questions 28
Chapter III 29

3. Materials and Methods 31
3.1. Reactors designs 31
3.1.1. L-MEC pilot plant 31
3.1.2. M-MEC pilot plant 33
3.1.3. Current and voltage monitoring 34
3.2. Chemical analysis 34
3.2.1. Chemical oxygen demand 34
3.2.2. Nitrogen and phosphorus 34
3.2.3. Solids 35
3.2.4. Volatile fatty acids (VFAs) 35
3.2.5. pH and conductivity 35
3.2.6. Gas chromatography 36
3.3. Molecular methods 38
3.4. Electrochemical techniques 38
3.5. Key performance indicators 40
3.5.1. Current density and hydrogen production 40
3.5.2. Cathodic recovery efficiency 40
3.5.3. Coulombic efficiency 41
3.5.4. Energy production 41
3.5.5. Energy consumption 41
3.5.6. Energy recovery 41
Chapter IV 43
4. Exploring key operational factors for improving H_2 production in a pilot-scale MEC treating UWW 45
4.1. Abstract 45
4.2. Introduction 46
4.3. Objectives 46
4.4. Specific experimental procedures and calculations 47
4.4.1. Reactor design 47
4.4.2. MEC operation 47
4.4.3. Analytical methods 48
4.4.4. KPIs 48

4.4.5. Temperature effect study on response modelling 48
4.4.6. CAS/HRAS comparison 49
4.5. Results and discussion 51
4.5.1. Start-up of the pilot plant with synthetic wastewater 51
4.5.2. Operation in continuous mode of the pilot plant with urban wastewater 53
4.5.2.1. Effect of the applied potential on the plant performance 54
4.5.2.2. Effect of the temperature on the plant performance 56
4.5.2.3. Effect of the hydraulic retention time on the plant performance 60
4.5.3. Comparison with previous cassette-type MEC pilot plants 62
4.5.4. Comparing MECs vs conventional wastewater treatment technologies 65
4.6. Conclusions 68
Chapter V 69
5. Enhancing bioelectrochemical hydrogen production from industrial wastewater using Ni-foam cathodes in a MEC pilot plant 71
5.1. Abstract 71
5.2. Introduction 72
5.3. Objectives 73
5.4. Specific experimental procedures and calculations 74
5.4.1. Reactor design 74
5.4.2. Characteristics of wastewater 76
5.4.3. MEC operation 77
5.4.4. Analytical methods 78
5.4.5. Molecular methods 78
5.4.6. KPIs 78
5.5. Results and discussion 78
5.5.1. Electrochemical characterization of the cathodes 78
5.5.2. Start-up of the pilot plant 79
5.5.3. Preliminary evaluation of the performance of Ni-foam 80
5.5.4. Performance and cost analysis of the different cathode configurations . 83
5.5.5. Effect of ΔV on hydrogen production and energy efficiency 85
5.5.6. Bacterial communities in the anode 88
5.6. Conclusions 91

Chapter VI 93
6. Scale-up of MECs: Design, construction and operation of a 1 m^3 MEC pilot plant in a real wastewater treatment plant 95
6.1. Abstract 95
6.2. Introduction 96
6.3. Objectives 96
6.4. Specific experimental procedures and calculations 97
6.4.1. Reactor design 97
6.4.2. MEC operation 97
6.4.2.1. Performance evaluation with synthetic wastewater 97
6.4.2.2. Performance evaluation with real urban wastewater 99
6.4.2.2.1. Stage I 99
6.4.2.2.2. Stage II 100
6.4.3. Analytical methods 102
6.4.4. KPIs 102
6.4.5. Preliminary techno-economic study 102
6.4.5.1. Profitability 103
6.4.5.2. Treatment cost 103
6.4.5.3. Net present value 104
6.5. Results and discussion 104
6.5.1. Design and construction of the prototype 104
6.5.1.1. Cell design basis 105
6.5.1.1.1. Dimensioning of the anodes 105
6.5.1.1.2. Dimensioning of the cathodes 107
6.5.1.1.3. Cassette assembly 108
6.5.1.2. Tank design basis 110
6.5.1.2.1. Hydraulic design parameters 110
6.5.1.2.2. Tank sizing 110
6.5.1.3. Construction of the pilot plant 113
6.5.2. First evaluation of a cassette performance with synthetic wastewater 116
6.5.2.1. Start-up and operation of the MEC 116
6.5.2.2. Current density and hydrogen production 117
6.5.3. Performance evaluation of the pilot plant with urban wastewater 121

6.5.3.1. Stage I: Three cells on a real environment 121
6.5.3.1.1. Inoculation and start-up of the MEC 121
6.5.3.1.2. Long-term performance 122
6.5.3.2. Stage II: Ten cells on a real environment 127
6.5.3.2.1. Inoculation and start-up of the MEC 127
6.5.3.2.2. Long-term performance 128
6.5.4. Preliminary techno-economic assessment of the MEC 133
6.5.4.1. Profitability 133
6.5.4.2. Treatment cost 136
6.5.4.3. Net present value 138
6.6. Conclusions 141
Chapter VII 143
7. General conclusions and future perspectives 145
7.1. General conclusions 145
7.2. Future perspectives 150
Chapter VIII 153
References 155
List of Abbreviations 175
List of Figures 177
List of Tables 183
Curriculum Vitae 185

Chapter I

General Introduction

1. General introduction

1.1. Wastewater treatment: From waste to resource

Access to clean water is often regarded as a fundamental human right. However, an important percentage of the global population is deprived of this essential resource. Given the increasing and predominantly urbanised global population, the delivery of clean water is anticipated to incur significant costs, deplete our diminishing reserves of carbon-based energy and, consequently, contribute to the emission of greenhouse gases into the atmosphere. As a result, the challenges related to water pollution are also expected to increase, leading to subsequent adverse effects on the environment. Therefore, it is imperative to thoroughly investigate every potential cost-saving, energy-efficient and eco-friendly strategy for wastewater treatment.

Wastewater is generated mostly in human water-using activities and is typically defined as the mixture of water-carried pollutants removed from residences, institutions, and industrial facilities, together with groundwater, surface water, and rainwater (Metcalf and Eddy, 2003). Wastewater is characterised by the presence of significant amounts of contaminants and the composition greatly varies depending on where it is generated. Biodegradable and non-biodegradable compounds, nutrients (primarily nitrogen and phosphorus), toxic substances, pathogens, and inorganic suspended particles are the main pollutants of wastewater. Therefore, wastewater should be treated before its discharge into water bodies to prevent potential public health risks arising from the transmission of infectious diseases, as well as to address environmental problems related to natural water. However, considering the urgent need for sustainable waste management practices, the limited resource availability, and the increasing interest in energy recovery (r_E), environmental engineering is undergoing a paradigm shift towards approaching wastewater as a resource rather than merely waste. This field has gained global recognition and possesses a rich technological background (van Loosdrecht and Brdjanovic, 2014).

Focusing on r_E, wastewater contains many different organic compounds (from simple carbohydrates to more complex molecules) that contain valuable energy stored within their chemical bonds (Dai et al., 2019). The quantification of the energy content of domestic wastewater is a complex and multifaceted challenge. Numerous studies have attempted to establish correlations between this energy content and widely used

parameters such as biological oxygen demand (BOD) or chemical oxygen demand (COD). Combustion enthalpy of typical wastewater compounds can be calculated from reference data (Lide, 2004), giving values (kJ g^{-1} COD) of 13.6 for acetic acid, 14.6 for glucose and 15.6 for glutamic acid. Then, a typical value around 15 kJ g^{-1} COD seems to be a reasonable approach considering the inherent variability of urban wastewater (UWW) fractionation, and it agrees with different reported values (Heidrich et al., 2011; Korth et al., 2017; Shizas and Bagley, 2004).

In a modern society, each population equivalent (PE) produces about 200 - 300 L of wastewater per day with an organic matter load about 80 - 120 g COD $person^{-1}$ d^{-1} (Kiely, 1997). This means that, for example, in the case of Spain, with a population about 47 million people, an ideal maximum of $3 \cdot 10^{16}$ J per year could be recovered from wastewater, which is equivalent to the energy of burning around 735,000 tonnes of crude oil in a modern power station. This value is certainly overestimated, and a realistic goal may be to recover between 25-50% of this energy (Logan, 2008). However, despite all this amount of energy to harness, wastewater treatment remains an energy-intensive process, mainly because of the large aeration requirements of the activated sludge process, which constitutes the primary energy consuming process of a standard wastewater treatment plant (WWTP) (Molinos-Senante et al., 2014). Consequently, there is a significant focus on conducting comprehensive research aimed at minimising the energy consumption associated with wastewater treatment, as well as investigating novel approaches for harnessing the unutilized resources contained in the form of value-added products.

1.2. Hydrogen: A clean and versatile energy-carrier

There are several methods for harnessing the energy present in wastewater. Among these, anaerobic digestion (AD) for biogas production stands out as the most widely adopted approach (Obileke et al., 2021). The energy content of biogas from AD varies depending on the composition of the biogas. Specifically, the methane content of biogas is the main factor that determines its energy content. The higher the methane content of biogas, the higher its energy content will be.

Other promising alternatives focus on generating green hydrogen as an energy carrier (Guo et al., 2019). Hydrogen has a higher energy content per unit mass compared to methane (122 kJ g^{-1} *vs* 55 kJ g^{-1}) and contributes to reducing the carbon footprint, as water

is its only combustion product. Furthermore, it may be used in a wide range of applications beyond being a fuel as it is a valuable feedstock for various industrial processes, making the hydrogen industry large and well-established. For instance, the chemical and petrochemical industry (oil refining, ammonia, methanol, etc.) is the largest consumer of hydrogen as a raw material (around 70%). The remaining percentage is used in metallurgy, electronics, and the propulsion of spacecraft (Von Zuben et al., 2022).

According to the International Energy Agency, hydrogen consumption in Spain is around 500,000 t per year, mainly produced from fossil fuels (Ruiz Lozano, 2021). The natural gas reforming is the most common approach (Equation 1.1). In this process, methane is mixed with steam under the presence of a metal catalyst, at high temperatures (700-850 ºC) and pressures (3-25 bar), to generate hydrogen and carbon monoxide (Faheem et al., 2021).

$$CH_4 + H_2O \rightarrow CO + 3H_2 \qquad \Delta H^0 = 205.9\ kJ/mol \tag{1.1}$$

The 4% left of the hydrogen consumption is produced by water electrolysis (Equation 1.2) using non-renewable energy, which is dedicated to applications requiring high hydrogen purity.

$$H_2O \rightarrow H_2 + \frac{1}{2}O_2 \qquad \Delta H^0 = 285.8\ kJ/mol \tag{1.2}$$

Thus, the global hydrogen production is not considered neither renewable nor carbon-neutral, since both reactions are endothermic (Lide, 2004) and hence require a significant amount of external energy.

In this sense, the biological approach emerges as a promising alternative to tackle these limitations (Singh and Das, 2019; Younas et al., 2022), offering several theoretical advantages that include lower energy requirements, reduced capital costs, enhanced sustainability, and the utilization of waste materials. Unlike water electrolysis, which demands significant external energy input in the form of electricity for water splitting, biological hydrogen production processes harness part of the energy from organic feedstocks, such as waste materials, enabling a more energy-efficient approach. In fact, the versatility of biological hydrogen production is further exemplified by its ability to utilize various waste materials, including manure, food waste, and agricultural residues,

effectively remediating environmental concerns associated with these discarded substances.

The most common biological technologies for hydrogen production are dark fermentation, photofermentation and microbial electrolysis cells (MECs), all of them employing microorganisms as biocatalysts (Lee et al., 2010). These technologies have reported promising results, but their practical application is still unfeasible due to the inherent limitations of each technology. Photosynthetic hydrogen production encounters technical complexities related to oxygen sensitivity. Hydrogen production by dark fermentation is usually low due to the predominant utilisation of electrons for the synthesis of organic molecules, rather than the production of hydrogen (Dhar et al., 2015). This limitation could be overcome by coupling the fermentation process with a complementary step that effectively transforms the energy content of the fermentation products into hydrogen. Lastly, microbial electrolysis cells (MECs), which are a specific type of Bioelectrochemical Systems (BES) (see Section 1.3), can generate hydrogen obtaining part of the energy from the biological consumption of organic compounds, but its practical application on a larger scale is widely unexplored.

Regardless of the source, whether or not hydrogen becomes the energy vector of the future depends not only on the development of production technologies, but also on economic and social policies, distribution, storage, and safety aspects (Züttel et al., 2010). However, the European Commission itself indicated the start of a sustainable hydrogen economy in Europe, together with renewable energy campaigns, including wind and solar projects. In fact, the European Green Deal plays a crucial role in the European recovery strategy. The proposed approach outlines a gradual path consisting of three stages aimed at boosting the clean hydrogen economy (Fetting, 2020). These phases are designed to be implemented at different intervals across numerous industrial sectors.

1.3. Fundamentals of Bioelectrochemical Systems

BES comprise emerging technologies that combine electrochemistry with the metabolism of microorganisms. As an electrochemical cell, the system consists of a pair of electrodes: an anode, where an oxidation reaction takes place (loss of electrons), and a cathode, where a reduction reaction occurs (gain of electrons). The electrical connection of both electrodes allows electrons to flow from the anode to the cathode. The electrodes are surrounded by an electrolyte, a conductive aqueous solution with ionic species. Both

electrodes can be physically separated in an anodic and a cathodic chamber if an ion exchange membrane (IEM) is used, containing the anolyte and the catholyte, respectively.

There are many different types of BES that allow the implementation of many interesting environmental applications (Figure 1.1). The most studied configurations are: microbial fuel cells (MFCs), MECs, microbial desalination cells (MDCs) and microbial electro-synthesis cells (MESs). In an MFC, chemical energy is converted directly into electrical energy (Logan et al., 2006). On the contrary, when a certain voltage needs to be applied to drive the reactions, then the system is known as MEC (Liu et al., 2005; Rozendal et al., 2007). An MDC has as target the removal of salts and generation of electricity at the same time (Cabrera et al., 2021) and MESs, are capable of generating organic compounds such as ethanol, acetate, formate, propionate, butyrate or isopropanol from the capture of CO_2 (Batlle-Vilanova et al., 2017; Kronenberg et al., 2017; Logan, 2008).

In BES, microorganisms catalyse the oxidation and/or reduction reactions. The metabolic processes of these microorganisms are closely linked to the electrodes and, therefore, they are generally called electroactive microorganisms. Microorganisms whose metabolism is related to the anodic processes are the ones with the most studied and best understood metabolic mechanisms. The so-called anode respiring bacteria (ARB), oxidize organic matter under anaerobic conditions (in absence of other possible electron acceptors such as oxygen, nitrate and/or sulphate), and use an insoluble anode as the terminal electron acceptor. ARB are also known as exoelectrogens, as they transfer electrons extracellularly to the anode (Logan, 2008).

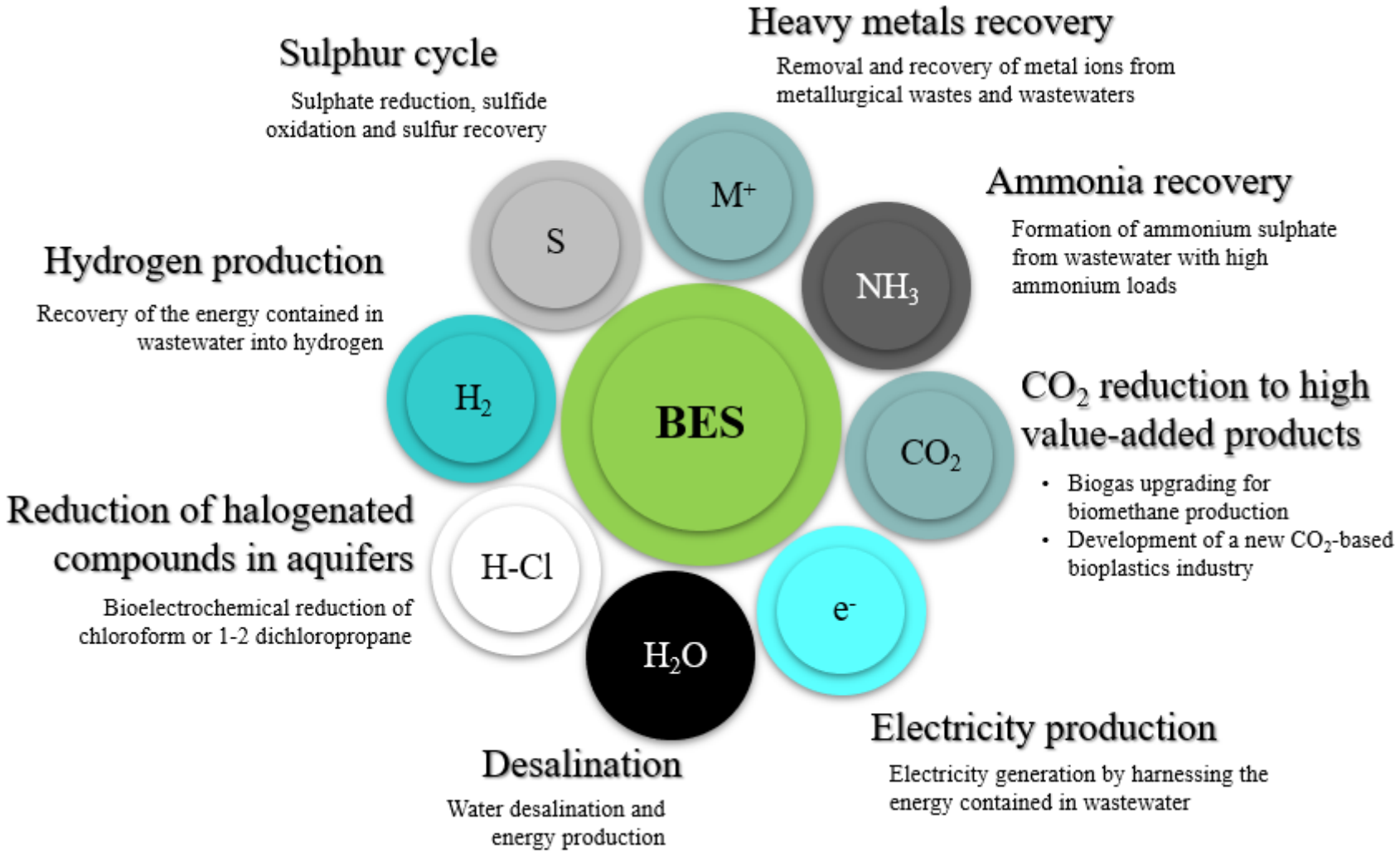

Figure 1.1. Examples of current applications of bioelectrochemical systems (BES).

1.3.1. Exoelectrogenic microorganisms

The first evidence of microorganisms with the ability to transfer electrons extracellularly was presented by Potter in 1911 (Potter, 1911). However, it was not until the end of the century that a more comprehensive understanding of their metabolic processes was established, leading to the beginning of research focused on their practical use (Joo Kim et al., 2002; Stirling et al., 1983). Since then, various mechanisms have been proposed to describe the extracellular transport of electrons in ARB (Figure 1.2):

- Direct electron transfer to the electrode requires physical contact between the microbe and the anode. The occurrence of this phenomenon is facilitated by the presence of outer membrane proteins, specifically c-type cytochromes, which play a crucial role in the electron transport chain (L. Shi et al., 2009). Furthermore, it can be facilitated by long and conductive filaments called nanowires (Reguera et al., 2005).
- Electron transfer between the cell and the anode can also occur through the involvement of mediators, or electro shuttles, that are continuously reduced and oxidized (Lovley, 2006). Electron shuttles may be synthesised endogenously by the same bacteria or externally added. Mechanisms are not exclusive for different species and are also linked to the operational mode of the BES (Borole et al., 2011; Busalmen et al., 2008).

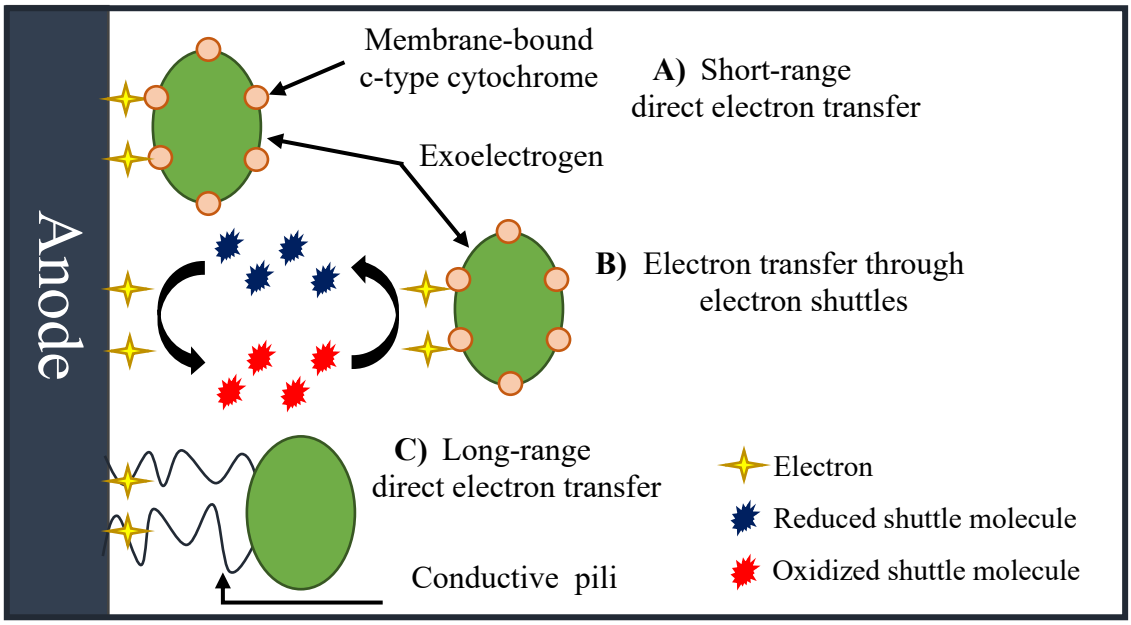

Figure 1.2. Extracellular electron transport mechanisms of exoelectrogens at the anode.

The first studied anodic microbial communities were both gram-negative and gram-positive bacteria. Examples of these bacteria include *Actinobacillus succinogenes* (Park et al., 1999), *Proteus vulgaris* (Kim et al., 2000), *Shewanella putrefaciens* (Kim et al., 2002), *Geobacter metallireducens* (Gregory et al., 2004), *Geobacter sulfurreducens* (Patil et al., 2012), *Pseudomonas sp.* (Pham et al., 2008; Venkataraman et al., 2010), *Bacillus subtilis* (Nimje et al., 2009), *Klebsiella pneumoniae* (Xia et al., 2010), *E. coli* (Weld et al., 2011), and *Corynebacterium sp*. (Liu et al., 2010). Previous studies have employed two different categories of microorganisms in BES: bacteria that require a mediator and the mediator-free ones. For instance, it has been reported that *E. coli*, *Bacillus subtilis*, *Proteus vulgaris*, *Actinobacillus succinogenes*, and *Pseudomonas fluorescens* require mediators. However, certain bacteria such as *Shewanella putrefaciens*, *Geobacteraceae*, *Geobacter*, *Rhodoferax ferrireducens*, and *D. desulfuricans* demonstrated the ability to work without mediators (Aghababaie et al., 2015; Bond and Lovley, 2003; Ieropoulos et al., 2005; Patil et al., 2012).

Substrate-consumption capabilities of most of these exoelectrogens are limited to simple fermentation products, such as acetate, though some members can use a wider range of substrates, such as propionate, butyrate, glucose, or lactate (Debabov, 2008; Holmes et al., 2004; Lovley et al., 1993). Therefore, in view of real-world applications of BES for wastewater treatment, a diverse consortium of bacteria is required, specially including fermentative and exoelectrogenic bacteria (Montpart et al., 2015). Fermentative bacteria would degrade the complex organic molecules present in wastewater into simpler compounds, which would then be consumed by exoelectrogenic bacteria.

1.3.2. Thermodynamics and electromotive force

The anodic oxidation of organic matter by ARB needs to be coupled to a cathodic reduction. The flow of electrons is favoured towards more positive potentials. Depending on the reduction reaction, the thermodynamics of the overall process may be favoured (negative Gibbs free energy) or it may require an energy input (positive Gibbs free energy).

In MFC, the reduction potential of the anode process is lower than that of the cathode process; therefore, the electrical connection between the anode and cathode spontaneously produces an electron flow that can be used as electricity elsewhere. In contrast, in MEC, the reduction potential of the reaction occurring at the cathode is lower

than that of the anode, and an energy input is required to drive the process and obtain the desired product. Both methodologies open a wide range of applications for BES.

The Gibbs free energy (ΔG, Equation 1.3) is used to determine whether a chemical process occurs spontaneously or requires additional energy. When Gibbs free energy is negative the process will proceed spontaneously (exergonic). Alternatively, when Gibbs free energy is positive the reaction requires additional energy input (endergonic).

$$\Delta G = \Delta H - T\Delta S \quad (1.3)$$

Where ΔG (J) is the change in Gibbs free energy; ΔH (J) is the change in the total heat content of the system (enthalpy); T (K) is the temperature; and ΔS (J K^{-1}) is the change in heat content unavailable for work (entropy). In this context, work and heat are considered flows of energy across system boundaries.

The thermodynamics of the overall reaction can be evaluated in terms of ΔG but in electrochemical systems it is useful to consider the electromotive force (emf). Equation 1.4 shows the relation of ΔG and emf:

$$\Delta G = -nFE \quad (1.4)$$

Where n is the number of moles exchanged in the electrochemical reaction; F (96485 C mol^{-1} e^-) is the Faraday constant; and E is the emf.

The emf in an electrochemical cell is determined by the differences in the electrode potentials, as shown in Equation 1.5:

$$emf = E_{cell} = E_{cathode} - E_{anode} \quad (1.5)$$

Where $E_{cathode}$ and E_{anode} are the reduction potential of the cathode and the anode, respectively.

The potential of each half reaction can be calculated according to Nernst equation (Equation 1.6):

$$E = E^o - \frac{R \cdot T}{n \cdot F} \ln(\Pi) \quad (1.6)$$

Where E^o (V) is the standard electrode potential, which by convention is reported as a reduction potential and can be found reported relative to the standard hydrogen electrode

(SHE). SHE is assigned a value of zero at standard conditions (298.15 K, 1 atm and pH=7); R (8.314 J K^{-1} mol^{-1}) is the ideal gas law constant; and *Π* is the reaction quotient calculated as the activities of the products divided by those of the reactants, raised to their respective stoichiometric coefficients. At low concentrations, activity coefficients typically approach to 1. As a result, the Nernst equation may be simplified by substituting the concentration values of the different species for their corresponding activity values.

1.3.2.1. Microbial Fuel Cells

The basic concept of an MFC is shown in Figure 1.3. The anodic exoelectrogenic biofilm oxidises organic matter using the anode as final electron acceptor. Typically, acetate is directly oxidised by the electrogenic organisms (Equation 1.7). However, metabolic pathways are only partially understood (Ishii et al., 2015). At standard conditions and neutral pH, the potential of this oxidation reaction is -0.28V (Equation 1.8).

Anode oxidation reaction: $CH_3COO^- + 4H_2O \rightarrow 2HCO_3^- + 9H^+ + 8e^-$ (1.7)

$$E_{(HCO3-|CH3COO-)} = E_{an} = E^o_{an} - \frac{R \cdot T}{b_{Ac} \cdot F} ln \frac{[CH_3COO^-]}{[HCO_3^-]^2\,[H^+]^9} \quad (1.8)$$

($E_{HCO3-|CH3COO-}$ = -0.28 V vs. SHE at standard conditions and pH = 7)

Where E^o_{an} (V) is the standard reduction potential for the oxidation reaction in Equation 1.7 (0.187 V vs. SHE); b_{Ac} are the moles of electrons transferred in the electrochemical reaction per mole of acetate (8 mol e^- mol^{-1} Ac); and [CH_3COO^-], [HCO_3^-] and [H^+] (mol L^{-1}) are the concentrations of acetate, bicarbonate and protons, respectively, raised to their stoichiometric coefficient.

In the cathode chamber, oxygen is available. The oxygen and protons in the solution are reduced to water (Equation 1.9). At standard conditions and neutral pH, the potential of this reduction reaction is +0.82V (Equation 1.10). This creates a charge gradient between the electrodes. As the resulting emf is positive (+1.1V) and the Gibbs free energy negative, the reaction occurs spontaneously and electrical current flows from the anode to the cathode, which could be used to charge external devices or be fed into the grid (Logan et al., 2006).

Cathode reduction reaction: $O_2 + 4H^+ + 4e^- \rightarrow 2H_2O$ (1.9)

$$E_{(O2|H2O)} = E_{cat} = E^o_{cat} - \frac{R \cdot T}{b_{O_2} \cdot F} ln \frac{1}{pO_2 \, [H^+]^4} \quad (1.10)$$

($E_{O2|H2O}$ = 0.82 V vs. SHE at standard conditions and pH = 7)

Where E^o_{cat} is the standard reduction potential for reaction 1.4 (1.229 V vs. ENH); b_{O2} are the moles of electrons transferred in the electrochemical reaction per mole of oxygen (4 mol e^- mol^{-1} O_2), and pO_2 (atm) is the partial pressure of oxygen.

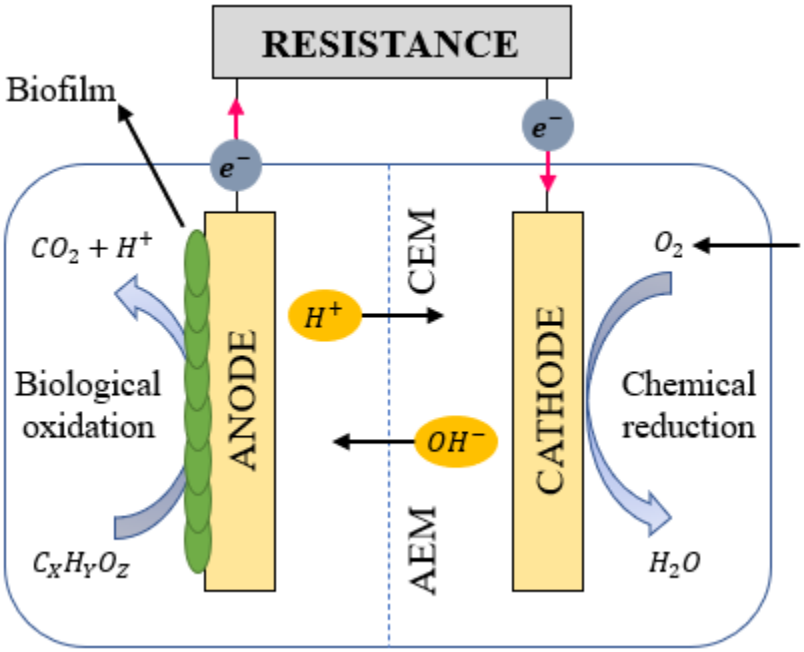

Figure 1.3. Diagram of a microbial fuel cell (MFC) for electricity production. CEM and AEM refers to cation and anion exchange membrane, respectively.

1.3.2.2. Microbial Electrolysis Cells

The basic concept of an MEC is shown in Figure 1.4. The oxidation reaction occurring in the anode is the same as in an MFC (Equations 1.7 and 1.8). The cathode reaction, however, must occur in anaerobic conditions. The electrons released in the oxidation reaction travel through the electrical circuit from the anode to the cathode, ultimately contributing to the hydrogen evolution reaction (HER, Equation 1.11) (Rozendal et al., 2007). At standard conditions and neutral pH, the reduction of protons to hydrogen gas occurs at a theoretical potential of -0.41V (Equation 1.12). The emf is -0.12V and the process is therefore endergonic.

Cathode reduction reaction: $2H^+ + 2e^- \rightarrow H_2$ (1.11)

$$E_{(H+|H2)} = E_{cat} = E^o_{cat} - \frac{R \cdot T}{b_{H_2} \cdot F} \ln \frac{pH_2}{[H^+]^2} \quad (1.12)$$

($E_{H+|H2}$ = -0.41 V vs. SHE at standard conditions and pH = 7)

Where E^o_{cat} is the standard reduction potential for Equation 1.11 (0.0 V vs. SHE); b_{H2} are the moles of electrons transferred in the electrochemical reaction per mole of hydrogen (2 mol e^- mol^{-1} H_2), and pH_2 (atm) is the partial pressure of hydrogen.

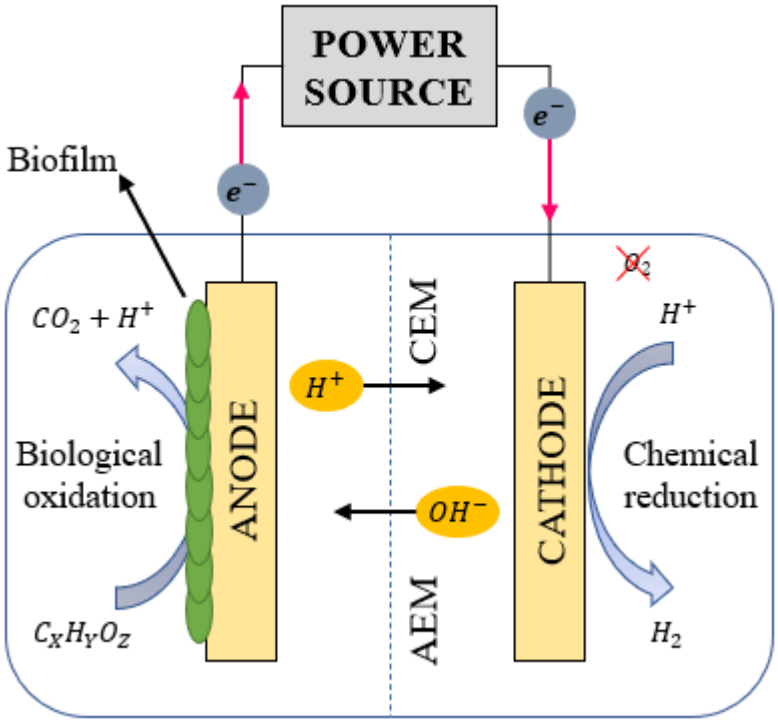

Figure 1.4. Diagram of a microbial electricity cell (MEC) for hydrogen production. CEM and AEM refers to cation and anion exchange membrane, respectively.

1.3.2.3. Voltage losses

The emf of an electrochemical cell, as expressed in Equation 1.5, is the basis for determining its theoretical potential. However, it is important to note that the real potential measured within the cell often differs significantly from the theoretical potential calculated using thermodynamic values. This value decreases in the case of an MFC, causing less electrical energy to be generated, and increases in the case of an MEC, causing more external energy requirements for the electrochemical reactions to take place.

The actual potential required in an electrochemical cell ($E_{applied}$) can be calculated with Equation 1.13 (Logan et al., 2008):

$$E_{applied} = E_{cell} - \eta_{cathode} - \eta_{anode} - \eta_{ohmic} \quad (1.13)$$

Where $\eta_{cathode}$ (V) and η_{anode} (V) are the overpotentials at the cathode and anode, respectively, and η_{ohmic} (V) is the ohmic overpotential or ohmic drop.

The cathodic and anodic overpotentials are the difference in potential between the actual (measured) value and the theoretical value, both at the cathode and at the anode. These overpotentials are a combination of an activation, concentration and bacterial metabolic overpotential in the case of the anode, as expressed in Equation 1.14 and 1.15 (Ki et al., 2016):

$$\eta_{cathode} = \eta_{act,c} - \eta_{conc,c} \quad (1.14)$$

$$\eta_{anode} = \eta_{act,a} - \eta_{conc,a} - \eta_{bact} \quad (1.15)$$

Where ηact,c (V) and ηact,a (V) are the cathode and anode activation overpotentials, respectively; ηconc,c (V) and ηconc,a (V) are the cathodic and anodic concentration overpotentials, respectively, and ηbact (V) is the bacterial metabolic overpotential of the anodic biofilm.

In addition, the ohmic overpotentials are caused by the resistance to the flow of ions in the electrolyte and across the IEM (if used), as well as the resistance to the flow of electrons through the electrodes and the existing interconnections (Logan et al., 2018).

Thus, the ohmic overpotential (η_{ohmic}) can be calculated following Ohm's law (Equation 1.16):

$$\eta_{ohmic} = I \cdot R_{int} \quad (1.16)$$

Where R_{int} (Ω) is the internal resistance of the cell, and I (A) is the current flowing through the cell.

1.3.3. Single-chamber vs double-chamber MECs

Single and double-chamber systems are the most common MEC configurations. In a double-chamber MEC, the anodic and cathodic chambers are separated by an IEM, while in a single-chamber MEC, the anode and cathode share the same electrolyte.

In the case of single-chamber MECs, the architecture is simplified, thus reducing the capital costs. Also, the pH gradient is reduced, and the potential required to carry out the electrochemical reactions is theoretically lower compared to a double-chamber MEC. This is because, in a double-chamber system, adding a separator between the cathodic and anodic chamber causes the internal resistance of the cell to increase significantly. Specifically, the potential losses associated with IEM are estimated to be between 0.26 and 0.38 V (Rozendal et al., 2007). However, the fact that both electrolytes are not physically separated contributes to the development of microorganisms that compete with ARB not only for the substrate but also for hydrogen. Methanogenic archaea that consume acetate (acetoclastic methanogens) and hydrogen (hydrogenotrophic methanogens) are able to grow in the system. As a consequence of their proliferation and increased activity, hydrogen production decreases and the resulting gas contains impurities (such as methane, carbon dioxide or hydrogen sulphide). This represents an energy loss for the MEC. Furthermore, a prior separation process would be required if the objective is to use hydrogen as a feedstock, resulting in higher costs. Other hydrogen scavengers, such as homoacetogenic and hydrogen-oxidizing ARB, may also develop in the system, resulting in a hydrogen recycling scenario, or, equivalently, an electron recycling scenario (Parameswaran et al., 2009; Ruiz et al., 2013). Since hydrogen produced on the cathode can be used by hydrogen-oxidizing ARB as the electron donor and by homoacetogenic bacteria to produce acetate, net hydrogen production in this scenario is reduced or entirely eliminated (Rago et al., 2015). Adding chemical inhibitors of hydrogen scavengers is not an economically feasible choice in view of future scale-up of the process, but some strategies have been developed to reduce the hydrogen retention time and decrease the effects of methanogenesis in MECs (Montpart et al., 2015).

In practice, double-chamber MECs are the most abundantly used among other reactor designs (Bora et al., 2022). However, the choice between these configurations should align with specific project goals, budget constraints, and the importance of product purity. Single-chamber MECs can be cost-effective but require strategies to manage microbial competition and impurity formation. In contrast, double-chamber MECs offer greater control over reactions but entail higher costs.

1.4. Unleashing the power of MECs

The choice between MFCs and MECs depends on a thorough evaluation of several parameters and specific objectives. Both systems have unique advantages and challenges. For instance:

i) MFCs rely on the availability of oxygen as the electron acceptor at the cathode. This requires the utilisation of either large-scale air-cathodes, which present design complexities, or the use of aeration in the cathode chamber, resulting in substantial EC.

ii) The power produced by MFCs must be directly used or stored in external batteries.

iii) Furthermore, MFCs are susceptible to a phenomenon referred to as voltage reversal, which has the potential to cause damage to the bioanode and incur significant expenses for replacement (Aiken et al., 2019). In contrast, this problem could be solved by MECs with the application of voltage (Li et al., 2017).

iv) Most importantly, MFCs face limitations in terms of commercial viability due to the relatively low cost of electricity (Christgen et al., 2015; Rozendal et al., 2008).

On the other hand, MECs may become a more economically feasible alternative for domestic wastewater treatment and sustainable energy production (E_P) through the generation of hydrogen gas or other value-added products (Cusick et al., 2011; Rozendal et al., 2008). Considering the current energy scenario and the dedicated efforts towards promoting green hydrogen (see Section 1.2), MECs appear to be a promising alternative. Hydrogen production requires only two electrons from the (bio)electrochemical oxidation and protons are readily abundant in water or wastewater. Previous studies estimated that the costs associated with hydrogen production by MECs were considerably lower than the actual market value of hydrogen (Cusick et al., 2010). Highlighting the benefits of MEC, prior studies have demonstrated that the anodic microbial communities may be influenced by the applied potential (Hasany et al., 2016), which could increase the exoelectrogenic activity, reduce start-up times (G. Kumar et al., 2017) and enable the oxidation of specific pollutants.

1.5. Critical parameters affecting MEC performance

The performance of MECs is influenced by several critical parameters. Substrate type and concentration significantly impact ARB performance, with highly biodegradable substrates yielding higher hydrogen production rates (Ullah and Zeshan, 2020). Additionally, the optimal anodic pH for MEC operation varies depending on the microbial community present, but most MECs typically operate at a pH of 7-8. Temperature also plays a crucial role, as MEC performance generally increases with temperature up to a certain point, beyond which microbial activity and hydrogen production decline (Ahn et al., 2017). The optimal temperature varies based on the microbial community.

The material and surface properties of electrodes can have a significant impact on MEC performance. Electrodes with high surface area and good catalytic activity tend to result in higher hydrogen production rates. Membranes, concerning their type and thickness, also affect performance (Leong et al., 2013). Cation exchange membranes (CEMs) with high proton conductivity and low resistance typically contribute to higher hydrogen production rates (Kumar and Himabindu, 2019). Additionally, the applied voltage and current density can affect MEC performance, with optimal electrical parameters varying depending on the specific MEC design and operating conditions.

Furthermore, other critical parameters can influence MEC performance. Effective mixing within the MEC is crucial to ensure substrate diffusion and microbial access to nutrients (Day et al., 2022). Biofouling on the electrodes can reduce MEC performance by increasing internal resistance and blocking ion and electron transfer (Koók et al., 2019). Inhibition from certain compounds in the substrate or wastewater, such as heavy metals and toxic organic compounds, can be detrimental to the microbial community (Sharma et al., 2021). In conclusion, MEC performance is influenced by a variety of critical factors. By carefully optimizing all of these parameters, it would be possible to increase hydrogen production rates and efficiencies.

1.6. Hydrogen production in MECs

MECs have shown promising results at laboratory scale in terms of hydrogen production, usually attaining values between 1 - 10 m^3 H_2 m^{-3} reactor d^{-1} (Guo et al., 2010; Montpart et al., 2015; Y. Wang et al., 2014), with high (>70 %) cathodic recoveries (r_{CAT}) and high

(>50 %) coulombic efficiencies (CEs) (Rago et al., 2016; Wagner et al., 2009). However, the majority of the studies were conducted in small reactors (i.e. reactor volumes below 100 mL) with the use of simple substrates and optimized and buffered culture media (Lu and Ren, 2016). As previously explained, acetate, among all the substrates tested is recognized to be the best candidate in terms of hydrogen production performances, leading to high hydrogen production rates and r_E efficiencies in most cases exceeding 100% (Cheng and Logan, 2011; Jeremiasse et al., 2010; Liang et al., 2011; Tartakovsky et al., 2009).

As of October 30th, 2023, a search on ScienceDirect yielded 11,207 items for the search term "microbial electrolysis cell". However, it is noteworthy that no commercially feasible design for wastewater treatment has been developed so far. The gap between the amount of research conducted in this particular subject and the absence of a commercially feasible design in practical applications is significant, but not necessarily damning for MEC. Over the past two decades, the field of MEC has experienced a surge in research activity, with more than 50% of all published papers being released since 2016 (Figure 1.5).

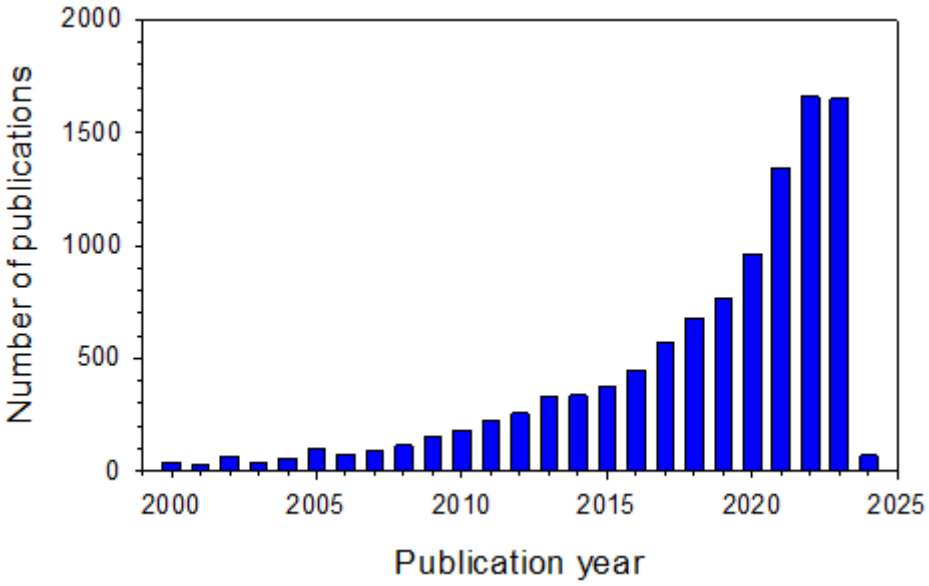

Figure 1.5. Number of articles related to microbial electrolysis cells (MECs) based on ScienceDirect database as of October 30th, 2023.

However, despite the large number of manuscripts published about the fundamentals of bioelectrochemical hydrogen production, few studies are conducted at pilot scale. Jadhav et al. specified that <1% of the >20,000 studies about microbial electrochemical technologies (MET) addressed the issue of scaling-up (Jadhav et al., 2022).

Among the few experiences of such systems at pilot scale, a general reduction in reactor performance is reported compared to bench-scale reactors (de Fouchécour et al., 2022; Guisasola et al., 2020a). Hydrogen production is usually poor, in the range 0.005 - 0.040 $m^3\ m^{-3}\ d^{-1}$ (Baeza et al., 2017; Escapa et al., 2015; Gil-Carrera et al., 2013; Heidrich et al., 2013), with low CE (< 50 %) and significant hydrogen leakages (Cotterill et al., 2017; Heidrich et al., 2014). Also, the reported range of organic matter removal in these studies is very broad (between 10 and 60%) due to the different influent load and composition, with reported hydraulic retention times (HRTs) between 4 and 48h.

1.7. Current challenges facing MEC development

The benefits of MECs for wastewater treatment and hydrogen production are clear. However, there are several challenges that need to be addressed before MECs can be widely adopted at industrial scale.

One of the biggest challenges is the high cost of MECs due to the specialized materials required for the electrodes and membranes. MEC materials need to be cheap, electrically conductive, biologically compatible, and electrochemically stable. This is a difficult combination of properties to achieve, especially at larger scale. For instance, Pt is one of the most common catalysts for electrochemical reactions because of its excellent catalytic properties, but its high cost leads to increased and unaffordable capital expenses.

Another challenge is the low current densities and limited organic removal rates (ORR) that can be achieved. Commonly organic loading rates (OLRs) in systems for UWW treatment are in the range 0.04 - 1.6 g COD $L^{-1}\ d^{-1}$ (Metcalf and Eddy, 2003). In this sense, MECs must operate at a short HRT to be competitive with other technologies (e.g., activated sludge or AD systems) (Fornero et al., 2010). Achieving high COD removal efficiencies under short HRTs is one of the recent objectives of WWTP designers aiming only at COD removal. However, poor anode-based oxidation rates are typically found in MECs due to low mixing (Michie et al., 2014), which is translated in higher volumes or higher HRTs and, consequently, in poor volumetric hydrogen production rates ($m^3\ H_2\ m^{-3}_{reactor}\ d^{-1}$). Conventional stirring or recycling pumps are implemented to improve turbulence in the reactor to avoid mass transfer limitations (Baeza et al., 2017; Cotterill et al., 2017; Day et al., 2022), but this may hinder the system energy balance.

Furthermore, a considerable variability in performance of pilot-scale MECs is usually reported in the literature. The ORR and hydrogen production depend on multiple factors (see Section 1.5), and even similar reactor configurations treating similar wastewater can lead to totally different performances (Baeza et al., 2017; Escapa et al., 2012; Heidrich et al., 2014). This represents a challenge not only for comparison, but also for the design and operation of MECs that are consistently reliable and efficient in different scenarios.

The limited advancement in the scale-up of MECs could potentially be attributed to the predominant focus of research in laboratory conditions, which mostly involve the use of simple substrates and controlled favourable conditions such as high conductivity and temperature, and use of phosphate as a buffer in usually short-term experiments. Even though lab-scale research is essential, it may put out of sight the challenging issues involved in the operation of MECs under real-scale conditions. MECs need to be operated under conditions like those of WWTPs to bridge the gap between lab and industrial adoption. If future scale-up designs are based on results obtained under non-representative conditions, such as the use of synthetic media, this could lead to significant underdimension of the system.

1.8. The LIFE+ NIMBUS project

1.8.1. Environmental problem targeted

The transport sector, which demands around 33% of the total primary E_C in Europe (Haasz et al., 2018), has recently diversified energy sources (natural gas and electricity) but more effort is needed to reduce the environmental impacts. While the production and use of renewable electricity in EU is growing and accounted for the 22.1%, the share of renewable fuels in the transport sector was just 10.3% in 2020 (Akimoto et al., 2022). Within this context, among renewable fuels for transport, biomethane is starting to play a key role among sustainable road transport solutions. On the other hand, the European Directive 2009/28/EC aims to achieve a 32% share of energy from renewable sources by 2030. In particular, the power sector can easily reach a high share of renewable sources thanks to wind and solar technologies, so that renewable power generation could grow up to 53% by 2050. However, the good perspectives for wind and solar sources into the power mix are limited by the storage capacity of the grid and often the renewable power plants are forced to decrease the supply during low demand periods.

Power-to-gas concept is a solution to store the 'excess' of renewable energy when the power generation is higher than the demand and use it to obtain a renewable biofuel, such as biomethane. Biomethane can be used for transport and thus contribute to reduce CO_2 emissions compared to fossil natural gas, which goes in the direction of European standards to reduce CO_2 emissions in transport (Regulation (EU) 2019/631). Therefore, biomethane produced from power-to-gas technologies is an opportunity to link renewable electricity generation with decarbonisation of the transport sector. It also improves the circular economy between the city and the WWTPs, which have a huge potential to produce biomethane, minimizing the city overall impacts. As the current use of biogas in WWTPs is cogeneration of heat and power, the solution proposed in this project allows to increase up to 68% the efficiency of the renewable E_P.

There are cities that have already taken actions to introduce biomethane fuelled buses in their fleet, as Stockholm, Bergen, Lille and Bristol, obtaining biomethane through different biogas upgrading technologies (separation of methane and carbon dioxide), such as water scrubbing or membranes. However, these technologies only provide the amount of biomethane that is already in the biogas, approximately 60-65%. In contrast, biological methanation is based on hydrogenotrophic methanogenesis, which is able to convert the remaining 35 - 40% of CO_2 into additional biomethane, therefore increasing the renewable biofuel production potential.

1.8.2. Project objectives

The aim of the LIFE+ NIMBUS project is to demonstrate a power-to-gas technology based on biological processes to produce biomethane by biological methanation and bioelectrochemical hydrogen by MECs (Figure 1.6). From a technical point of view, the main objective is to produce biomethane that accomplishes the quality to be used as a biofuel.

In order to tackle this objective, a biological methanation demonstration plant was designed, built and operated in the Baix Llobregat WWTP (2,000,000 PE) in Barcelona. The biomethane produced by this demonstration plant was used to fuel one public bus that covers a daily route of 100 km of the fleet of Transports Metropolitans de Barcelona (TMB), consequently reducing 72 t CO_2 $year^{-1}$. Two hydrogen production technologies were evaluated in the biomethanation: water electrolysis and a BES. In this sense, a 1 m^3 pilot-scale MEC was designed, built and operated in the WWTP to produce hydrogen

from UWW. The project evaluated the technical and economic feasibility of the solution proposed, and also included a business and a replication plan to ensure the implementation of the proposed power-to-gas technology in other sites, such as Sète WWTP in France.

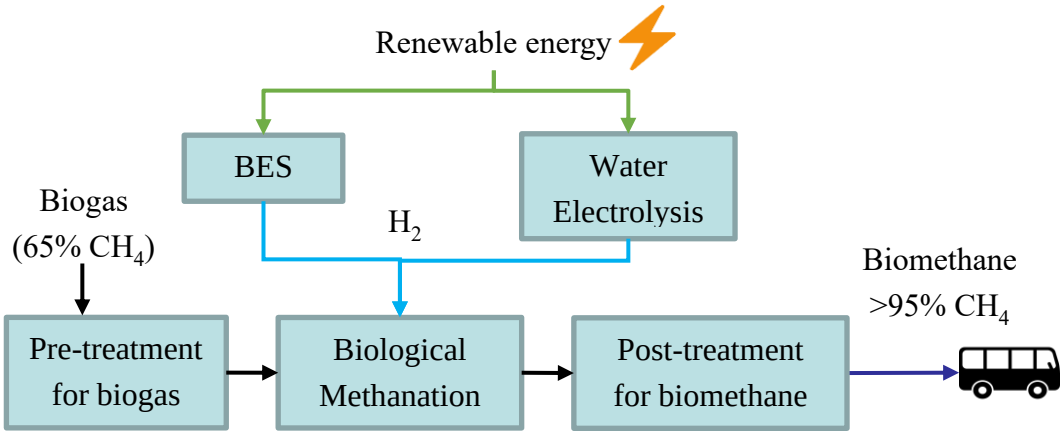

Figure 1.6. Diagram of the biomethane production process proposed in the LIFE+ NIMBUS project.

Chapter II

Objectives and research questions

2. Objectives and research questions

2.1. Objectives

Aim	To investigate pilot-scale MECs for wastewater treatment and hydrogen production, focusing on optimizing performance, demonstrating reactor scale-up, and assessing the techno-economic viability for future large-scale implementation.
Objective 1	To understand key operational parameters affecting MEC performance
Objective 2	To test different MEC components and configurations at pilot-scale
Objective 3	To compare MECs with alternative technologies
Objective 4	To design , construct and operate a 1 m^3 MEC pilot plant
Objective 5	To evaluate commercial viability of MECs

2.2. Research questions

Research question	Chapter
What are the key knowledge gaps and limitations identified in the existing literature related to the practical applications of MECs?	I
What are the optimal operational parameters for maximizing hydrogen yield and energy efficiency in pilot-scale MECs treating different wastewaters?	IV
Can MECs achieve superior treatment performance and r_E compared to CAS/HRAS?	IV
How does the composition and strength of real wastewater impact the performance and efficiency of MECs?	IV & V
Can Ni-foam improve current density and hydrogen production in pilot-scale MECs treating real wastewater?	V
What are the key technical and economic challenges that need to be addressed for scaling-up MECs?	VI
How is the performance of a 1 m^3 MEC operating within a real WWTP?	VI
How far are MECs from being a commercially viable alternative to existing wastewater treatment technologies?	VI
What are the most promising areas for future research and development to address the remaining challenges and accelerate the commercialization of MECs?	VII

Chapter III

Materials and Methods

3. Materials and Methods

3.1. Reactors designs

Throughout this thesis, different types of MEC configurations and volumes have been used for each experiment. The following is a general description of the main configurations and the specific details of each can be found in the results and discussion chapters.

3.1.1. L-MEC pilot plant

The litre-scale microbial electrolysis cell (L-MEC) pilot plant (Figures 3.1 - 3.3) was based on a cassette-style design (Heidrich et al., 2013), with a series of cassette-type cells being placed into a rectangular stainless-steel (SS) tank of 220 L of total volume. Each cassette worked as a double-chamber MEC and contained two anodes and a cathode that were separated by anion exchange membranes (AEMs). During operation, the cassettes were strategically positioned on alternating sides of the reactor with the intention to facilitate a zig-zag flow. Hydrogen gas was produced in the internal frames and further collected for analysis. The top of the tank was closed by two SS plates placed over the liquid to maintain anaerobic conditions. A small head space of around 2.5 L was left in the anodic chamber for the gas tubbing and electrical connections.

The cells consisted of a central polyvinyl chloride (PVC) frame (3 cm width x 36 cm length x 46 cm height) acting as a cathode chamber (i.e., containing the cathode and the catholyte). The internal cathode section of each cell had a volume of 3.7 L. Two different cathode materials were evaluated in this reactor configuration: i) Pressed SS wool (Steel wool #2, Barlesa SL, Spain) and ii) Nickel (Ni) foam (RCM-Ni4753, Recemat BV, The Netherlands).

The cathode chamber was separated from the anodes using AEMs on both sides. The following AEMs were tested: i) AEM made of polystyrene cross-linked with divinylbenzene (AMI-7001S, Membranes International Inc., United States) and ii) AEM made of a mix of polyethylene and polyester conjugate fibres (RALEX® AMHPP, Mega, Czechia).

In all experiments, the anodes were made of carbon felt (PX35 Carbon Felt, Zoltek™, United States) and were pressed to the membranes on both sides of the cathode through a SS mesh. A 1 mm SS cross wire was wounded into the SS mesh for the electrical

connections. The anodes were thermally pre-treated (400ºC for 20 min) to improve biomass adhesion. The membranes and the anodes were located between the cathode compartment and two outer PVC frames (1 cm length x 36 cm width x 46 cm height in external dimensions with a 6 cm frame).

The central frame was provided with an olive fitting at the top that allowed the gas collection via a tube (Marprene® Tubing 9.6 mm BORE, Watson Marlow, United Kingdom) connected to a 10 L gas sample bag (FlexFoil® Standard, SKC, United States). All pieces were sandwiched using 2 mm rubber gaskets and held together by tightening 34 wing nuts onto bolts through 5 mm holes in the PVC frames.

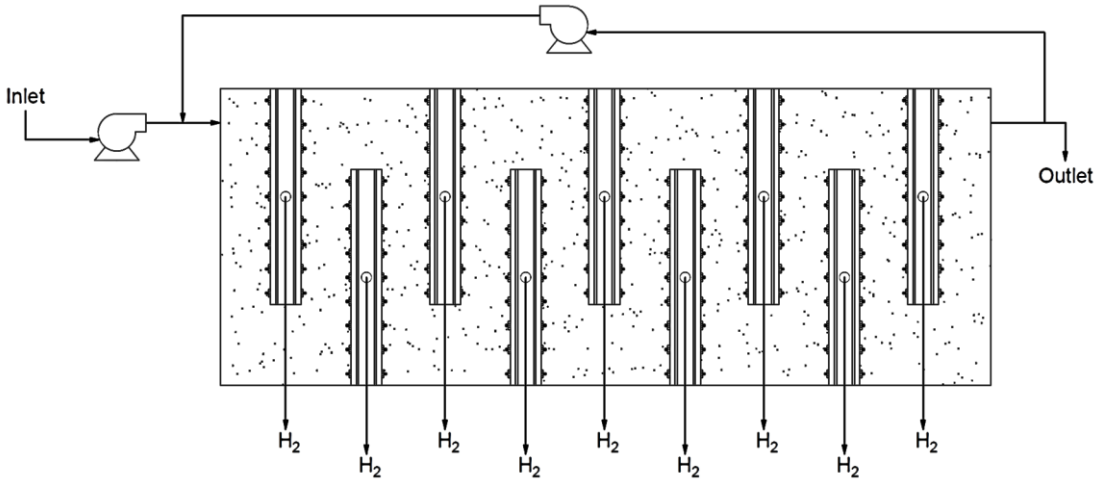

Figure 3.1. Top view flow diagram of the L-MEC pilot plant with nine cassette cells.

Figure 3.2. L-MEC pilot plant.

3.1.2. M-MEC pilot plant

The m^3-scale microbial electrolysis cell (M-MEC) pilot plant (Figure 3.4 – 3.6) was the scaled-up version of the L-MEC, in the frame of the LIFE+ NIMBUS project (see Section 1.8). The M-MEC was constructed following the same cassette-style and consisted of a rectangular SS tank with a working volume of 1000 L, capable of accommodating several cassette cells. In the same way, wastewater circulated through the anode chamber on both sides of each cell and hydrogen gas was produced in the internal frames.

A comprehensive design and engineering process was undertaken during the scale-up to ensure the optimal configuration and performance of the pilot plant. This included detailed calculations of reactor dimensions, electrode specifications, hydraulics, and electrical systems. Specialized components that required custom fabrication were workshop-manufactured. The pilot plant was carefully installed and assembled within the real WWTP, ensuring proper integration with the existing infrastructure. Comprehensive commissioning and testing procedures were conducted to verify the functionality and performance of all systems and components. This included initial tests with water and gradual integration with the actual wastewater stream. A detailed discussion about the design of the pilot plant scale-up is presented in Chapter VI (Section 6.5.1).

Figure 3.3. M-MEC pilot plant.

3.1.3. Current and voltage monitoring

Each individual cell was powered by a separate power source (Programmable DC LAB Power Supply LABPS3005DN, Velleman Group, Belgium). Both voltage and current were digitally monitored using the AddControl software developed in LabWindows CVI by the research group (Baeza, 2022). The current intensity for each cell was monitored online for calculating several performance parameters.

3.2. Chemical analysis

3.2.1. Chemical oxygen demand

Liquid samples from the anode chamber were characterized after filtering with 0.22 μm pore filters (Millipore). Organic matter was measured using commercial COD kits (Hach, LCK 514, United States) that covered the range of 0.1 - 2 g O_2 L^{-1} and a spectrophotometer (Hach, DR2800).

3.2.2. Nitrogen and phosphorus

Nitrogen and phosphate were analysed after filtering anolyte samples with 0.22 μm pore filters (Millipore). Ammonium concentration was measured with an ammonium analyser (AMTAXsc, Hach Lange), based on the potentiometric determination of ammonia, where the ammonium concentration is determined from the potential readings of a gas-sensing electrode in which ammonia gas diffuses. Total N was analysed by the high temperature combustion device multi N/C® 2100S (Analytik Jena, Germany). Phosphate was measured by a phosphate analyser (PHOSPHAXsc, Hach Lange), which is based on the

vanadomolybdate yellow method, where the intensity of the yellow colour of the sample is measured by a spectrophotometer and is correlated with the phosphate concentration.

3.2.3. Solids

Volatile suspended solids (VSS) and total suspended solids (TSS) were measured according to Standard Methods (Rice et al., 2012). The Standard Methods for TSS and VSS are based on the following steps:

i) A sample of the wastewater is filtered through a pre-weighed filter paper.
ii) The filter paper is dried at 120 ºC and weighed to determine the TSS.
iii) The filter paper is then introduced in a furnace at 550°C to volatilize the organic suspended solids.
iv) The filter paper is weighed again to determine the VSS.

3.2.4. Volatile fatty acids (VFAs)

Ethanol and volatile fatty acids (VFAs), including acetic, propionic, isobutyric, butyric, isovaleric, valeric, isocaproic and caproic acids, were analysed in a gas chromatograph (GC) equipped with a DB FFAP column (30 m x 0.25 mm x 0.25 μm) and a flame ionization detector (Agilent Technologies, 7820-A). Helium was used as carrier gas with a split ratio of 10:1 to 2.9 mL min^{-1}. 800 μL of filtered anolyte were transferred to a chromatography vial to which 200 μL of a stabilizing solution composed of crotonic acid (2 g L^{-1}) and phosphoric acid (2%) was subsequently added.

Afterwards, 1 μL of the sample was injected into the GC at a temperature of 275 ºC under split conditions (29 psi). The column temperature was 85 ºC for one minute, followed by a temperature ramp of 3 ºC min^{-1} until reaching a value of 130 ºC. Next, there was a second temperature ramp of 35 ºC min^{-1} up to 220 ºC. The flame ionization detector temperature was set to 275 ºC, with a supply of 350 mL min^{-1} of air, 40 mL min^{-1} of H_2, and 30 mL min^{-1} of helium. The analysis time for each sample was 18 minutes. Finally, the column was cleaned with hexanol to remove all the compounds that could have adhered to the column.

3.2.5. pH and conductivity

pH was measured through pH probes (HACH pH electrode Crison5233, Spain) and conductivity was measured using a conductivity meter (XS Instruments COND 8, Italy).

3.2.6. Gas chromatography

The cathodic gas was analysed in a GC (Agilent Technologies, 7820-A) with a thermal conductivity detector. The GC was equipped with two columns: a packed column Porapaq Q 80/100 3 ft G3591-81136 (1.38 m ± 2 mm) and a second column MolSieve 5 A 80/100 3 ft. G3591-80017 (1.83m ± 2mm), from Agilent Technologies. Both columns were connected via a pneumatic valve. Nitrogen was used as carrier gas. The temperature of the oven was initially set at 70 ºC for 2 min, followed by a temperature ramp of 20 ºC min^{-1} until reaching a temperature of 140 ºC. Dionex Chromeleon 6.8 (ThermoFisher Scientific) was used for data acquisition and processing to estimate the concentrations of each gas.

To analyse the cathodic gas produced in the cells, 1 mL of sample was manually injected using a gastight syringe (1 mL Vici Samplelock Syrenge) at a temperature of 200 °C under Split conditions (8 psi). The oven temperature was adjusted to a constant temperature of 40 °C. The injector was set to 250 ºC and the detector temperature was set to 220 °C, with a nitrogen flow of 20 mL min^{-1} and a negative polarity signal. The analysis time for each sample was 6 minutes.

The total hydrogen or methane production was calculated using the Gas Bag Method presented by Ambler and Logan (Ambler and Logan, 2011). The procedure consists of a first analysis in which the initial composition of the gas in the bag is determined. Next, a well-known volume of a tracer gas (carbon dioxide) is introduced into the bag and, subsequently, the new gas composition is analysed. From these two analyses, and according to the mass balances calculations, the volumes of hydrogen and methane can be calculated. The development of the calculations is detailed below.

The gas bag can be represented as in Figure 3.4:

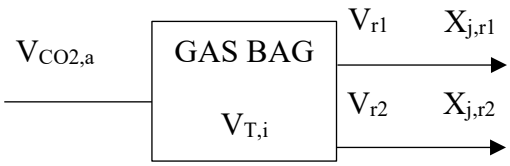

Figure 3.4. Scheme of the gas bag used for the gas quantification. $V_{CO2,a}$ refers to the well-known volume of CO_2 added; $V_{T,I}$ is the initial total gas volume in the bag; V_{r1} is the volume of gas injected in the GC in the first analysis; V_{r2} is the volume of gas injected in the GC in the second analysis; $X_{j,r1}$ and $X_{j,r2}$ refer to the molar fractions of compound j in the first and second analysis, respectively.

The final volume of CO_2 in the gas bag ($V_{CO2,f}$) can be expressed as in Equation 3.1:

$$V_{CO2,f} = V_{CO2,i} + V_{CO2,a} - V_{CO2,r1} - V_{CO2,r2} \quad (3.1)$$

Diving both sides of the equation by the final total volume of the gas ($V_{T,f}$), the equation results in Equation 3.2:

$$\frac{V_{CO2,f}}{V_{T,f}} = x_{CO2,f} = \frac{V_{CO2,i}+V_{CO2,a}-V_{CO2,r1}-V_{CO2,r2}}{V_{T,f}} \quad (3.2)$$

The term of $V_{T,f}$ can be further developed, resulting in Equation 3.3:

$$x_{CO2,f} = \frac{V_{CO2,i}+V_{CO2,a}-V_{CO2,r1}-V_{CO2,r2}}{V_{T,i}+V_{CO2,a}-V_{r1}-V_{r2}} \quad (3.3)$$

Rearranging the equation in view of isolating $V_{T,I,}$ the equation can be expressed as (Equation 3.4):

$$x_{CO2,r2} \cdot \left(V_{T,i} + V_{CO2,a} - V_{r1} - V_{r2}\right) = V_{CO2,i} + V_{CO2,a} - V_{CO2,r1} - V_{CO2,r2} \quad (3.4)$$

$V_{CO2,i}$ can be expressed as $\left[V_{CO2,i} = V_{T,i} \cdot X_{CO2,r1}\right]$, which combined with Equation 3.4, results in Equation 3.5:

$$V_{T,i} \cdot x_{CO2,r2} + V_{CO2,a} \cdot x_{CO2,r2} - V_{r1} \cdot x_{CO2,r2} - V_{r2} \cdot x_{CO2,r2} =$$

$$= V_{T,i} \cdot x_{CO2,r1} + V_{CO2,a} - V_{CO2,r1} - V_{CO2,r2} \quad (3.5)$$

Further developing Equation 3.5, the equation can be expressed as (Equation 3.6 and 3.7):

$$V_{T,i} \cdot \left(x_{CO2,r2} - x_{CO2,r1}\right) =$$

$$= V_{CO2,a} - V_{CO2,r1} - V_{CO2,r2} - (V_{CO2,a} \cdot X_{CO2,r2} - V_{r1} \cdot X_{CO2,r2} - V_{r2} \cdot X_{CO2,r2} \quad (3.6)$$

$$V_{T,i} = \frac{V_{CO2,a}-V_{CO2,r1}-V_{CO2,r2}-V_{CO2,a}\cdot X_{CO2,r2}+V_{r1}\cdot X_{CO2,r2}+V_{r2}\cdot X_{CO2,r2}}{X_{CO2,r2}-X_{CO2,r1}} \quad (3.7)$$

Since $\left[V_{CO2,r2} = V_{r2} \cdot X_{CO2,r2}\right]$, both terms cancel, obtaining Equation 3.8:

$$V_{T,i} = \frac{V_{CO2,a}\cdot\left(1-X_{CO2,r2}\right)+V_{r1}\cdot\left(X_{CO2,r2}-X_{CO2,r1}\right)}{X_{CO2,r2}-X_{CO2,r1}} \quad (3.8)$$

Once the total volume of gas is determined, the total volume of hydrogen ($V_{H2,i}$) or methane ($V_{CH4,i}$) can be calculated as the product of their initial mole fractions and the total volume of gas in the bag, as shown in Equation 3.9 and 3.10:

$$V_{H2,i} = X_{H2,r1} \cdot V_{T,i} \quad (3.9)$$

$$V_{CH4,i} = X_{CH4,r1} \cdot V_{T,i} \quad (3.10)$$

3.3. Molecular methods

The microbial community composition was determined by Illumina amplicon sequencing of the 16S ribosomal ribonucleic acid (rRNA) gene. Anode samples were taken during the decommissioning process at the end of the experimental trial. The desoxyribonucleic acid (DNA) extraction process was performed using the Soil DNA isolation plus kits (Norgen Biotek CORP, Canada) according to manufacturer's protocol. A sterilized scalpel was used to cut the carbon felt into small pieces and were then added to a lysing matrix tube. Each tube contained 10.00 g ± 0.02 g of wet carbon felt. The manufacturer's instructions were followed for cell lysis, DNA isolation and purification. The concentration and the quality of the DNA extracted were determined by using the NanoDrop 1000 Spectrophotometer (Thermo Fischer Scientific, USA). A 260/280 ratio of 1.8 ± 0.1 was selected as a good quality indicator and a DNA concentration of 5 ng μL^{-1} was required as the minimum concentration needed for sequencing. Prior to further analyses, DNA samples were stored at -20ºC. Sequencing analyses were performed by the Genomics Service (SG) of the Universitat Autònoma de Barcelona (UAB, Spain). The organisms were categorized using the RefSeq+RDP database (Alishum, 2022) and the sequence reads were examined using Usearch software. Each anode sample was extracted and sequenced twice, one for each carbon felt of the same cassette, so the results presented in this work correspond to the average of two sequencing analyses.

3.4. Electrochemical techniques

Cyclic voltammetry (CV) is a powerful electrochemical technique used to study the electrochemical properties of materials. CV has also been widely used to study the behaviour of BES because it allows characterising the interactions between microorganisms or microbial biofilms and BES electrodes (Fricke et al., 2008; Logan et al., 2006). The technique is based on a cyclic potential sweep applied to a working

electrode, where the reaction of interest takes place. The current response is then analysed to provide information about the redox processes occurring at the electrode.

In a CV experiment, the working electrode potential is measured relative to a reference electrode, while the current is measured between the working electrode and a counter electrode. The applied potential sweep is characterized by three parameters: the sweep speed, the initial potential, and the final potential. These parameters define the range of potentials to be applied to the working electrode.

If the applied potential goes towards positive values (anodic direction), the working electrode becomes an oxidizing agent. On the contrary, if the potential goes towards negative values (cathodic direction), the working electrode becomes a reducing agent. When a potential value is reached that is favourable for the oxidation of the electroactive species, the intensity of the anodic current increases notably until it reaches a maximum value. This maximum value corresponds to the maximum polarization condition of the electrode. The analyses are performed under non-mixing conditions, so that, when the scanning direction is reversed, the oxidized electroactive species on the electrode surface are reduced, generating a cathodic current up to a maximum value, forming a characteristic reduction peak.

For an ideal electroactive material, the anodic and cathodic peaks should exhibit a value of 0.059/n, where 'n' represents the number of electrons transferred in the electrochemical reaction. Additionally, both peak currents should have the same absolute value, and the peak potentials should remain unaffected by variations in the sweep speed. Furthermore, the peak current should follow a square root relationship with the sweep speed, as dictated by the Randles-Ševčik equation (Equation 3.11):

$$I_p = 3.01 \cdot 10^5 \cdot n^{3/2} \cdot (\alpha \cdot D_a \cdot \upsilon)^{1/2} \cdot A \cdot C_a \quad (3.11)$$

With I_p: Peak intensity (A), α: Transfer coefficient, D_a: Diffusion coefficient ($cm^2\ s^{-1}$), υ: Sweep speed ($V\ s^{-1}$), A: Electrode area (cm^2), and C_a: Concentration of the species ($mol\ cm^{-3}$). D_a is usually estimated using a solution of potassium ferro/ferricyanide ($[Fe(CN)_6]^{3-}/[Fe(CN)_6]^{4-}$), which is fully reversible.

The CV is usually represented as the current intensity obtained in the working electrode versus the applied potential (Gosser, 1993).

CVs were performed using a potentiostat/galvanostat (Multi Autolab PGSTAT204, Methrom Inc.) and a the three-electrode configuration. The reference electrode was a commercial $Ag/AgCl_{(sat)}$ electrode (BioLogic), the working electrode was Ni-foam or SS-wool with a projected surface of 1 cm^2, and the reference electrode was a Pt electrode (Biologic). The redox pair $[Fe(CN)_6]^{3-}/[Fe(CN)_6]^{4-}$ was the redox marker in a 30 mL of 0.1 M KCl solution containing 0.01 M $K_4Fe(CN)_6/K_3Fe(CN)_6$. The cell was left for 15 minutes in open circuit voltage (OCV) to stabilise the potential. This was followed by three cycles to obtain a fully stabilised current intensity. The scan rate was 10 mV s^{-1} and the voltage range [-1.0 - 0.2].

3.5. Key performance indicators

This section includes the key performance indicators (KPIs) that have been used in this thesis to assess the performance of the proposed wastewater treatment technology.

3.5.1. Current density and hydrogen production

Current density (*j*) in each cell was expressed as function of the projected anodic surface (A m^{-2}). Hydrogen production was expressed considering the total production in the plant and the projected anodic surface (L m^{-2} d^{-1}) or the reactor volume (m^3 m^{-3} d^{-1}).

3.5.2. Cathodic recovery efficiency

The cathodic recovery (r_{CAT}) compares the moles of electrons required for hydrogen production with the moles of electrons arriving to the cathode as a current. The r_{CAT} was calculated using Equation (3.16):

$$r_{CAT} = \frac{V_{H_2} \cdot {V_{m,H_2}}^{-1} \cdot b_{H_2} \cdot F}{\int_{t_0}^{t_f} I \, dt} \quad (3.16)$$

Being V_{H2}: Volume of hydrogen produced (L), $V_{m,H2}$: Molar volume of hydrogen (24.06 L mol^{-1} at 1 atm, 20 ºC), b_{H2}: Number of electrons transferred per mole of hydrogen (2 mol e^- mol^{-1} H_2), F: Faraday's constant (96485 C mol^{-1} e^-), t_0: Initial time of the cycle (s), t_f: Final time of the cycle (s), and I: Current intensity (A).

3.5.3. Coulombic efficiency

The coulombic efficiency (CE) refers to the ratio between the coulombs recovered as current and the coulombs that could be theoretically generated from the substrate oxidation. The CE was calculated using Equation (3.17):

$$CE = \frac{\int_{t_0}^{t_f} I\ dt}{\Delta C \cdot V_L \cdot {M_{O_2}}^{-1} \cdot b_s \cdot F} \quad (3.17)$$

Being ΔC: Difference of substrate concentration between the inlet and the outlet of the reactor (g L^{-1}), V_L: Anodic volume (150 L), M_{O2}: Molar mass of oxygen (32 g mol^{-1}), and b_s: Number of moles of electrons transferred per mol of COD (4 mol e^- mol^{-1} COD).

3.5.4. Energy production

The energy production (E_P) is the amount of energy recovered as hydrogen. The E_p was calculated using Equation (3.18):

$$E_P = n_{H_2} \cdot \Delta H_{H_2} \quad (3.18)$$

With n_{H2}: Number of moles of hydrogen produced, ΔH_{H2}: Heat enthalpy of hydrogen (-285.8 kJ mol^{-1}).

3.5.5. Energy consumption

The energy consumption (E_C) is the amount of energy consumed as electrical input. The E_C was calculated using Equation (3.19):

$$E_C = \int_{t_0}^{t_f} I \cdot \Delta V\ dt \quad (3.19)$$

With ΔV: Applied potential (V).

3.5.6. Energy recovery

The energy recovery (r_E) refers to the ratio of E_P to E_C. The r_E was calculated using Equation (3.20):

$$r_E = \frac{E_P}{E_C} \cdot 100 \quad (3.20)$$

Chapter IV

Exploring key operational factors for improving H_2 production in a pilot-scale MEC treating UWW

4. Exploring key operational factors for improving H_2 production in a pilot-scale MEC treating UWW

4.1. Abstract

BES are becoming popular technologies with a plethora of applications in the environmental field. However, research on the scale-up of these systems is scarce. To understand the limiting factors of hydrogen production in MEC at pilot scale, a 135 L MEC was operated for six months under a wide range of operational conditions: applied potential [0.8 - 1.1 V], hydraulic residence time [1.1 - 3.9 d], and temperature [18 - 30 ºC], using three types of wastewater; synthetic (900 mg CODs L^{-1}), raw UWW (200 mg CODs L^{-1}) and urban wastewater amended with acetate (UWW_A) (1000 mg CODs L^{-1}). The synthetic wastewater (SWW) yielded the maximum current density (1.23 A m^{-2}) and hydrogen production (0.1 m^3 m^{-3} d^{-1}) ever reported in a pilot scale MEC, with a r_{CAT} of 70% and a CE of 27%. In contrast, the use of low COD UWW limited the plant performance. Interestingly, it was possible to improve hydrogen production by reducing the hydraulic residence time, finding the optimal applied potential or increasing the temperature. Further, the pilot plant demonstrated a robust capacity to remove the organic matter present in the wastewater under different conditions, with removal efficiencies above 70%. This study shows improved results compared to similar MEC pilot plants treating domestic wastewater in terms of hydrogen production and treatment efficiency and also compares its performance against activated sludge processes.

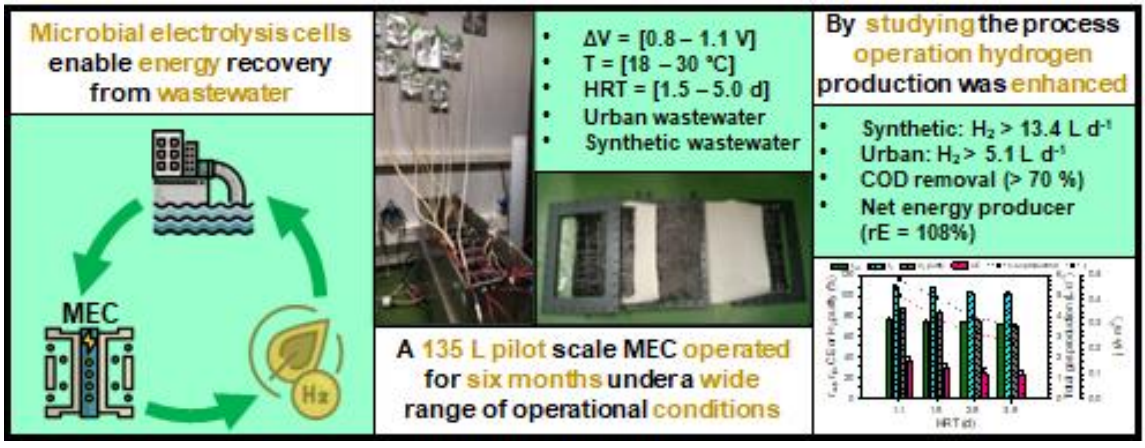

Figure 4.1. Graphical abstract.

4.2. Introduction

In the face of a changing climate and the increasing demand for sustainable practices, the challenge of achieving effective wastewater treatment has become more critical than ever. Traditional wastewater treatment methods, such as the activated sludge process, have been the mainstay of the industry for decades. However, these methods are often energy-intensive and rely on external sources of power, making them less environmentally friendly and less sustainable. In response to these concerns, researchers have turned their attention to exploring alternative approaches that can address the environmental impact of wastewater treatment while also recovering valuable resources from the waste stream. Among these promising technologies, MECs, which utilize the metabolism of electroactive microorganisms to simultaneously degrade organic matter and produce hydrogen gas, have emerged as a promising solution.

MECs have shown great potential at lab-scale, but their performance has been hampered when scaled-up to pilot plant. The key challenge lies in overcoming the inherent limitations of MECs, including low mass transfer rates at the anode, poor hydrogen production at short HRTs, and the hydrogen leakages. To address these challenges, research is focused on improving reactor design, optimizing operating parameters, and developing strategies to enhance anode performance and hydrogen recovery. The successful scaling-up of MECs holds immense potential for the future of wastewater treatment and renewable E_P. By addressing the current challenges and continuously refining the technology, MECs can play a pivotal role in transitioning towards a more sustainable and environmentally friendly approach to wastewater management and energy generation.

4.3. Objectives

The highest hydrogen production in a double-chamber MEC pilot plant (0.031 $m^3\ m^{-3}\ d^{-1}$) was reported in a previous study of the research group (Baeza et al., 2017) and has been used as a reference to evaluate the technical feasibility of MECs (Leicester et al., 2020a), its environmental performance (Chen et al., 2019), and discussed in many other works (Dange et al., 2021; Fudge et al., 2021; Rousseau et al., 2020). Despite promising results were obtained with this reactor configuration, limited operational conditions were tested. Hence, it was considered appropriate to further study the reactor in other scenarios to understand the limiting factors of MEC operation at pilot scale, and

gain technical knowledge on reactor scale-up for the design of the LIFE+ NIMBUS MEC pilot plant. The 135 L double-chamber MEC was operated under a wide range of operational conditions and a critical assessment was performed to determine how hydrogen yield and energy efficiency can be improved by modifying the operational parameters. Finally, the experimental efficiency obtained in this study was used to evaluate the treatment of 1 m^3 of UWW by an MEC and the results were compared with two existing technologies reported in the literature: conventional activated sludge (CAS) and high-rate activated sludge (HRAS).

4.4. Specific experimental procedures and calculations

4.4.1. Reactor design

The L-MEC was used to carry out the experimental trial (see Materials and Methods, Section 3.1.1). The reactor had a total anodic volume of 135 L once the nine cells were placed inside the reactor. The cathode chamber contained pressed SS wool (Steel wool #2, Barlesa SL, Spain). The cathode was separated from the anodes using an AEM on both sides (AMI-7001S, Membranes International Inc., United States). The anodes were made of carbon felt (PX35 Carbon Felt, Zoltek™, United States) and were pressed to the membranes on both sides of the cathode through a SS mesh. The projected anode surface was 0.163 m^2 per cell (i.e. a total of 1.47 m^2 in the reactor), which yielded a total area/volume ratio of 10.9 m^2 m^{-3}.

4.4.2. MEC operation

Three different types of wastewaters were used during the operation of the plant (Table 4.1). In the first period, SWW with acetate as sole carbon source and macronutrients was used. It was prepared in a refrigerated 2000 L tank with tap water, sodium acetate (2335 g), NH_4Cl (305.67 g), K_2HPO_4 (56.19 g), KH_2PO_4 (43.91 g) and 50 mL of micronutrient solution (Smolders et al., 1994), obtaining the concentrations reported in Table 4.1. In the second period, real UWW from a municipal WWTP (Manresa, Spain) after primary settling was used, refilling the 2000 L tank approximately every 10 days. The levels of organic matter in the raw UWW after filtration (0.22 µm) were in the range of 200 - 300 mg COD L^{-1}. Also, the raw influent was amended with acetate during the temperature experiments to increase the organic concentration up to 1000 mg L^{-1} of COD. The catholyte was a 5 g L^{-1} NaCl solution. It was only renewed on day 30 before the

continuous operation with UWW and its pH was measured weekly (it remained around 11 - 12 during the whole operation).

Table 4.1. Average characteristics of the different wastewaters treated.

Wastewater	COD_S (mg L^{-1})	$N\text{-}NH_4^+$ (mg L^{-1})	$P\text{-}PO_4^{3-}$ (mg L^{-1})	σ (mS cm^{-1})	pH
SWW	903 ± 6	40 ± 2	10 ± 1	2.8 ± 0.1	6.9 ± 0.1
UWW	247 ± 34	51 ± 4	5 ± 1	1.1 ± 0.2	6.7 ± 0.2
UWW_A	1069 ± 39			3.2 ± 0.2	7.2 ± 0.1

σ: Electrical conductivity; SWW: Synthetic wastewater; UWW: Urban wastewater; UWW_A: Urban wastewater amended with acetate

The pilot plant was started-up with nine non-colonised cells, using an anaerobic sludge inoculum from the same WWTP. The anodic chamber was filled with synthetic medium and 5 L of sludge (VSS = 2 g L^{-1}) and operated in batch mode with an internal recycle of 150 L d^{-1} to improve mixing conditions, using a timed peristaltic pump (520 FAM/R2, Watson Marlow, United Kingdom). After 20 days of enrichment period, the plant was moved to continuous operation. During the whole operation, the influent was fed in the range 46 - 125 L d^{-1} from a 2000 L supply tank and using 150 L d^{-1} of recirculation flowrate.

4.4.3. Analytical methods

Liquid and gas samples were analysed following the previously described procedure (see Materials and Methods, Section 3.2)

4.4.4. KPIs

Reactor performance was evaluated using the previously described KPIs (see Materials and Methods, Section 3.5).

4.4.5. Temperature effect study on response modelling

The effect of temperature on hydrogen production and current density was studied experimentally. The anodic temperature was controlled using the AddControl software, a thermoresistance (Pt1000, Axiomatic, Spain), and a silicone heating tape (HBSI 10m, HORST GmbH, Germany) placed around the tank. The temperature range (18 - 30 ºC) was selected based on typical wastewater temperatures in an urban WWTP, which

commonly varies between 10 and 25 ºC depending on the season and geographic location, while temperatures above 30 ºC are highly unlikely (Metcalf and Eddy, 2003). To model the response, the Arrhenius equation (Equation 4.1) was used and fitted to the experimental data:

$$k(T) = k(20ºC) \cdot \theta^{(T-20)} \quad (4.1)$$

with k(T) and k(20 ºC) being hydrogen production rate or current density at temperature T (ºC) and at 20 ºC.

The model was fit to the experimental data by minimising the sum of the quadratic differences between the experimental and predicted data using the GRG nonlinear method of Excel Solver. The goodness of fit of the models was evaluated with the coefficient of determination R^2 calculated with Equation 4.2:

$$R^2 = 1 - \frac{\sum_{i=1}^{n}(y_i - \hat{y}_i)^2}{\sum_{i=1}^{n}(y_i - \bar{y})^2} \quad (4.2)$$

4.4.6. CAS/HRAS comparison

The MEC performance was compared to CAS and HRAS systems by calculating the energy requirements of each technology for treating 1 m^3 of UWW with an organic matter concentration of 300 mg COD L^{-1}. As these aerobic technologies only treat wastewater and do not produce energy by themselves, methane production by AD of the purged sludge in the CAS and HRAS was considered as a revenue. CAS and HRAS performances were assessed using data reported in the literature. The E_C was calculated considering the dominant energy requirements for municipal wastewater treatment (Pakenas, 1995): aeration energy for the biological processes and heating for anaerobic digester. Pumping energy was discarded as it was assumed that all technologies would account for similar E_C. The energy needs of the biological processes were considered as the amount of oxygen consumed in the aerobic bioreactor, and were calculated with Equation 4.3 as proposed by Svardal and Kroiss (2011):

$$Aeration\ energy = \frac{Mineralized\ COD}{AE} \frac{SatDO}{(SatDO - DO)} \quad (4.3)$$

With Aeration energy: Energy requirements for aeration (kWh d^{-1}), Mineralized COD: The influent COD mineralized fraction COD (kg d^{-1}), AE: Aeration efficiency (1.5 kg O_2 kWh^{-1}), (Tchobanoglous et al., 2014), SatDO: Dissolved oxygen concentration at

saturation (10mg L^{-1} at 15 ºC), (Svardal and Kroiss, 2011), and DO: Dissolved oxygen concentration in the bioreactor (mg L^{-1}).

The energy requirements of the anaerobic digester were considered as the amount of energy needed to increase the temperature of the incoming waste activated sludge (WAS) to the digestor. A conservative value of 0.12 kWh m^{-3} wastewater was assumed for the comparison (Khiewwijit et al., 2015), but the actual requirements were also calculated for each case with Equation 4.4:

$$Q = m\, C_p\, \Delta T \tag{4.4}$$

Being Q: Heating energy requirements (kWh d^{-1}), m: Mass flow rate of WAS (kg d^{-1}), Cp: Specific heat of WAS (considered as water: 1.17 10^{-3} kWh kg^{-1} $ºC^{-1}$), and ΔT: Temperature difference between the digestor and the incoming WAS (ºC).

The operational temperature in the anaerobic digestor was assumed to be 35ºC, and the temperature of the A-stage was considered for the incoming WAS (15ºC). Heat losses through the surface of the tank were not considered.

The gas mass flow rates were estimated using the ideal gas law under normal conditions (20 ºC and 1 atm). Both the hydrogen produced by the MEC pilot plant, and the methane produced by AD were considered to be completely transformed into electricity. Thus, only the combustion enthalpy of each gas was used. The amount of WAS generated was calculated performing the COD balances. Methane production was estimated considering the VSS in the WAS (no primary), using a yield of 205 L CH_4 kg^{-1} VSS_{added} reported under similar conditions (Trzcinski et al., 2017). On the other hand, hydrogen production in the MEC was calculated considering the efficiencies obtained in this study during the continuous operation with raw UWW at 20ºC.

The net energy production (NE_P) was calculated as the difference between the E_C and the E_P, and the process energy efficiency (EE) was defined as the amount of energy recovered as hydrogen or methane with respect to E_C.

4.5. Results and discussion

4.5.1. Start-up of the pilot plant with synthetic wastewater

The cells were inoculated with anaerobic sludge and started in batch mode using synthetic medium for a period of 20 days. Once a stable current density was obtained (around 1.0 A m^{-2}), the plant was shifted to continuous mode with an inlet flowrate of 46 L d^{-1} and an OLR of 0.33 g L^{-1} d^{-1}. The synthetic feeding was maintained for the first days under continuous conditions to assess the performance of the MEC pilot plant in an ideal scenario: i.e. readily biodegradable carbon source and a moderate conductive medium (> 2.5 mS cm^{-1}).

The performance of the plant was studied under different fixed intensities (Stage 1) in each cassette cell: 0.10, 0.15 and 0.20 A $cell^{-1}$ (or 0.61, 0.92 and 1.22 A m^{-2}, respectively) (Figures 4.2 and 4.3). The power sources were configured to maintain the current intensity through each cell by automatically modifying the applied voltage within a range of [0.00 - 1.00 V]. The maximum total gas production of 14.74 L d^{-1} (0.01 m^3 m^{-2} d^{-1} or 0.11 m^3 m^{-3} d^{-1}) with a 90% of hydrogen purity was obtained at the highest current intensity tested (0.20 A $cell^{-1}$) and at an applied potential of 0.93 V. This is the highest hydrogen production reported at such a high MEC scale (>100 L) and represents a significant advancement on the way towards reaching viable hydrogen efficiencies. Most of the studies on hydrogen production from UWW in cassette-type pilot-scale MECs report values in the range 0.005 - 0.031 m^3 m^{-3} d^{-1} (Guisasola et al., 2020). However, the performance and efficiency parameters obtained with the synthetic medium should be treated with caution, and not exactly considered for future scaling-up processes, since the characteristics of real UWW hinder to obtain these high-performance values, as will be discussed below. It was observed that r_{CAT} varied as a function of the current intensity used and increased from 36 ± 1% with 0.10 A $cell^{-1}$ to 68 ± 2% with 0.20 A $cell^{-1}$. The major reported cause of low r_{CAT} are hydrogen leakages. It was determined that hydrogen leakages were constant in the range studied (6.23 ± 0.19 L H_2 d^{-1}). Hence, the higher the hydrogen production, the lower the effect of hydrogen losses due to leakages, causing r_{CAT} to increase with intensity.

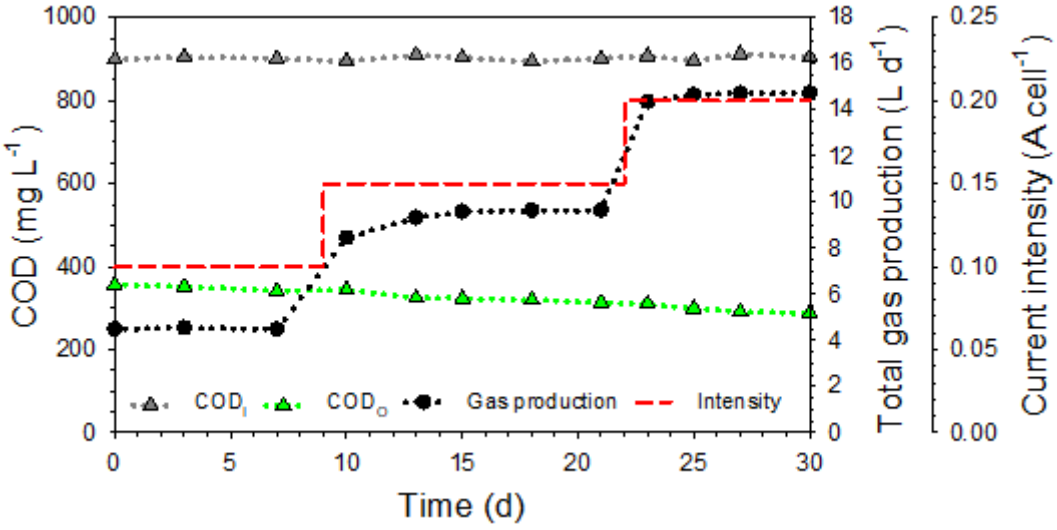

Figure 4.2. Inlet (COD_I) and outlet (COD_O) COD, and total gas production over time at different fixed intensities during the synthetic wastewater period in continuous mode (Stage 1).

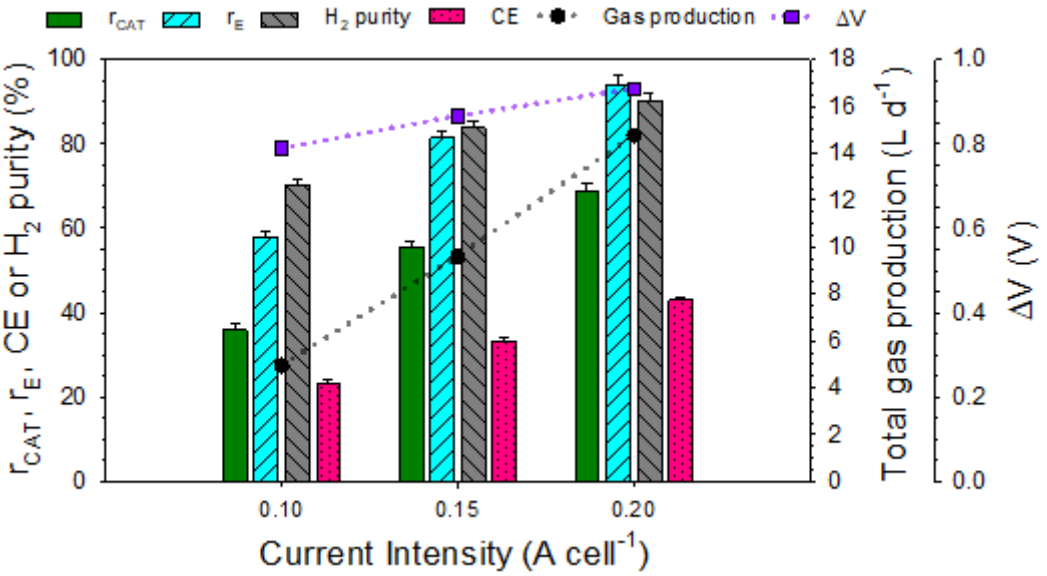

Figure 4.3. Average key performance indices, applied potential and total gas production at different fixed intensities during the continuous operation with synthetic wastewater. Standard deviations are shown in the figure.

Hydrogen was the major compound in the gas collected, followed by methane. In all cases, the methane production remained constant (around 1.48 ± 0.05 L CH_4 d^{-1}). Methane could come from either the anodic or the cathodic chamber. In the first case, methane from anaerobic organic matter degradation would be transferred to the cathode through the AEM. This hypothesis implies that most of the methane is produced in the bulk liquid and, therefore, methanogenesis depends on the anolyte conditions rather than on the anodic biofilm. Under this hypothesis, the methane flux through the membrane should

have been independent of the different applied potential, which seems to be in line with the observed results. Moreover, if methane had been produced in the anode, CE would have been very low, since part of the entering substrate would be diverted to methanogenesis rather than to exoelectrogenesis. The CE values obtained were below 50% in all cases, which seems to corroborate that part of the COD was not consumed by the exoelectrogens.

On the other hand, cathodic methane production implies the presence of hydrogenotrophic methanogens in the cathode, which would occur if the cells were not completely sealed. In this scenario, the pH gradient would have been reduced by the direct contact between electrolytes and the cathode may have become biocompatible (otherwise, the theoretical cathodic pH in a double chamber MEC should be around 12). Additionally, methanogenesis would depend on the current intensity values as there would be different concentrations of hydrogen for each case, thus affecting the methane formation kinetics. The pH of the catholyte was over 12, and hence it can be concluded that most of the methane collected came from the anodic chamber. Thus, it is necessary to use IEM with lower permeability to prevent methane diffusion produced anaerobically in the anode.

The highest r_E attained (94 ± 2%) corresponded to the highest current density and hydrogen production, but energy neutrality was not attained yet. The applied potential required was much higher than the theoretical value of 0.13 V (calculated under standard conditions, at a pH of 7 and with acetate as sole electron donor) due to the potential losses of the system. As high current densities are required to obtain significant hydrogen production, reducing the energy loss is essential to achieve energy neutrality.

4.5.2. Operation in continuous mode of the pilot plant with urban wastewater

After the period with SWW, the feed was entirely replaced by wastewater from a municipal WWTP after primary settling without any amendment. As expected, this real effluent showed reduced electrical conductivity (1.1 ± 0.2 mS cm^{-1}) and concentration of organic matter (COD_S = 247 ± 34 mg L^{-1}). The organic matter fractionation of real influents is very relevant because the substrate-utilization capabilities of most exoelectrogenic bacteria are limited to fermentation products, basically VFA. Thus, fermentative bacteria are essential to provide the substrate required for current generation from the potential complex molecules present in domestic effluents. A very diverse microbial community needs to be developed in the reactor, including exoelectrogens,

hydrolytic and fermentative bacteria (Kokko et al., 2018; Montpart et al., 2015). These populations establish a syntrophic relation with positive interactions that favour an efficient anodic-based oxidation of the complex organic compounds, which is the first step to obtain hydrogen at the cathode. However, the inherent variability of UWW properties challenges the ARB predominance in the reactor and competitors for substrate can appear, thereby reducing the CE. For this reason, a comprehensive analysis of the plant performance under different scenarios is essential to understand the opportunities of these systems under real conditions.

The plant was operated for more than 100 days under different operational conditions. In a first period (Stage 2), different applied potentials were tested to find the conditions with better energy efficiency (Section 4.5.2.1). Afterwards (Stage 3), the reactor was operated for more than 40 days at the optimal applied potential of 0.90 V to understand the effect of temperature on the plant performance (Section 4.5.2.2). Finally (Stage 4), the plant was operated under different HRT values to determine its effect on the COD removal efficiency (Section 4.5.2.3). The key operational parameters are shown in Table 4.2.

Table 4.2. Key operational parameters of each experimental stage.

Period	ΔV (V)	Inlet flowrate (L d^{-1})	T (ºC)
Stage 1	0.8 - 0.9	50	18
Stage 2	0.8 - 1.1	50	18
Stage 3	0.9	50	18 - 30
Stage 4	0.9	35 - 123	18

4.5.2.1. Effect of the applied potential on the plant performance

Increasing the input voltage can enhance H_2 production and boost current density as shown by previous authors (Hu et al., 2008) at expenses of higher energy requirements. However, undesired electrochemical oxidation of the compounds in the wastewater and even water electrolysis may occur when the applied potential is too high, resulting in a decrease of exoelectrogenic activity (Tice and Kim, 2014). The applied potential has a significant impact on energy efficiency since it is directly proportional to the power consumption. Thus, it is important to find its optimal value to improve MEC performance at the lowest applied potential possible.

Figure 4.4 shows the average current density and gas production values obtained at different applied potentials and Figure 4.5 shows the current density profiles. The applied potential was increased in 0.10 V intervals, from 0.50 V to 1.10 V, which is the typical range for the pilot-scale operation with UWW. The best results for this set of experiments were obtained with an ΔV of 0.90 V, showing a maximum current density (0.21 A m^{-2}) and hydrogen production of 0.016 m^3 m^{-3} d^{-1} (1.5 10^{-3} m^3 m^{-2} d^{-1}), with r_{CAT} = 64 ± 2%, r_E = 91 ± 2%, and CE = 30 ± 7%. Higher ΔV were detrimental as they had no significant effect on the performance and only decreased energy efficiency to r_E = 68 ± 2%. Due to the inherent characteristics of real wastewater, current density and hydrogen production were down to 6 times lower than the reported in Section 4.5.1 using SWW. The most likely reason is that the limiting step was the fermentation of complex organic matter to VFA rather than the exoelectrogenic activity. At ΔV above 0.90 V, the exoelectrogenic ability to consume VFA was likely higher than the VFA production by fermentation. The composition of the gas was also richer in methane (around 30%), and although r_E remained at similar values, r_{CAT} and CE were approximately 10% lower. The low COD strength of domestic effluents can limit MEC performance when compared to SWW. This difference in performance can lead to undersized designs if the productions and efficiencies of studies carried out under unrealistic conditions are taken as a reference for future scale-up. Laboratory-scale research is essential but understanding the limitations of such systems at larger scales with real effluents is crucial too.

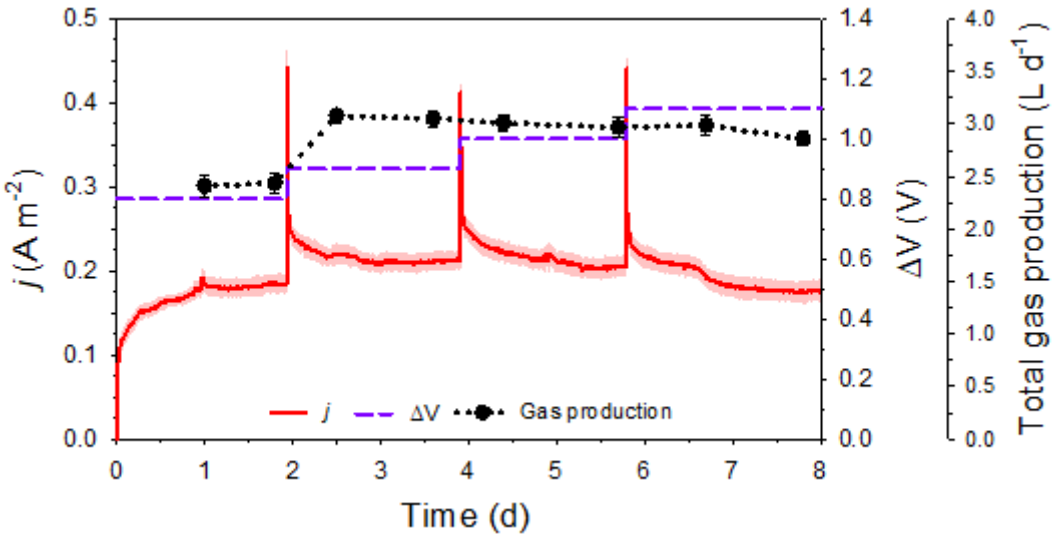

Figure 4.4. Average current density and total gas production over time at different applied potentials during the urban wastewater period in continuous mode (Stage 2). ΔV < 0.8 V are not shown in the figure. Shade indicates standard deviation of current density.

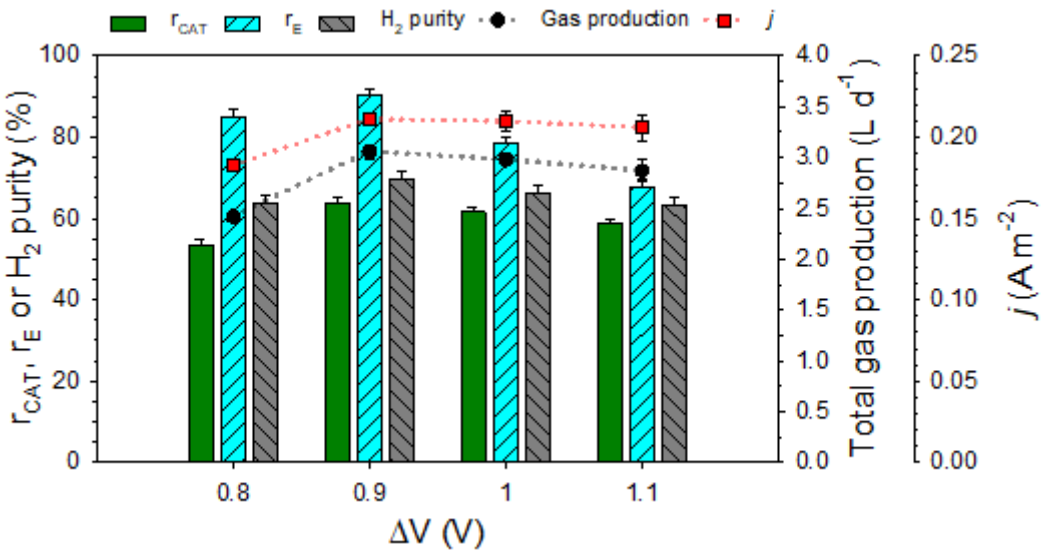

Figure 4.5. Average key performance indices, current density and total gas production at different applied potential during the continuous operation with urban wastewater. ΔV < 0.8 V are not shown in the figure. Standard deviations are shown in the figure.

Any voltage below 0.8 V was not enough to drive hydrogen production. Again, the minimum ΔV to drive evolution was higher than the theoretical value (i.e. 0.13 V) due to overpotentials and ohmic losses of the system. Increasing the electrode surface area, improving the electrode catalytic effect, increasing the temperature, or increasing the ARB-enrichment in the anodic biofilm can decrease the overpotential losses (Rozendal et al., 2006). Furthermore, ohmic losses can generally be minimized by reducing the electrode spacing, using a membrane with low resistivity, and increasing the solution conductivity (Liu et al., 2005). In real WWTPs, the use of externally enriched cultures is unfeasible considering the large microbial diversity that is entering in the reactor and the potential evolution of the population and increasing the load or the conductivity by dosing chemicals to the reactor is unfeasible (Pant et al., 2011). Thus, research should focus on improving the structural design of the cells, enhancing the physical, chemical, and spatial properties of the electrodes and the membrane, to reduce the overall internal resistance to current flow.

4.5.2.2. Effect of the temperature on the plant performance

In this second experimental period, the effect of temperature was studied for the first time in a pilot-scale MEC using both raw and amended (acetate addition) UWW to decouple the fermentation step from exoelectrogenesis. Temperature was progressively increased from 18 ºC to 30 ºC in 39 days feeding raw UWW. Afterwards, the reverse operation was

carried out until room temperature was reached again, using UWW_A. Figure 4.6 shows all the experimental profiles obtained during this period.

The reactor showed a robust capacity to remove the organic matter present in the wastewater under different temperatures, with COD removal efficiencies above 70% (75 ± 4%) in the case of raw UWW, and around 60% in the case of UWW_A (63 ± 5%). Figure 4.7 displays the dependence of current density and hydrogen production on temperature for both raw and amended UWW. The current density increased at 30 °C up to 0.36 ± 0.02 A m^{-2} with raw UWW which was 91 % higher than that obtained when operating at 18 ºC, while an increase of 40 % was observed when the influent was amended with acetate (0.50 ± 0.01 A m^{-2}).

The simplified Arrhenius equation model fits are also presented in Figure 4.7, showing a good agreement (R^2 up to 0.972) between experimental data and model prediction. The highest deviation appears for the current density of UWW at the higher temperature tested (T = 30ºC). Typical activated sludge models (Henze et al., 2000) categorize biological processes based on their temperature dependency θ: none (1.00), low (1.04), medium (1.07), and high (1.12). In this study, the operation with UWW leads to a medium value (θ = 1.065), while operating with VFA-amended UWW resulted in a low temperature dependency (θ = 1.031). These results suggest that the operation with raw UWW was more sensitive to temperature changes than the operation with VFA-amended UWW. This observation agrees with fermentation being the limiting step, and that temperature has a strong effect on the rate of the fermentation processes required to transform complex carbon sources into VFA. When increasing the temperature with raw UWW, the limitation due to fermentation was mitigated and VFA production increased. In contrast, when the pilot plant was fed with acetate in excess, fermentative bacteria did not play a limiting role because there was already enough substrate for exoelectrogens and the effect of temperature on fermentation was not observed in the experimental results.

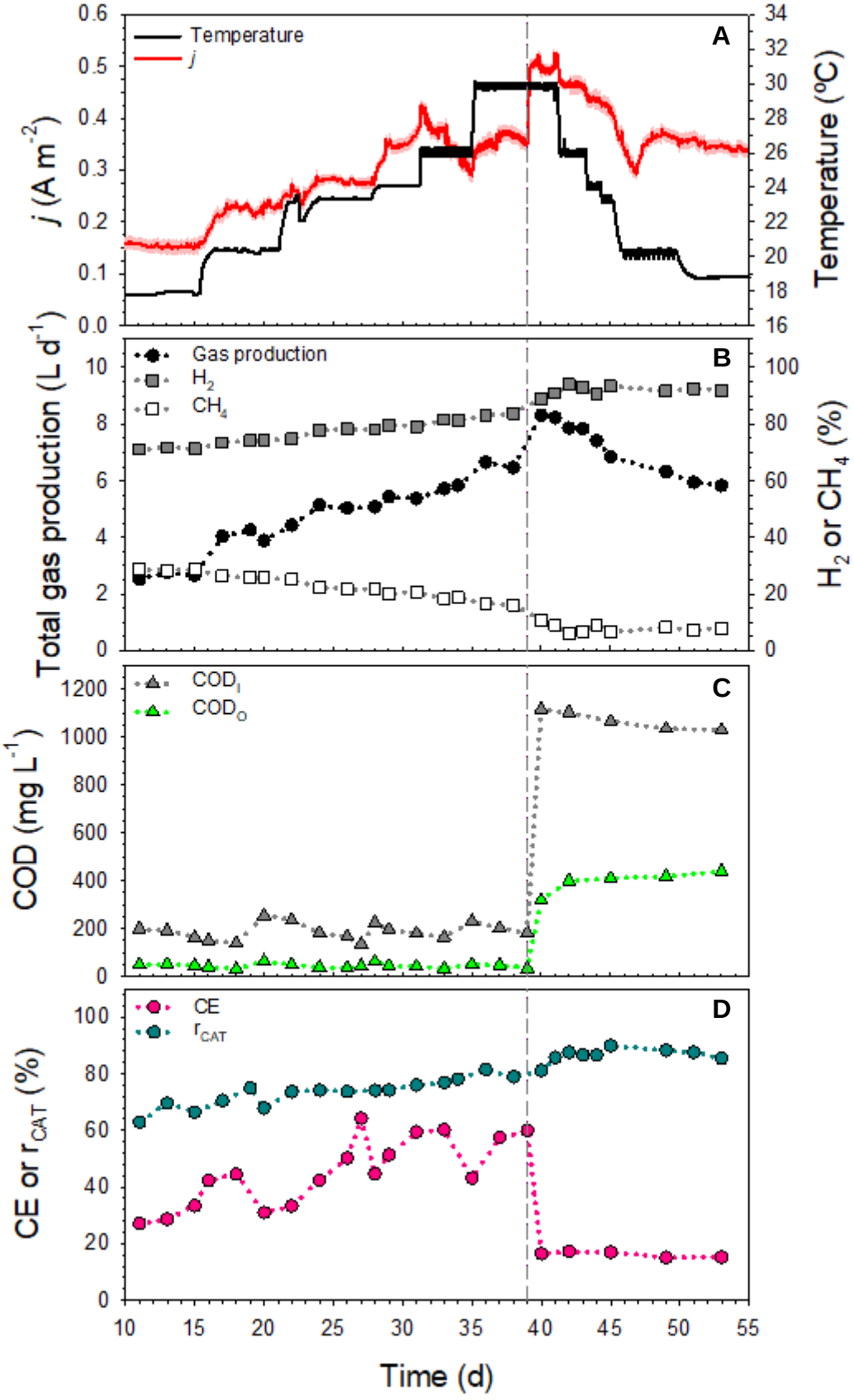

Figure 4.6. Experimental profiles over time at different temperatures during the urban wastewater period in continuous mode (Stage 3). Dashed line indicates the change from raw to amended wastewater. Shade indicates standard deviation of current density.

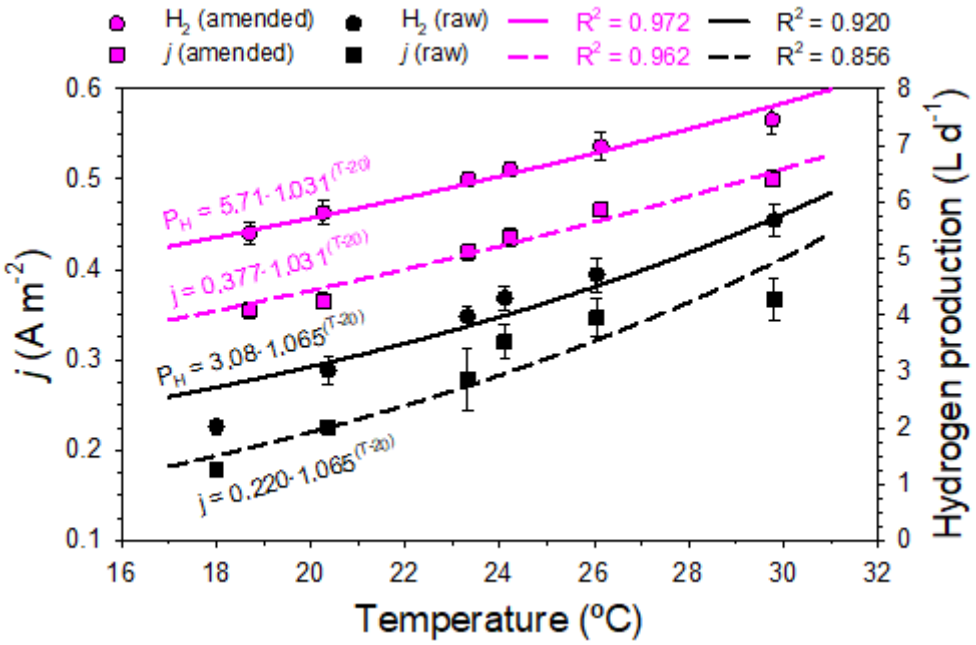

Figure 4.7. Average current density and hydrogen production at different temperatures during the continuous operation with raw and amended urban wastewater. Experimental data are presented with standard deviation. Lines represent the model predictions (Equation 4.3).

The value of r_{CAT} (Figure 4.6D) increased progressively with temperature to a value of 80 ± 2% for raw UWW, and in the case of amended, up to 85 ± 3%. Methane production was also present in this scenario for both substrates, but it was not significantly affected by temperature. As a result, the gas produced had a higher percentage of hydrogen. CE was also improved by increasing the temperature with raw UWW. On one hand, the ORR was not substantially influenced by temperature because it appeared to be limited by the low COD concentration in the reactor. These low COD concentrations did not have much room to be reduced. On the other hand, current density did increase with temperature because COD was being fermented faster and VFAs availability for ARBs improved. These results suggest that ARBs uptake VFAs faster than methanogens. Nevertheless, a large variability in this parameter can be observed because of the variable influent concentration. CE decreased drastically below 15 ± 2% when the OLR was increased from day 39 onwards (Figure 4.6, UWW_A period), indicating an increase of the substrate consumed by other planktonic microorganisms present in the anode chamber, causing the reactor to show lower current density and gas production than that with only SWW, despite the OLR was increased to 0.40 g L^{-1} d^{-1}.

Some studies also showed a reduction in the MEC performance under low temperatures (Larrosa-Guerrero et al., 2010). Heidrich et al. (2014) operated a MEC pilot plant fed

with domestic wastewater at room temperature for 12 months of operation, but the general low levels of performance and high variance in the data masked any temperature trend that may have occurred. Moreover, the influence of temperature on the composition and production of VFAs in AD has been investigated by several authors. These systems share some of the hydrolytic and acetogenic steps with MECs and are limited by low temperatures (Bowen et al., 2014). For instance, significant changes on the performance while increasing the temperature from 10 ºC to 35 ºC under mesophilic conditions have been reported (Deng et al., 2014; Komemoto et al., 2009) Thus, it can be stated that temperature plays an important role in MEC operated with UWW as the metabolism of the entire microbial community is altered. Considering the daily and seasonal temperature fluctuations, this system will provide variable hydrogen production when operating at a constant ΔV if temperature is not controlled.

4.5.2.3. Effect of the hydraulic retention time on the plant performance

HRT is a critical parameter for MEC performance. Low HRTs imply an increase of the organic matter load at expenses of not having enough time for an efficient substrate conversion to hydrogen. In our previous work, the HRT was increased from 1 to 2 days to tackle an unsuccessful organic matter removal (Baeza et al., 2017). In fact, batch experiments showed that 10 days were needed to reach 72% of organic matter removal. Up to date, there are no reports on the effect of HRT on a double-chamber pilot-scale MEC treating UWW, but some dynamic models are being used to study its effect (Day et al., 2022; Recio-Garrido et al., 2016). In any case, reducing the HRT remains a critical factor in making MEC technology feasible.

In the last experimental period (from day 60 onwards), different volumetric flow rates were tested to study the effect of HRT on the reactor performance (Figure 4.8). Surprisingly, the plant showed 23 ± 2% increase in current density compared to Stage 2, although the same operational conditions were maintained (HRT = 2.9 d; ΔV = 0.9 V and T = 18 ºC), probably caused by a change in the biofilm populations after the period with UWW_A. As a result, the pilot plant achieved energy neutrality with all volumetric flow rates tested.

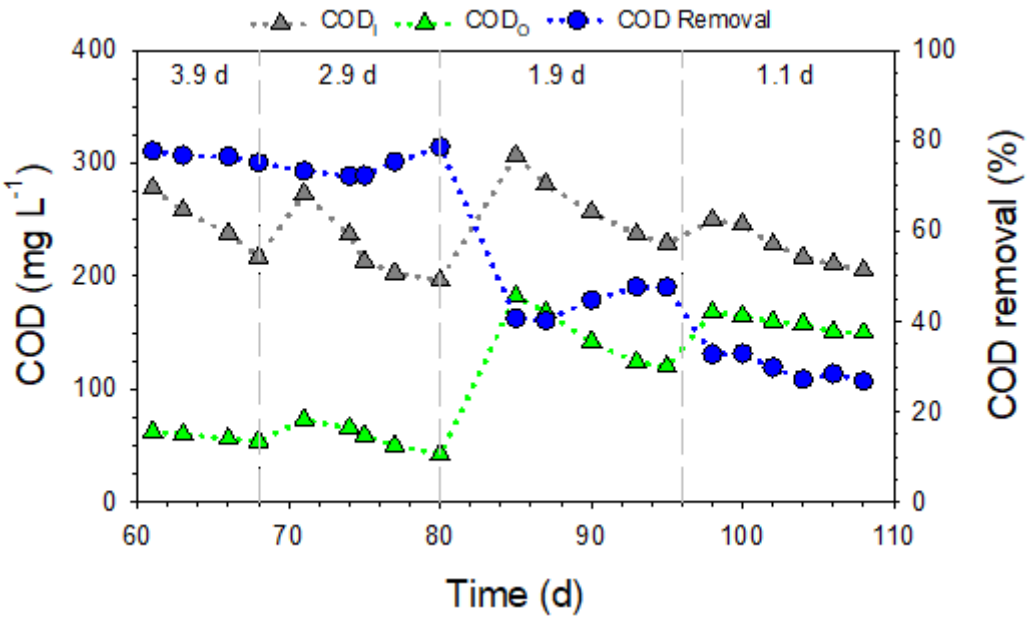

Figure 4.8. Inlet (COD_I) and outlet (COD_O) COD, and removal trend over time at different HRTs during the urban wastewater period (Stage 4). Four periods with different HRT between 1.1 and 3.9 d were evaluated.

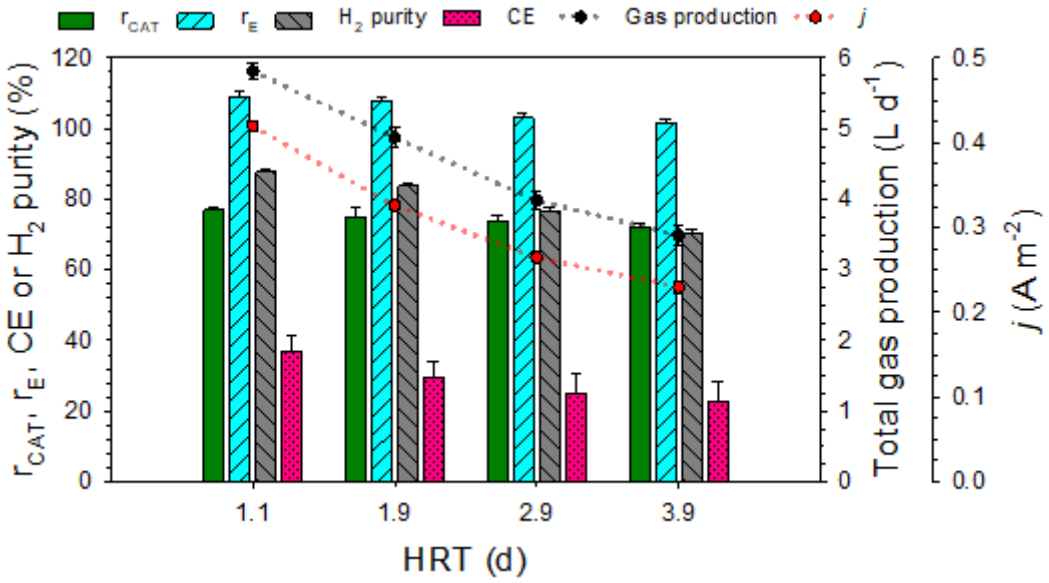

Figure 4.9. Average key performance indices, current density, and total gas production at different HRTs during the continuous operation with urban wastewater. Standard deviations are shown in the figure.

Figure 4.9 shows the average results for each HRT during the continuous operation with raw UWW. Decreasing the HRT from 4 to 1 d caused an increase of 86% in current density, reaching 0.42 A m^{-2}, with hydrogen production following the same trend and a r_{CAT} of 77 ± 2%. Specifically, hydrogen production increased from 0.024 to 0.038 m^3 m^{-3} d^{-1} when the HRT decreased from 4 to 1 d (i.e. 52% increase). This boost in current

density or hydrogen production through the inlet flowrate can be attributed to two factors: i) increasing the OLR increases both the COD concentration in the reactor and the exoelectrogenic kinetics and ii) it also decreases the residence time of the planktonic biomass in the system, favouring the washout of methanogens (i.e. less anodic methane production and higher CE). On the other hand, higher flowrates increase the velocity of the liquid in the anode chamber, increasing the turbulence and improving external mass transfer from the bulk to the biofilm surface. However, the quality of the treated water was drastically reduced at low HRT. The OLR was increased from 63 ± 6 mg COD L^{-1} d^{-1} at HRT = 4 d to 200 ± 15 mg COD L^{-1} d^{-1} at HRT = 1 d, but the maximum ORR achieved was around 70 ± 9 mg COD L^{-1} d^{-1} at HRT = 1 d, leading to a significant reduction in the percentage of COD removed (from 75 ± 4% to 30 ± 3%, Figure 4.8). Despite the higher water treatment efficiencies at high HRTs, CEs were still lower due to biological organic matter degradation pathways different than exoelectrogenesis. In fact, an increase in CE from 23 to 37% can be observed as the HRT decreases to 1 d. Despite the percentage of COD removed decreased at lower HRT, the r_E was higher. For the same reason, the amount of methane produced and transferred from the anode was lower at low HRTs: 1.14 ± 0.22 L CH_4 d^{-1} at HRT = 4 d whereas 0.72 ± 0.11 L CH_4 d^{-1} were recovered at HRT = 1 d. Thus, there is a trade-off between effluent quality and hydrogen production in the choice of the optimal HRT. High HRT will result in higher percentage of COD removal, whereas low HRT will result in higher hydrogen production. Low HRT configurations would require higher anodic surface to volume ratios (m^2_{anode} $m^{-3}_{reactor}$) to promote the exoelectrogenic substrate consumption over other biological processes. However, the changes in the biofilm structure due to these new hydraulic conditions could play an important role and deserve more study.

4.5.3. Comparison with previous cassette-type MEC pilot plants

The implementation of MECs in current WWTPs has the potential to transform organic pollutants into energy and valuable products as well as reducing the current treatment costs with environmental benefits. However, there is a wide gap between theoretical and practical performance. As indicated in Table 4.3, the current densities and hydrogen production rates reported with pilot-scale cassette MECs are far from those obtained in lab-scale systems. Current densities reported in pilot plants usually range between 0.25-0.30 A m^{-2}; only the plant presented by Leicester et al. (2020b) reported a value of 1.11 A m^{-2} but working with a smaller sized plant with anodic volume of 36 L, and

treating return sludge liquor with higher organic matter concentration. On the other hand, lab-scale MECs can yield up to 2 A m^{-2} (Rago et al., 2017; Tenca et al., 2013). Hydrogen production in double-chamber cassette-type MEC pilot reactors is usually in the range 0.005 - 0.031 m^3 m^{-3} d^{-1}. This is much lower than 1 - 1.3 m^3 m^{-3} d^{-1} reported in bench-scale (Wagner et al., 2009; Wang et al., 2014). In this study, a maximum hydrogen production of 0.099 m^3 m^{-3} d^{-1} was obtained with SWW. Furthermore, 0.038 m^3 m^{-3} d^{-1} of hydrogen were obtained feeding UWW, which is 23% higher than the maximum value reported previously under similar conditions (Baeza et al., 2017). This is equal to a 60% increase in the specific hydrogen production (L m^{-2} d^{-1}). We attribute this improvement in performance to different upgrades implemented in the pilot plant: i) the replacement of the current and voltage monitoring system, removing the external resistance to determine the intensity in the cells, ii) the enhancement of the electrical wiring, replacing the crocodile clips with SS connection strips to avoid rusting and iii) the replacement of polytetrafluoroethylene (PTFE) tubbing with Marprene® in the gas collection system. Furthermore, the microbial populations established in the anodic compartment could have played a critical role.

The organic matter removal efficiencies were similar to those obtained in other studies, and HRT greater than 3 days was required to achieve organic matter removal of 70%. The only exception appears in Cotterill et al. (2017), who proved at pilot-scale that increasing the anode surface to volume ratio can result in a significant reduction of the required HRT, obtaining a good quality effluent. However, the lack of pilot-scale MEC experiences available in the literature does not allow a reliable comparison. More research is needed in the field.

Table 4.3. Summary of the data reported with cassette-type MEC at pilot-scale for urban wastewater treatment.

Pilot plant	V (L)	COD (g COD L^{-1})	OLR (g L^{-1} d^{-1})	S / V (m^2 m^{-3})	HRT (h)	T (ºC)	CODr (%)	r_{CAT} (%)	CE (%)	ΔV (V)	j_{max} (A m^{-2})	H_2 (m^3 m^{-3} d^{-1})
Heidrich et al. 2013	120	0.45	0.14	16.4	24	16	34	70	55	1.1	0.30	0.015
Heidrich et al. 2014	100	0.07 - 0.4	0.54			1 / 22	33	49	41	0.7	0.25	0.007
Baeza et al. 2017	130	0.3 - 0.5	0.5 / 0.25	12.6	24 / 48	22	6 / 25	82	28	1.0	0.30	0.031 / 0.020
Cotterill et al. 2017	175	0.3 - 0.5	1.60	34	5	11.5	63	10	21	0.9	0.29	0.005
Leicester et al. 2020b	36	(2.2 - 4.3)[a]	4.4 - 8.6	20.2	0.36 - 432	10 - 20	52[b]	1[b]	6[b]	-	1.11[b]	0.011[b]
This work	135	SWW (0.9)	0.33	10.9	65	18	64	70	26	0.9	1.23	0.099
		UWW (0.2 - 0.3)	0.2 - 0.07		26 - 94		30 - 77	77 - 66	37 - 23		0.42 - 0.27	0.038 - 0.022
		UWW_A (1.0)	0.40		65		63	88	17		0.34	0.040

V: Anodic working volume; S / V: Projected anodic surface to reactor volume ratio; CODr: COD removal; j_{max}: Maximum current density.

[a] Reactor fed with return sludge liquor (concentrated filtrate of AD sludge)

[b] Results reported at the optimal HRT found (0.5 d)

4.5.4. Comparing MECs versus conventional wastewater treatment technologies

MECs need to achieve high COD removal efficiencies with short HRT to compete with other existing technologies for municipal wastewater treatment, such as the A/B configuration (Boehnke et al., 1997; Wett et al., 2007). A/B systems consist of an A-stage with short HRT and a B-stage where autotrophic nitrogen removal occurs. The A-stage aims at converting the influent particulate, colloidal, and soluble COD into a single solid stream with minimum mineralisation and low E_C by the stimulation of sludge production, bacterial storage, and bioflocculation (Jimenez et al., 2015). The surplus sludge of the A-stage is diverted to an r_E process such as AD, while the supernatant is treated in the B-stage.

The costs and possible revenues of the treatment of 1 m^3 of UWW with a COD concentration of 300 mg L^{-1} by different systems (CAS+AD, HRAS+AD and a MEC) were compared (Table 4.4). Wastewater treatment was successful in CAS with 85% of COD removal, but the energy efficiency was the lowest (59 %) of all technologies investigated and the HRT required was higher than in a HRAS. Rey-Martínez et al. (2021) reported the highest E_C of all HRAS studied due to a higher COD mineralization, even though the maximum COD removal was achieved. On the other hand, the best results were obtained in the HRAS published by Kinyua et al. (2017), with a NE_P of -0.140 kWh kg^{-1} COD degraded and a COD removal of 77%. Negative values of NE_P indicated that the methane produced contained more energy than the required by the system. Guven et al. (2019) reported lower percentages of mineralized and purged COD (operating at HRT<1 h and SRT<14 h) than those of Kinyua et al. (2017), which resulted in a 23% reduction in methane production, decreasing energy efficiency (EE) to 91%.

Considering the results of our MEC pilot plant, 0.066 m^3 d^{-1} of hydrogen could be produced with a NE_P of -0.031 kWh kg^{-1} COD degraded at HRT = 70 h, while an average of 0.019 ± 0.004 m^3 d^{-1} of methane would be generated with the HRAS+AD (average NE_P = 0.095 ± 0.024 kWh kg^{-1} COD degraded). Additionally, a NE_P of -0.104 kWh kg^{-1} COD degraded could be achieved with an EE of 109%, if HRT in the MEC was decreased to 26 h. Nonetheless, the MEC E_C at HRT = 26 h was the highest of all technologies compared (1.19 kWh kg^{-1} COD degraded). Therefore, the applied potential in the MEC must be decreased to make it less energy-intensive, since the E_C is directly proportional to the ΔV.

MECs have the potential to become a realistic alternative to CAS or HRAS in terms of r_E because they recover similar or even more energy from the organic compounds in wastewater compared to CAS/HRAS+AD. Additionally, the sludge post-treatment requirements appear to be considerably lower considering the TSS in the outlet of the MEC pilot plant (< 20 mg L^{-1}). Also, during the operation with the MEC pilot plant, an average of 15 ± 3% of N-NH_4^+ and 8 ± 1% of P-PO_4^{3-} removal was observed, possibly to cover the nutrient requirements of ARB and other microorganisms that might have activity. By contrast, in a HRAS, N-NH_4^+ and P-PO_4^{3-} removal can account up to a 30% and 12%, respectively (Rey-Martínez et al., 2021). Thus, it appears to be more feasible to avoid nitrification in an MEC than in a HRAS (if it is intended to be used as A-stage in an A/B system). However, the HRT required in an MEC to achieve a similar COD removal to that of a HRAS may be several times higher. The successful implementation of such technology on a larger scale is currently hindered by the important differences in volumetric treatment capacity between MECs and conventional wastewater treatment processes. Hence, future designs should be aimed at: i) maximizing the anode surface to reactor volume ratio, making the exoelectrogenic activity in the reactor prevalent to achieve high COD removal efficiencies at low HRT, and ii) optimizing the cassette design to reduce the electrical resistance to current flow in the cells.

Table 4.4. Comparison of conventional and high-rate activated sludge versus microbial electrolysis cell.

	Guven 2019	**Kinyua 2017**	**Guven 2019**	**Rey-Martínez 2021**	**This study**	
Technology	CAS	HRAS	HRAS	HRAS	MEC	
T (ºC)	20	20	20	18 - 22	18	
DO (mg L^{-1})	2	1	0.5	1	-	
HRT (h)	6	0.5	1	2.5	70	26
SRT (h)	96	13.4	9.6	28.8	-	
CODr (%)	86	77	59	88	74	30
H_2 or CH_4 (m^3 d^{-1})	0.015	0.023	0.017	0.016	0.066	0.041
H_2 or CH_4 (m^3 kg^{-1} COD degraded)	0.057	0.098	0.098	0.059	0.325	0.455
E_C (kWh d^{-1})	0.238	0.168	0.160	0.234	0.198	0.107
E_P (kWh d^{-1})	0.139	0.200	0.145	0.144	0.188	0.116
E_C (kWh kg^{-1} COD degraded)	0.924	0.727	0.904	0.886	0.892	1.189
E_P (kWh kg^{-1} COD degraded)	0.541	0.867	0.819	0.545	0.924	1.293
E_PCOD (%)	14	22	21	14	24	33
NE_P (kWh/kg COD degraded)	0.383	-0.140	0.085	0.341	-0.031	-0.104
EE (%)	59	119	91	62	95	109

DO: Dissolved oxygen; SRT: Solids retention time; E_C: Energy consumption; E_P: Energy production; E_PCOD: Energy recovered from removed COD from influent; NE_P: Net energy production; EE: Energy efficiency

4.6. Conclusions

- The MEC pilot plant achieved the best results with SWW, yielding the maximum current density (1.23 A m^{-2}) and hydrogen production (13.40 L d^{-1}, 0.10 m^3 m^{-3} d^{-1} and 10 L m^{-2} d^{-1}) ever reported in a pilot-scale MEC (>100 L).
- Low COD concentration in the UWW limited the plant performance. Specifically, an average hydrogen production of 5.1 ± 0.2 L d^{-1} (0.038 m^3 m^{-3} d^{-1} or 3.9 L m^{-2} d^{-1}) were obtained at HRT = 1 d. These are better results than similar MEC pilot plants treating domestic wastewater.
- High COD removal efficiencies (>60 %) were obtained with UWW under a wide range of operational conditions.
- The double-chamber configuration achieved viable current densities and recovered most of the hydrogen produced (r_{CAT} > 80%).
- The optimum applied potential for this configuration was found to be 0.9 V, far from the theoretical 0.123V.
- Low-moderate temperatures (< 20 ºC) resulted in poor anode-based oxidation but when temperature was increased (> 30 ºC), the fermentation step was improved, and hydrogen production increased from 2.0 to 5.7 L d^{-1}.
- The plant was able to produce 5.1 L H_2 d^{-1} at HRT = 1 d, which was 52% more than that obtained operating at HRT = 4 d. However, lower HRTs resulted in a significant reduction in COD removal (from 77 ± 1% to 30 ± 3%).
- The MEC performance was compared to CAS and HRAS. MEC have the potential to become an alternative to conventional wastewater treatment in terms of r_E, but the limited volumetric treatment capacity hinders its full-scale implementation.

Chapter V

Enhancing bioelectrochemical hydrogen production from industrial wastewater using Ni-foam cathodes in a MEC pilot plant

5. Enhancing bioelectrochemical hydrogen production from industrial wastewater using Ni-foam cathodes in a MEC pilot plant

5.1. Abstract

Developing efficient and cost-effective cathodes to drive the HER is crucial for the viability of MECs as a sustainable technology. While numerous lab-scale studies have been conducted to investigate different cathode materials, the transition to pilot-scale applications remains limited, leaving the actual performance of these scaled-up cathodes largely unknown. In this thesis, Ni-foam and SS-wool cathodes were used as catalysts to critically assess hydrogen production in a 150 L MEC pilot plant treating sugar-based industrial wastewater (IWW). Continuous hydrogen production was achieved in the reactor for more than 80 days, with a maximum COD removal efficiency of 40%. Ni-foam cathodes exhibited better performance at non-limiting substrate concentration, yielding the maximum hydrogen production ever reported at pilot-scale (19.07 ± 0.46 L H_2 m^{-2} d^{-1}). This is a 3.0-fold increase in hydrogen production compared to the SS wool cathode. However, the higher current cost of Ni-foam compared to SS-wool may constrain its use in real applications. The energy balance of the system demonstrated that MECs have the potential to be net energy producers, in addition to effectively oxidize organic matter in wastewater. While higher applied potentials increased the energy requirements, they also resulted in enhanced hydrogen production. For our system, a conservative applied potential range of 0.9 to 1.0 V was found to be optimal. Finally, the microbial community established on the anode was found to be a syntrophic consortium of exoelectrogenic and fermentative bacteria, predominantly *Geobacter* and *Bacteroides*, which appeared to be well-suited to transform complex organic matter into hydrogen.

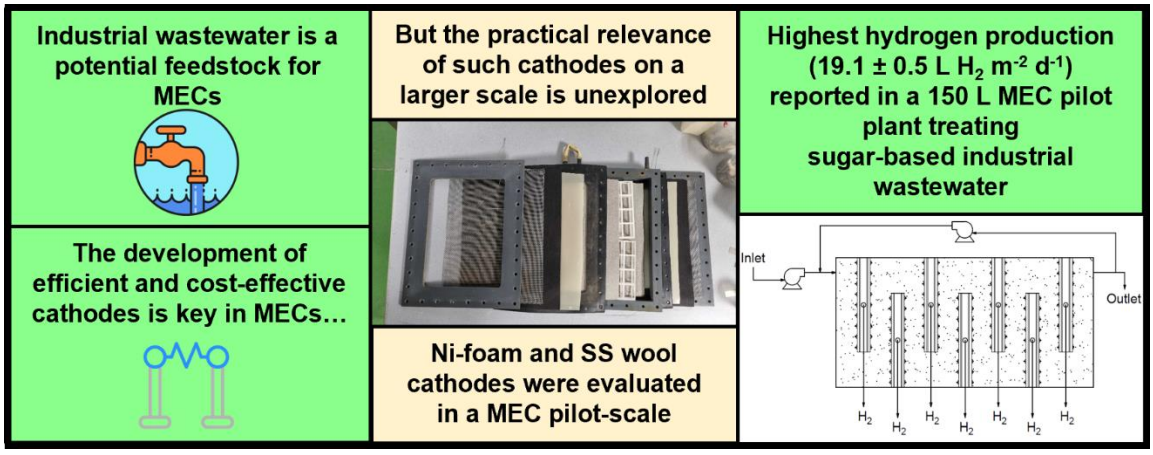

Figure 5.1. Graphical abstract.

5.2. Introduction

One of the primary factors contributing to the limited performance of MECs at pilot-scale is the use of low organic strength UWWs (0.25 - 0.80 g L^{-1}) (Metcalf and Eddy, 2003). In contrast, IWWs, generated by various manufacturing processes, exhibit distinct characteristics compared to UWWs. They typically have a higher organic strength, ranging from strong (>1 g COD L^{-1}) to extremely strong (>200 g L^{-1}), as observed in olive mills (Paraskeva and Diamadopoulos, 2006), textile industries (Walker and Weatherley, 2001), and beverage production facilities (Valta et al., 2015). This high organic content makes IWW a potential feedstock for MECs, as it provides a rich source of electron donors for hydrogen production. Nonetheless, other physicochemical properties such as pH, salinity or toxicity, must be evaluated to ensure the suitability for MEC operation. The presence of inhibitory compounds or recalcitrant organic matter in IWWs may require pretreatment steps before being fed to MECs.

One of the current focuses of research when scaling-up MECs is to minimize ΔV losses to obtain a high hydrogen yield at a low energy input. Membrane-less MECs offer significantly lower resistance to current flow, but if metabolic inhibitors are not used, the gas produced contains impurities (such as methane, carbon dioxide or hydrogen sulphide) that require further post-treatment (Kadier et al., 2015). Additionally, hydrogen recycling to the anode, which has been documented in these systems and decreased the net hydrogen production, can also readily occur (Ruiz et al., 2013). Other researchers focus on minimising anodic mass transfer limitations by implementing a recirculation (Escapa et al., 2015; Zhang et al., 2010) or a flow-through anode (Rossi et al., 2020; Sleutels et al., 2009). Similarly, the cathode overpotential can be reduced by decreasing mass transfer issues and improving the catalytic properties of the electrode to drive HER (Escapa et al., 2016). In this frame, Pt is one of the most common catalysts for electrochemical reactions, but its high-cost leads to increased and unaffordable capital expenses for MECs (Ambler and Logan, 2011). Therefore, there is a growing emphasis on the development of non-noble metal cathodes to ensure the economic viability of MECs.

Among the various non-noble metal cathodes investigated for MECs, those based on Ni have received significant attention (Kundu et al., 2013). Ni exhibits a lower HER overpotential and greater stability under alkaline conditions compared to other common non-noble metals like SS (Chaurasia and Mondal, 2022; Lu et al., 2016). Also, Ni exhibits

a significantly lower cost compared to Pt, and it is abundantly accessible on a large scale (it is a crucial material to produce SS and battery manufacturing) (Kadier et al., 2015). Ni and Ni alloys have been used as cathode in different formats, including as a metal sheet (Selembo et al., 2009), as a metal foam (Jayabalan et al., 2019; Jeremiasse et al., 2010), or as a powder (Kim and Logan, 2019; Selembo et al., 2010). In most of the lab tests, higher hydrogen production rates with Ni-based cathodes than other non-noble metal cathodes have been reported. However, its practical relevance on a larger scale is still unexplored. With this view, the objective of this study was to test, for the first time at pilot-scale (>100 L), the use of Ni-foam as cathode material in a double-chamber cassette-type MEC treating IWW. The selection of Ni-foam was based on its high specific surface area, which leads to a lower activation overpotential compared to other Ni-based cathodes (Jeremiasse et al., 2010). The 150 L double-chamber MEC was operated in batch and continuous mode for more than three months with real diluted IWW from a confectionery industry. The effect of Ni-foam in current generation and hydrogen production was studied and compared to a cassette operating with SS wool cathode (Baeza et al., 2017; Guerrero-Sodric et al., 2023). By exploring the limitations and challenges that arise when working on a larger scale, this research provides valuable insights into the practical feasibility and scalability of implementing Ni-foam as a cathode material in MECs treating wastewater.

5.3. Objectives

The objective of this study was to test, for the first time at pilot-scale (>100 L), the use of Ni-foam as cathode material in a double-chamber cassette-type MEC treating IWW. The 150 L double-chamber MEC was operated in batch and continuous mode for more than three months with real diluted IWW from a confectionery industry. The effect of Ni-foam in current generation and hydrogen production was studied and compared to a cassette operating with SS wool cathode (Baeza et al., 2017; Guerrero-Sodric et al., 2023). By exploring the limitations and challenges that arise when working on a larger scale, this research provides valuable insights into the practical feasibility and scalability of implementing Ni-foam as a cathode material in MECs treating wastewater.

5.4. Specific experimental procedures and calculations

5.4.1. Reactor design

The L-MEC was used to carry out the experimental trial (see Materials and Methods, Section 3.1.1). The reactor had a total anodic volume of 150 L once the seven cells were placed inside the reactor. The anodes were made of carbon felt (PX35 Carbon Felt, Zoltek™, United States) and were pressed against the membranes on both sides of the cathode through a SS mesh. The anodes and the cathode were separated with an AEM (RALEX® AMHPP, Mega, Czechia). The projected anode surface was 0.163 m^2 per cell (i.e., a total of 1.14 m^2 in the reactor), yielding a total area-to-volume ratio of 7.6 $m^2 \cdot m^{-3}$.

Ni-foam (RCM-Ni4753, Recemat BV, The Netherlands) was used as cathode material to drive the HER. Ni-foam purity was 99.5%, with surface density of 79 ± 3 g m^{-2}, porosity 95.2%, with 0.4 mm pore diameter, and a specific surface of 5400 m^2 m^{-3}. The effect of Ni-foam in performance was studied under two cathode configurations (Figure 5.2): i) Configuration NF_S (S stands for single), using a 15 x 20 cm sheet of Ni-foam placed in the centre of the cathodic chamber; ii) Configuration NF_D (D stands for double), with two 25 x 33 cm interconnected Ni-foam sheets attached to the membranes. For this second configuration, polypropylene (PP) 3D-printed separators were used to fix the Ni-foam sheets in contact with the membranes (Figure 5.3-5.5). Additionally, a cell (MEC 5) with a SS wool cathode (Steel wool #2, Barlesa SL, Spain) (Baeza et al., 2017; Guerrero-Sodric et al., 2023) was operated for comparison purposes. Table 5.1 shows the cathode configuration used in each cassette for each operational mode.

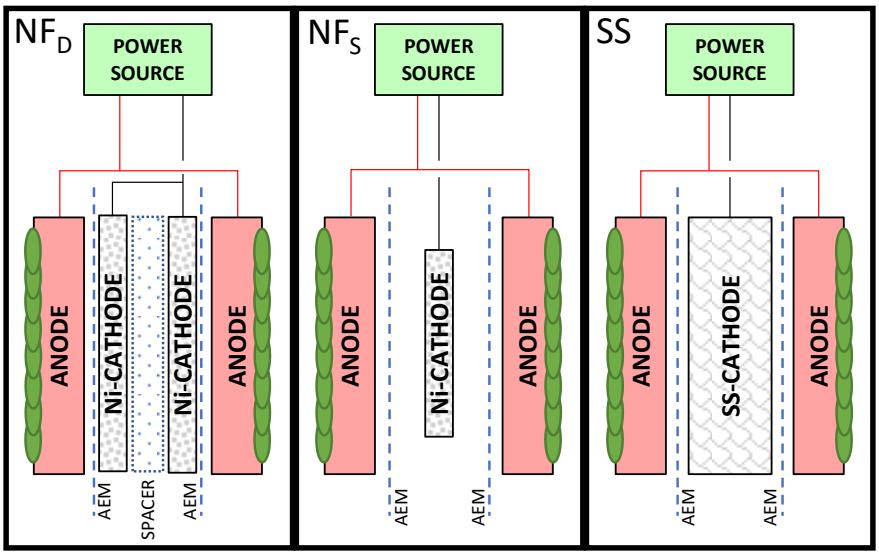

Figure 5.2. Schematic representation of the cathode configurations tested.

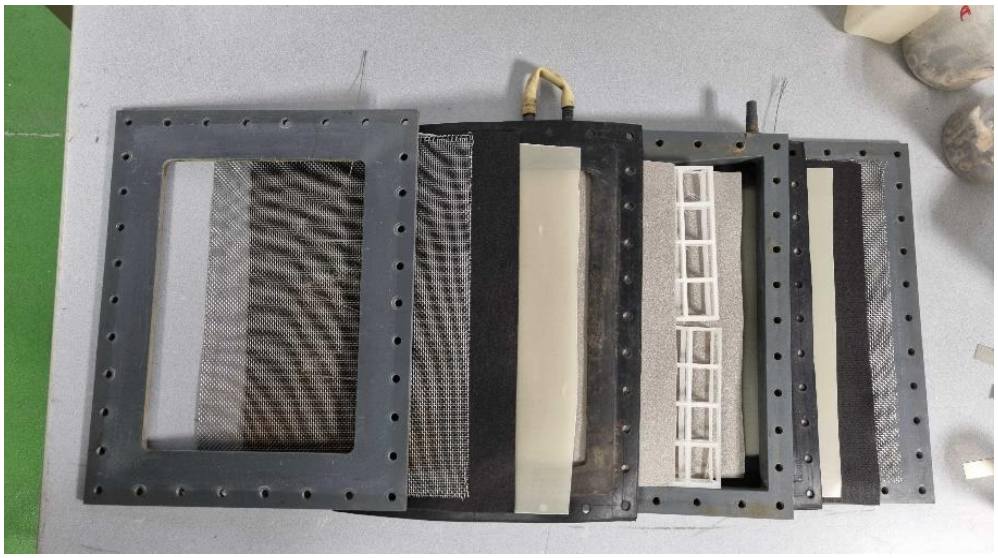

Figure 5.4. Dissembled cassette-cell with a double-sheet Ni-foam cathode (NF_D).

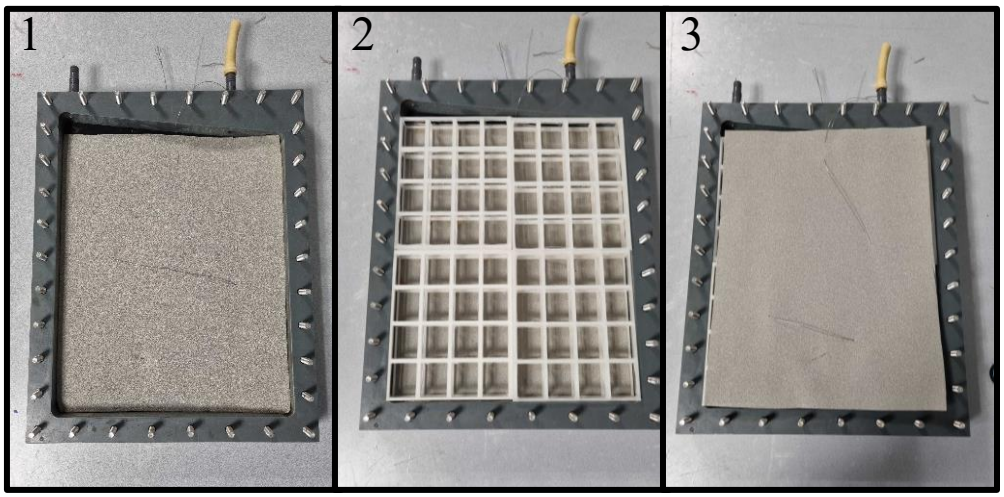

Figure 5.3. Detail of the NF_D configuration (1: First Ni-foam sheet, 2: 3D-printed PP spacer, 3: Second Ni-foam sheet).

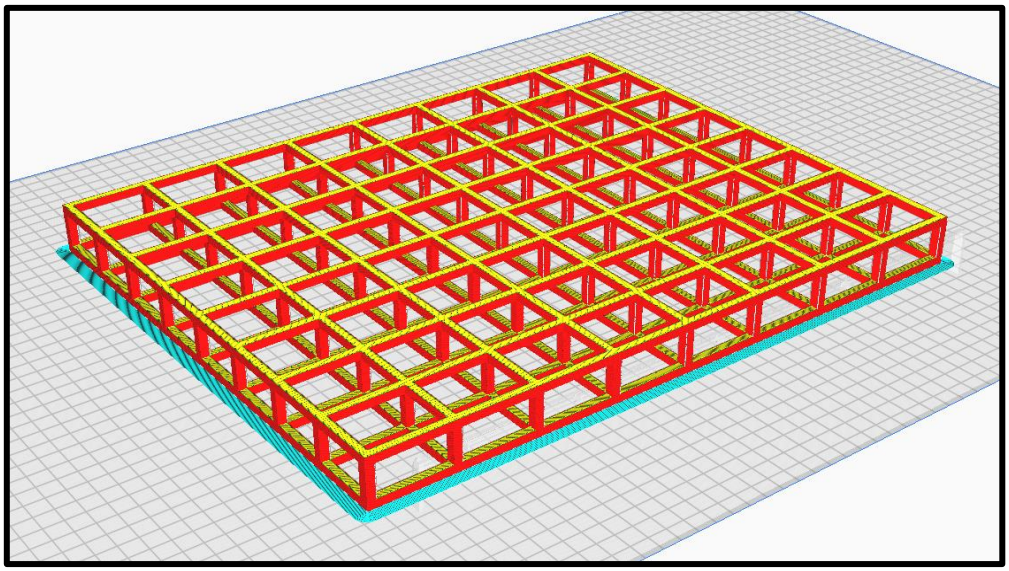

Figure 5.5. Detail of the 3D-printed separator.

Table 5.1. Cathode configuration employed in each cassette MEC.

Cell ID	Batch	Continuous
MEC 1		NF_S
MEC 2		NF_S
MEC 3		NF_S
MEC 4		SS
MEC 5	NF_S	NF_D
MEC 6	NF_S	NF_D
MEC 7		NF_S

5.4.2. Characteristics of wastewater

The IWW was collected from a sugar confectionery factory nearby Barcelona, Spain, and stored at 5ºC before their use. The wastewater had a turbid appearance, pale orange colour and sweet odour. The wastewater contained 22.1 g L^{-1} saccharose, 18.4 g L^{-1} glucose, 16.2 g L^{-1} fructose, 8.6 g L^{-1} lactose, 4.3 g L^{-1} maltose, and contained proteins and fats. Diluted IWW was used as substrate for the microbial community in the anode chamber. All dilutions were prepared with demineralized water with no extra addition of buffer solution or nutrients. The important physicochemical properties of the raw wastewater and the dilutions are listed in Table 5.2.

Table 5.2. Physicochemical properties of the raw and diluted industrial wastewater.

Wastewater	COD_S (g L^{-1})	Total N (mg L^{-1})	$P\text{-}PO_4^{3-}$ (mg L^{-1})	Conductivity (mS cm^{-1})	pH
Raw IWW	74 ± 2	642 ± 37	26 ± 1	1.4 ± 0.1	4.1 ± 0.1
Diluted IWW	2.04 ± 0.02	8 ± 1	1 ± 1	0.3 ± 0.1	6.8 ± 0.1
	5.01 ± 0.02	18 ± 2	2 ± 1	0.6 ± 0.1	6.5 ± 0.1

5.4.3. MEC operation

The cells were inoculated with anaerobic sludge from a nearby WWTP (Sabadell WWTP). The anodic chamber was filled with diluted wastewater and 5 L of sludge. The initial concentration of VSS in the anolyte was 1.5 g L^{-1}. The different modes of operation that were established in the pilot plant are schematically represented in Figure 5.6. The reactor was started-up with six NF_S and one SS cells, in continuous mode at ΔV = 0.8 V, HRT = 2 d and OLR = 1.00 g L^{-1} d^{-1}. An internal recycle flowrate of 200 L d^{-1} was maintained during the entire experimental trial. Influent and internal recycle were established using two timed peristaltic pumps (520 FAM/R2, Watson Marlow, United Kingdom). Wastewater was fed continuously during inoculation to reduce the solids retention time of the sludge, minimizing undesired precipitation and subsequent proliferation of the biomass.

At day ~12, ΔV was increased from 0.8 V to 1.0 V, and the reactor was operated in discontinuous mode to understand the effect of substrate concentration on reactor performance. A total of four batches were performed using diluted wastewater. The initial COD concentration was 2 g L^{-1} in batches I/II and 5 g L^{-1} in batches III/IV. During this stage, the pH in the anolyte was monitored but not controlled.

After the batch period, MEC 4 and MEC 5 were reassembled with the cathode configuration NF_D. Continuous operation with anodic pH control (20 g L^{-1} $NaHCO_3$ buffer solution addition, pH setpoint 7.0) was started in day 45 using diluted IWW with COD = 2 g L^{-1}, operating at HRT = 2.5 d, OLR = 0.82 g L^{-1} d^{-1} and ΔV = 1.0 V. Lastly, from day 70 onwards, the effect of the ΔV on the reactor performance was studied. ΔV was increased in 0.10 V intervals from 0.60 V to 1.40 V, to cover a wide range of potentials. Hydrogen production was measured a minimum of three times at each ΔV tested.

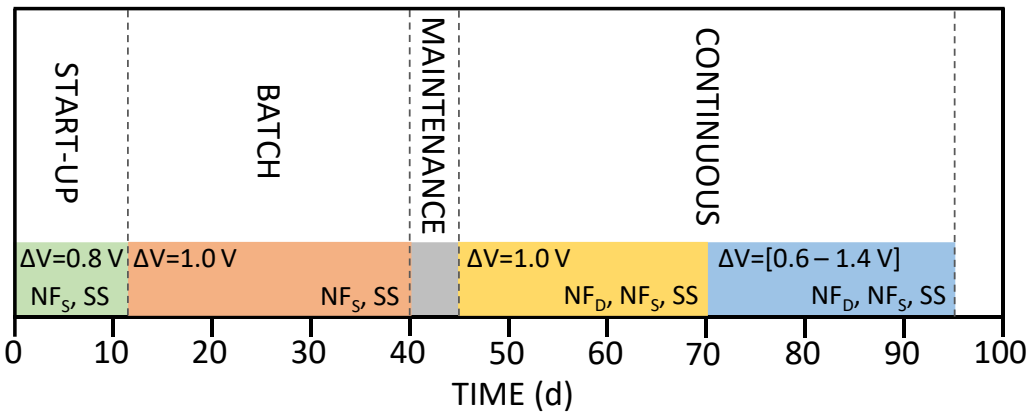

Figure 5.6. Operational schedule of the MEC pilot plant.

5.4.4. Analytical methods

Liquid and gas samples were analysed following the previously described procedure (see Materials and Methods, Section 3.2)

5.4.5. Molecular methods

The microbial community composition was determined following the previously described procedure (see Materials and Methods, Section 3.3)

5.4.6. KPIs

Reactor performance was evaluated using the previously described KPIs (see Materials and Methods, Section 3.5).

5.5. Results and discussion

5.5.1. Electrochemical characterization of the cathodes

CV was used to identify the best cathode material in terms of lowest overpotential and higher current generation. Figure 5.7 presents the results obtained with the two cathode materials studied, revealing the distinct behaviour of SS-wool compared to Ni-foam. Both materials exhibit a similar electrochemical behaviour, characterized by the absence of evident Fe oxidation or reduction peaks in the CV curves. This can be attributed to the consistent intensity throughout the CV range, effectively masking the peaks associated with Fe redox processes. This phenomenon is indicative of highly capacitive materials, which operate independently of Faraday's law. Consequently, their response is not influenced by the redox species present or their concentration. This is because these materials possess the capability to store energy rather than immediately dissipating it, as is observed in the case of faradaic processes, which generate distinct peaks. The sharper

slope exhibited by Ni-foam at negative potentials, clearly indicate its superior performance for effective hydrogen production, allowing for higher current densities at the same potential. Furthermore, at positive potentials, the observed current density is higher in the SS-wool, likely attributed to the oxidation of the electrode or other electrochemical processes. This observation suggests that SS-wool is less stable under oxidative potentials. These results are in line with the electrochemical characterization reported in the literature (Jayabalan et al., 2019), and indicate that Ni-foam exhibits better performance than SS-wool for hydrogen production.

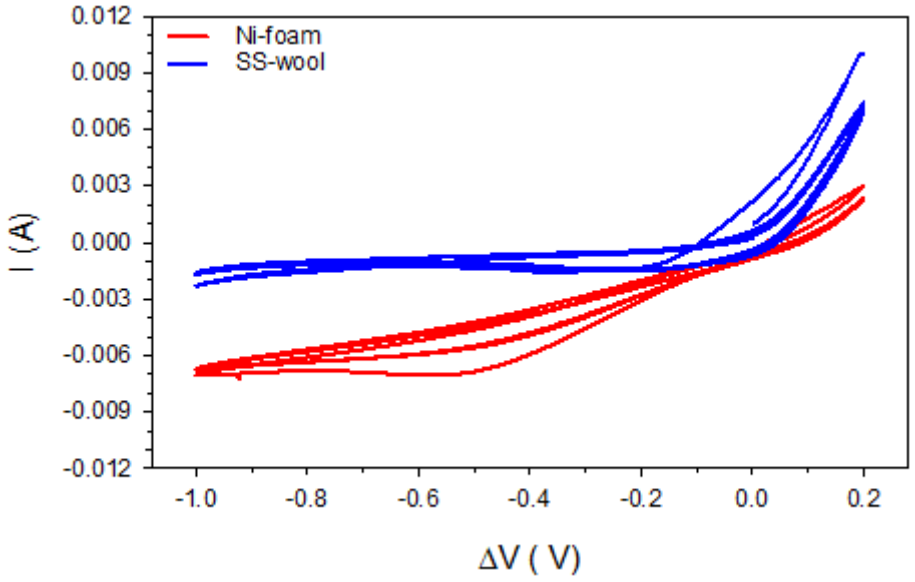

Figure 5.7. Cyclic voltammetry (CV) of Ni-foam and SS-wool against counter electrode (Pt), and reference electrode ($Ag/AgCl_{(sat)}$).

5.5.2. Start-up of the pilot plant

The reactor was inoculated with anaerobic sludge and started-up in continuous mode at ΔV = 0.8 V, HRT = 2 d and OLR = 1.00 g L^{-1} d^{-1}, with an internal recycle of 200 L d^{-1}. All MECs showed similar exponential intensity profiles during inoculation, with a lag phase of ~3.5 d and reaching a stable current after approximately 10 d of operation (Figure 5.8). Despite the six NFs MECs were assembled and started-up identically, some variability was observed among the cells regarding their current density and hydrogen production. The maximum intensity in the NFs cells during inoculation ranged from 0.118 A to 0.152 A, the average current density was 0.82 ± 0.09 A m^{-2}, and the specific H_2 production rate was 7.29 ± 1.57 L H_2 m^{-2} d^{-1}. Inoculation was considered to be finished at day ≈ 12 (t = 11.89 d) when stable performance over time was observed in all cells.

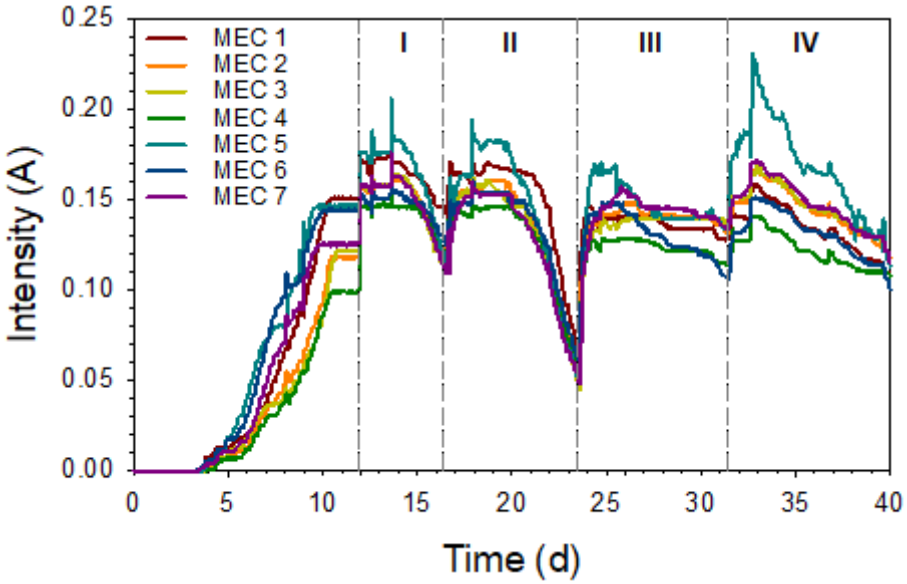

Figure 5.8. Intensity profiles of each cassette during the start-up and batch operation. The grey dashed line indicates the start of a new batch.

5.5.3. Preliminary evaluation of the performance of Ni-foam

A series of batch tests were conducted with the objective of gaining initial insights into the material's behaviour and to understand the influence of concentration on the plant performance. In batches I/II (ΔV = 1.0 V; initial COD = 2 g L^{-1}), current density and hydrogen production showed a close relation with the COD concentration in the anolyte (Figure 5.9). Current density peaked two days after the substrate was loaded and gradually dropped at COD concentrations below ~1 g L^{-1} (Figure 5.9B). The profiles obtained are consistent with the proposed synergistic mechanisms for the oxidation of complex substrates in BES (Montpart et al., 2015). Sugars, proteins, and fats in the wastewater need to be hydrolyzed and fermented to VFA in order to be used by the exoelectrogenic community. Hence, when complex organics were fed, there was a first stage in the batch when ARB were limited by low VFA presence. As the complex organic compounds were fermented, VFA production increased and, therefore, the anodic biofilm activity. Then, current density declined when substrate was depleted.

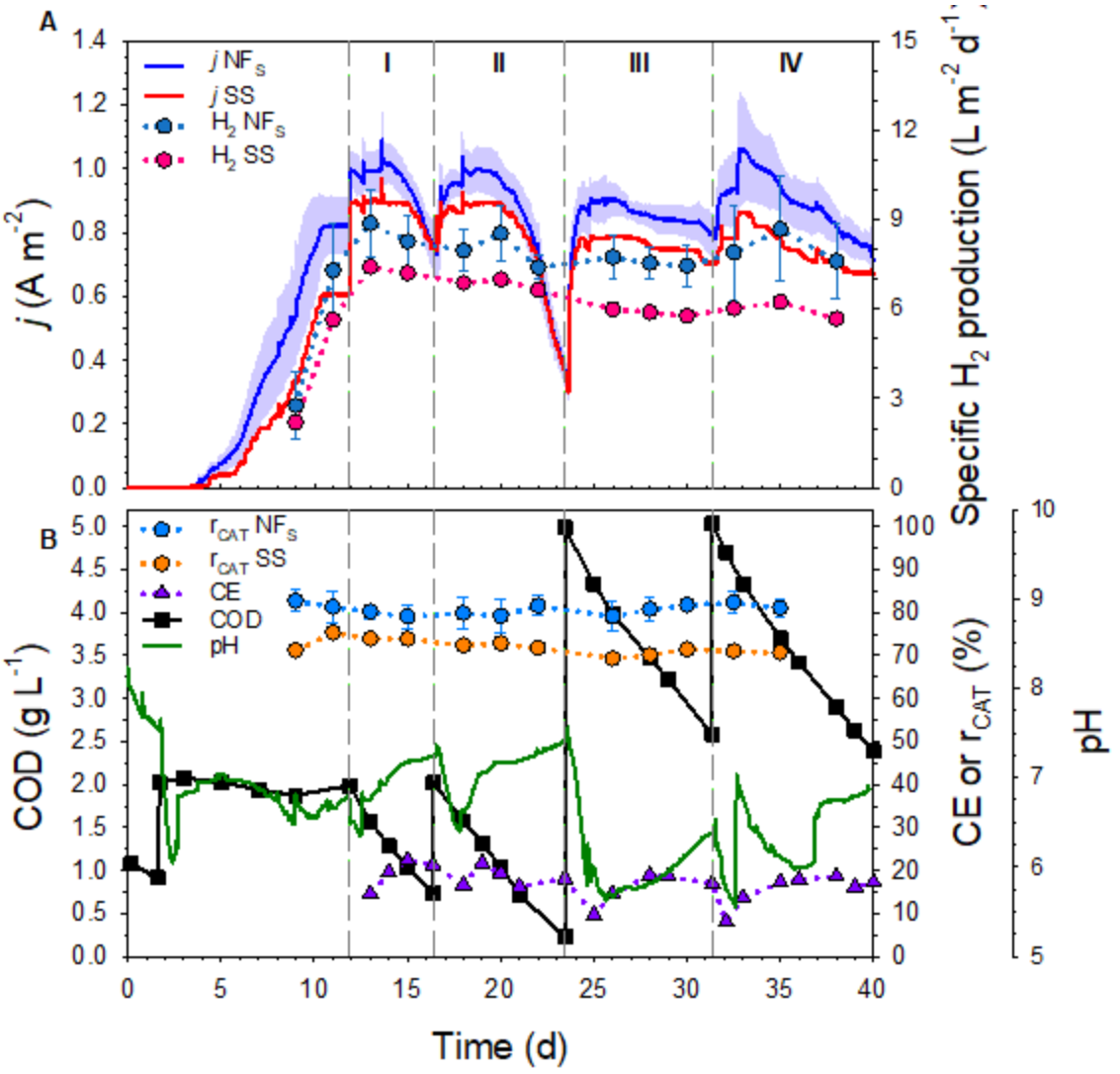

Figure 5.9. Start-up and batch operation profiles. A) Average current densities (*j*) and specific hydrogen production rates of the single-sheet nickel-foam cells (NF_S) and the stainless-steel cell (SS). B) Anodic COD concentration, pH and coulombic efficiency (CE); Average cathodic recovery efficiencies (r_{CAT}) of the NF_S and SS cells. Shade indicates standard deviation of current density in the NF_S cells. The grey dashed line indicates the start of a new batch.

At high COD concentrations (>1 g L^{-1}), NF_S cells reached a maximum average current density of 1.01 ± 0.02 A m^{-2} and H_2 production of 8.87 ± 1.15 L m^{-2} d^{-1}, which was a 1.1-fold and 1.2-fold higher, respectively, than those values obtained in the SS cell (0.89 A m^{-2} and 7.41 L H_2 m^{-2} d^{-1}). In contrast, NF_S and SS cells exhibited similar performance at low COD concentrations (<1 g L^{-1}), with less than 5% of difference between both cathode materials under such conditions. For instance, the current density observed with both cathode materials was around 0.73 A m^{-2} at the end of batch I (t = 16.37 d; COD ~ 0.70 g L^{-1}), and 0.30 A m^{-2} at the end of batch II (t = 23.43 d; COD ~ 0.25 g L^{-1}).

This behaviour could be attributed to the low COD concentration limiting the anodic biofilm activity. This is an important fact to consider in future MEC designs: anode performance is likely to be the limiting factor in low-strength wastewater treatment applications. Then, the use of expensive cathode materials to enhance HER may not be cost-effective, as the activation and concentration overpotentials in the anode would be the dominant limiting factor.

During batches III/IV, there was no significant enhancement in performance despite increasing the initial COD concentration up to 5 g L^{-1}. Current density peaks were similar to those recorded in batches I/II but more sustained over time, with NFs cells yielding between 30 - 40% higher specific hydrogen production rate than the SS cell (Table 5.3). NFs cells achieved slightly higher r_{CAT} efficiencies among the different batches (81 ± 1% for NFs vs 73 ± 2% for SS, Figure 5.9B). These are promising results considering that the cathodic efficiencies reported at pilot-scale are usually below 60% (Jiang et al., 2023). This achievement underscores the efficacy of the double-chamber configuration in efficiently capturing the hydrogen generated at the cathode.

Table 5.3. Summary of the important results obtained during the batch tests.

					NFs (MEC 1-3, 5-7)		SS (MEC 4)	
Batch ID	Batch length (d)	ΔCOD (mg L^{-1})	CE (%)	pH	j_{max} (A m^{-2})	H_{2max} (L m^{-2} d^{-1})	j_{max} (A m^{-2})	H_{2max} (L m^{-2} d^{-1})
I	4.5	1262	19	6.95 ± 0.26	1.02 ± 0.02	8.87 ± 1.15	0.89	7.42
II	7.1	1784	18	7.08 ± 0.26	1.01 ± 0.07	8.54 ± 0.94	0.90	6.99
III	7.9	2409	15	6.08 ± 0.45	0.91 ± 0.06	7.75 ± 0.75	0.79	5.98
IV	8.6	2647	16	6.37 ± 0.37	1.06 ± 0.12	8.68 ± 1.75	0.85	6.24

j_{max}: Maximum current density; H_{2max}: Maximum specific hydrogen production rate; pH: Average pH; ΔCOD: COD concentration difference between the start and the end of the batch; CE: Coulombic efficiency

Despite achieving significant COD degradation (Table 5.3), CEs lower than 20% (17 ± 2%) were observed, indicating that considerable biological organic matter oxidation other than exoelectrogenesis was occurring. These alternative pathways likely involved heterotrophic oxidation in the upper reactor layers and methanogenesis in the lower

anaerobic regions. Thus, the ORRs observed were not significantly dependent on hydrogen production or current generation. This scenario is frequently observed in pilot-scale double-chamber MECs and is linked to the elevated biological activity of planktonic biomass present in the anode chamber (Guisasola et al., 2020). As shown in Figure 5.9 and detailed in Table 5.3, batches III/IV reached lower pH levels compared to batches I/II as the higher initial COD concentration led to the accumulation of fermentation products. The impact of pH was evident at day ~ 32 (t = 32.40 days), when the pH of the anolyte was risen from 5.6 to a neutral value, boosting current density and hydrogen production. However, the COD concentration was still high, and the reactor was again acidified by fermentation. These differences in pH had considerable implications on the composition of the microbial community within the bioreactor. Therefore, the lack of improvement compared to batches I/II was mainly attributed to significant anolyte acidification (pH < 6), which masked any potential effects of the increased COD on current generation. For this reason, a pH control was implemented from day 37 (t = 36.88 d) onwards to maintain a neutral pH in the anolyte for the next experiments.

5.5.4. Performance and cost analysis of the different cathode configurations

Following the 40 days of batch operation, MEC 4 and MEC 5 were reassembled with a new bi-cathode configuration using two 30 x 35 cm interconnected Ni-foam sheets attached to the membranes (NF_D in Figure 5.2). The continuous operation with anodic pH control (pH = 7) was started in day 45 using diluted IWW with an inlet COD concentration around 2 g L^{-1}, operating at ΔV = 1.0 V; HRT = 2.5 d; and OLR = 0.82 g L^{-1} (Figure 5.10). The ORR remained around 0.33 ± 0.02 g L^{-1} d^{-1} during the whole continuous operation and the chemical composition of the effluent was 0.40 ± 0.01 g L^{-1} acetic acid, 0.11 ± 0.00 g L^{-1} propionic acid, 0.10 ± 0.00 g L^{-1} ethanol, and 0.05 ± 0.00 g L^{-1} butyric acid. These compounds represented ~95% of the total COD in the effluent, suggesting that the organic macromolecules in the influent were effectively transformed into fermentation products. The measured CE was generally low as reported in batch mode (CE = 21 ± 2 %), indicating room for improvement in terms of energy efficiency in future MEC designs (Figure 5.10A). Furthermore, there were no substantial differences in the r_{CAT}, being the NF_D cells those with the highest value: 86 ± 2 %.

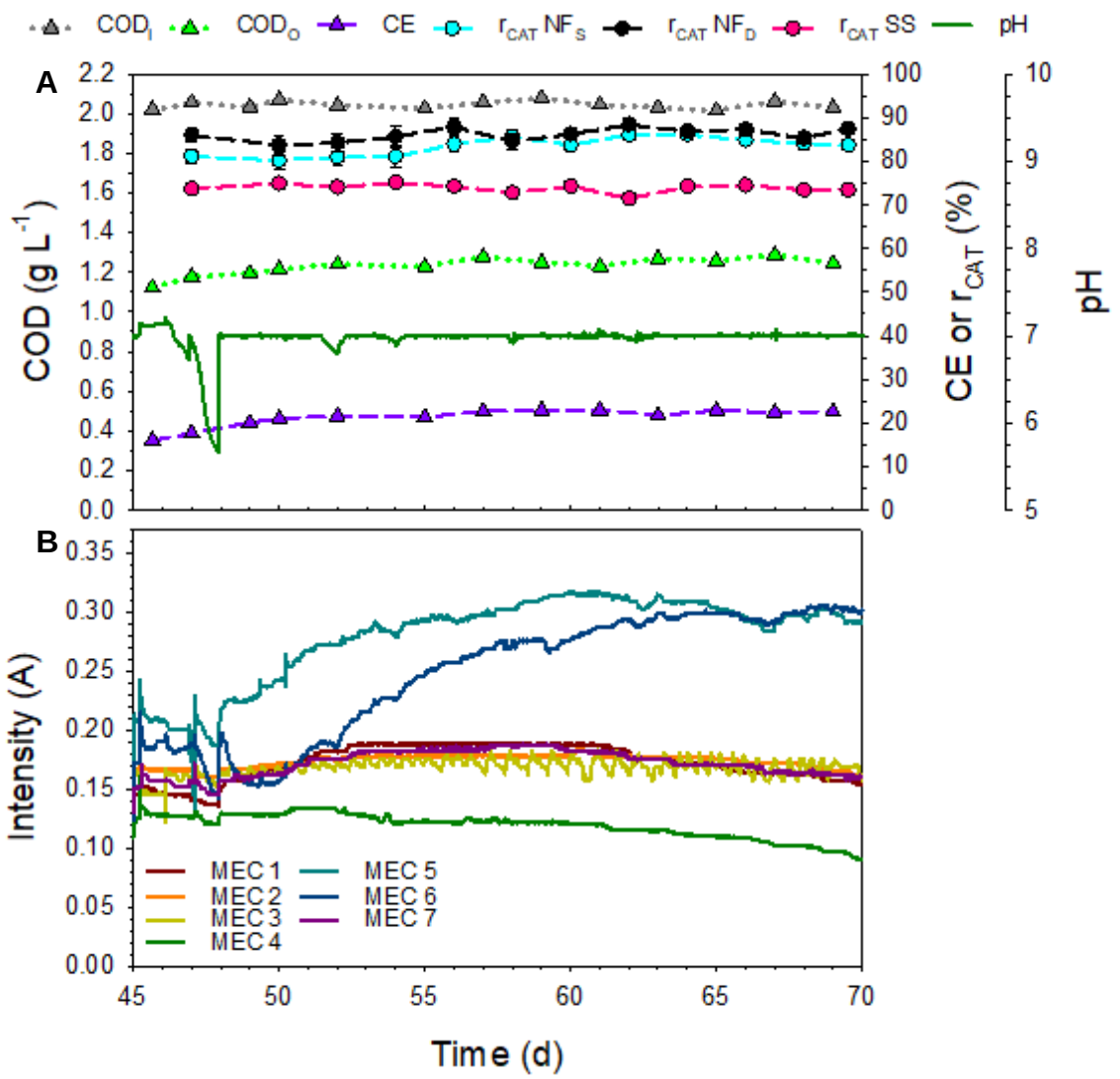

Figure 5.10. Start-up and batch operation profiles. A) Average current densities (*j*) and specific hydrogen production rates of the single-sheet nickel-foam cells (NFS) and the stainless-steel cell (SS). B) Anodic COD concentration, pH and coulombic efficiency (CE); Average cathodic recovery efficiencies (rCAT) of the NFS and SS cells. Shade indicates standard deviation of current density in the NFS cells. The grey dashed line indicates the start of a new batch.

The start-up of the two NF_D cells led to different current densities and hydrogen production rates but reached similar values (around 1.85 A m^{-2} and 17.86 ± 0.89 L H_2 m^{-2} d^{-1}) from day ~ 62 onwards (Figure 5.10). The average hydrogen production rate observed in the NF_D configuration was 3.0-fold higher than that obtained with the SS cell and 1.8-fold higher than the NF_S cells (Figure 5.11). This enhancement in performance was attributed to the higher cathode surface and lower electrode spacing, which resulted in a reduction of the overall ohmic resistance and a more efficient energy utilisation. However, the NF_D configuration was more expensive due to the higher price of Ni-foam

compared to SS wool (540 € kg^{-1} vs. 10 € kg^{-1}). The amount of cathode employed was 0.04 kg and 0.22 kg of Ni-foam for the NF_S and NF_D configurations, respectively, and 0.38 kg of SS wool for the SS cell. Therefore, the cathode cost of a cassette was 22 € MEC^{-1}, 119 € MEC^{-1} and 4 € MEC^{-1} for the NF_S, NF_D and SS configurations, respectively. This is a 5.5-fold and 29.8-fold increase in the cathode cost compared to the SS wool configuration, which is not corresponded by the cell performance in terms of current density and/or hydrogen production. However, the selection of the optimal cathode material depends on the specific system requirements or potential budget constraints.

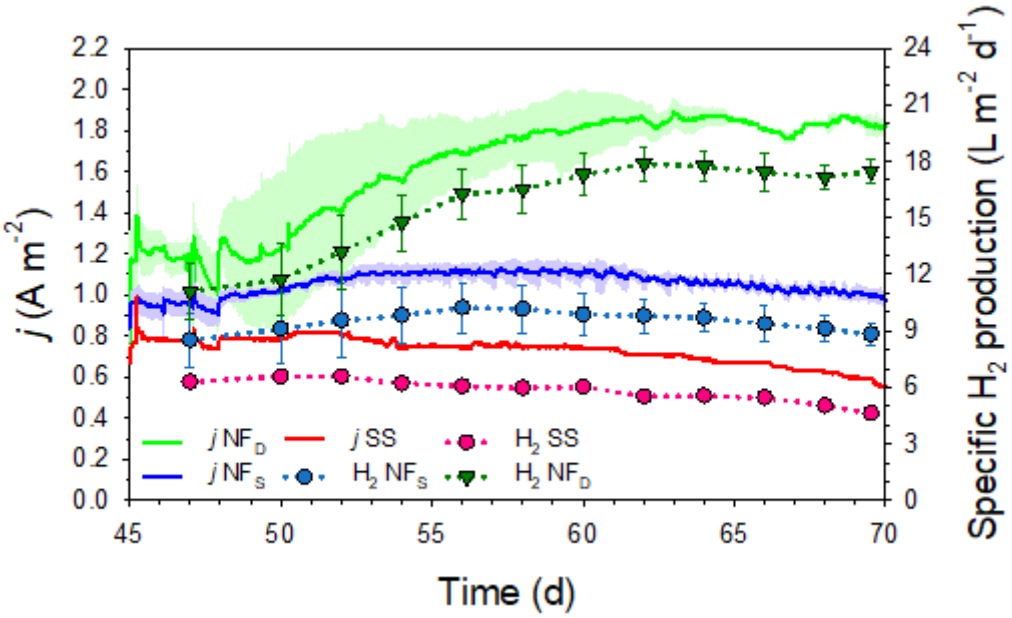

Figure 5.11. Average current density (*j*) and specific hydrogen production over time in each configuration during the continuous operation with diluted industrial wastewater.

5.5.5. Effect of ΔV on hydrogen production and energy efficiency

At day 70, different ΔVs were tested maintaining the same hydraulic conditions and temperature to understand the effect of the energy applied on the plant performance. ΔV was increased from 0.60 V to 1.40 V, in 0.10 V intervals (Figure 5.12). After a short non-steady state period, stable current density and hydrogen production over time was observed in all cells for every ΔV tested. The only exception was at an ΔV of 1.4 V when the performance declined in all configurations, indicating the occurrence of side reactions or electrode degradation processes that adversely affected the bioelectrochemical behaviour of the cells.

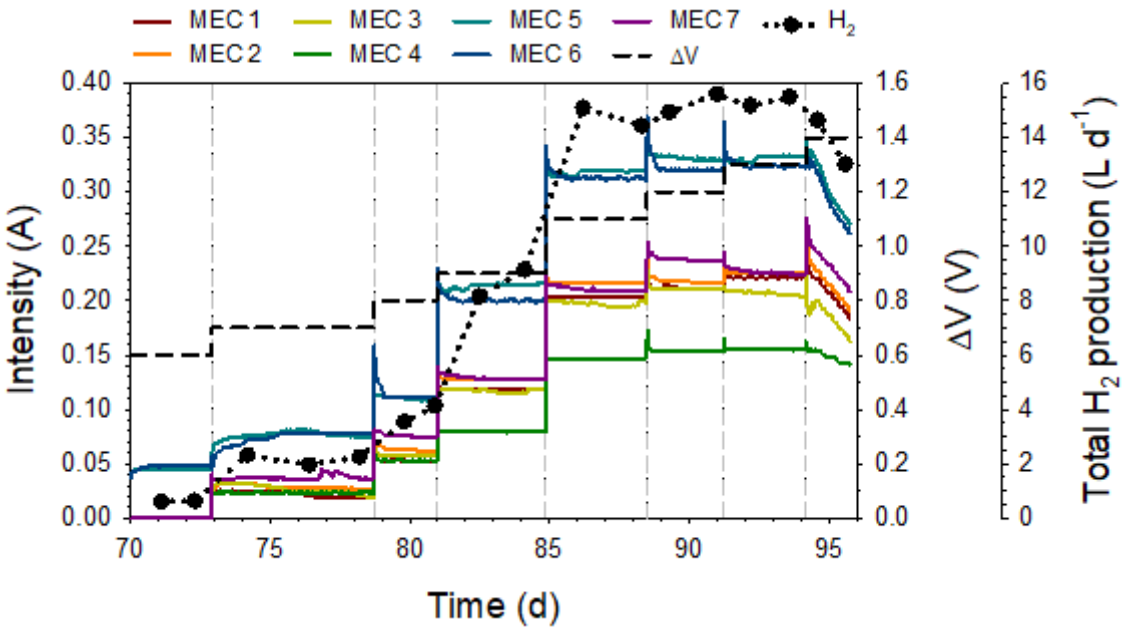

Figure 5.12. Intensity profiles of each cassette at different applied potentials (ΔV) during continuous operation with diluted industrial wastewater.

NF_D cells showed the lowest potential loss of all configurations tested, exhibiting a minimum ΔV requirement of 0.60 V to produce hydrogen (1.90 ± 0.14 L H_2 m^{-2} d^{-1}) (Figure 5.13A), with a current density of 0.28 ± 0.00 A m^{-2}. In contrast, SS and NF_S MECs required a higher minimum ΔV of 0.70 V and generated around 1 L H_2 m^{-2} d^{-1} with a current density of 0.14 A m^{-2}. Notably, NF_D and NF_S cells exhibited a sigmoidal trend, with a maximum average hydrogen production of 19.07 ± 0.46 L H_2 m^{-2} d^{-1} and 11.85 ± 0.40 L H_2 m^{-2} d^{-1}, respectively. On the other hand, SS cell displayed a more gradual increase in hydrogen production with the ΔV, eventually reaching a maximum of 7.72 ± 0.39 L H_2 m^{-2} d^{-1} at ΔV = 1.2 V. The initial region of the sigmoidal curve (low ΔV) indicates limitations of ΔV whereas the last region indicates mass transfer limitations since the current density does not depend on the ΔV.

The hydrogen production rates under different ΔVs resulted in different r_E efficiencies (r_E) of the system (Figure 5.13B). Regardless of the cathode configuration, a higher ΔV within the cells correlated with reduced r_E. The highest r_E efficiency (r_E = 132 ± 1 %) was obtained in the NF_D cells at the minimum applied potential (ΔV = 0.60 V). The optimal ΔV (i.e. balancing energy input/output) for all configurations was found to be in the range 0.9 - 1.0 V, in which a reasonable hydrogen production can be reached without compromising the energy efficiency of the process. NF_D and NF_S cells not only achieved energy neutrality but were net energy producers in a wide range of ΔV, since the hydrogen

would yield up to 0.05 kWh m^{-2} and 0.01 kWh m^{-2}, respectively. In contrast, the SS cell exhibited higher energy requirements with lower E_P yields for all ΔV investigated, but could reach energy neutrality in some cases (e.g. ΔV = 0.7/0.9 V).

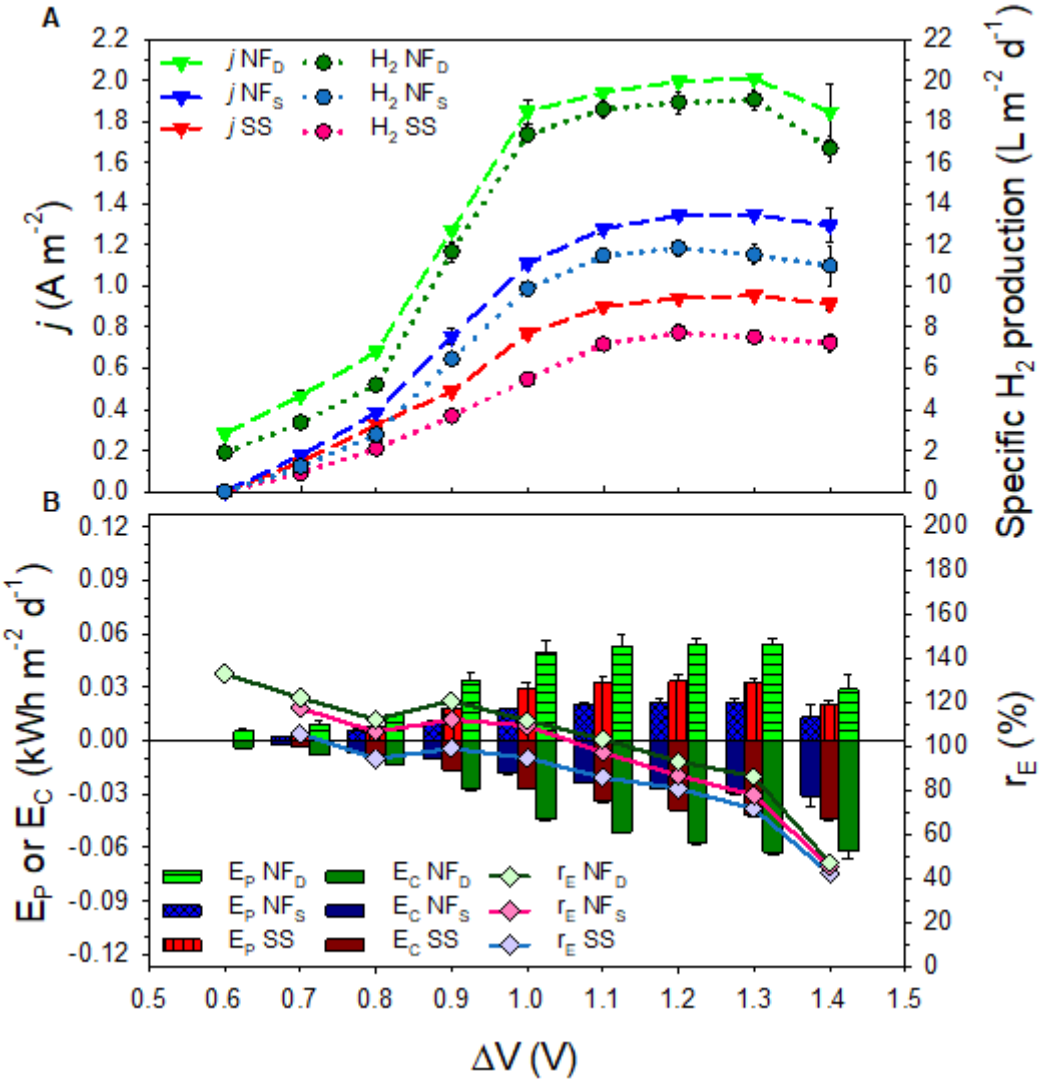

Figure 5.13. Key performance indices of the double-sheet nickel-foam MECs (NF_D), single-sheet nickel-foam MECs (NF_S) and the stainless-steel MEC (SS), at different applied potentials (ΔV) during continuous operation. A) Average current densities (*j*) and specific hydrogen production rates. B) Average energy production (E_P), energy consumption (E_C) and energy recovery efficiency (r_E).

Assuming full-operation of the pilot plant with 10 NF_D cells in the bioreactor (S / V = 12.6 m^2 m^{-3}), this configuration could potentially generate up to 0.21 m^3 H_2 m^{-3} d^{-1} with r_E >100 %. This is a significant outcome of this work since the reported H_2 production rates in double-chamber MEC pilot reactors (>100 L) are usually in the range of 0.005 - 0.040 m^3 m^{-3} d^{-1} (Guisasola et al., 2020). The benefits of using Ni-based cathode

materials have already been reported at lab-scale and compared to Pt sheets (Hu et al., 2009; Selembo et al., 2009), enabling theoretical volumetric hydrogen production rates as high as 50 m^3 H_2 m^{-3} d^{-1} (Jeremiasse et al., 2010). However, scaling-up and obtaining similar performance to lab-scale set-ups is the current bottleneck of BES. Scaling-up at volumes >100 L entails additional complexities and challenges, including mass transport limitations and reactor design considerations. Therefore, while lab-scale experiments provide valuable insights, further investigation and validation at pilot scale are necessary to determine the true potential and performance of new cathode materials in practical applications.

5.5.6. Bacterial communities in the anode

Samples from the anodes of the NF_D and SS MECs were analysed by Illumina 16s. The microbial community analysis indicated that the cathode material affected the distribution of the enriched microbiome. The microbial community that developed on the anode of both types of MECs was a mixed consortium with similar dominant orders but with different relative abundances. For instance, in the NF_D samples, the dominant orders were *Desulfuromonadales* (26.8%), *Bacteroidales* (24.9%), *Enterobacteriales* (15.1%), *Desulfovibrionales* (8.5%) and *Clostridiales* (4.5%). For the SS sample, the relative abundance was *Desulfuromonadales* (15.8%), *Bacteroidales* (12.9%), *Enterobacteriales* (15.1%), *Clostridiales* (7.5%) and *Desulfovibrionales* (7.1%).

The dominant genus in the NF_D cells were *Geobacter* (16.9%) and *Bacteroides* (15.4%) (Figure 5.14). *Geobacter* species are known as efficient exoelectrogens, capable of harvesting electrical energy from organic compounds (Kumar et al., 2015; Logan and Regan, 2006). On the other hand, *Bacteroides* species are known to be capable of hydrolysing a wide variety of particulate proteins and carbohydrates (Mahadevan et al., 1980). As suggested in other studies about MECs, they could have the role of hydrolysis and fermentation of complex organics into VFAs (Wang et al., 2010). Previous works have already demonstrated the need to develop an anodic biofilm with a syntrophic consortium between fermentative bacteria and exoelectrogens to treat complex substrates with BES (Montpart et al., 2015). Other dominant genera were *Desulfovibrio* (8.5%) and *Klebsiella* (7.0%). *Desulfovibrio* species are sulphate-reducing bacteria (Postgate and Campbell, 1966) that can participate in syntrophic relationships with exoelectrogens, facilitating the removal of sulphate and promoting the overall performance of the MEC.

Klebsiella is a genus of facultative anaerobic bacteria that can carry out different metabolic processes, including fermentation and nitrogen fixation (Drancourt et al., 2001; Rosenblueth et al., 2004).

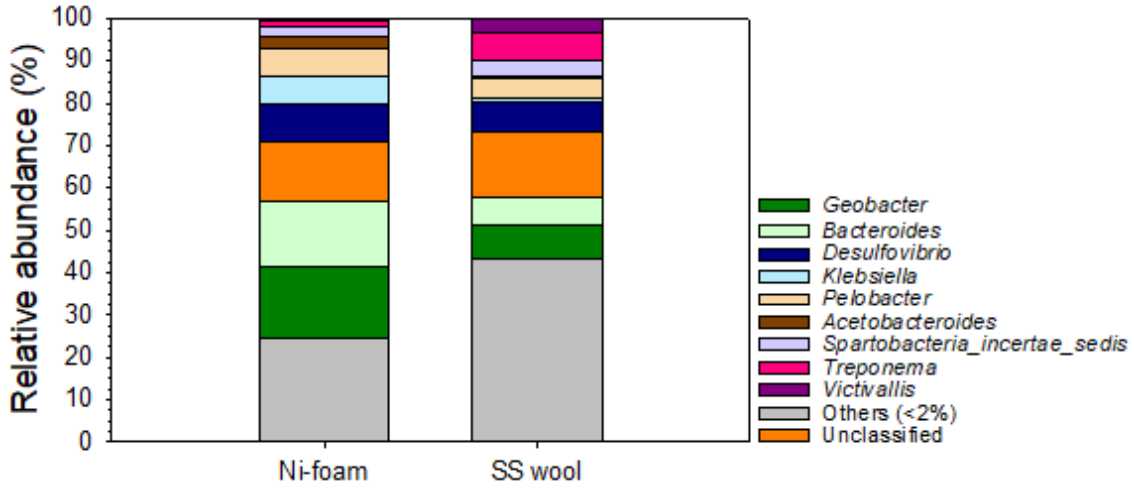

Figure 5.14. Anodic bacterial communities at genus level based on cloned 16S rRNA gene sequence distribution for the double-sheet nickel foam (NF_D) and stainless-steel (SS) MECs after reactor decommissioning.

The results at genus level clearly show an important fraction of unclassified and other microorganisms, which implies a high diversity because of working with a complex IWW. Comparing the results of NF_D with those of SS, the proportion of *Geobacter* is reduced to 8.1% in the latter, which is clearly correlated with the lower exoelectrogenic activity observed. A lower proportion of *Bacteroides* is also observed (6.6% for SS), which implies a higher proportion of other microorganisms and corroborates the hypothesis that biofilms developed using NF_D as cathode have higher specificity and seem to be more suitable for generating exoelectrogenic activity. The Shannon Diversity index at the genus level further supports this statement, with values of 3.06 and 3.72 for the NF_D and SS configurations, respectively, indicating a higher level of microbial diversity in the SS biofilm.

The 16S rRNA clone libraries indicate three *Geobacter* strains comprise a total of 15.4% of the NF_D community: *Geobacter chapellei* (7.8%), *Geobacter pickeringii* (6.3%) and *Geobacter sulfurreducens* (1.3%). *Bacteroides_oleiciplenus*, a fermentative gram-negative bacterium belonging to the *Bacteroides* genus, comprised ~15% of the anodic communities. The major end products of glucose metabolism in peptone yeast extract glucose broth (PYG) are acetic, succinic, formic and lactic acids (Watanabe et al., 2010).

Due to the limitations of the sampling method, microbial data could only be collected at the end of the study, which restricted the scope of analysis regarding the influence of microbial composition on performance. However, the microbial consortium in both configurations appears to be well-suited for the transformation of organic macromolecules into energy. *Geobacter* species contribute significantly to the exoelectrogenic activity, while *Bacteroides* and other fermentative bacteria are involved in the production of VFAs from sugar metabolism. These VFAs can then be consumed by exoelectrogens, completing the energy conversion process in the MEC. The higher prevalence of exoelectrogenic microorganisms, along with the presence of fermentative bacteria, creates a more favourable environment for electron transfer and organic matter degradation in the NF_D MECs, resulting in improved performance.

In the symbiotic relationship between exoelectrogenic and fermentative bacteria in the biofilm, ARB are likely to grow in the inner layers, closer to the conductive material, to efficiently donate the electrons generated in the anaerobic oxidation. In contrast, fermentative bacteria are likely to occupy the outer layers, providing a metabolic advantage by readily accessing fermentable substrates. These fermentative bacteria metabolize these substrates, generating acetate as a primary byproduct. Acetate, being a diffusible molecule, permeates the biofilm, reaching the exoelectrogenic population in the inner layers. If acetate availability is sufficient, ARB consume it, fuelling their growth and electron uptake. However, mass transfer limitations within the biofilm can restrict acetate diffusion, potentially limiting ARB growth. Fermentative bacteria, unaffected by acetate limitations, continue to produce and release acetate into the surroundings, contributing to the overall metabolic exchange within the biofilm. It is important to note that there may be other planktonic microorganisms in the anodic chamber that also produce and consume acetate.

5.6. Conclusions

- A MEC pilot plant (>100 L) can be successfully run with real IWW from the confectionery industry with i) good hydrogen production results (19.07 L m^{-2} d^{-1} and 0.21 m^3 m^{-3} d^{-1}), ii) reasonably high current density (>2 A m^{-2}) and iii) substantial organic matter removal efficiency (>40 %).
- High COD concentration allows high current densities but the CE (around 20 %) shows that other simultaneous organic matter removal processes occur, possibly related to heterotrophic oxidation in the upper layers of the reactor and methanogenesis in the lower part due to anaerobic conditions.
- The novel cassette configuration with a double Ni-foam sheet cathode that offers the best current density and hydrogen production rates observed so far at this scale. The improvement with the novel configuration is 202% over the SS-wool cathode and by 81% over the configuration with only a single Ni-foam sheet. However, the performance gains achieved with Ni-foam do not justify its higher cost .
- The applied potential has two opposite consequences regarding the energy efficiency of the system: on the one hand, higher ΔV imply higher energy requirements but also higher hydrogen (and thus, energy) recovery. A conservative value of 0.9 - 1.0 V was found to be successful for this system.
- The microbial community developed on the anode is a syntrophic culture of exoelectrogens and fermenters (mostly *Geobacter* and *Bacteroides*), which correlates well with the observed exoelectrogenic activity.

Chapter VI

Scale-up of MECs: Design, construction and operation of a 1 m^3 MEC pilot plant in a real wastewater treatment plant

6. Scale-up of MECs: Design, construction and operation of a 1 m^3 MEC pilot plant in a real wastewater treatment plant

6.1. Abstract

MECs hold significant promise for transforming wastewater treatment processes into energy-efficient and sustainable operations, but their scale-up presents substantial technical challenges, hampering widespread adoption in real-world applications. This chapter presents the design, construction, and operation of a 1 m^3 MEC pilot plant integrated into an UWW treatment plant for evaluating MEC performance and hydrogen production at a large scale. The experimental trials conducted with synthetic and real UWW showcased the MEC performance under varying operational conditions. The scalability of the pilot plant was demonstrated without a significant decrease in performance, achieving continuous hydrogen production at a maximum rate of 8.59 L m^{-2} d^{-1} and 3.45 L m^{-2} d^{-1} with synthetic and UWW, respectively, and a maximum total COD removal of 51 %. Furthermore, a preliminary techno-economic assessment evaluated the commercial potential of the pilot plant, considering factors such as revenue from hydrogen production, electricity consumption costs, and capital expenses. The outcomes of this study suggest that future research should focus on minimizing material costs, hydrogen leakages and voltage losses to enhance scalability, as well as exploring the applicability of MECs for high-strength wastewater treatment. The novel 1 m^3 pilot plant represents a significant advancement in MEC scale-up, offering valuable insights into the challenges and opportunities associated with real-world implementation.

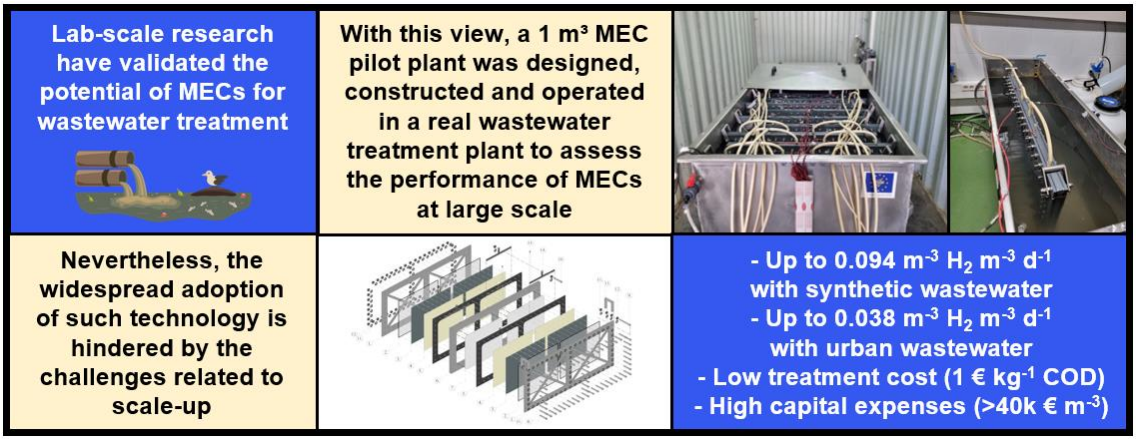

Figure 6.1. Graphical abstract.

6.2. Introduction

Evidence from lab-scale research have validated the potential of MEC technology, transforming wastewater treatment into an energy self-sufficient or even energy-producing process that simultaneously offers economic and environmental benefits (Osset-Álvarez et al., 2019). However, their widespread adoption is hindered by the technical challenges associated with their scale-up. The lack of pilot-scale research contributes to hamper the transition to large-scale implementation. In fact, most studies about MECs for wastewater treatment have been conducted at lab-scale with anodic volumes lower than 1 L (Jiang et al., 2023). Thus, there is a lack of understanding of the fundamental challenges of MEC operation at larger scales that ultimately constrain the development of robust and scalable MEC systems for commercial applications.

The first pilot-scale MEC fed with wastewater was reported by Cusick et al. (2011) in a 1000 L reactor. It was a visionary attempt to demonstrate MEC performance for real applications. However, the results were not satisfactory enough and the initial low hydrogen production was replaced for methanogenesis. Currently, several reviews have summarized the substrates, materials, and operational modes of pilot-scale MEC studies, providing valuable insights into the factors influencing the poor MEC performance typically reported (Aiken et al., 2021; Fathima et al., 2024; Jiang et al., 2023; et al., 2020; Rousseau et al., 2020). In a nutshell, the key bottlenecks detected are the need of optimal reactor configurations to maximize the OLR, the enhancement of mass transfer rates and electrode materials for boosting current density, the improvement of the energy efficiency of the process and the development of cost-effective materials that decrease the cost of the process without hindering its performance. Once these limitations are addressed, MEC technology can be expected to provide a sustainable and energy-efficient approach to wastewater treatment and valuable resource recovery. Then, MECs widespread adoption is highly dependent on a deep understanding of the critical factors influencing scale-up, enabling the development of next-generation MEC systems that are practical, scalable, and economically viable.

6.3. Objectives

The objective of this study was to design, build, and operate a 1 m^3 MEC pilot plant (M-MEC) in a real WWTP to evaluate the performance of MEC technology for UWW treatment and hydrogen production at larger scale. The main engineering goal was to

assess whether the performance achieved in the L-MEC could be maintained in a real scenario using a scaled-up version of the previous prototype.

The M-MEC was operated for more than 250 days under different operational conditions, including a preliminary evaluation of the novel cassette configuration and a stepwise integration with the actual wastewater stream. The M-MEC is the largest double-chamber MEC pilot plant built so far in terms of anodic volume, representing a significant step forward in the scale-up of this technology.

This chapter also aims at conducting, using the experimental long-term results, a preliminary techno-economic analysis of MEC technology to assess its commercial potential. Three key factors will be studied: (i) the revenue generated from hydrogen production, (ii) the costs associated with external electricity consumption, and (iii) the capital expenses required for the MEC construction and implementation.

6.4. Specific experimental procedures and calculations

6.4.1. Reactor design

A comprehensive design and engineering process was undertaken to ensure significant improvements in the configuration and performance of the pilot plant. This design included detailed calculations of reactor dimensions, electrode specifications, hydraulics, and electrical systems. Specialized components that required custom fabrication were workshop-manufactured. The pilot plant was carefully installed and assembled within the WWTP of El Prat de Llobregat (Barcelona, Spain), ensuring proper integration with the existing infrastructure. Before starting-up, comprehensive commissioning and testing procedures were conducted to verify the functionality and performance of all systems and components. A detailed discussion of the reactor design is provided in Section 6.5.1.

6.4.2. MEC operation

6.4.2.1. Performance evaluation with synthetic wastewater

The first experimental trial of the novel cells was carried out at the UAB facilities using a single cassette (Configuration A; Ni-foam cathode (RCM-Ni4753, Recemat BV, The Netherlands). This cell was integrated into the L-MEC pilot plant (Figure 6.2), resulting in most of the tank being the anodic chamber, with a working volume of 193 L.

The anodic chamber was inoculated with anaerobic sludge from the same WWTP and started-up in continuous mode with acetate as sole carbon source, at ΔV = 1.0 V, HRT = 2 d, and OLR = 0.50 g L^{-1} d^{-1}. Following the same strategy as previous experiences, the initial concentration of VSS in the anolyte was 1.5 g L^{-1}. An internal recycle of 200 L d^{-1} was used to improve turbulence in the reactor (i.e. decrease external mass transfer resistance near the biofilm). Both the influent and internal recycle flows were established using two timed peristaltic pumps (520 FAM/R2, Watson Marlow, United Kingdom). The feeding solution was prepared with demineralized water with no extra addition of buffer or nutrients solution and stored in a 120 L tank. The catholyte was a 4 g L^{-1} NaCl solution, it was not renewed during the whole experiment and its pH was measured weekly. These hydraulic conditions were maintained during the whole experiment.

After inoculation, the effect of the ΔV on performance was studied. ΔV was incrementally reduced from 1.40 V to 0.40 V, within 0.10 V intervals. This range was selected to prevent the cell from experiencing excessively high or low potentials, as these could cause irreversible damage. Hydrogen production was measured twice at each ΔV tested. Furthermore, to fully evaluate the resilience of the MEC to low voltage exposure, ΔV was raised back to the highest value tested until the end of the experiment.

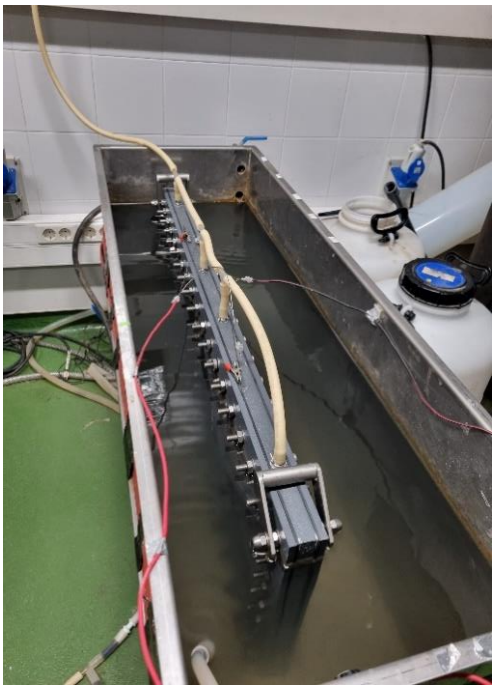

Figure 6.2. Experimental set-up during the performance evaluation of a cassette with synthetic wastewater in the L-MEC.

6.4.2.2. Performance evaluation with real urban wastewater

The second experimental trial of the novel cells was carried out at the WWTP of El Prat de Llobregat (Barcelona, Spain), to evaluate their performance under real operational conditions.

6.4.2.2.1. Stage I

In a first stage, three cells (Configuration A) were integrated into the 1380 L SS tank of the M-MEC (Figure 6.3), resulting in an anodic working volume of 1310 L. The cathodes used in the cassette were Ni-foam (RCM-Ni4753, Recemat BV, The Netherlands) and SS-wool (Steel wool #2, Barlesa SL, Spain) for MEC1-2 and MEC 3, respectively.

The cells were inoculated with UWW in continuous mode and started-up at $\Delta V = 1.0$ V, HRT = 1 d and an OLR ranging between 0.31 – 0.69 g L^{-1} d^{-1}, with an internal recycle of 2000 L d^{-1}. In this case, the initial concentration of VSS in the anolyte ranged between 0.08 – 0.32 g L^{-1} due to the inherent variability of the UWW composition. Throughout the entire experiment, the wastewater was directly pumped from the main collector at the outlet of the primary settlers to the M-MEC without any amendment, except for the addition of acetate (~1.5 kg; final COD concentration = 1415 mg L^{-1}) performed at day 80. The average wastewater composition during Stage I is shown in Table 6.1. The influent stream was equipped with a prefilter (FD246, Ferdom, Poland) to remove large particles that may have not been removed during primary treatment. The influent, effluent and internal recycle were established using three timed peristaltic pumps (520 FAM/R2, Watson Marlow, United Kingdom). The catholyte was a 4 g L^{-1} NaCl solution, it was not renewed during the whole experiment and its pH was measured every two weeks.

Figure 6.3. Experimental set-up during the performance evaluation of three cassettes with urban wastewater in the M-MEC.

6.4.2.2.2. Stage II

In a second stage, the M-MEC capacity was increased to ten cells to further evaluate its performance and stability, resulting in an anodic working volume of 1168 L (Figure 6.4). In this case, all cells were assembled with Ni-foam cathodes (RCM-Ni4753, Recemat BV, The Netherlands), and both cell configurations A and B (Figure 6.5) were studied under different conditions for over 100 days.

The previous start-up strategy was followed and the MEC was inoculated under the same operational conditions as described in Section 6.4.2.2.1. The initial concentration of VSS in the anolyte ranged between 0.08 – 0.32 g L^{-1}. After inoculation, the plant was operated under continuous mode with UWW at ΔV = 1.0 V, under two different HRT: 1 and 2 d. The average wastewater composition during Stage II is shown in Table 6.1. The wastewater was again directly pumped from the main collector at the outlet of the primary settlers without any amendment. The influent, effluent and internal recycle were established using the same timed peristaltic pumps (520 FAM/R2, Watson Marlow, United Kingdom). The same catholyte was used (4 g L^{-1} NaCl solution), it was not renewed during the whole experiment and its pH was measured every two weeks.

Table 6.1. Average characteristics of the urban wastewater during Stage I and II.

Parameter	Stage I	Stage II
COD (mg L^{-1})	509 ± 144	352 ± 105
COD_S (mg L^{-1})	371 ± 103	253 ± 87
Total N (mg L^{-1})	76 ± 6	64 ± 14
$P\text{-}PO_4^{3-}$ (mg L^{-1})	7 ± 3	8 ± 2
SST (mg L^{-1})	187 ± 97	115 ± 59
σ (mS cm^{-1})	2.7 ± 0.2	2.7 ± 0.3
pH	7.5 ± 0.1	7.7 ± 0.1

Figure 6.4. Experimental set-up during the performance evaluation of the M-MEC with ten cassettes with urban wastewater.

Figure 6.5. Comparison of the two cell configurations studied; Left (A) and right (B).

6.4.3. Analytical methods

Liquid and gas samples were analysed following the previously described procedure (see Materials and Methods, Section 3.2). The anodic temperature, pH and conductivity were monitored using the AddControl software. During the first days of Stage 1, temperature values from the average temperature in the primary settlers were considered. Afterwards, the temperature was measured online from the MEC through a thermoresistance (Pt1000, Axiomatic, Spain). pH was measured using a pH probe (HACH pH electrode Crison5335, and conductivity was measured with a conductivity probe (HACH conductivity electrode Crison5388).

6.4.4. KPIs

Reactor performance was evaluated using the previously described KPIs (see Materials and Methods, Section 3.5).

6.4.5. Preliminary techno-economic study

To assess the economic viability of the M-MEC pilot plant, a preliminary techno-economic evaluation was conducted. In addition to the real performance of the MEC, this assessment considered various scenarios including, changes in the applied potential, hydrogen production rates, cathodic and CEs, and replacement costs.

6.4.5.1. Profitability

The profitability of the pilot plant was evaluated through the methodology proposed by (Jiang et al., 2023). Profitability was defined as the ratio of hydrogen revenue (€) to electricity cost (€), as shown in Equation 6.1. The equation was further developed to isolate two different terms, one exclusively related to the MEC performance (hydrogen production per kWh electricity (kg H_2 kWh^{-1})) and the other associated with the market prices (the hydrogen selling price (€ kg^{-1} H_2) and electricity price (€ kWh^{-1})):

$$Profitability = \frac{Revenue\ from\ hydrogen}{Electricity\ cost} = \frac{H_2\ production}{Electricity\ consumption} \cdot \frac{H_2\ selling\ price}{Electricity\ price} \quad (6.1)$$

The kg of hydrogen per kWh electricity was calculated based on the operational performance of the MEC (Equation 6.3):

$$\frac{kg\ H2}{kWh} = \frac{\left(\frac{r_{CAT} \cdot \int_{t_0}^{t_f} I\ dt}{b_{H_2} \cdot F} \frac{M_{H_2}}{1000}\right)}{\left(\int_{t_0}^{t_f} I \cdot \Delta V\ dt \frac{1h}{3600s} \frac{1kWh}{1000VAh}\right)} = \frac{1}{26.8} \cdot \frac{r_{CAT}}{\Delta V} \quad (6.2)$$

The price ratio (PR, Equation 6.3), in kWh kg^{-1}, was defined as the ratio of the hydrogen selling price and the electricity price:

$$PR = \frac{H_2\ selling\ price}{Electricity\ price} \quad (6.3)$$

Combining these terms in equation 6.1, the profitability (dimensionless) was ultimately calculated through equation 6.4:

$$Profitability = \frac{1}{26.8} \cdot \frac{r_{CAT}}{\Delta V} \cdot PR \quad (6.4)$$

6.4.5.2. Treatment cost

The treatment cost was calculated as the ratio of the electricity cost (€) and the treatment capacity (kg of COD removed), as shown in Equation 6.5. Similar to the profitability, the equation was reformulated to isolate two different terms, one exclusively related to the MEC performance (kWh consumed per kg COD removed) and the other associated with the electricity price:

$$Treatment\ cost = \frac{Electricity\ cost}{Treatment\ capacity} = \frac{kWh}{kg\ COD} \cdot Electricity\ price \quad (6.5)$$

The kWh of electricity per kg of COD removed were calculated based on the operational performance of the MEC (Equation 6.6):

$$\frac{kWh}{kg\ COD} = \frac{\left(CE \cdot \left(\frac{M_{O_2}}{1000}\right)^{-1} \cdot b_S \cdot F\right)}{\int_{t_0}^{t_f} I\ dt} \cdot \left(\int_{t_0}^{t_f} I \cdot \Delta V\ dt \cdot \frac{1h}{3600s} \cdot \frac{1kWh}{1000\ VAh}\right) = 3.35 \cdot \Delta V \cdot CE \quad (6.6)$$

Combining Equation 6.5 and 6.6, the treatment cost (€ kg^{-1} COD) was ultimately calculated through Equation 6.7:

$$Treatment\ cost = 3.35 \cdot \Delta V \cdot CE \cdot Electricity\ price \quad (6.7)$$

6.4.5.3. Net present value

The net present value (NPV) was employed to evaluate the economic viability over a hypothetical twenty-year operational lifespan, including a one-year construction phase. It was calculated with Equation 6.8:

$$NPV = \sum_{t=0}^{n} \frac{C_t}{(1+r)^t} \quad (6.8)$$

With t = Time period; Ct = Cash flow in period t; and r = Discount rate (%).

The cash flows represent the net income generated by the system after deducting operating expenses and any additional expenses incurred. These cash flows were estimated considering the initial investment of the pilot plant, the electricity costs and the hydrogen selling revenue. On the other hand, the discount rate represents the investor's minimum acceptable rate of return, also known as the cost of capital. This rate reflects the opportunity cost of investing in the project versus other available options. The discount rate (r) was assumed to be equal to that of the Spanish government, at 2% (https://www.bde.es).

6.5. Results and discussion

6.5.1. Design and construction of the prototype

The M-MEC was based on the cassette-style design previously described by Heidrich (2013,2014), and adapted by Baeza (2017) and Guerrero-Sodric (2023). The reactor included several modifications based on the previous know-how of the group in the

scaling of MECs. As a specific objective of the LIFE+ NIMBUS project, the design volume was set at an order of magnitude higher than the previous scale tested (from 0.135 m^3 to 1 m^3).

In addition to budget constraints, there were several reasons for not increasing the capacity further: i) Scaling up the MEC by an order of magnitude allows for a more gradual increase in the size and complexity of the reactor, which can help to mitigate safety risks; ii) It also allows the collection of data at multiple scales, which can be used to optimize the process and identify potential challenges; iii) Most importantly, there is an important lack of research about the scale-up of BES and there are no experiences with double-chamber MEC reported at such scale, leaving the effect of scaling on performance certainly unknown.

6.5.1.1. Cell design basis

6.5.1.1.1. Dimensioning of the anodes

Once the anodic volume was determined, the design of the cassette was based on maintaining the projected anode surface to volume ratio of the L-MEC (10.9 m^2 m^{-3}), yielding a total anode surface of 10.9 m^2. The work of Cotterill et al. (2017) for the scaling-up of a 175 L MEC pilot plant was also used as a reference during the design process. Their cassettes had a projected anode surface area of 2 m^2 $cell^{-1}$ (1.0 m^2 of anode on each side of the cassette). They tested two reactors of different volumes and cassette sizes but with similar projected anode surface to reactor volume ratio (34 m^2 m^{-3}). Despite considerable proportion of organic matter was removed at a low HRT (COD removal efficiency of 50% at an HRT of 5 h), poor cathodic recoveries were obtained (< 10 %). The smaller MEC exhibited a hydrogen production rate that was four times greater per unit of anode surface area (2.07 compared to 0.52 L m^{-2} d^{-1}). As the author suggested, if this finding indicates a linear decline in the amount of hydrogen gas obtained with a rise in the anode scale, then a 30% more increase in the anodic surface (from 1.0 m^2 to 1.3 m^2) could potentially lead to a module where no gas is produced. This would be in line with Fornero's predictions that scaling from the millilitre to litre scale is the critical challenge (Fornero et al., 2010).

Therefore, the cassette design was not mainly focused on increasing the size of the anodes. Instead, special attention was paid to technical aspects such as reducing the gas

leakages or minimising the overpotential losses. Initially, the possibility of maintaining the same dimensions of the L-MEC cassettes was considered. However, this approach would have required 66 modules to achieve the desired anodic surface, which would significantly introduce complexity to the reactor operation. Therefore, it was decided to increase the anodic surface per cell (i.e. bigger cells and lower number of cells). The challenge was to find the optimal anodic surface area per cell, and thus the number of modules.

The most critical dimension was the height of the cassette, as this limits the reactor depth, which is an unexplored factor in MECs. Water pressure and its effects on the membrane, undesired accumulation of solids and turbulence, are difficult factors to predict based on lab-scale experiences and may have a negative impact on performance. For instance, water pressure at a depth of only 0.85 m was reported to be problematic in an MFC with large air-cathodes (0.62 m^2, (Rossi et al., 2019)). Thus, the height of the cell was maintained at 50 cm as in the L-MEC design, giving a useful height for the anode of around 40 cm (considering the space required for hardware).

The cell length and number of modules were determined to achieve the desired total anodic surface area after evaluating different frame styles designed in AutoCAD®2D/3D software. The final design of the anode frame is shown in Figure 6.6. This version consisted of two pairs of smaller anodes (one in each side of the cell) instead of a pair of large anodes. Each anodic window was divided and supported by an X-bracing frame to prevent membrane and electrode deformations due to water pressure and to ensure sealing. This design offered a total projected anode surface area of 0.73 m^2 per cell (0.18 m^2 per window and two windows per side).

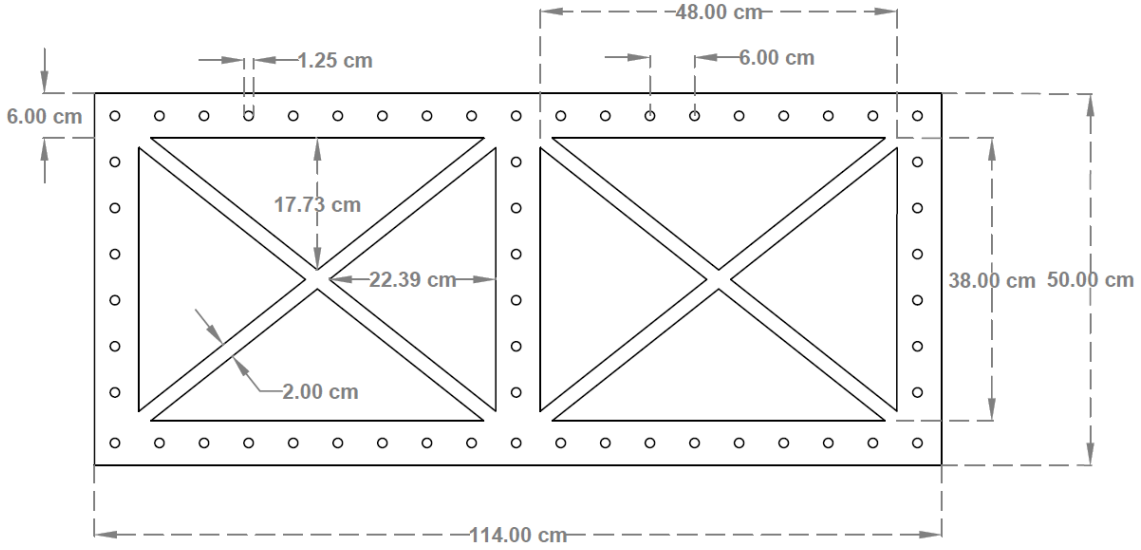

Figure 6.6. Dimensions of the anode frame (external frame).

6.5.1.1.2. Dimensioning of the cathodes

The L-MEC operation with UWW (see Chapter IV) showed that the anode rather than the cathode was the limiting factor due to the low COD concentration of the influent. Thus, it was decided to reduce the thickness of the internal cathode frame compared to that in the L-MEC in view of optimizing the projected anode surface area to cathode volume ratio (m^2 m^{-3}). This would also minimize the cathode overcapacity and reduce the cell overpotential by decreasing the inter-electrode distance.

Two different sizes of internal cathode section were proposed and tested during this thesis: i) Configuration A, with an internal frame thickness of 2.5 cm; ii) Configuration B, with an internal frame thickness of 1.5 cm (Figure 6.5). Both configurations were in line with the anode design and consisted of two cathodic chambers (Figure 6.7), each containing a cathode bounded on each side by an AEM, leaving the corresponding anode on the other side. The total cathodic volume per cell was 9 L in Configuration A and 5.5 L in Configuration B, yielding a projected anode surface area to cathode volume ratio of 80.0 and 133.4 m^2 m^{-3}, respectively (Table 6.2). These values represented an increase of this ratio in 101% and 236% compared to the L-MEC cassette design, which would lead to a more efficient use of the applied potential and a lower cell volume.

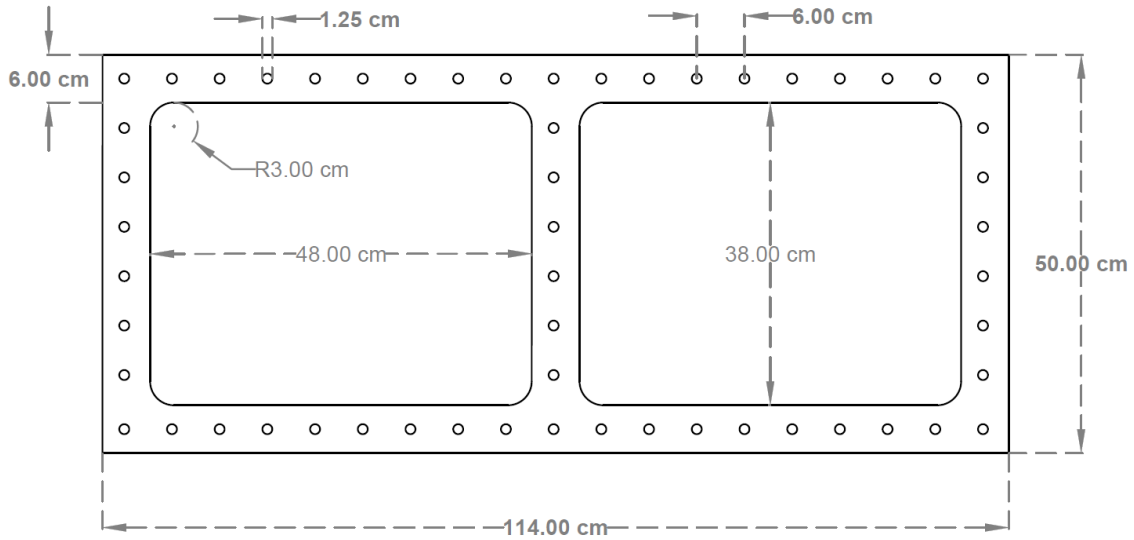

Figure 6.7. Dimensions of the cathode frame (internal frame).

Table 6.2. Design parameters of the L-MEC and the M-MEC.

Parameter	L-MEC	M-MEC (A)	M-MEC (B)
Nº cells	10	15	
Anodic volume (m^3)	0.135	1	
Cassette anodic surface (m^2)	0.16	0.73	
Total anodic surface (m^2)	1.47	10.95	
Anodic surface / Anodic volume ratio (m^2 m^{-3})	10.89	10.95	
Cassette cathodic volume (m^3)	0.004	0.009	0.005
Total cathodic volume (m^3)	0.037	0.137	0.082
Anodic surface / Cathodic volume ratio (m^2 m^{-3})	39.73	80.04	133.41

6.5.1.1.3. Cassette assembly

different components that collectively form each cassette and their description is listed in Table 6.3. The choice of the materials for each component was carefully considered to ensure compatibility, durability, and efficient performance: The PVC frame and ethylene propylene diene monomer (EPDM) gaskets provide structural integrity and prevent leaks; The AEMs have low permeability to methane, allow anions to flow and prevent the mixing of the electrolytes; The carbon felt anodes and SS-wool cathodes offer a balance of cost-effectiveness and performance, while Ni-foam cathodes have the potential to deliver higher current densities; The SS bolts and nuts ensure tight assembly and

corrosion resistance, while the hanging shackles facilitate easy insertion and removal of the cassette; Finally, the SS gas collector minimizes hydrogen leakages.

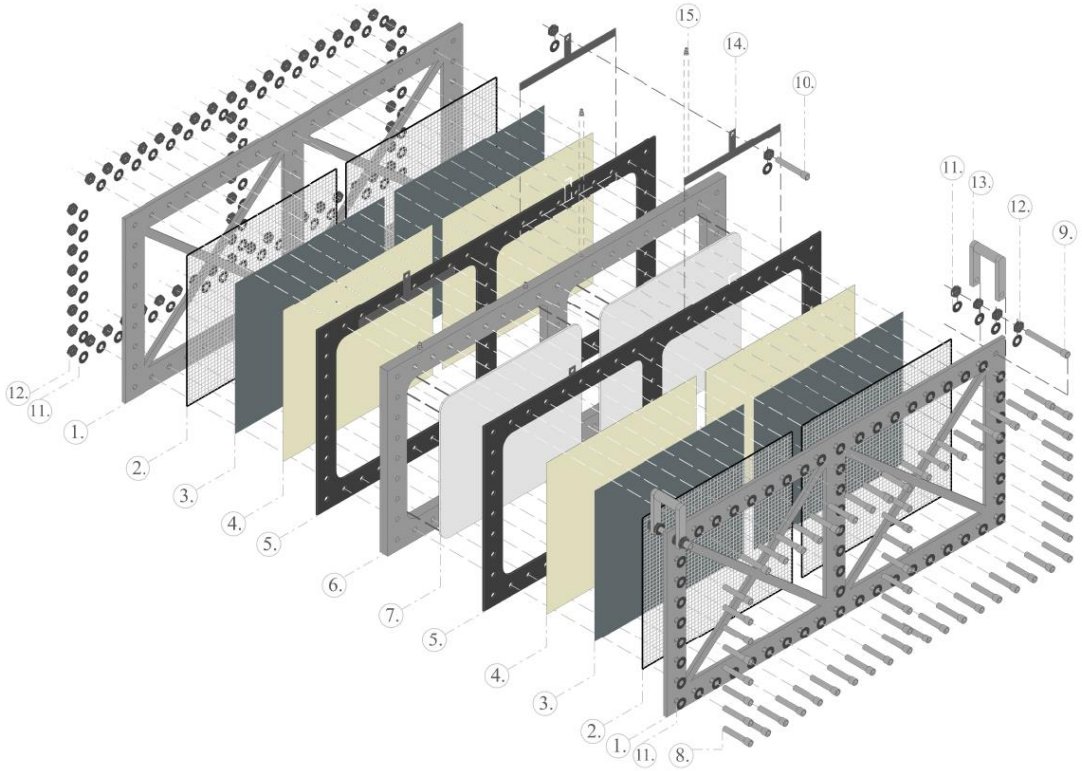

Figure 6.8. Exploded view of the M-MEC cassette prototype.

Table 6.3. Body parts of a M-MEC cassette.

Body part	Description	Material
1	External frame	PVC
2	Anode current collector	SS-316L mesh
3	Anode	Carbon felt
4	Ion exchange membrane	PP AEM
5	Gasket	EPDM
6	Internal frame	PVC
7	Cathode	Ni-foam / SS-304L wool
8	Cassette bolt	SS-316L
9	Shackle bolt	
10	Cathode current collector bolt	
11	Cassette washer	
12	Cassette nut	
13	Hanging shackle	
14	Cathode current collector	
15	Gas collector	

6.5.1.2. Tank design basis

6.5.1.2.1. Hydraulic design parameters

The design inlet and recirculation flowrates were chosen considering the results obtained in the L-MEC treating UWW (see Chapter IV). Two different inlet flowrates and thus, two different HRTs (1 and 2 days), were compared in view of maximizing hydrogen production and optimizing wastewater treatment efficiency. The recirculation flowrate was set to 2000 L d^{-1} to maintain a similar ratio as in the L-MEC.

6.5.1.2.2. Tank sizing

The tank was sized based on the design flowrates and the dimensions of the cassettes. SS 316L was chosen as construction material to prevent the deterioration of the reactor. The design was focused on increasing the Reynolds number of the anolyte compared to that in the L-MEC configuration to improve turbulence, prevent mass transfer limitations, and enhance substrate diffusion into the biofilm (Day et al., 2022; Michie et al., 2014). However, very high liquid velocities can induce the detachment of biofilms due to the increase in the shear stress (τ) (Picioreanu et al., 2001). Specifically, shear forces $\tau \geq 1$ N m^{-2} have been reported to significantly affect biofilm detachment (Ohashi and Harada, 1994).

The optimal liquid velocity was determined through an iterative calculation process testing different channel widths between adjacent cassettes. The minimum practical channel width for this configuration was around 10 cm to prevent the contact of the terminal screws of the different cells, which could lead to short circuits and irreversible damage. Furthermore, the reactor depth was set at 48 cm in all cases (2 cm lower than the height of the cassettes) to prevent direct contact between the anolyte and the electrical connections.

Table 6.4 reports the important parameters obtained during the iterative process and compares them with the L-MEC configuration. The Reynolds numbers are higher in the M-MEC and large enough to consider non-laminar flow regime but low enough that the flow may be non-turbulent. Furthermore, the shear forces are also considerably higher and below the threshold required for significant biofilm detachment (1 N m^{-2}). This a is consequence of the reduction in the channel width, which increases the anolyte velocity between the cassettes.

Table 6.4. Key design parameters of the L-MEC and M-MEC tanks.

Parameter	L-MEC		M-MEC	
HRT (d)	1.1	2.9	1.0	2.0
Q_{IN} (m^3 s^{-1})	1.45E-06	5.32E-07	1.16E-05	5.79E-06
Q_{REC} (m^3 s^{-1})	1.74E-06		3.70E-05	
H (m)	0.44		0.48	
W (m)	0.15		0.10	
v (m s^{-1})	4.82E-05	3.44E-05	1.01E-03	8.92E-04
Re	3.29	1.21	101.27	89.22
τ (N m^{-2})	3.22E-07	2.29E-07	1.01E-05	8.92E-06

Q_{IN}: Inlet flowrate; Q_{REC}: Recirculation flowrate; H: Height of the liquid in the reactor; W_C: Channel width between adjacent cassettes; v: Anolyte velocity; Re: Reynolds number; τ: Shear stress

Another significant improvement over the previous prototype was the implementation of a bottom with a 3% negative slope to effectively collect and discharge any solid particle that had not been removed during the primary treatment. This decision aimed to enhance the CE by preventing the undesired accumulation of biomass that could potentially have microbial activity (i.e. methanogenesis). Therefore, a PES coated fibreglass grating was used to keep the cells standing upright and allow the solids to settle. Figure 6.9 shows the final reactor design, including the 15 cells needed to reach the target anodic surface.

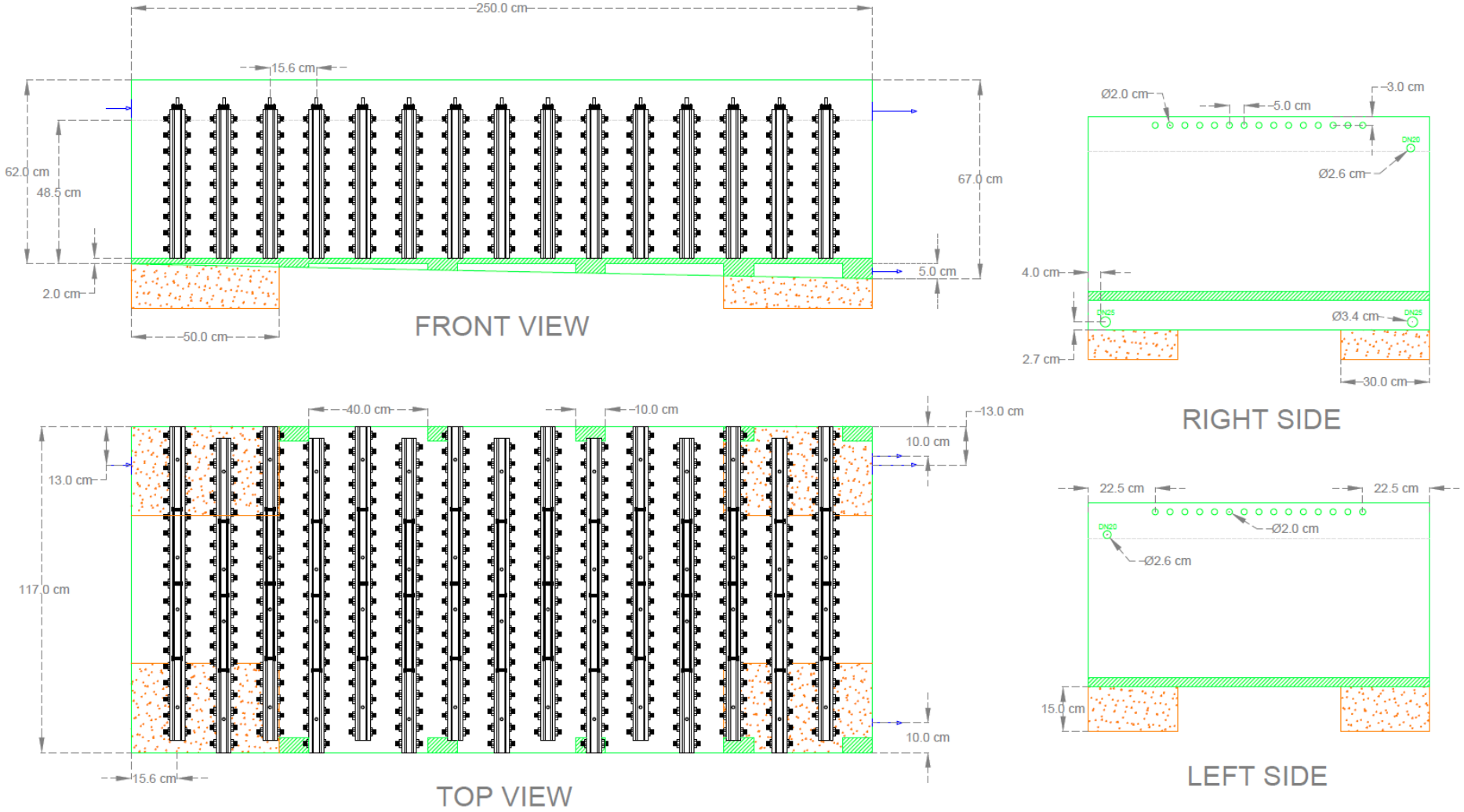

Figure 6.9. Layout of the M-MEC.

6.5.1.3. Construction of the pilot plant

The wastewater composition at different stages of the treatment process was evaluated to select the location of the M-MEC within the WWTP. The most suitable stream was the primary effluent because: i) the wastewater has undergone pre-treatment, removing most of the inorganic particles and some organic compounds that could negatively impact the reactor performance (i.e., foaming), and ii) the concentration of organic matter was higher than in other subsequent steps of the treatment process. Therefore, the M-MEC was located next to the primary settlers. The reactor was located inside a shipping container to protect the plant and instrumentation from adverse weather conditions.

In terms of execution, no civil works were necessary, as an existing concrete slab was used. The technical engineering tasks required to safely perform the mechanical and electrical connections of the pilot plant to the general supply were carried out.

One of the objectives of the MEC pilot plant was to show the feasibility of feeding the hydrogen produced bioelectrochemically to the biomethanation plant in the frame of the LIFE+ NIMBUS project. Due to the distance between the biomethanation unit (BMU) and the M-MEC location (600 meters), it was not possible to establish a continuous connection. Instead, the connection on batch mode was envisaged. Unlike the M-MEC pilot plant, the biomethanation reactor had to be located close to the anaerobic digestors. Figure 6.10 shows the location of the MEC pilot plant and the BMU in the WWTP of El Prat de Llobregat (Barcelona, Spain), and Figure 6.11 shows the actual MEC pilot plant.

.

Figure 6.10. A) Location of the MEC pilot and the BMU in the wastewater treatment plant of El Prat de Llobregat (Barcelona, Spain). B) Detail of the MEC pilot plant location next to the primary settlers.

Figure 6.11. A) Shipping container located next to the primary settlers; B) Monitoring system and power sources; C) M-MEC; and D) Different cassette-type cells placed inside the reactor.

6.5.2. First evaluation of a cassette performance with synthetic wastewater

A preliminary experimental trial using a single cassette (Configuration A) was conducted in the 220 L SS tank of the L-MEC under controlled conditions to evaluate the performance and integrity of the cassettes.

6.5.2.1. Start-up and operation of the MEC

The cell was inoculated with anaerobic sludge from the WWTP of El Prat de Llobregat (Barcelona, Spain) and started-up in continuous mode with acetate as sole carbon source at ΔV = 1.0 V, HRT = 2 d and OLR = 0.50 g L^{-1} d^{-1}, with an internal recycle of 200 L d^{-1}. During this stage, the current intensity displayed an exponential trend, consistent with the previous experiments conducted in the L-MEC. This trend involves an initial lag phase of around 3.5 d and an exponential increase that reaches a plateau after approximately two weeks of operation (Figure 6.12). The maximum current density during inoculation was 0.74 A m^{-2}, and the specific hydrogen production rate was 5.03 L H_2 m^{-2} d^{-1}. Inoculation was finished at day ~13 when stable performance over time was observed.

Afterwards, different ΔVs were tested maintaining the same hydraulic conditions and temperature, to understand the effect of the energy applied on the plant performance. ΔV was incrementally reduced from 1.40 V to 0.40 V in 0.10 V intervals. This range was selected to ensure that the cell was not subjected to excessively high or low potentials that could lead to irreversible damage.

During each ΔV tested, stable current density and hydrogen production over time was observed in the MEC. ΔV was increased again to further assess the cell performance after applying low ΔV. When ΔV was fixed to 1.4 V, current density or hydrogen production rate did not immediately increase. Instead, it took some time for the microbial community to adapt to the higher ΔV and, therefore, current density increased gradually. The remarkable ability of the MEC to maintain its performance (1.02 ± 0.00 A m^{-2} and 8.05 ± 0.00 L H_2 m^{-2} d^{-1}) despite exposure to very low ΔV values suggests that the system possesses a robust resilience that enables it to restore its functional capacity, even under suboptimal ΔV conditions.

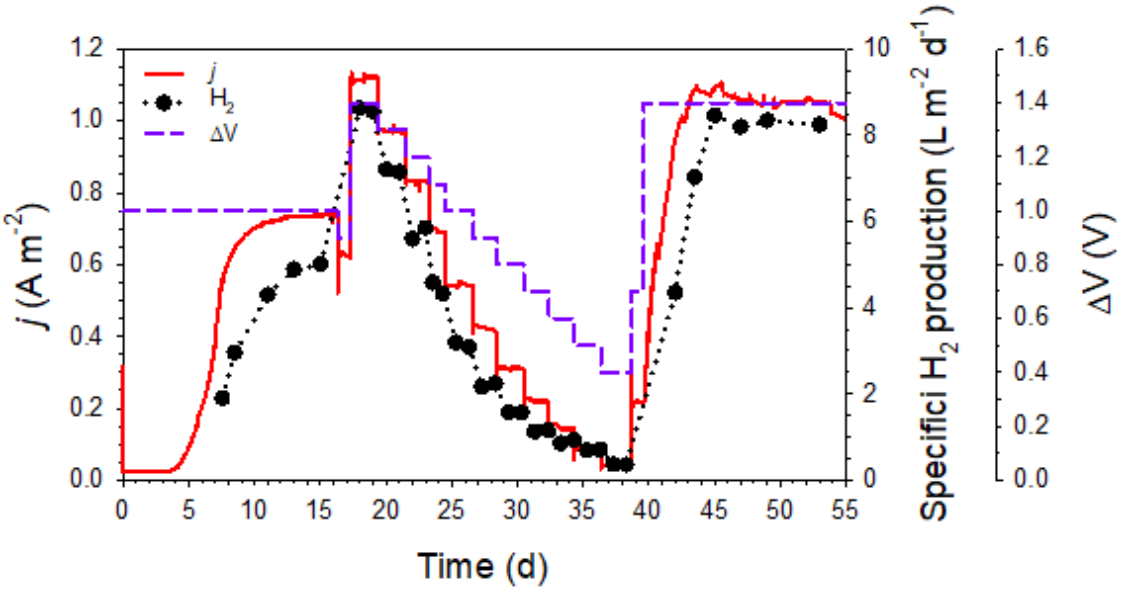

Figure 6.12. Current density (*j*), specific hydrogen production rate and applied potential (ΔV) over time during the preliminary evaluation of a cassette (Configuration A, 2.5 cm).

6.5.2.2. Current density and hydrogen production

The effect of ΔV on hydrogen production and current density is presented in Figure 6.13A. The profiles obtained clearly show a significant impact of the ΔV on the MEC performance, with higher ΔV leading to higher current densities and hydrogen production rates. In contrast to previous studies conducted in the L-MEC (Figure 4.5), no region is observed where current density or hydrogen production rate remains unaffected by the ΔV. This behaviour is likely attributed to the non-limiting substrate conditions under which the MEC operated, which allowed the bioelectrochemical reactions to be mostly dependent on ΔV rather than on COD concentration or external mass transfer rates.

The minimum ΔV requirement to drive HER was 0.40 V, yielding 0.35 ± 0.00 L H_2 m^{-2} d^{-1} and 0.04 ± 0.00 A m^{-2}. Even though hydrogen production was relatively low at this ΔV, it demonstrated that hydrogen can be produced at pilot-scale under low ΔV, which is important for improving the efficiency of the process.

On the other hand, the maximum specific hydrogen production rate was observed at the highest ΔV tested, obtaining 8.59 ± 0.06 L H_2 m^{-2} d^{-1} at ΔV = 1.4 V. Assuming full-operation of the M-MEC with 15 cassettes in the bioreactor (S / V = 10.95 m^2 m^{-3}), under these operational conditions, this configuration could potentially generate up to 0.094 m^3 H_2 m^{-3} d^{-1}.

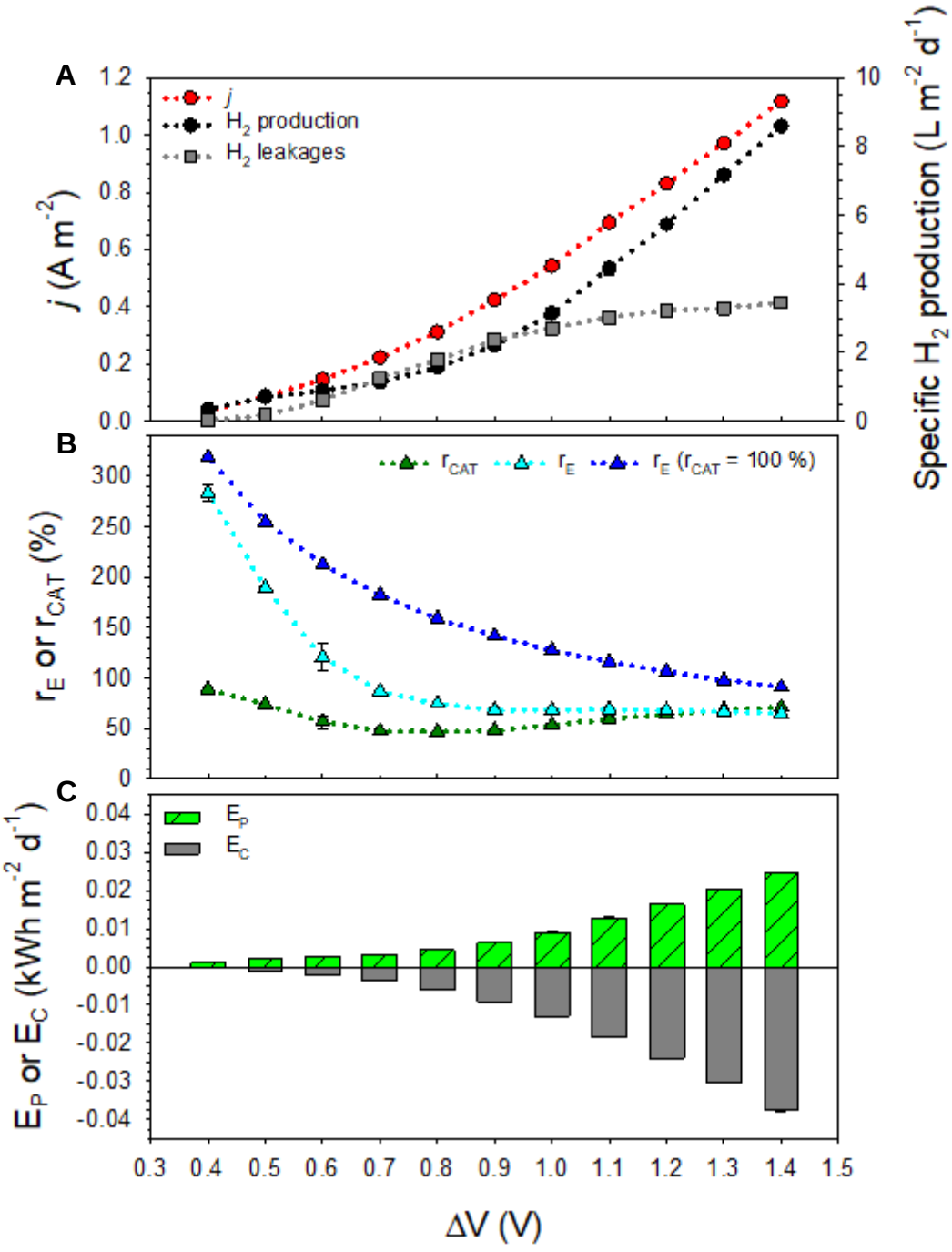

Figure 6.13. Key performance indices of the cassette at different applied potentials (ΔV). A) Current density (*j*), specific hydrogen production rate and estimated hydrogen leakages. B) Cathodic recovery (r_{CAT}), experimental energy recovery (r_E) and theoretical energy recovery (assuming r_{CAT} = 100 %). C) Energy production (E_P) and energy consumption (E_C).

This is a significant outcome of this study since the reported H_2 production rates in double-chamber MEC pilot reactors (>100 L) are usually lower (0.005 - 0.040 m^3 m^{-3} d^{-1}, Guisasola et al., 2020). However, it is important to note that most of these reported volumetric hydrogen production rates were obtained with UWW.

UWW exhibits a more complex composition and lower COD concentration compared to SWW, which hinders the ability of the microbial community to effectively use the organic matter as substrate for hydrogen production. Therefore, the results obtained with the novel cassette cell using SWW further emphasize the potential of MECs for hydrogen production when operating with a more concentrated and readily biodegradable stream.

The high r_E (r_E > 200%) observed at low ΔV (Figure 6.13B), highlights the remarkable potential of MEC to generate hydrogen efficiently since the hydrogen produced contained the double of energy than that required to drive the process. However, r_E decreases as the ΔV increases until 0.9 V, where r_E reaches a plateau around 67 ± 2%. This made obtaining significant E_P inefficient due to increased E_C (Figure 6.13C).

Higher current densities are generally desired as they lead to higher hydrogen production rates. However, it is important to note that the energy efficiency of the MEC decreases with increasing ΔV. Therefore, it is important to find a balance between the current density and energy efficiency in the choice of the optimal ΔV. Balancing the energy input and output, the optimal ΔV for this configuration, under these conditions, was found to be in the range 0.6 - 0.7 V, in which a reasonable hydrogen production can be obtained without sacrificing the energy efficiency of the process.

The hydrogen losses were also significantly influenced by the ΔV. The initial region of the curve (low ΔV) followed a linear relation, whereas the last region was not significantly affected by the ΔV (Figure 6.13A). This resulted in a substantial impact on the r_{CAT}, which decreased importantly until reaching its minimum value at ΔV = 0.8 V (r_{CAT} = 47%). Further, at ΔV > 0.8V, r_{CAT} increased again as hydrogen losses stabilized. It is noteworthy that the hydrogen purity remained above 93% throughout the entire experiment, with less than 2% of methane, indicating that the hydrogen losses could be mainly attributed to leakages and not to biological hydrogen consumption. Hence, the variability of hydrogen leakages over time may be attributed to the existence of potential problems related to pressure variations in the cathode chamber.

Maintaining a constant pressure in the cathode chamber appears to be crucial for achieving efficient hydrogen production and preventing leakages. As hydrogen production rates vary, pressure fluctuations in the cathode chamber can lead to increased leakages, compromising the overall process efficiency. In other terms. hydrogen must be

collected quickly enough to avoid overpressurization of the cathode chamber. To address this challenge, several engineering solutions are proposed:

- Pressure Control Valves: Implementing pressure control valves (PCVs) to regulate the outflow of gas, ensuring that the pressure in the cathode chamber remains within a specified range.
- Pressure Monitoring Systems: Installing pressure monitoring systems to provide real-time data on the pressure fluctuations in the cathode chamber. This allows for timely adjustments of the PCVs or identifying potential leaks before they cause significant losses.
- Diaphragm Seals: Employing diaphragm seals between the cathode chamber and the hydrogen collection system to effectively prevent gas leaks. Diaphragm seals are flexible membranes that provide a gas-tight seal while allowing for controlled gas flow. They can accommodate pressure fluctuations without compromising their sealing integrity.
- Regular Maintenance: Implementing regular maintenance protocols, including leak detection and repair, could proactively address any potential leaks in the cathode chamber and gas collection system before damage is exacerbated. This includes inspecting welds, seals, and gaskets for signs of wear or damage and replacing components as needed.
- Forced extraction of hydrogen: Removing hydrogen from the cathode chamber by forced extraction methods like vacuum pumps can mitigate overpressurization and enable higher production rates (Feng et al., 2018).

By implementing these engineering solutions, the pressure in the cathode chamber could be maintained low, ensuring efficient hydrogen production and minimizing gas leakages. This would improve the overall performance and economic viability of the system. Figure 6.13B shows the r_E considering no hydrogen losses in the system (i.e., r_{CAT} = 100%) and the MEC would yield significant hydrogen production rates with high r_E efficiencies (r_E >100%) under a wide range of ΔV, achieving values as high as r_E = 319% (ΔV = 0.4 V) or 8.96 ± 0.20 L H_2 m^{-2} d^{-1} with r_E = 106% (ΔV = 1.2 V). Thus, addressing gas leakage issues in double-chamber MECs at pilot-scale remains a critical challenge and should be a priority in future scaled-up reactors.

6.5.3. Performance evaluation of the pilot plant with urban wastewater

6.5.3.1. Stage I: Three cells on a real environment

The performance of the cells under real operational conditions was evaluated after the successful experiments with SWW in a controlled environment. Three cells (Configuration A) were operated for over 100 days in the M-MEC under different influent characteristics with UWW. Furthermore, two different cathode materials (already successful in the L-MEC) were evaluated in this real scenario. This comprehensive investigation aimed to assess the long-term stability, efficiency, and adaptability of the cassettes to a real environment.

6.5.3.1.1. Inoculation and start-up of the MEC

The M-MEC was inoculated under continuous mode with UWW at ΔV = 1.0 V, HRT = 1 d and an OLR ranging between 0.31 - 0.69 g L^{-1} d^{-1}, with an internal recycle of 2000 L d^{-1}. Again, the expected exponential current density profile was observed during inoculation in all cells (Figure 6.14). Under these conditions, the start-up was significantly slower than that observed in the laboratory. The cells exhibited a lag phase of ~3.0 d and required over 20 days to stabilize. The longer acclimatation period can be attributed to several factors, including the variability of wastewater properties (e.g., COD content and fractionation, conductivity, temperature, etc.) under real operating conditions and the inoculation strategy (i.e., UWW had lower biomass concentration compared to the anaerobic sludge used in previous experiments). These inherent characteristics of the real wastewater also resulted in a 40% and 30% reduction in current density and hydrogen production, respectively, compared to the results obtained with SWW under controlled conditions (Section 6.5.2). Specifically, the maximum current density during inoculation was observed in the cells with Ni-foam cathodes (MEC 1 - 2), yielding 0.54 A m^{-2} and a specific hydrogen production rate of 3.85 L m^{-2} d^{-1}. In contrast, the current density (0.26 A m^{-2}) and hydrogen production (1.65 L m^{-2} d^{-1}) in the cell with SS-wool cathode (MEC 3), was a 108% and 133% lower, respectively. This represents a lower degree of improvement than in the case of using Ni-foam with high-strength wastewater (Chapter V), mainly due to the limiting properties of UWW.

Unlike previous studies that relied on the addition of acetate or buffer solution to induce exoelectrogenic activity, this work demonstrated the ability of our MEC configuration to establish a functional biofilm directly from real UWW in a relatively short term. The high

recirculation ratio and continuous feeding, combined with the inherent characteristics of the MEC design, enabled the rapid and efficient inoculation of the MEC. This finding is very promising for practical MEC applications, as it eliminates the need for external substrates and simplifies the inoculation process.

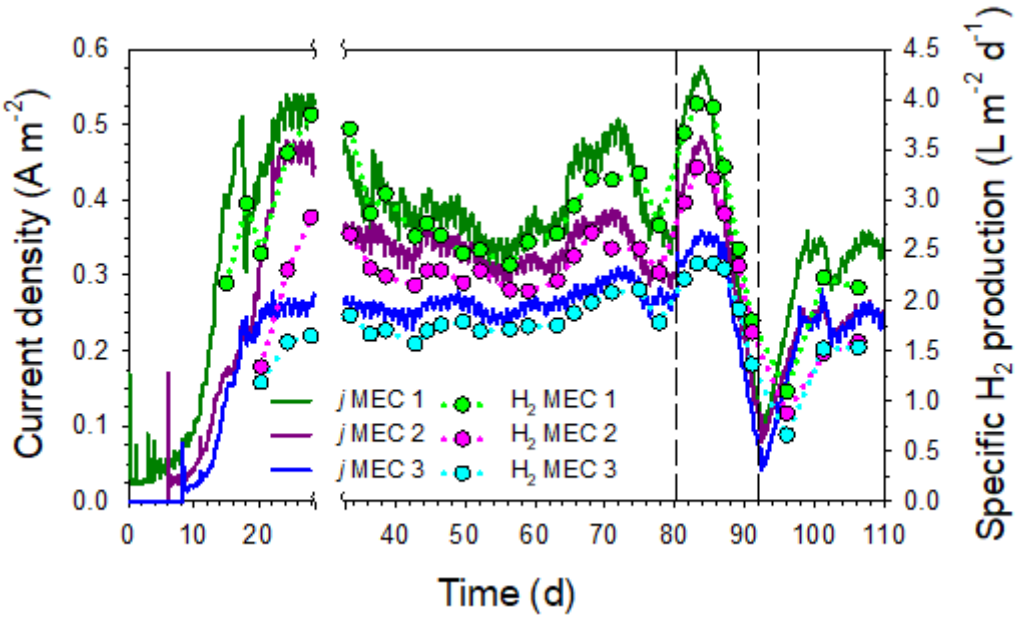

Figure 6.14. Current density (*j*) and specific hydrogen production rate (H_2) during the preliminary evaluation of the cassettes with real wastewater. Dashed lines indicate the start and end time of the batch period.

6.5.3.1.2. Long-term performance

Once semi-stable current density and hydrogen production was obtained, the plant was operated under the previously described hydraulic conditions and ΔV. The organic content of the UWW varied widely during the experiment, ranging from 217 to 595 mg COD L^{-1}. This variability resulted in OLRs in the range of 0.17 to 0.47 g L^{-1} d^{-1}. The water treatment efficiency was generally poor, with an average total COD removal of 22 ± 6 % and a soluble COD removal of 13 ± 4 % (at HRT = 1 d).

Furthermore, CEs lower than 20% were also observed and the maximum efficiency achieved was around 17%. These relatively low values of the KPIs related to wastewater treatment efficiency were expected considering the low HRT imposed and that only three MEC modules were present, limiting the available anodic surface for exoelectrogenic activity and favouring the prevalence of other microorganisms in the reactor.

Temperature variations were a prominent feature throughout the experimental period (Figure 6.15A). The temperature remained below 20°C for the first 70 days of operation, including the initial acclimatisation phase of the microbial community. Subsequently, the temperature gradually increased, reaching a maximum of 27.5°C towards the end of the experiment. This temperature increase was due to the increase in the external temperature and long periods of exposure to direct sunlight. In addition, daily water temperature fluctuations of approximately 1.5°C between day and night were observed during the whole experiment.

It is interesting to note the significant drop in temperature on day 16, which coincided with an unusual snowfall event. The average inlet wastewater temperature dropped to 15°C, with a minimum of 12°C. This abrupt temperature decline had a noticeable impact on the performance of MEC 1, the first inoculated cassette which was still in the exponential growth phase. The current density in MEC 1 decreased from 0.50 A m^{-2} to 0.31 A m^{-2}, reflecting the sensitivity of microbial activity to temperature fluctuations. The effect of this temperature drop was less pronounced in MEC 2-3, as they had recently been inoculated and were still in the early stages of biofilm formation.

Despite the inherent variability in influent characteristics, which impact MEC performance, the current density and hydrogen production in all cells consistently exhibited a relation with temperature (Figure 6.14 and 6.15A). For instance, the average current densities were 0.34 ± 0.02 A m^{-2} in MEC 1, 0.31 ± 0.01 A m^{-2} in MEC 2, and 0.25 ± 0.01 A m^{-2} in MEC 3 at around 18 °C (from day 50 to 60). In contrast, the values around 22 °C (from day 65 to 75), notably increased to 0.46 ± 0.03 A m^{-2} in MEC 1, 0.36 ± 0.02 A m^{-2} in MEC 2, and 0.29 ± 0.01 A m^{-2} in MEC 3. This resulted in an average increase in total hydrogen production of around 45% with only an average increase of 4ºC. On the contrary, the daily temperature fluctuations did not significantly influence the reactor performance, causing less than 5% (3 ± 1%) reduction between the current densities observed during day and night. Nevertheless, the shape of current density profiles closely reflected the daily temperature trend.

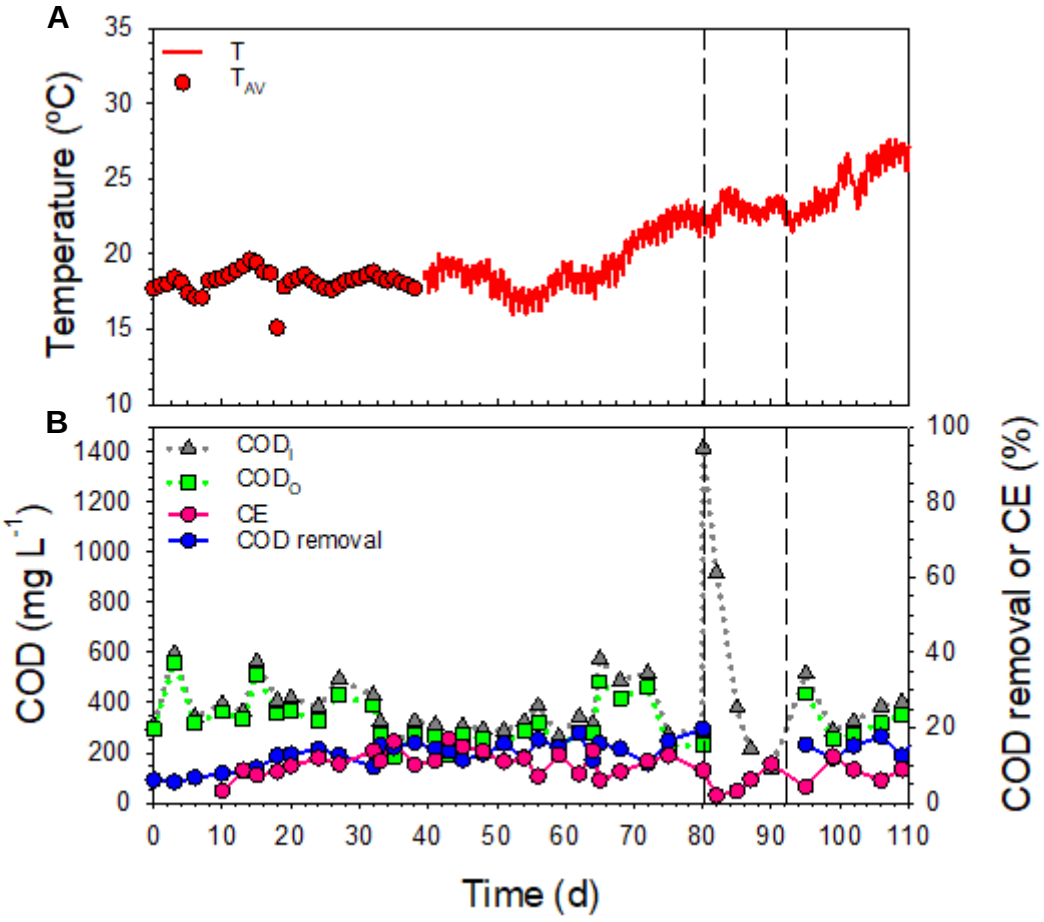

Figure 6.15. A) Average temperature (T_{AV}) and online temperature (T) of the reactor. B) Inlet soluble COD concentration (COD_I), outlet soluble COD concentration (COD_O), coulombic efficiency and soluble COD removal efficiency (COD removal). Dashed lines indicate the start and end time of the batch period.

Continuous hydrogen production was achieved in all cassettes, demonstrating robust operation and stability (Figure 6.14). The volume of gas produced per day remained relatively stable throughout the experimental period despite the inherent variations in wastewater characteristics. The average specific hydrogen production rates were 2.80 ± 0.65 L m^{-2} d^{-1}, 2.25 ± 0.54 L m^{-2} d-1, and 1.77 ± 0.35 L m^{-2} d^{-1}, and the cumulative hydrogen production (Figure 6.16) was 174.27 L, 129.43 L and 100.81 L, for MECs 1, 2, and 3, respectively. These results imply that a fully operational pilot plant equipped with 15 cassettes containing Ni-foam cathodes in the bioreactor (S / V = 10.95 m^2 m^{-3}), could potentially generate up to 0.042 m^3 H_2 m^{-3} d^{-1}. This value is higher than the volumetric hydrogen production rates typically reported in smaller MEC pilot plants fed with UWW (Leicester et al., 2020a). Moreover, these results represent a significant advancement in the scale-up of MECs, since the maximum hydrogen production rate observed in the

L-MEC (135 L) treating UWW at HRT = 1 d was 0.038 m^3 H_2 m^{-3} d^{-1}, validating the successful scale-up of the cassette-style MEC without compromising its performance.

There were no substantial differences in the r_{CAT} between the cells and it remained around 65%, which supports the hypothesis that this KPI in a double-chamber MEC is fundamentally related to the nature of the cells and not significantly influenced by the operational conditions. The r_{CAT} observed are in accordance with the previous experimental trial with SWW, considering a similar hydrogen production rate. On the other hand, r_E was neither variable, achieving an average efficiency of 81 ± 6 %. The peak values of r_E at day 90 (87 %), were related with very low COD concentrations, making current density very poor and, therefore, are not representative of the true performance of the reactor.

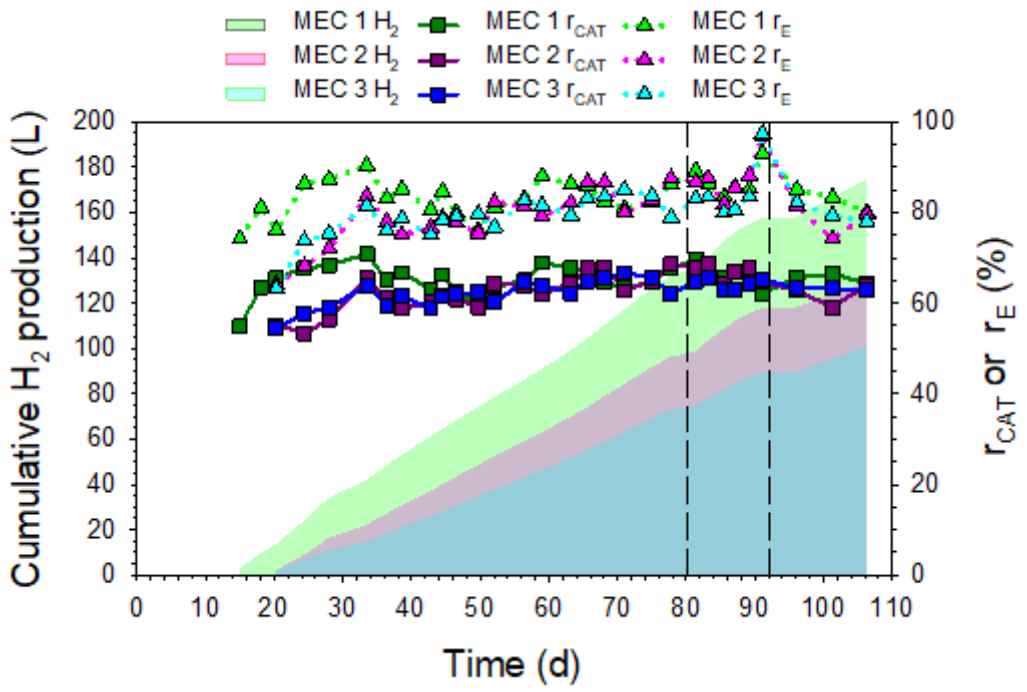

Figure 6.16. Cumulative hydrogen production (H_2), cathodic recovery efficiency (r_{CAT}) and energy recovery efficiency (r_E) during the preliminary evaluation of the cassettes with real wastewater. Dashed lines indicate the start and end time of the batch period.

Between days 80 and 92, the plant was operated in batch mode by increasing the COD concentration up to 1400 mg COD L^{-1} through the addition of concentrated acetate. The aim of this period was to simultaneously improve hydrogen production and to unravel the underlying constraints, whether associated with the anode, the cathode, or the balance between fermenting and exoelectrogenic bacteria. A sudden increase in current density

and hydrogen production was observed in all cells, reaching a peak of 0.56 A m^{-2} and 3.96 L m^{-2} d^{-1} in MEC 1. However, a few days later, the reactor performance began to decrease progressively due to the lower COD concentration, reaching values below 0.15 A m^{-2} (2.00 L H_2 m^{-2} d^{-1}). The total average hydrogen production rate was 2.67 ± 0.77 L m^{-2} d^{-1} and did not vary significantly from that obtained in continuous operation with raw wastewater (2.19 ± 0.63 L m^{-2} d^{-1}). These results are most likely attributed to the restricted ability of exoelectrogens to consume the substrate. The biofilm was adapted to the low substrate levels encountered in continuous operation with UWW, establishing a diverse and specific microbial community tailored to those conditions. The biofilm community under these operational conditions is characterized by a diverse metabolic profile, encompassing hydrolytic, fermentative, exoelectrogenic, and other bacterial species (Montpart et al., 2015). However, when acetate is the sole carbon source, the current density may be limited because the presence of exoelectrogenic bacteria is not sufficient for the new amount of acetate available, whose growth would require a certain period of adaptation to the new operational conditions. In this sense, the biofilm formation could have been limited by the short exposure time to the new feeding conditions, as the fast depletion of COD would have prevented the formation of a stable biofilm enriched in exoelectrogens, resulting in negligible changes in performance. The fact that all cells exhibited reduced performance after the batch operation, even at a higher temperature and similar COD concentration, indicates that there were indeed changes in the biofilm composition, which seems to be in line with this hypothesis.

These findings raise concerns about the performance fluctuations in response to abrupt changes in wastewater characteristics. While the capacity of the biofilm can resist temporary COD peaks, wastewater treatment efficiency could be challenged by significant variations in COD composition or other wastewater properties, since a microbial adaptation of the biofilm would be required. Thus, dealing with wastewater streams with highly variable or unpredictable compositions may present significant challenges for MEC at larger scale.

Table 6.5. Summary of the most important results obtained during Stage I.

				Ni-foam (MEC 1/2)		SS-wool (MEC 3)	
Operational phase	OLR (g COD L^{-1} d^{-1})	ORR (g COD L^{-1} d^{-1})	T (ºC)	j_{max} (A m^{-2})	H_{2max} (L m^{-2} d^{-1})	j_{max} (A m^{-2})	H_{2max} (L m^{-2} d^{-1})
Inoculation t=(0 – 25)	0.43 ± 0.13	0.08 ± 0.03	18 ± 1	0.51 ± 0.05	2.58 ± 1.25	0.28	1.58
Continuous t=(35 – 80)	0.39 ± 0.11	0.09 ± 0.03	19 ± 2	0.45 ± 0.04	3.33 ± 0.72	0.31	2.11
Batch t=(80 – 92)	-	0.14 ± 0.10	23 ± 1	0.53 ± 0.07	3.64 ± 0.45	0.36	2.37
Continuous t=(92-110)	0.40 ± 0.06	0.07 ± 0.02	25 ± 2	0.31 ± 0.05	2.13 ± 0.54	0.20	1.83

6.5.3.2. Stage II: Ten cells on a real environment

After the successful operation of the cassettes under real conditions, the capacity of the pilot plant was increased to ten cells to further evaluate the performance and stability of the M-MEC. The main objective of Stage II was to evaluate hydrogen production and wastewater treatment efficiency operating at a representative capacity for the pilot plant. Both cassette configurations A and B were studied under different conditions for over 100 days.

6.5.3.2.1. Inoculation and start-up of the MEC

Following the previous start-up strategy, the MEC was inoculated under continuous mode with UWW at under the same operational conditions than in Stage I. The initial operation was hampered by intermittent communication failures between the power supplies and the control system, which, despite not affecting the performance of the cells, resulted in the loss of part of the inoculation data. Nonetheless, all cells achieved satisfactory current densities and hydrogen production within a remarkably short period (<10 d). For instance, the last cells inoculated (MEC 8 - 10) exhibited a brief lag phase of just over one day, followed by a fast stabilization of current density profiles within less than a week (Figure 6.17). The inherent presence of exoelectrogenic biomass in the bulk liquid from the previous stage likely contributed to a faster establishment of an active biofilm. Additionally, the operating temperature (>30 °C) also favoured the microbial inoculation process. These high temperatures were a consequence of the summer season and the

specific location of the pilot plant (inside a steel shipping container), which favoured temperature increase and reduced daily temperature fluctuations. Such high temperatures should not be expected when considering integrating MEC technology outdoors.

The maximum average current density during inoculation was 0.38 ± 0.09 A m^{-2} and 0.50 ± 0.09 A m^{-2}, with a specific H_2 production rate of 2.65 ± 0.66 L H_2 m^{-2} d^{-1} and 3.03 ± 0.33 L H_2 m^{-2} d^{-1}, for configuration A and B, respectively. These values are slightly lower than those obtained in Stage I. The influent COD concentration in Stage II was around 50% lower than in Stage I, which limited the exoelectrogenic activity.

6.5.3.2.2. Long-term performance

By day 25 of operation, all cells had established stable performance and exhibited continuous hydrogen production until the end of Stage II. The plant was operated under continuous mode with UWW at ΔV = 1.0 V under two different HRT: 1 and 2 d. The inlet COD_S concentration ranged from 103 to 345 mg L^{-1} (average soluble COD_I = 253 ± 87 mg L^{-1}) and the OLRs were in the range 0.12 – 0.44 g L^{-1} d^{-1}, depending on the hydraulic conditions. The M-MEC showed higher COD removal efficiencies compared to Stage I due to the higher number of modules, yielding an average total COD removal of 34 ± 5 % and a soluble COD removal of 25 ± 6 %. The removal efficiencies increased up to 51 ± 4 % and 45 ± 2 % when operating at HRT = 2 d (Figure 6.18B). Furthermore, CE was boosted, yielding an average efficiency of 31 ± 7 % and 28 ± 4 %, at an HRT of 1 and 2 d, respectively. These results are comparable to the CEs typically reported at pilot-scale (>30 %, (Rousseau et al., 2020)), but still far from the reported at lab-scale with acetate (>70 %, (Guisasola et al., 2020)), which indicates the effect of a more complex microbial community, and that further optimization would be required to favour exoelectrogenic activity over other biological processes, ultimately leading to enhanced CEs. Nonetheless, the operation of the M-MEC at full capacity should be expected to yield slightly higher COD removal efficiencies and CEs, due to the increased anode surface to volume ratio (m^2 m^{-3}). This increased capacity would also result in slightly lower current densities and specific hydrogen production rates (L m^{-2} d^{-1}), as the COD concentration in the reactor would be lower

The temperature profile (Figure 6.18A) exhibited a comparable trend to that observed during the previous phase and according to the ambient temperature fluctuations. A consistent temperature of around 30°C was observed during the first 50 days of operation.

Then, the temperature gradually declined down to 20°C. These temperature variations were also reflected in the observed current density and hydrogen production profiles.

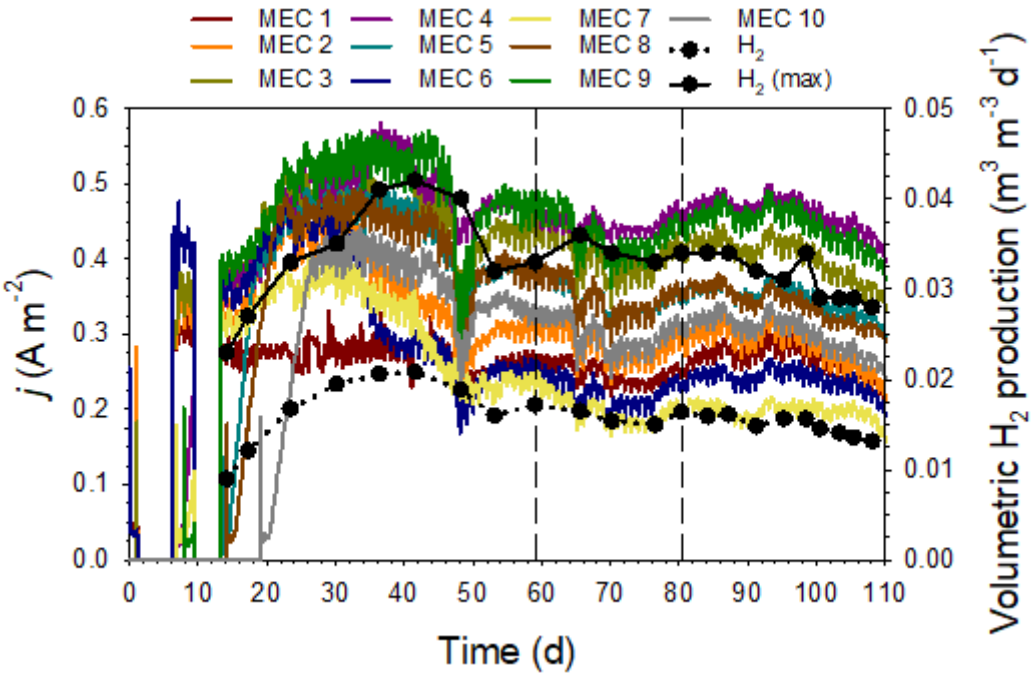

Figure 6.17. Current density (*j*) and volumetric hydrogen production rate (H_2) during the continuous operation of the M-MEC (10 cells) with real wastewater. (H_2 (max)) refers to the estimated volumetric hydrogen production rate considering 15 cells yielding the maximum performance obtained. Dashed lines indicate the start and end time of the continuous operation at HRT = 2 d.

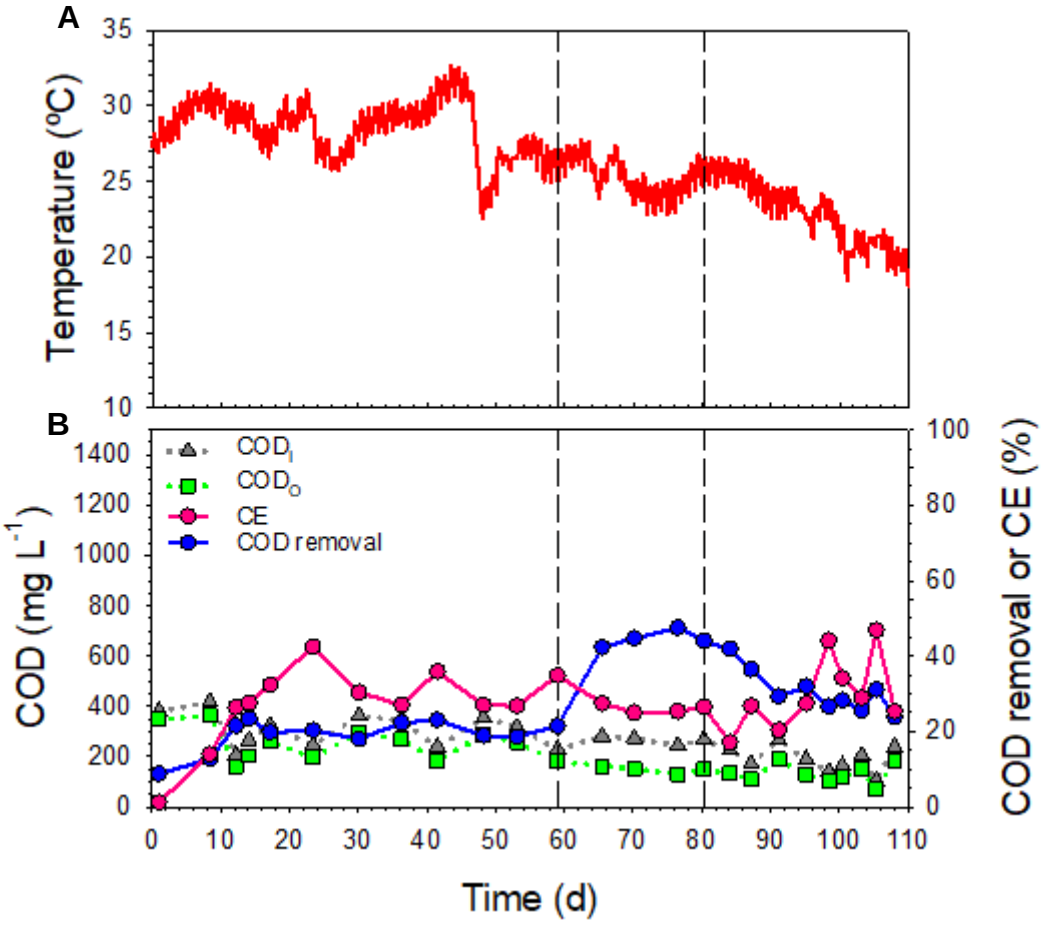

Figure 6.18. Continuous operation of the M-MEC (10 cells) with real wastewater. A) Temperature profile of the reactor. B) Inlet soluble COD concentration (COD_I), outlet soluble COD concentration (COD_O), coulombic efficiency (CE) and soluble COD removal efficiency (COD removal). Dashed lines indicate the start and end time of the continuous operation at an HRT of 2 d.

Again, continuous hydrogen production was achieved in all cassettes, demonstrating robust operation and stability. Specifically, more than 1.5 m^3 of hydrogen with a purity >92% was collected during Stage II (Figure 6.19). In contrast to the COD removal efficiencies, no significant variations in hydrogen production rates were observed between the different HRTs tested. The average volumetric hydrogen production rate was 0.015 ± 0.005 m^3 m^{-3} d^{-1} and the maximum production was 0.021 m^3 H_2 m^{-3} d^{-1} (Figure 6.17). This may be attributed to the influence of the varying temperature in the anolyte or to the fact that COD concentration did not vary importantly, masking the effect of HRT in performance. Specifically, the microbial activity could be more sensitive to the lower temperature rather than to the HRT, as long as there is enough COD in the liquid phase. For instance, the effect of temperature was particularly important around day 50, when

the hydrogen production rate decreased from 0.015 to 0.010 m^3 m^{-3} d^{-1}. Based on these findings, an HRT of 2 days would be considered optimal for reactor operation, as higher COD removal efficiencies would be achieved without compromising hydrogen production.

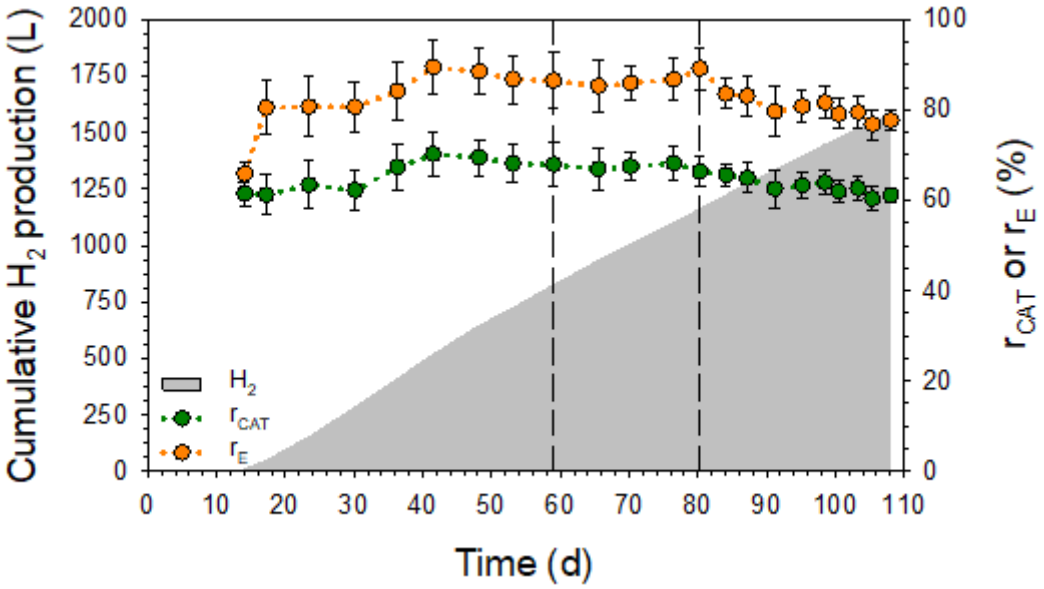

Figure 6.19. Cumulative hydrogen production (H_2), average cathodic recovery (r_{CAT}) and energy recovery (r_E) efficiency, during the continuous operation of the M-MEC. Dashed lines indicate the start and end time of the continuous operation at HRT = 2 d.

The average r_{CAT} and r_E were also stable throughout Stage II, consistently maintaining values around 65% and 80%, respectively (Figure 6.19). The highest r_E (90%) was observed in the cells with configuration B, demonstrating the benefits of this configuration for enhanced r_E. Despite these promising results, energy neutrality was not attained, primarily attributable to the significant hydrogen losses, and the overpotentials and ohmic losses arising from the intrinsic characteristics of UWW and reactor design.

Figure 6.20 compares the performance of configurations A and B during the continuous operation of the M-MEC. Configuration B exhibited better performance than the cells with configuration A during the whole operation, yielding an average current density and hydrogen production of 0.39 ± 0.04 A m^{-2} and 2.69 ± 0.35 L H_2 m^{-2} d^{-1}. This represents a 57% and 53 % increase in current density and hydrogen production compared to configuration A. These improved results were mainly attributed to the reduced inter-electrode distance compared to that used in configuration A, which led to a decrease in the cell overpotential. Considering the possible operation of the M-MEC with 15 cassettes

(Configuration B, S / V = 10.95 m^2 m^{-3}), yielding the maximum current density and hydrogen production observed during the experiment (MEC 4, H_{2max} = 7.29 L m^{-2} d^{-1}), the reactor could potentially generate up to 0.042 m^3 H_2 m^{-3} d^{-1} (Figure 6.17).

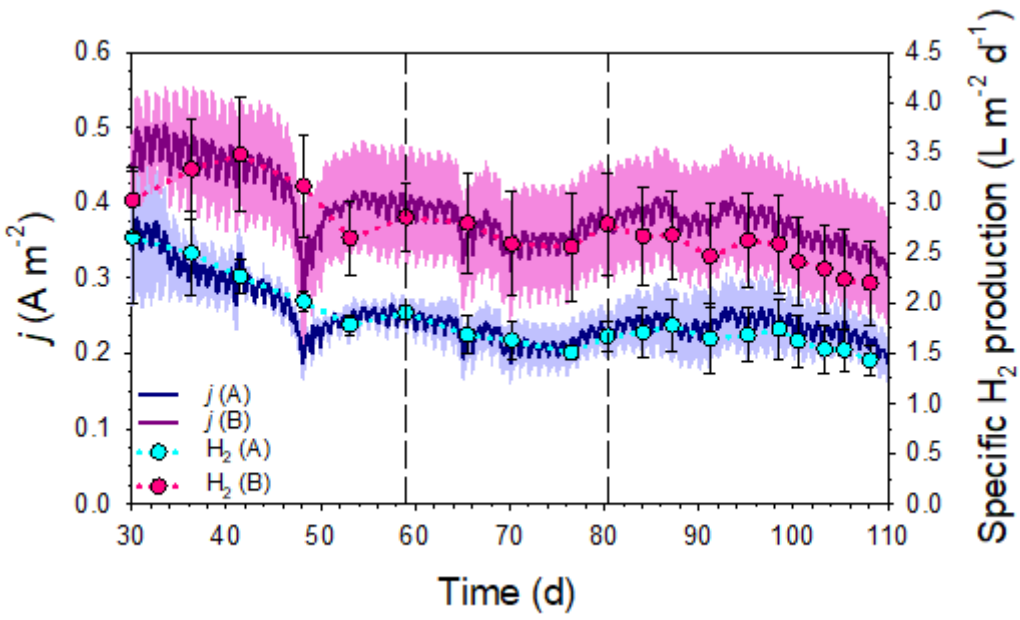

Figure 6.20. Comparison of the current density (*j*) and specific hydrogen production rate (H_2), during the continuous operation of the M-MEC (10 cells) with real wastewater, between configuration A and B. Shade indicates standard deviation of current density. Dashed lines indicate the start and end time of the continuous operation at HRT = 2 d.

Considering the typical hydrogen production rates reported in MEC pilot reactors (>100 L), these results are remarkably promising. The largest MEC reactor to date is the 1000 L single-chamber reactor proposed by Cusick et al. (2011), which was operated for 100 days with winery wastewater but, over the long term, methanogenesis became dominant, consuming the produced hydrogen. Subsequent MEC pilot plant studies have adopted a double-chamber configuration in various reactor architectures to inhibit methanogenesis, demonstrating reasonable performance (Jiang et al., 2023). However, only litre-scale reactors have yielded high hydrogen production rates using real wastewater (>1 m^3 m^{-3} d^{-1}), with reactors larger than 10 L typically producing significantly lower values (>0.1 m^3 m^{-3} d^{-1}). The highest hydrogen production rate reported in a semi pilot-scale MEC (V_{anode} = 10 L) to date, using lignocellulosic hydrolysate as a substrate, was 0.71 m^3 m^{-3} d^{-1} (L. Wang et al., 2021). In double-chamber MECs with anodic volumes larger than 100 L treating UWW, performance further diminishes, yielding hydrogen production rates ranging from 0.005 to 0.038

m^3 H_2 m^{-3} d^{-1} (Cotterill et al., 2017; Guerrero-Sodric et al., 2023). Internal resistance, hydrogen leakages, and the low-strength nature of UWW have been identified as the primary causes of these reduced current densities and hydrogen production rates. In conclusion, the results obtained in the M-MEC pilot are promising, as the reactor was scaled-up without a significant decrease in performance. This demonstrates the potential of the MEC design proposed in this thesis to address the challenges associated with large-scale MEC pilot plants. Currently, further research is needed to bridge the gap between theoretical and practical performance. Specifically, efforts should be directed towards minimizing the internal resistance and hydrogen leakages, which are known to hinder the scalability of MEC technology. Future research should explore the applicability of MEC technology to treating high-strength wastewater streams, where its benefits are most pronounced.

6.5.4. Preliminary techno-economic assessment of the MEC

Assessing the techno-economic viability of MECs is crucial for understanding their market potential and identifying key challenges, but only few studies have addressed this aspect (Aiken et al., 2019, 2021; Jiang et al., 2023; Savla et al., 2021). Considering the results obtained in the M-MEC, a preliminary techno-economic assessment was conducted to evaluate the economic viability of the M-MEC pilot plant under different scenarios.

6.5.4.1. Profitability

The profitability was defined as the ratio of hydrogen revenue and the electricity cost (Equation 6.1-6.5), as proposed by Jiang et al. (2023). Profitability (Equation 6.5) is the product of two terms: i) the kg of hydrogen production per kWh of electricity, and; ii) the ratio of the hydrogen selling price and the electricity price (price ratio, PR, (€ kg^{-1})/(€ kWh^{-1}) = kWh kg^{-1}). When the profitability ratio exceeds 1, the system generates more revenue from hydrogen sales than the cost of electricity consumed in the process. On one hand, the hydrogen production per kWh of electricity input is solely related to the ΔV and the r_{CAT} as the current and time terms cancel out. Specifically, higher r_{CAT} and lower ΔV would lead to increased hydrogen production per kWh of electricity. On the other hand, the price ratio is exclusively linked to the market selling prices of hydrogen and electricity. A low price ratio arises from a combination of low hydrogen

selling price and high electricity price, whereas a high price ratio reflects a high hydrogen selling price and low electricity price.

Based on the hydrogen sales revenue and the electricity consumption costs, profitability was calculated for the different MEC performance reported in Table 6.6. Figure 6.21 shows the results obtained for the different cases evaluated. Considering the current average electricity cost for the industrial sector in Spain (0.1 € kWh^{-1}, (https://www.statista.com/statistics), and the EU's target hydrogen selling price for 2030 (3 € kg^{-1} H_2, (Wurster and Wietschel, 2008)), the price ratio would be 30 kWh kg^{-1} H_2. At this price ratio, the operation of the pilot plant becomes profitable only in the case of treating SWW with low ΔV and high r_{CAT} (Case 4). Under these conditions, profitability was 2.5, i.e., the revenue from the sale of hydrogen would be 2.5 times the cost of electricity. In contrast, the operation of the M-MEC with UWW (Case 1) would not be profitable due to the relatively low r_{CAT} achieved and high ΔV required. This economic inefficiency is not directly correlated to the hydrogen production rate. For instance, the performance with UWW (Case 1) and SWW at ΔV of 1.0 V (Case 5) or 1.4 V (Case 6) revealed significantly different hydrogen yields while maintaining comparable profitability. Nonetheless, considering the actual price of hydrogen (6 - 10 € kg^{-1} H_2, (Panah et al., 2022)), the PR would be around 60 - 100 kWh kg^{-1} H_2, making these three cases become profitable.

Table 6.6. Description of the different cases evaluated to assess profitability in the M-MEC. PR limit refers to the lowest price ratio threshold for a profitability of 1.

Case	Description	PR limit (kWh kg^{-1} H_2)
1	Average performance with UWW (r_{CAT} = 65%; ΔV = 1.0V)	41.23
2	Theoretical performance with acetate (r_{CAT} = 100%; ΔV = 0.123V)	3.30
3	Theoretical performance with acetate (r_{CAT} = 65%; ΔV = 0.123V)	5.07
4	Average performance with acetate (r_{CAT} = 89%; ΔV = 0.4V)	12.04
5	Average performance with acetate (r_{CAT} = 54%; ΔV = 1.0V)	49.63
6	Average performance with acetate (r_{CAT} = 71%; ΔV = 1.4V)	52.85

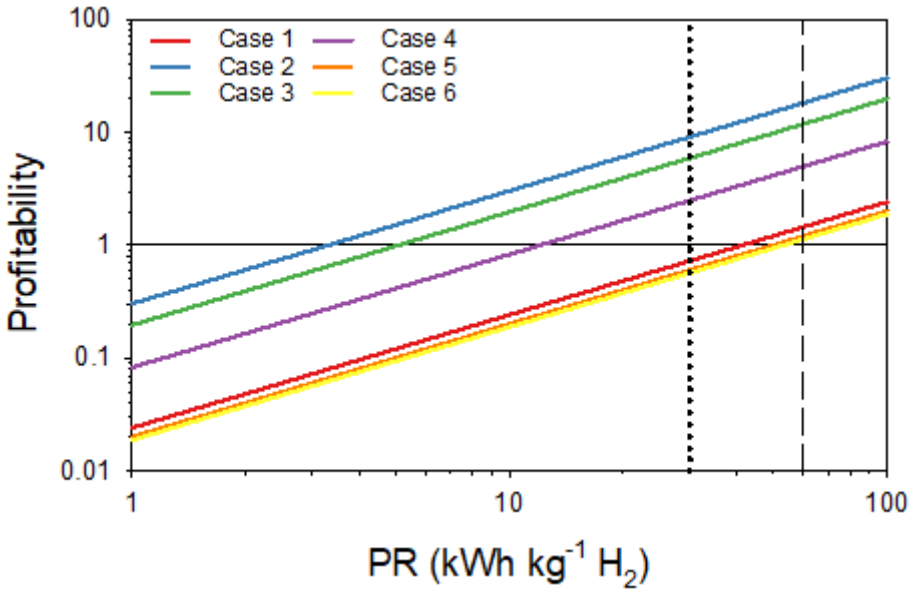

Figure 6.21. Profitability of the M-MEC pilot plant at different price ratios (PR) and different performance cases. Black dashed line indicates the PR yielded by the current price of electricity and the EU's hydrogen target price for 2030. Black dotted line indicates the PR yielded by the current prices of electricity and hydrogen.

The M-MEC should be operated at lower ΔV and hydrogen losses should be minimized to reduce the reliance on market fluctuations. Achieving r_{CAT} close to 100% in double-chamber systems seems to be an exclusively technical/engineering challenge, and therefore achievable, but obtaining significant hydrogen production by applying a low ΔV (i.e. close to the theoretical potential value, 0.123 V) is practically unattainable due to the intrinsic properties of UWW and the voltage losses observed in the reactor. However, a substantial reduction in the ΔV is feasible by improving the reactor design and/or using high-strength or high-conductive wastewaters. Ideal wastewater streams for MECs include those derived from food, beverage, alcohol or biofuel processing, and other similar industries (Chung and Dhar, 2021). In an ideal scenario, where the theoretical potential (ΔV = 0.123 V) is enough to drive HER and no hydrogen losses occur (r_{CAT} = 100%), the PR limit would be very low (3.30 kWh kg^{-1} H_2, Table 6.6), and the M-MEC could potentially generate 10 times more revenue from hydrogen sales than electricity costs. This favourable economic outlook would ensure the profitability of the MEC system across a wide range of PRs, thereby significantly reducing the investment risk associated with its implementation.

6.5.4.2. Treatment cost

The treatment cost was defined as the ratio of the electricity cost and the treatment capacity (Equation 6.6 - 6.9). It was calculated based on the product of two terms: i) the kWh of electricity per kg COD removed, and; ii) the electricity price. The E_C per kg COD removed depends on the performance of the MEC, while the electricity price is only linked to external market-related factors.

Figure 6.22 presents a comparative analysis of the treatment cost of the M-MEC pilot plant under four different performance cases, with detailed descriptions provided in Table 6.7. The results obtained highlight the pivotal role of both CE and ΔV in determining the treatment cost of the MEC technology. Considering the theoretical performance with acetate (Case C), a remarkable 3.7-fold reduction in the treatment cost compared to CAS process would be achieved. Furthermore, 3.75 kWh kg^{-1} COD would be produced under these conditions (considering 33 kWh kg^{-1} H_2, (Dolle et al., 2022)). The treatment cost considering the current performance of the pilot plant with UWW (Case A), would still yield a 2.5-fold decrease in electricity consumption per kg COD removed compared to the reference CAS. A substantial portion of the organic matter removed is not consumed by the exoelectrogenic bacteria (CE = 31%), resulting in lower current density and reduced power consumption. If CE was improved, the current density would increase to treat all the input organic matter under the same ΔV, leading to higher treatment costs when compared to the reference CAS. However, more hydrogen would be generated and, specifically, the net balance would not be affected. As high CE are generally desired, the only viable strategy to reduce the treatment costs of MEC lies in minimizing the ΔV.

Table 6.7. Description of the different cases evaluated to assess the treatment cost in the M-MEC, kWh of electricity consumed per kg COD removed, kg of hydrogen produced per kg COD removed, and kWh of electricity produced per kg COD removed.

Case	Description	kWh kg^{-1} COD	kg H_2 kg^{-1} COD	kWh kg^{-1} COD (33 kWh kg^{-1} H_2)
A	Average performance with UWW (CE = 31%; ΔV = 1.0V)	1.04	0.03	0.21
B	Improved performance with UWW (CE = 100%; ΔV = 1.0V)	3.35	0.08	0.65
C	Theoretical performance with acetate (CE = 100%; ΔV = 0.123V)	0.41	0.13	-3.75
CAS	Reference conventional activated sludge	1.50	0.000	1.50

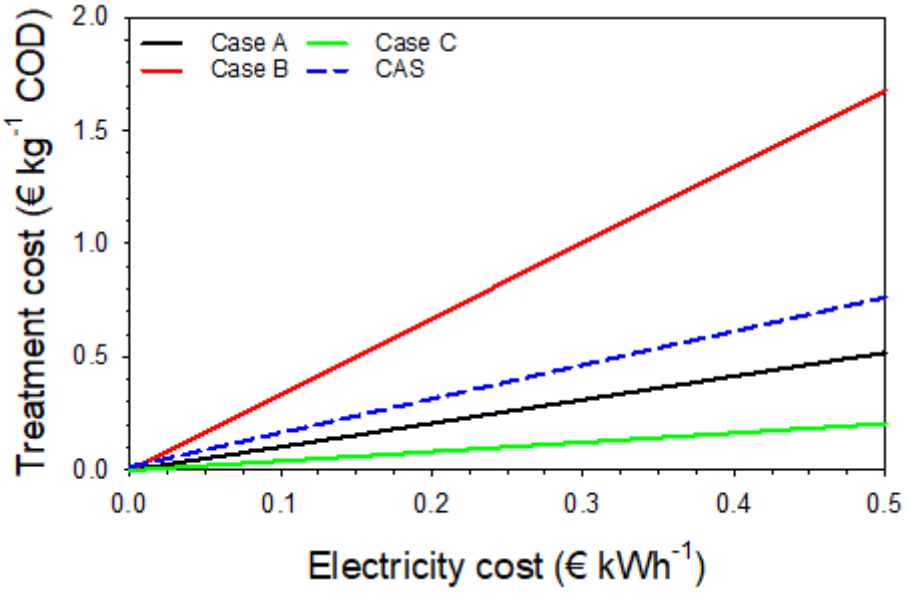

Figure 6.22. Treatment cost of the M-MEC at different electricity prices, for different performance cases. CAS refers to the treatment cost of a reference conventional activated sludge.

6.5.4.3. Net present value

The NPV was employed to evaluate the economic viability of five different scenarios of the M-MEC pilot plant over a hypothetical twenty-year operational lifespan, including a one-year construction phase (Table 6.8). An increase in the NPV is economically favourable for the technology, whereas a decrease detrimental. The five scenarios, ranging from practical to theoretical performance, considered various factors that impact the economic performance of MECs, including hydrogen production rate and its revenue, r_{CAT}, ΔV, maintenance costs, and capital expenses.

Table 6.8. NPV for a 20 year operational period of the M-MEC under different scenarios.

Scenario	Description	NPV
Scenario A	Average performance (H_2 = 0.031 m^3 m^{-3} d^{-1}; r_{CAT} = 65%; ΔV = 1.0V)	-44,132.09 €
Scenario B	Scenario A; annually replacement of AEMs and electrical connections	-72,166.56 €
Scenario C	Maximum performance (H_2 = 0.042 m^3 m^{-3} d^{-1}; r_{CAT} = 65%; ΔV = 1.0V)	-44,135.25 €
Scenario D	Theoretical performance (H_2 = 1 m^3 m^{-3} d^{-1}; r_{CAT} = 100%; ΔV = 0.123V)	-42,745.25 €
Scenario E	Scenario D; 50% reduction on capital expenses	-21,279.25 €

Considering the average performance levels observed in the M-MEC with UWW (Scenario A), the NPV was -44,132.09 €. Even with the pilot plant operating at the theoretical potential, yielding a high hydrogen production of 1 m^3 m^{-3} d^{-1} and a r_{CAT} = 100 % (Scenario D), the NPV did not vary importantly (-42,745.25 €). Furthermore, those scenarios did not contemplate the impact of maintenance costs on the economic viability of the MEC. Some components such as the membranes or the electrical connections could require regular maintenance to ensure optimal performance and prevent system failures. Considering the annual replacement of the membranes and the electrical connections (Scenario B), the NPV decreased down to -72,166.56 €. Only with a significant reduction of the material costs (Scenario E) the NPV was improved. These results highlight the considerable impact of material costs on the economic viability of the MEC.

In fact, the material costs accounted for 99% of the NPV, making the electricity costs and the hydrogen selling revenue negligible in most of the cases. For a 1 m^3 M-MEC operating

at an HRT of 1 d, material costs accounted for 44,123 €, which were considerably higher than the material costs per unit flowrate (< 3000 €/(m^3 d^{-1}) estimated by Aiken et al. (2019). This change is mainly related to the higher costs associated to manufacture the cells. Specifically, the cassette bodies constituted the greatest proportion of the material costs (49%), followed by the control system and instrumentation (23%), and the electrodes and membranes (13%) (Figure 6.23). These components accounted for 85% of total the total costs.

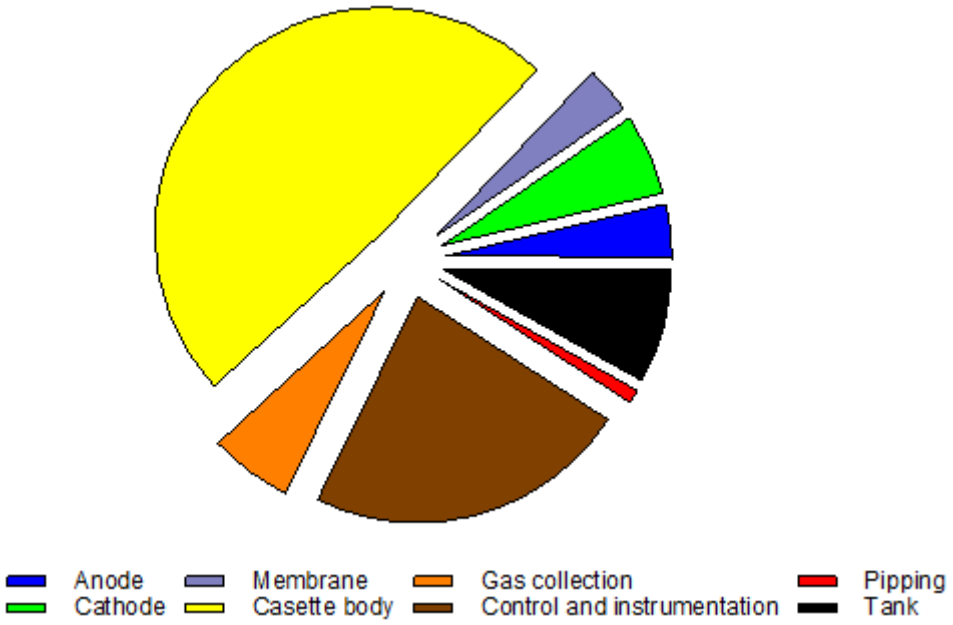

Figure 6.23. Distribution of material costs among major components of a 1 m^3 M-MEC pilot plant.

MECs hold promise as a sustainable and eco-friendly technology for wastewater treatment and hydrogen production. Extensive research has demonstrated that MECs have the potential to achieve energy neutrality, even NE_P, whereas CAS systems typically consume around 0.2 kWh m^{-3} for aeration throughout their whole operational lifespan (Shi, 2011). However, the techno-economic analysis revealed that the high material costs pose a major hurdle in making MECs commercially viable. The capital expenses typically reported for CAS are in the range 350 - 4290 €/(m^3 d^{-1}) (Gao et al., 2022) due to the higher volumetric treatment capacities achieved, representing down to two orders of magnitude lower capital costs compared to MECs. Even at optimal conditions, the NPV of MECs remains very negative because the revenue generated from hydrogen production is negligible compared to the high capital expenses. This huge gap in the initial investment hinders commercial adoption, pointing to the need for research efforts to focus on

developing and implementing cost-effective materials for MEC components, prioritizing affordability over maximizing performance at any cost. This includes exploring alternative materials for cassette bodies, optimizing electrode and membrane fabrication techniques, and employing innovative materials that can enhance performance while reducing costs. Furthermore, the long-term durability of materials remains a critical aspect impacting their commercial viability, yet poorly understood, which limits the identification of the optimal materials for large-scale applications. For instance, electrode dissipation or membrane fouling are major issues in MECs (Fudge et al., 2021), which can potentially result in reduced efficiency and increased maintenance costs. Developing anti-fouling strategies or preventive electrode deterioration techniques could open new avenues for designing robust and efficient MECs that minimize maintenance requirements. Ultimately, standardizing MEC designs and adopting efficient manufacturing techniques for modularization, using recycled materials, could significantly reduce production costs.

6.6. Conclusions

- The novel cassette MEC fed with SWW yielded significant hydrogen production rates under a wide range of ΔV, with higher ΔV leading to higher current densities and hydrogen production rates. Under these conditions, the minimum ΔV requirement to drive the HER (0.35 L H_2 m^{-2}) was 0.4 V, demonstrating that hydrogen production can be produced in a large-scale MEC at a low ΔV. On the other hand, a maximum hydrogen production of was achieved at 1.4 V.
- The operation of the pilot plant with UWW demonstrated the ability to establish functional biofilms directly from UWW, eliminating the need for an initial dosage of suitable external carbon sources and simplifying the inoculation process. Furthermore, continuous hydrogen production was achieved in all cases, demonstrating robust operation and stability, even under temperature variations and changes in influent characteristics. An average total COD removal of 34 ± 5 % and 51 ± 4 % was achieved at an HRT of 1 and 2 days, respectively.
- When comparing SS-wool and Ni-foam cathodes, the maximum specific hydrogen production rates observed with UWW were 2.12 L m^{-2} d^{-1} and 3.45 L m^{-2} d^{-1}, respectively. This represents a lower degree of improvement than in the case of using Ni-foam with high-strength wastewaters.
- Configuration B exhibited an average current density and hydrogen production of 0.39 ± 0.04 A m^{-2} and 2.69 ± 0.35 L H_2 m^{-2} d^{-1}, respectively. This represents a 57% and 53 % increase in current density and hydrogen production compared to configuration A, which is attributed to the lower ohmic losses and overpotentials of the cell.
- Considering the operation of the pilot plant at full capacity (S/V = 10.95 m^2 m^{-3}) and the maximum current density and hydrogen production obtained (7.29 L m^{-2} d^{-1}), the reactor could potentially generate up to 0.042 m^3 H_2 m^{-3} d^{-1}. These results are comparable to those obtained in the L-MEC, demonstrating the successful scale-up of the M-MEC.
- Gas leakages were identified as a significant challenge, potentially compromising the overall process efficiency. Effective management of pressure fluctuations in the cathode chamber could be an important factor for efficient hydrogen production, underscoring the importance of implementing control strategies and proactive maintenance.

- Based on the hydrogen sales revenue and the electricity consumption costs, the pilot plant could be profitable only under very specific conditions. Furthermore, a significant reduction in the treatment cost per unit of COD removed is achieved compared to CAS.
- The high capital expenses associated with MEC components hinder commercial viability, emphasizing the need for cost-effective materials and manufacturing techniques. Material costs represent a 99% of the NPV, overshadowing the benefits of lower electricity costs and the hydrogen revenue.

Chapter VII

General conclusions and future perspectives

7. General conclusions and future perspectives

7.1. General conclusions

The past two decades have witnessed an exponential rise in MECs research, with over 50% of studies published since 2016. However, most of the reports primarily focus on fundamental aspects of bioelectrochemical hydrogen production at laboratory scale, employing readily biodegradable substrates, highly conductive media, and well-controlled operational conditions. The obtained results in terms of current densities and hydrogen production rates were good enough to begin its industrial adoption but, scaling-up BES is not a straightforward issue. This thesis addresses this critical gap by shifting the focus towards pilot-scale MECs for real wastewater treatment applications.

The first objective of the thesis dealt with gaining a comprehensive understanding of key factors influencing pilot-scale MEC performance for wastewater treatment. This included the operation of a 135 L MEC pilot plant under a wide range of operational conditions (temperature, HRT and applied potential), treating wastewaters with diverse loads and testing different materials. Building upon this knowledge, a critical scale-up of a 1 m^3 MEC pilot reactor was conducted within a real WWTP facility. The scale-up performance experimental results were not only used to assess the performance under realistic conditions but also to assess the economic viability of the process. This thesis provides valuable insights towards bridging the gap between lab-scale research and practical MEC implementation. Moreover, several promising avenues were identified for future research to further advance in the development of MECs and contribute to the realization of its full-scale implementation. The most important conclusions of each specific Chapter are detailed below.

Chapter IV critically assesses the operation of a 135 L double-chamber MEC under a wide range of conditions to determine how hydrogen yield and energy efficiency depend on the operational parameters. The experimental outcomes were compared to those from the treatment of 1 m^3 of UWW by MECs and two conventional technologies reported in the literature (CAS/HRAS + AD). The key findings were:

- The MEC pilot plant achieved the best results with SWW, yielding the maximum current density (1.23 A m^{-2}) and hydrogen production (13.40 L d^{-1}, 0.10 m^3 m^{-3} d^{-1} and 10 L m^{-2} d^{-1}) ever reported in a pilot-scale MEC (>100 L).
- Low COD concentration in the UWW limited the plant performance. Specifically, an average hydrogen production of 5.1 ± 0.2 L d^{-1} (0.038 m^3 m^{-3} d^{-1} or 3.9 L m^{-2} d^{-1}) were obtained at HRT = 1 d. These are better results than similar MEC pilot plants treating domestic wastewater.
- High COD removal efficiencies (>60 %) were obtained with UWW under a wide range of operational conditions.
- The double-chamber configuration achieved viable current densities and recovered most of the hydrogen produced (r_{CAT} > 80%).
- The optimum applied potential for this configuration was found to be 0.9 V, far from the theoretical 0.123V.
- Low-moderate temperatures (< 20 ºC) resulted in poor anode-based oxidation but when temperature was increased (> 30 ºC), the fermentation step was improved, and hydrogen production increased from 2.0 to 5.7 L d^{-1}.
- The plant was able to produce 5.1 L H_2 d^{-1} at HRT = 1 d, which was 52% more than that obtained operating at HRT = 4 d. However, lower HRTs resulted in a significant reduction in COD removal (from 77 ± 1% to 30 ± 3%).
- The MEC performance was compared to CAS and HRAS. MEC have the potential to become an alternative to conventional wastewater treatment in terms of r_E, but the limited volumetric treatment capacity hinders its full-scale implementation.

Chapter V evaluates, for the first time at pilot-scale (>100 L), the use of Ni-foam as cathode material in a double-chamber MEC treating IWW. The effect of Ni-foam in current generation and hydrogen production was studied and compared to a cassette operating with SS-wool cathode. The main conclusions were:

- A MEC pilot plant (>100L) can be successfully run with real IWW from the confectionery industry with i) good hydrogen production results (19.07 L m^{-2} d^{-1} and 0.21 m^3 m^{-3} d^{-1}), ii) reasonably high current density (>2 A m^{-2}) and iii) substantial organic matter removal efficiency (>40 %).
- High COD concentration allows high current densities but the CE (around 20 %) shows that other simultaneous organic matter removal processes occur, possibly related to heterotrophic oxidation in the upper layers of the reactor and methanogenesis in the lower part due to anaerobic conditions.
- The novel cassette configuration with a double Ni-foam sheet cathode that offers the best current density and hydrogen production rates observed so far at this scale. The improvement with the novel configuration is 202% over the SS-wool cathode and by 81% over the configuration with only a single Ni-foam sheet. However, the performance gains achieved with Ni-foam do not justify its higher cost .
- The applied potential has two opposite consequences regarding the energy efficiency of the system: on the one hand, higher ΔV imply higher energy requirements but also higher hydrogen (and thus, energy) recovery. A conservative value of 0.9 - 1.0 V was found to be successful for this system.
- The microbial community developed on the anode is a syntrophic culture of exoelectrogens and fermenters (mostly *Geobacter* and *Bacteroides*), which correlates well with the observed exoelectrogenic activity.

Chapter VI shows the scale-up design, construction, and operation of a 1 m^3 MEC pilot to assess its performance under real-conditions. The experimental outcomes obtained were used to evaluate the techno-economic viability of the process and the results were compared with CAS. The main conclusions were:

- The novel cassette MEC fed with SWW yielded significant hydrogen production rates under a wide range of ΔV, with higher ΔV leading to higher current densities and hydrogen production rates. Under these conditions, the minimum ΔV requirement to drive the HER (0.35 L H_2 m^{-2}) was 0.4 V, demonstrating that hydrogen production can be produced in a large-scale MEC at a low ΔV. On the other hand, a maximum hydrogen production of was achieved at 1.4 V.
- The operation of the pilot plant with UWW demonstrated the ability to establish functional biofilms directly from UWW, eliminating the need for an initial dosage of suitable external carbon sources and simplifying the inoculation process. Furthermore, continuous hydrogen production was achieved in all cases, demonstrating robust operation and stability, even under temperature variations and changes in influent characteristics. An average total COD removal of 34 ± 5 % and 51 ± 4 % was achieved at an HRT of 1 and 2 days, respectively.
- When comparing SS-wool and Ni-foam cathodes, the maximum specific hydrogen production rates observed with UWW were 2.12 L m^{-2} d^{-1} and 3.45 L m^{-2} d^{-1}, respectively. This represents a lower degree of improvement than in the case of using Ni-foam with high-strength wastewaters.
- Configuration B exhibited an average current density and hydrogen production of 0.39 ± 0.04 A m^{-2} and 2.69 ± 0.35 L H_2 m^{-2} d^{-1}, respectively. This represents a 57% and 53 % increase in current density and hydrogen production compared to configuration A, which is attributed to the lower ohmic losses and overpotentials of the cell.
- Considering the operation of the pilot plant at full capacity (S/V = 10.95 m^2 m^{-3}) and the maximum current density and hydrogen production obtained (7.29 L m^{-2} d^{-1}), the reactor could potentially generate up to 0.042 m^3 H_2 m^{-3} d^{-1}. These results are comparable to those obtained in the L-MEC, demonstrating the successful scale-up of the M-MEC.
- Gas leakages were identified as a significant challenge, potentially compromising the overall process efficiency. Effective management of pressure fluctuations in

the cathode chamber could be an important factor for efficient hydrogen production, underscoring the importance of implementing control strategies and proactive maintenance.

- Based on the hydrogen sales revenue and the electricity consumption costs, the pilot plant could be profitable only under very specific conditions. Furthermore, a significant reduction in the treatment cost per unit of COD removed is achieved compared to CAS.
- The high capital expenses associated with MEC components hinder commercial viability, emphasizing the need for cost-effective materials and manufacturing techniques. Material costs represent a 99% of the NPV, overshadowing the benefits of lower electricity costs and the hydrogen revenue.

In summary, this thesis represents a significant advancement in the field of MECs by transitioning from small-scale laboratory investigations to larger pilot-scale applications for real-world wastewater treatment scenarios. Through meticulous experimentation and analysis, critical insights have been gained into the operational dynamics, performance characteristics, and economic feasibility of MEC systems across varying scales and conditions. Notably, the examination of pilot-scale MEC performance has revealed key factors influencing hydrogen production, current densities, and the removal of organic matter. The findings underscore the potential of MECs as a sustainable alternative to conventional treatment methods in terms of energy efficiency, under diverse influent characteristics and operational conditions. Despite the promising results, challenges such as scale-up complexities, high capital costs, and process optimization, persist as important areas for further investigation. As the pursuit of sustainable wastewater treatment solutions continues, the insights generated in this thesis serve as a foundational framework for future innovations aimed at realizing the widespread implementation of MEC technology, thus advancing environmental sustainability and resource recovery in wastewater management practices.

7.2. Future perspectives

Based on the insights and findings presented, this section explores potential future directions and challenges to advance MEC technology towards full-scale implementation.

- **Optimizing MEC design and operation:**

  Further efforts are needed to address the limited volumetric treatment capacity hindering full-scale implementation. This could involve exploring novel modular reactor configurations and electrode materials, optimizing hydrodynamics for efficient mass transfer, and investigating alternative operational approaches. Furthermore, strategies to minimize the voltage losses and hydrogen leakages should be identified to enhance the overall energy efficiency of the process.

- **Reducing costs:**

  The high capital cost of MEC components, particularly the body, electrodes, and membranes, hinders their economic viability. Efforts should focus on developing gas-tight cost-effective body parts, alternative electrode materials and membranes with comparable performance but lower costs. Exploring innovative manufacturing processes for MEC components may also contribute to achieve economies of scale and reduce production costs.

- **Integrating MECs into existing wastewater treatment processes:**

  Future research should explore the integration of MECs into existing wastewater treatment processes, considering factors such as influent characteristics, pre-treatment requirements, and compatibility with existing infrastructure. Identifying synergistic interactions between MECs and other treatment processes could further enhance overall treatment efficiency and resource recovery.

- **Expanding applications and resource recovery:** While this thesis focused on hydrogen production, future research should explore the potential of MECs for generating other valuable products. Moreover, integrating MECs with nutrient recovery and water reuse technologies could create sustainable and circular treatment systems, maximizing resource recovery. This could broaden the application scope and economic feasibility of MEC technology.

- **Assessing life cycle assessment and sustainability:** Conducting comprehensive life cycle assessments of MECs based on real data to evaluate their environmental impact and identify potential areas for improvement in terms of resource utilization and sustainability.

- **Policy and regulatory frameworks:** Supportive policy and regulatory frameworks are crucial to incentivize the adoption of innovative technologies like MECs. Future efforts should focus on developing clear guidelines and standards for MEC design, operation, and performance to ensure safety, reliability, and effluent quality.

Chapter VIII

References

References

Aghababaie, M., Farhadian, M., Jeihanipour, A., & Biria, D. (2015). Effective factors on the performance of microbial fuel cells in wastewater treatment–a review. *Environmental Technology Reviews* (Vol. 4, Issue 1, pp. 71–89). Taylor and Francis Ltd. https://doi.org/10.1080/09593330.2015.1077896

Ahn, Y., Im, S., & Chung, J. W. (2017). Optimizing the operating temperature for microbial electrolysis cell treating sewage sludge. *International Journal of Hydrogen Energy*, *42*(45), 27784–27791. https://doi.org/10.1016/j.ijhydene.2017.05.139

Aiken, D. C., Curtis, T. P., & Heidrich, E. S. (2019). Avenues to the financial viability of microbial electrolysis cells [MEC] for domestic wastewater treatment and hydrogen production. *International Journal of Hydrogen Energy*, *44*(5), 2426–2434. https://doi.org/10.1016/j.ijhydene.2018.12.029

Aiken, D. C., Curtis, T. P., & Heidrich, E. S. (2021). The Rational Design of a Financially Viable Microbial Electrolysis Cell for Domestic Wastewater Treatment. *Frontiers in Chemical Engineering*, *3*. https://doi.org/10.3389/fceng.2021.796805

Akimoto, K., Sano, F., & Nakano, Y. (2022). Assessment of comprehensive energy systems for achieving carbon neutrality in road transport. *Transportation Research Part D: Transport and Environment*, *112*. https://doi.org/10.1016/j.trd.2022.103487

Ambler, J. R., & Logan, B. E. (2011). Evaluation of stainless steel cathodes and a bicarbonate buffer for hydrogen production in microbial electrolysis cells using a new method for measuring gas production. *International Journal of Hydrogen Energy*, *36*(1), 160–166. https://doi.org/10.1016/j.ijhydene.2010.09.044

Average monthly electricity wholesale price in Spain from January 2019 to January 2024 https://www.statista.com/statistics/1267552/spain-monthly-wholesale-electricity-price (accessed January 5, 2024)

Baeza, J. A., Martínez-Miró, À., Guerrero, J., Ruiz, Y., & Guisasola, A. (2017). Bioelectrochemical hydrogen production from urban wastewater on a pilot scale. *Journal of Power Sources*, *356*, 500–509. https://doi.org/10.1016/j.jpowsour.2017.02.087

Baeza, J.A., 2022. Advanced Direct Digital Control (AddControl): lessons learned from 20 years of adding control to lab and pilot scale treatment systems, in: 13th IWA Conference on Instrumentation, Control and Automation. ICA 2022. Tsinghua University, Beijing (China), pp. 13–15.

Banco de España, Agregado de tasas de descuento 2023 https://www.bde.es/app/sif/es/publicacion/descuento (accessed December 24, 2023)

Batlle-Vilanova, P., Ganigué, R., Ramió-Pujol, S., Bañeras, L., Jiménez, G., Hidalgo, M., Balaguer, M. D., Colprim, J., & Puig, S. (2017). Microbial electrosynthesis of butyrate from carbon dioxide: Production and extraction. *Bioelectrochemistry*, *117*, 57–64. https://doi.org/10.1016/j.bioelechem.2017.06.004

Boehnke, B., Diering, B., & Zuckut, S. W. (1997). Ab process removes organics and nutrients: Adsorption/bio-oxidation combines high food-to-microorganism ratio efficiency with advanced activated sludge operations. *Water Environment & Technology*, *9*(3), 23–27.

Bond, D. R., & Lovley, D. R. (2003). Electricity production by Geobacter sulfurreducens attached to electrodes. *Applied and Environmental Microbiology*, *69*(3), 1548–1555. https://doi.org/10.1128/AEM.69.3.1548-1555.2003

Bora, A., Mohanrasu, K., Swetha, T. A., Ananthi, V., Sindhu, R., Chi, N. T. L., Pugazhendhi, A., Arun, A., & Mathimani, T. (2022). Microbial electrolysis cell (MEC): Reactor configurations, recent advances and strategies in biohydrogen production. *Fuel*, *328*, 125269.

Borole, A. P., Reguera, G., Ringeisen, B., Wang, Z. W., Feng, Y., & Kim, B. H. (2011). Electroactive biofilms: Current status and future research needs. *Energy and Environmental Science* (Vol. 4, Issue 12, pp. 4813–4834). https://doi.org/10.1039/c1ee02511b

Bowen, E. J., Dolfing, J., Davenport, R. J., Read, F. L., & Curtis, T. P. (2014). Low-temperature limitation of bioreactor sludge in anaerobic treatment of domestic wastewater. *Water Science and Technology*, *69*(5), 1004–1013. https://doi.org/10.2166/wst.2013.821

Busalmen, J. P., Esteve-Nuñez, A., & Feliu, J. M. (2008). Whole cell electrochemistry of electricity-producing microorganisms evidence an adaptation for optimal exocellular electron transport. *Environmental Science and Technology*, *42*(7), 2445–2450. https://doi.org/10.1021/es702569y

Cabrera, J., Irfan, M., Dai, Y., Zhang, P., Zong, Y., & Liu, X. (2021). Bioelectrochemical system as an innovative technology for treatment of produced water from oil and gas industry: A review. *Chemosphere*, *285*. https://doi.org/10.1016/j.chemosphere.2021.131428

Chaurasia, A. K., & Mondal, P. (2022). Enhancing biohydrogen production from sugar industry wastewater using Ni, Ni–Co and Ni–Co–P electrodeposits as cathodes in

microbial electrolysis cells. *Chemosphere*, *286*. https://doi.org/10.1016/j.chemosphere.2021.131728

Chen, J., Xu, W., Wu, X., E, J., Lu, N., Wang, T., & Zuo, H. (2019). System development and environmental performance analysis of a pilot scale microbial electrolysis cell for hydrogen production using urban wastewater. *Energy Conversion and Management*, *193*, 52–63. https://doi.org/10.1016/j.enconman.2019.04.060

Cheng, S., & Logan, B. E. (2011). High hydrogen production rate of microbial electrolysis cell (MEC) with reduced electrode spacing. *Bioresource Technology*, *102*(3), 3571–3574. https://doi.org/10.1016/j.biortech.2010.10.025

Christgen, B., Scott, K., Dolfing, J., Head, I. M., & Curtis, T. P. (2015). An evaluation of the performance and economics of membranes and separators in single chamber microbial fuel cells treating domestic wastewater. *PLoS One*, *10*(8), e0136108.

Cotterill, S. E., Dolfing, J., Jones, C., Curtis, T. P., & Heidrich, E. S. (2017). Low Temperature Domestic Wastewater Treatment in a Microbial Electrolysis Cell with 1 m2 Anodes: Towards System Scale-Up. *Fuel Cells*, *17*(5), 584–592. https://doi.org/10.1002/fuce.201700034

Cusick, R. D., Bryan, B., Parker, D. S., Merrill, M. D., Mehanna, M., Kiely, P. D., Liu, G., & Logan, B. E. (2011). Performance of a pilot-scale continuous flow microbial electrolysis cell fed winery wastewater. *Applied Microbiology and Biotechnology*, *89*(6), 2053–2063. https://doi.org/10.1007/s00253-011-3130-9

Cusick, R. D., Kiely, P. D., & Logan, B. E. (2010). A monetary comparison of energy recovered from microbial fuel cells and microbial electrolysis cells fed winery or domestic wastewaters. *International Journal of Hydrogen Energy*, *35*(17), 8855–8861. https://doi.org/10.1016/j.ijhydene.2010.06.077

Dai, Z., Heidrich, E. S., Dolfing, J., & Jarvis, A. P. (2019). Determination of the Relationship between the Energy Content of Municipal Wastewater and Its Chemical Oxygen Demand. *Environmental Science and Technology Letters*, *6*(7), 396–400. https://doi.org/10.1021/acs.estlett.9b00253

Dange, P., Pandit, S., Jadhav, D., Shanmugam, P., Gupta, P. K., Kumar, S., Kumar, M., Yang, Y.-H., & Bhatia, S. K. (2021). Recent developments in microbial electrolysis cell-based biohydrogen production utilizing wastewater as a feedstock. *Sustainability*, *13*(16), 8796.

Day, J. R., Heidrich, E. S., & Wood, T. S. (2022). A scalable model of fluid flow, substrate removal and current production in microbial fuel cells. *Chemosphere*, *291*. https://doi.org/10.1016/j.chemosphere.2021.132686

de Fouchécour, F., Larzillière, V., Bouchez, T., & Moscoviz, R. (2022). Systematic and quantitative analysis of two decades of anodic wastewater treatment in bioelectrochemical reactors. *Water Research* (Vol. 214). Elsevier Ltd. https://doi.org/10.1016/j.watres.2022.118142

Debabov, V. G. (2008). Electricity from microorganisms. In *Microbiology* (Vol. 77, Issue 2, pp. 123–131). https://doi.org/10.1134/S002626170802001X

Deng, L., Yang, H., Liu, G., Zheng, D., Chen, Z., Liu, Y., Pu, X., Song, L., Wang, Z., & Lei, Y. (2014). Kinetics of temperature effects and its significance to the heating strategy for anaerobic digestion of swine wastewater. *Applied Energy*, *134*, 349–355. https://doi.org/10.1016/j.apenergy.2014.08.027

Dhar, B. R., Elbeshbishy, E., Hafez, H., & Lee, H. S. (2015). Hydrogen production from sugar beet juice using an integrated biohydrogen process of dark fermentation and microbial electrolysis cell. *Bioresource Technology*, *198*, 223–230. https://doi.org/10.1016/j.biortech.2015.08.048

Dolle, C., Neha, N., & Coutanceau, C. (2022). Electrochemical hydrogen production from biomass. *Current Opinion in Electrochemistry* (Vol. 31). Elsevier B.V. https://doi.org/10.1016/j.coelec.2021.100841

Drancourt, M., Bollet, C., Carta, A., & Rousselier, P. (2001). Phylogenetic analyses of Klebsiella species delineate Klebsiella and Raoultella gen. nov., with description of Raoultella ornithinolytica comb. nov., Raoultella terrigena comb. nov. and Raoultella planticola comb. nov. *International Journal of Systematic and Evolutionary Microbiology*, *51*(3), 925–932. https://doi.org/10.1099/00207713-51-3-925

Escapa, A., Gil-Carrera, L., García, V., & Morán, A. (2012). Performance of a continuous flow microbial electrolysis cell (MEC) fed with domestic wastewater. *Bioresource Technology*, *117*, 55–62.

Escapa, A., Mateos, R., Martínez, E. J., & Blanes, J. (2016). Microbial electrolysis cells: An emerging technology for wastewater treatment and energy recovery. from laboratory to pilot plant and beyond. *Renewable and Sustainable Energy Reviews* (Vol. 55, pp. 942–956). Elsevier Ltd. https://doi.org/10.1016/j.rser.2015.11.029

Escapa, A., San-Martín, M. I., Mateos, R., & Morán, A. (2015). Scaling-up of membraneless microbial electrolysis cells (MECs) for domestic wastewater treatment: Bottlenecks and limitations. *Bioresource Technology*, *180*, 72–78. https://doi.org/10.1016/j.biortech.2014.12.096

Faheem, H. H., Tanveer, H. U., Abbas, S. Z., & Maqbool, F. (2021). Comparative study of conventional steam-methane-reforming (SMR) and auto-thermal-reforming (ATR) with their hybrid sorption enhanced (SE-SMR & SE-ATR) and environmentally benign process models for the hydrogen production. *Fuel*, *297*. https://doi.org/10.1016/j.fuel.2021.120769

Fathima, A., Ilankoon, I. M. S. K., Zhang, Y., & Chong, M. N. (2024). Scaling up of dual-chamber microbial electrochemical systems – An appraisal using systems design approach. *Science of the Total Environment* (Vol. 912). Elsevier B.V. https://doi.org/10.1016/j.scitotenv.2023.169186

Feng, H., Huang, L., Wang, M., Xu, Y., Shen, D., Li, N., Chen, T., & Guo, K. (2018). An effective method for hydrogen production in a single-chamber microbial electrolysis by negative pressure control. *International Journal of Hydrogen Energy*, *43*(37), 17556–17561. https://doi.org/10.1016/j.ijhydene.2018.07.197

Fetting, C. (2020). The European green deal. *ESDN Report*, *53*.

Fornero, J. J., Rosenbaum, M., & Angenent, L. T. (2010). Electric power generation from municipal, food, and animal wastewaters using microbial fuel cells. *Electroanalysis* (Vol. 22, Issues 7–8, pp. 832–843). Wiley-VCH Verlag. https://doi.org/10.1002/elan.200980011

Fricke, K., Harnisch, F., & Schröder, U. (2008). On the use of cyclic voltammetry for the study of anodic electron transfer in microbial fuel cells. *Energy & Environmental Science*, *1*(1), 144–147.

Fudge, T., Bulmer, I., Bowman, K., Pathmakanthan, S., Gambier, W., Dehouche, Z., Al-Salem, S. M., & Constantinou, A. (2021). Microbial electrolysis cells for decentralisedwastewater treatment: The next steps. *Water (Switzerland)*, *13*(4). https://doi.org/10.3390/w13040445

Gao, T., Xiao, K., Zhang, J., Xue, W., Wei, C., Zhang, X., Liang, S., Wang, X., & Huang, X. (2022). Techno-economic characteristics of wastewater treatment plants retrofitted from the conventional activated sludge process to the membrane bioreactor process. *Frontiers of Environmental Science and Engineering*, *16*(4). https://doi.org/10.1007/s11783-021-1483-6

Ghaebi Panah, P., Cui, X., Bornapour, M., Hooshmand, R. A., & Guerrero, J. M. (2022). Marketability analysis of green hydrogen production in Denmark: Scale-up effects on grid-connected electrolysis. *International Journal of Hydrogen Energy*, *47*(25), 12443–12455. https://doi.org/10.1016/j.ijhydene.2022.01.254

Gil-Carrera, L., Escapa, A., Carracedo, B., Morán, A., & Gómez, X. (2013). Performance of a semi-pilot tubular microbial electrolysis cell (MEC) under several hydraulic retention times and applied voltages. *Bioresource Technology*, *146*, 63–69. https://doi.org/10.1016/j.biortech.2013.07.020

Gosser, D. K. (1993). *Cyclic voltammetry: simulation and analysis of reaction mechanisms* (Vol. 43). VCH New York.

Gregory, K. B., Bond, D. R., & Lovley, D. R. (2004). Graphite electrodes as electron donors for anaerobic respiration. *Environmental Microbiology*, *6*(6), 596–604. https://doi.org/10.1111/j.1462-2920.2004.00593.x

Guerrero-Sodric, O., Baeza, J. A., & Guisasola, A. (2023). Exploring key operational factors for improving hydrogen production in a pilot-scale microbial electrolysis cell treating urban wastewater. *Chemical Engineering Journal*, *469*. https://doi.org/10.1016/j.cej.2023.144001

Guisasola, A., Baeza, J. A., Marone, A., Trably, É., & Bernet, N. (2020). Opportunities for Hydrogen Production from Urban/Industrial Wastewater in Bioelectrochemical Systems. *Microbial Electrochemical Technologies*, 225–243.

Guo, X. M., Trably, E., Latrille, E., Carrre, H., & Steyer, J. P. (2010). Hydrogen production from agricultural waste by dark fermentation: A review. *International Journal of Hydrogen Energy*, *35*(19), 10660–10673. https://doi.org/10.1016/j.ijhydene.2010.03.008

Guo, Z., Sun, Y., Pan, S. Y., & Chiang, P. C. (2019). Integration of green energy and advanced energy-efficient technologies for municipal wastewater treatment plants. *International Journal of Environmental Research and Public Health* (Vol. 16, Issue 7). MDPI AG. https://doi.org/10.3390/ijerph16071282

Haasz, T., Vilchez, J. J. G., Kunze, R., Deane, P., Fraboulet, D., Fahl, U., & Mulholland, E. (2018). Perspectives on decarbonizing the transport sector in the EU-28. *Energy Strategy Reviews*, *20*, 124–132.

Hasany, M., Mardanpour, M. M., & Yaghmaei, S. (2016). Biocatalysts in microbial electrolysis cells: A review. *International Journal of Hydrogen Energy*, *41*(3), 1477–1493.

Heidrich, E. S., Curtis, T. P., & Dolfing, J. (2011). Determination of the internal chemical energy of wastewater. *Environmental Science and Technology*, *45*(2), 827–832. https://doi.org/10.1021/es103058w

Heidrich, E. S., Dolfing, J., Scott, K., Edwards, S. R., Jones, C., & Curtis, T. P. (2013). Production of hydrogen from domestic wastewater in a pilot-scale microbial electrolysis cell. *Applied Microbiology and Biotechnology*, *97*(15), 6979–6989. https://doi.org/10.1007/s00253-012-4456-7

Heidrich, E. S., Edwards, S. R., Dolfing, J., Cotterill, S. E., & Curtis, T. P. (2014). Performance of a pilot scale microbial electrolysis cell fed on domestic wastewater at ambient temperatures for a 12month period. *Bioresource Technology*, *173*, 87–95. https://doi.org/10.1016/j.biortech.2014.09.083

Holmes, D. E., Nevin, K. P., & Lovley, D. R. (2004). Comparison of 16S rRNA, nifD, recA, gyrB, rpoB and fusA genes within the family Geobacteraceae fam. nov. *International Journal of Systematic and Evolutionary Microbiology*, *54*(5), 1591–1599. https://doi.org/10.1099/ijs.0.02958-0

Hu, H., Fan, Y., & Liu, H. (2008). Hydrogen production using single-chamber membrane-free microbial electrolysis cells. *Water Research*, *42*(15), 4172–4178. https://doi.org/10.1016/j.watres.2008.06.015

Hu, H., Fan, Y., & Liu, H. (2009). Hydrogen production in single-chamber tubular microbial electrolysis cells using non-precious-metal catalysts. *International Journal of Hydrogen Energy*, *34*(20), 8535–8542. https://doi.org/10.1016/j.ijhydene.2009.08.011

Hyun Chung, T., & Ranjan Dhar, B. (2021). A multi-perspective review on microbial electrochemical technologies for food waste valorization. *Bioresource Technology* (Vol. 342). Elsevier Ltd. https://doi.org/10.1016/j.biortech.2021.125950

Ieropoulos, I. A., Greenman, J., Melhuish, C., & Hart, J. (2005). Comparative study of three types of microbial fuel cell. *Enzyme and Microbial Technology*, *37*(2), 238–245. https://doi.org/10.1016/j.enzmictec.2005.03.006

Ishii, S., Suzuki, S., Tenney, A., Norden-Krichmar, T. M., Nealson, K. H., & Bretschger, O. (2015). Microbial metabolic networks in a complex electrogenic biofilm recovered from a stimulus-induced metatranscriptomics approach. *Scientific Reports*, *5*. https://doi.org/10.1038/srep14840

Jadhav, D. A., Park, S.-G., Pandit, S., Yang, E., Abdelkareem, M. A., Jang, J.-K., & Chae, K.-J. (2022). Scalability of microbial electrochemical technologies: Applications and challenges. *Bioresource Technology*, *345*, 126498.

Jayabalan, T., Matheswaran, M., & Naina Mohammed, S. (2019). Biohydrogen production from sugar industry effluents using nickel based electrode materials in

microbial electrolysis cell. *International Journal of Hydrogen Energy*, 17381–17388. https://doi.org/10.1016/j.ijhydene.2018.09.219

Jeremiasse, A. W., Hamelers, H. V. M., Saakes, M., & Buisman, C. J. N. (2010). Ni foam cathode enables high volumetric H2 production in a microbial electrolysis cell. *International Journal of Hydrogen Energy*, *35*(23), 12716–12723. https://doi.org/10.1016/j.ijhydene.2010.08.131

Jiang, J., Lopez-Ruiz, J. A., Bian, Y., Sun, D., Yan, Y., Chen, X., Zhu, J., May, H. D., & Ren, Z. J. (2023). Scale-up and techno-economic analysis of microbial electrolysis cells for hydrogen production from wastewater. *Water Research*, *241*, 120139. https://doi.org/10.1016/j.watres.2023.120139

Jimenez, J., Miller, M., Bott, C., Murthy, S., De Clippeleir, H., & Wett, B. (2015). High-rate activated sludge system for carbon management - Evaluation of crucial process mechanisms and design parameters. *Water Research*, *87*, 476–482. https://doi.org/10.1016/j.watres.2015.07.032

Joo Kim, H., Soo Park, H., Sik Hyun, M., Seop Chang, I., Kim, M., & Hong Kim, B. (2002). *A mediator-less microbial fuel cell using a metal reducing bacterium, Shewanella putrefaciens*. www.elsevier.com/locate/enzmictec

Kadier, A., Simayi, Y., Chandrasekhar, K., Ismail, M., & Kalil, M. S. (2015). Hydrogen gas production with an electroformed Ni mesh cathode catalysts in a single-chamber microbial electrolysis cell (MEC). *International Journal of Hydrogen Energy*, *40*(41), 14095–14103. https://doi.org/10.1016/j.ijhydene.2015.08.095

Khiewwijit, R., Temmink, H., Rijnaarts, H., & Keesman, K. J. (2015). Energy and nutrient recovery for municipal wastewater treatment: How to design a feasible plant layout? *Environmental Modelling and Software*, *68*, 156–165. https://doi.org/10.1016/j.envsoft.2015.02.011

Ki, D., Popat, S. C., & Torres, C. I. (2016). Reduced overpotentials in microbial electrolysis cells through improved design, operation, and electrochemical characterization. *Chemical Engineering Journal*, *287*, 181–188. https://doi.org/10.1016/j.cej.2015.11.022

Kim, K. Y., & Logan, B. E. (2019). Nickel powder blended activated carbon cathodes for hydrogen production in microbial electrolysis cells. *International Journal of Hydrogen Energy*, *44*(26), 13169–13174. https://doi.org/10.1016/j.ijhydene.2019.04.041

Kim, N., Choi, Y., Jung, S., & Kim, S. (2000). Effect of initial carbon sources on the performance of microbial fuel cells containing Proteus vulgaris. *Biotechnology and Bioengineering*, *70*(1), 109–114.

Kokko, M., Epple, S., Gescher, J., & Kerzenmacher, S. (2018). Effects of wastewater constituents and operational conditions on the composition and dynamics of anodic microbial communities in bioelectrochemical systems. *Bioresource Technology* (Vol. 258, pp. 376–389). Elsevier Ltd. https://doi.org/10.1016/j.biortech.2018.01.090

Komemoto, K., Lim, Y. G., Nagao, N., Onoue, Y., Niwa, C., & Toda, T. (2009). Effect of temperature on VFA's and biogas production in anaerobic solubilization of food waste. *Waste Management*, *29*(12), 2950–2955. https://doi.org/10.1016/j.wasman.2009.07.011

Koók, L., Bakonyi, P., Harnisch, F., Kretzschmar, J., Chae, K. J., Zhen, G., Kumar, G., Rózsenberszki, T., Tóth, G., Nemestóthy, N., & Bélafi-Bakó, K. (2019). Biofouling of membranes in microbial electrochemical technologies: Causes, characterization methods and mitigation strategies. *Bioresource Technology* (Vol. 279, pp. 327–338). Elsevier Ltd. https://doi.org/10.1016/j.biortech.2019.02.001

Korth, B., Maskow, T., Günther, S., & Harnisch, F. (2017). Estimating the Energy Content of Wastewater Using Combustion Calorimetry and Different Drying Processes. *Frontiers in Energy Research*, *5*. https://doi.org/10.3389/fenrg.2017.00023

Kronenberg, M., Trably, E., Bernet, N., & Patureau, D. (2017). Biodegradation of polycyclic aromatic hydrocarbons: Using microbial bioelectrochemical systems to overcome an impasse. *Environmental Pollution* (Vol. 231, pp. 509–523). Elsevier Ltd. https://doi.org/10.1016/j.envpol.2017.08.048

Kumar, G., Bakonyi, P., Zhen, G., Sivagurunathan, P., Koók, L., Kim, S.-H., Tóth, G., Nemestóthy, N., & Bélafi-Bakó, K. (2017). Microbial electrochemical systems for sustainable biohydrogen production: surveying the experiences from a start-up viewpoint. *Renewable and Sustainable Energy Reviews*, *70*, 589–597.

Kumar, R., Singh, L., Wahid, Z. A., & Din, M. F. M. (2015). Exoelectrogens in microbial fuel cells toward bioelectricity generation: A review. *International Journal of Energy Research* (Vol. 39, Issue 8, pp. 1048–1067). John Wiley and Sons Ltd. https://doi.org/10.1002/er.3305

Kundu, A., Sahu, J. N., Redzwan, G., & Hashim, M. A. (2013). An overview of cathode material and catalysts suitable for generating hydrogen in microbial electrolysis cell.

International Journal of Hydrogen Energy (Vol. 38, Issue 4, pp. 1745–1757). https://doi.org/10.1016/j.ijhydene.2012.11.031

Larrosa-Guerrero, A., Scott, K., Head, I. M., Mateo, F., Ginesta, A., & Godinez, C. (2010). Effect of temperature on the performance of microbial fuel cells. *Fuel*, *89*(12), 3985–3994. https://doi.org/10.1016/j.fuel.2010.06.025

Lee, H. S., Vermaas, W. F. J., & Rittmann, B. E. (2010). Biological hydrogen production: Prospects and challenges. *Trends in Biotechnology* (Vol. 28, Issue 5, pp. 262–271). https://doi.org/10.1016/j.tibtech.2010.01.007

Leicester, D., Amezaga, J., & Heidrich, E. (2020a). Is bioelectrochemical energy production from wastewater a reality? Identifying and standardising the progress made in scaling up microbial electrolysis cells. *Renewable and Sustainable Energy Reviews* (Vol. 133). Elsevier Ltd. https://doi.org/10.1016/j.rser.2020.110279

Leicester, D. D., Amezaga, J. M., Moore, A., & Heidrich, E. S. (2020b). Optimising the hydraulic retention time in a pilot-scale microbial electrolysis cell to achieve high volumetric treatment rates using concentrated domestic wastewater. Molecules, 25(12), 2945.

Leong, J. X., Daud, W. R. W., Ghasemi, M., Liew, K. Ben, & Ismail, M. (2013). Ion exchange membranes as separators in microbial fuel cells for bioenergy conversion: A comprehensive review. *Renewable and Sustainable Energy Reviews* (Vol. 28, pp. 575–587). https://doi.org/10.1016/j.rser.2013.08.052

Li, J., Li, H., Fu, Q., Liao, Q., Zhu, X., Kobayashi, H., & Ye, D. (2017). Voltage reversal causes bioanode corrosion in microbial fuel cell stacks. *International Journal of Hydrogen Energy*, *42*(45), 27649–27656.

Liang, D. W., Peng, S. K., Lu, S. F., Liu, Y. Y., Lan, F., & Xiang, Y. (2011). Enhancement of hydrogen production in a single chamber microbial electrolysis cell through anode arrangement optimization. *Bioresource Technology*, *102*(23), 10881–10885. https://doi.org/10.1016/j.biortech.2011.09.028

Lide, D. R. (2004). *CRC Handbook of Chemistry and Physics* (Vol. 85). CRC press.

Liu, H., Grot, S., & Logan, B. E. (2005a). Electrochemically assisted microbial production of hydrogen from acetate. *Environmental Science and Technology*, *39*(11), 4317–4320. https://doi.org/10.1021/es050244p

Liu, M., Yuan, Y., Zhang, L. X., Zhuang, L., Zhou, S. G., & Ni, J. R. (2010). Bioelectricity generation by a Gram-positive Corynebacterium sp. strain MFC03

under alkaline condition in microbial fuel cells. *Bioresource Technology*, *101*(6), 1807–1811. https://doi.org/10.1016/j.biortech.2009.10.003

Logan, B. E. (2008). *Microbial fuel cells*. John Wiley & Sons.

Logan, B. E., Call, D., Cheng, S., Hamelers, H. V. M., Sleutels, T. H. J. A., Jeremiasse, A. W., & Rozendal, R. A. (2008). Microbial electrolysis cells for high yield hydrogen gas production from organic matter. *Environmental Science and Technology* (Vol. 42, Issue 23, pp. 8630–8640). https://doi.org/10.1021/es801553z

Logan, B. E., Hamelers, B., Rozendal, R., Schröder, U., Keller, J., Freguia, S., Aelterman, P., Verstraete, W., & Rabaey, K. (2006). Microbial fuel cells: Methodology and technology. *Environmental Science and Technology* (Vol. 40, Issue 17, pp. 5181–5192). https://doi.org/10.1021/es0605016

Logan, B. E., & Regan, J. M. (2006). Electricity-producing bacterial communities in microbial fuel cells. *Trends in Microbiology* (Vol. 14, Issue 12, pp. 512–518). https://doi.org/10.1016/j.tim.2006.10.003

Logan, B. E., Zikmund, E., Yang, W., Rossi, R., Kim, K. Y., Saikaly, P. E., & Zhang, F. (2018). Impact of Ohmic Resistance on Measured Electrode Potentials and Maximum Power Production in Microbial Fuel Cells. *Environmental Science and Technology*, *52*(15), 8977–8985. https://doi.org/10.1021/acs.est.8b02055

Lovley, D. R. (2006). Bug juice: Harvesting electricity with microorganisms. *Nature Reviews Microbiology* (Vol. 4, Issue 7, pp. 497–508). Nature Publishing Group. https://doi.org/10.1038/nrmicro1442

Lovley, D. R., Giovannoni, S. J., White, D. C., Champine, J. E., Phillips, E. J. P., Gorby, Y. A., & Goodwin, S. (1993). Geobacter metallireducens gen. nov. sp. nov., a microorganism capable of coupling the complete oxidation of organic compounds to the reduction of iron and other metals. *Archives of Microbiology*, *159*, 336–344.

Lu, L., Hou, D., Fang, Y., Huang, Y., & Ren, Z. J. (2016). Nickel based catalysts for highly efficient H2 evolution from wastewater in microbial electrolysis cells. *Electrochimica Acta*, *206*, 381–387. https://doi.org/10.1016/J.ELECTACTA.2016.04.167

Lu, L., & Ren, Z. J. (2016). Microbial electrolysis cells for waste biorefinery: A state of the art review. *Bioresource Technology* (Vol. 215, pp. 254–264). Elsevier Ltd. https://doi.org/10.1016/j.biortech.2016.03.034

Mahadevan, S., Erfle, J. D., & Sauer, F. D. (1980). Degradation of Soluble and Insoluble Proteins by Bacteroides Amylophilus Protease and by Rumen Microorganisms.

Journal of Animal Science, *50*(4), 723–728. https://doi.org/10.2527/JAS1980.504723X

Metcalf & Eddy. (2003). *Wastewater Engineering: Treatment and Reuse* (4th ed.). McGraw-Hill.

Michie, I. S., Kim, J. R., Dinsdale, R. M., Guwy, A. J., & Premier, G. C. (2014). The influence of anodic helical design on fluid flow and bioelectrochemical performance. *Bioresource Technology*, *165*(C), 13–20. https://doi.org/10.1016/j.biortech.2014.03.069

Molinos-Senante, M., Hernandez-Sancho, F., & Sala-Garrido, R. (2014). Benchmarking in wastewater treatment plants: A tool to save operational costs. *Clean Technologies and Environmental Policy*, *16*(1), 149–161. https://doi.org/10.1007/s10098-013-0612-8

Montpart, N., Rago, L., Baeza, J. A., & Guisasola, A. (2015). Hydrogen production in single chamber microbial electrolysis cells with different complex substrates. *Water Research*, *68*, 601–615. https://doi.org/10.1016/j.watres.2014.10.026

Nimje, V. R., Chen, C. Y., Chen, C. C., Jean, J. S., Reddy, A. S., Fan, C. W., Pan, K. Y., Liu, H. T., & Chen, J. L. (2009). Stable and high energy generation by a strain of Bacillus subtilis in a microbial fuel cell. *Journal of Power Sources*, *190*(2), 258–263. https://doi.org/10.1016/j.jpowsour.2009.01.019

Obileke, K. C., Nwokolo, N., Makaka, G., Mukumba, P., & Onyeaka, H. (2021). Anaerobic digestion: Technology for biogas production as a source of renewable energy—A review. *Energy and Environment* (Vol. 32, Issue 2, pp. 191–225). SAGE Publications Inc. https://doi.org/10.1177/0958305X20923117

Ohashi, A., & Harada, H. (1994). Adhesion strength of biofilm developed in an attached-growth reactor. *Water Science and Technology*, *29*(10), 281–288.

Osset-Álvarez, M., Rovira-Alsina, L., Pous, N., Blasco-Gómez, R., Colprim, J., Balaguer, M. D., & Puig, S. (2019). Niches for bioelectrochemical systems on the recovery of water, carbon and nitrogen in wastewater treatment plants. *Biomass and Bioenergy*, *130*. https://doi.org/10.1016/j.biombioe.2019.105380

Pakenas, L. J. (1995). *Energy efficiency in municipal wastewater treatment plants: technology assessment*. New York State Energy Research and Development Authority.

Pant, D., Singh, A., Van Bogaert, G., Gallego, Y. A., Diels, L., & Vanbroekhoven, K. (2011). An introduction to the life cycle assessment (LCA) of bioelectrochemical

systems (BES) for sustainable energy and product generation: Relevance and key aspects. *Renewable and Sustainable Energy Reviews* (Vol. 15, Issue 2, pp. 1305–1313). https://doi.org/10.1016/j.rser.2010.10.005

Parameswaran, P., Torres, C. I., Lee, H. S., Krajmalnik-Brown, R., & Rittmann, B. E. (2009). Syntrophic interactions among anode respiring bacteria (ARB) and non-ARB in a biofilm anode: Electron balances. *Biotechnology and Bioengineering*, *103*(3), 513–523. https://doi.org/10.1002/bit.22267

Paraskeva, P., & Diamadopoulos, E. (2006). Technologies for olive mill wastewater (OMW) treatment: A review. *Journal of Chemical Technology and Biotechnology* (Vol. 81, Issue 9, pp. 1475–1485). https://doi.org/10.1002/jctb.1553

Park, D. H., And, †, & Zeikus, J. G. (1999). Utilization of Electrically Reduced Neutral Red by Actinobacillus succinogenes: Physiological Function of Neutral Red in Membrane-Driven Fumarate Reduction and Energy Conservation. In *JOURNAL OF BACTERIOLOGY* (Vol. 181, Issue 8). https://journals.asm.org/journal/jb

Patil, S. A., Hägerhäll, C., & Gorton, L. (2012). Electron transfer mechanisms between microorganisms and electrodes in bioelectrochemical systems. *Bioanalytical Reviews* (Vol. 4, Issues 2–4, pp. 159–192). Springer-Verlag Wien. https://doi.org/10.1007/s12566-012-0033-x

Pham, T. H., Boon, N., Aelterman, P., Clauwaert, P., De Schamphelaire, L., Vanhaecke, L., De Maeyer, K., Höfte, M., Verstraete, W., & Rabaey, K. (2008). Metabolites produced by Pseudomonas sp. enable a Gram-positive bacterium to achieve extracellular electron transfer. *Applied Microbiology and Biotechnology*, *77*(5), 1119–1129. https://doi.org/10.1007/s00253-007-1248-6

Picioreanu, C., Van Loosdrecht, M. C. M., & Heijnen, J. J. (2001). Two-dimensional model of biofilm detachment caused by internal stress from liquid flow. *Biotechnology and Bioengineering*, *72*(2), 205–218. https://doi.org/10.1002/1097-0290

Postgate, J. R., & Leon Campbell, L. (1966). *Classification of DesulJovibrio Species, the Nonsporulating Sulfate-reducing Bacteria* (Vol. 30, Issue 4). https://journals.asm.org/journal/br

Potter, M. C. (1911). Electrical effects accompanying the decomposition of organic compounds. *Proceedings of the Royal Society of London. Series b, Containing Papers of a Biological Character*, *84*(571), 260–276.

Rago, L., Baeza, J. A., & Guisasola, A. (2016). Increased performance of hydrogen production in microbial electrolysis cells under alkaline conditions. *Bioelectrochemistry*, *109*, 57–62.

Rago, L., Baeza, J. A., & Guisasola, A. (2017). Bioelectrochemical hydrogen production with cheese whey as sole substrate. *Journal of Chemical Technology and Biotechnology*, *92*(1), 173–179. https://doi.org/10.1002/jctb.4987

Rago, L., Ruiz, Y., Baeza, J. A., Guisasola, A., & Cortés, P. (2015). Microbial community analysis in a long-term membrane-less microbial electrolysis cell with hydrogen and methane production. *Bioelectrochemistry*, *106*, 359–368. https://doi.org/10.1016/j.bioelechem.2015.06.003

Recio-Garrido, D., Perrier, M., & Tartakovsky, B. (2016). Modeling, optimization and control of bioelectrochemical systems. *Chemical Engineering Journal* (Vol. 289, pp. 180–190). Elsevier. https://doi.org/10.1016/j.cej.2015.11.112

Reguera, G., McCarthy, K. D., Mehta, T., Nicoll, J. S., Tuominen, M. T., & Lovley, D. R. (2005). Extracellular electron transfer via microbial nanowires. *Nature*, *435*(7045), 1098–1101. https://doi.org/10.1038/nature03661

Rey-Martínez, N., Barreiro-López, A., Guisasola, A., & Baeza, J. A. (2021). Comparing continuous and batch operation for high-rate treatment of urban wastewater. *Biomass and Bioenergy*, *149*. https://doi.org/10.1016/j.biombioe.2021.106077

Rice, E. W., Bridgewater, L., & Association, A. P. H. (2012). *Standard methods for the examination of water and wastewater* (Vol. 10). American public health association Washington, DC.

Rosenblueth, M., Martínez, L., Silva, J., & Martínez-Romero, E. (2004). Klebsiella variicola, A Novel Species with Clinical and Plant-Associated Isolates. In *System. Appl. Microbiol* (Vol. 27). http://www.elsevier-deutschland.de/syapm

Rossi, R., Jones, D., Myung, J., Zikmund, E., Yang, W., Gallego, Y. A., Pant, D., Evans, P. J., Page, M. A., Cropek, D. M., & Logan, B. E. (2019). Evaluating a multi-panel air cathode through electrochemical and biotic tests. *Water Research*, *148*, 51–59. https://doi.org/10.1016/j.watres.2018.10.022

Rossi, R., Wang, X., & Logan, B. E. (2020). High performance flow through microbial fuel cells with anion exchange membrane. *Journal of Power Sources*, *475*. https://doi.org/10.1016/j.jpowsour.2020.228633

Rousseau, R., Etcheverry, L., Roubaud, E., Basséguy, R., Délia, M. L., & Bergel, A. (2020). Microbial electrolysis cell (MEC): Strengths, weaknesses and research needs

from electrochemical engineering standpoint. *Applied Energy* (Vol. 257). Elsevier Ltd. https://doi.org/10.1016/j.apenergy.2019.113938

Rozendal, R. A., Hamelers, H. V. M., Euverink, G. J. W., Metz, S. J., & Buisman, C. J. N. (2006). Principle and perspectives of hydrogen production through biocatalyzed electrolysis. *International Journal of Hydrogen Energy*, *31*(12), 1632–1640.

Rozendal, R. A., Hamelers, H. V. M., Molenkamp, R. J., & Buisman, C. J. N. (2007). Performance of single chamber biocatalyzed electrolysis with different types of ion exchange membranes. *Water Research*, *41*(9), 1984–1994. https://doi.org/10.1016/j.watres.2007.01.019

Rozendal, R. A., Hamelers, H. V. M., Rabaey, K., Keller, J., & Buisman, C. J. N. (2008). Towards practical implementation of bioelectrochemical wastewater treatment. *Trends in Biotechnology*, *26*(8), 450–459.

Ruiz Lozano, L. (2021). *Economic models to optimize green hydrogen production with a PV farm in Spain. Case study for a solar 50MW site with an H2 electrolyzer on site*.

Savla, N., Suman, Pandit, S., Verma, J. P., Awasthi, A. K., Sana, S. S., & Prasad, R. (2021). Techno-economical evaluation and life cycle assessment of microbial electrochemical systems: A review. *Current Research in Green and Sustainable Chemistry* (Vol. 4). Elsevier B.V. https://doi.org/10.1016/j.crgsc.2021.100111

Selembo, P. A., Merrill, M. D., & Logan, B. E. (2009). The use of stainless steel and nickel alloys as low-cost cathodes in microbial electrolysis cells. *Journal of Power Sources*, *190*(2), 271–278. https://doi.org/10.1016/j.jpowsour.2008.12.144

Selembo, P. A., Merrill, M. D., & Logan, B. E. (2010). Hydrogen production with nickel powder cathode catalysts in microbial electrolysis cells. *International Journal of Hydrogen Energy*, *35*(2), 428–437. https://doi.org/10.1016/j.ijhydene.2009.11.014

Sharma, P., Pandey, A. K., Kim, S. H., Singh, S. P., Chaturvedi, P., & Varjani, S. (2021). Critical review on microbial community during in-situ bioremediation of heavy metals from industrial wastewater. *Environmental Technology and Innovation*, *24*. https://doi.org/10.1016/j.eti.2021.101826

Shi, C. Y. (2011). *Mass flow and energy efficiency of municipal wastewater treatment plants*. IWA Publishing.

Shi, L., Richardson, D. J., Wang, Z., Kerisit, S. N., Rosso, K. M., Zachara, J. M., & Fredrickson, J. K. (2009). The roles of outer membrane cytochromes of Shewanella and Geobacter in extracellular electron transfer. *Environmental Microbiology*

Reports (Vol. 1, Issue 4, pp. 220–227). https://doi.org/10.1111/j.1758-2229.2009.00035.x

Shiva Kumar, S., & Himabindu, V. (2019). Hydrogen production by PEM water electrolysis – A review. *Materials Science for Energy Technologies* (Vol. 2, Issue 3, pp. 442–454). KeAi Communications Co. https://doi.org/10.1016/j.mset.2019.03.002

Shizas, I., & Bagley, D. M. (2004). Experimental determination of energy content of unknown organics in municipal wastewater streams. *Journal of Energy Engineering*, *130*(2), 45–53.

Singh, V., & Das, D. (2019). Chapter 3 - Potential of Hydrogen Production From Biomass. In P. E. V de Miranda (Ed.), *Science and Engineering of Hydrogen-Based Energy Technologies* (pp. 123–164). Academic Press. https://doi.org/https://doi.org/10.1016/B978-0-12-814251-6.00003-4

Sleutels, T. H. J. A., Lodder, R., Hamelers, H. V. M., & Buisman, C. J. N. (2009). Improved performance of porous bio-anodes in microbial electrolysis cells by enhancing mass and charge transport. *International Journal of Hydrogen Energy*, *34*(24), 9655–9661. https://doi.org/10.1016/j.ijhydene.2009.09.089

Smolders, G. J. F., Van der Meij, J., Van Loosdrecht, M. C. M., & Heijnen, J. J. (1994). Stoichiometric model of the aerobic metabolism of the biological phosphorus removal process. *Biotechnology and Bioengineering*, *44*(7), 837–848.

Stirling, J., Bennetto, H. P., Delaney, G. M., Mason, J. R., Roller, S. D., Tanaka, K., & Thurston, C. F. (1983). Microbial fuel cells. *Biochemical Society Transactions*, *11*(4), 451–453. https://doi.org/10.1042/bst0110451

Svardal, K., & Kroiss, H. (2011). Energy requirements for waste water treatment. *Water Science and Technology*, *64*(6), 1355–1361. https://doi.org/10.2166/wst.2011.221

Tartakovsky, B., Manuel, M. F., Wang, H., & Guiot, S. R. (2009). High rate membrane-less microbial electrolysis cell for continuous hydrogen production. *International Journal of Hydrogen Energy*, *34*(2), 672–677. https://doi.org/10.1016/j.ijhydene.2008.11.003

Tchobanoglous, G., Stensel, H. D., Tsuchihashi, R., Burton, F., Abu-Orf, M., Bowden, G., & Pfrang, W. (2014). *Metcalf & Eddy. Wastewater Engineering. Treatment and resource recovery* (M.-H. Education, Ed.; 5th ed.). McGray-Hill Education.

Tenca, A., Cusick, R. D., Schievano, A., Oberti, R., & Logan, B. E. (2013). Evaluation of low cost cathode materials for treatment of industrial and food processing

wastewater using microbial electrolysis cells. *International Journal of Hydrogen Energy*, *38*(4), 1859–1865. https://doi.org/10.1016/j.ijhydene.2012.11.103

Tice, R. C., & Kim, Y. (2014). Methanogenesis control by electrolytic oxygen production in microbial electrolysis cells. *International Journal of Hydrogen Energy*, *39*(7), 3079–3086. https://doi.org/10.1016/j.ijhydene.2013.12.103

Trzcinski, A. P., Wang, C., Zhang, D., Ang, W. S., Lin, L. L., Niwa, T., Fukuzaki, Y., & Ng, W. J. (2017). Performance of A-stage process treating combined municipal-industrial wastewater. *Water Science and Technology*, *75*(1), 228–238.

Ullah, Z., & Zeshan, S. (2020). Effect of substrate type and concentration on the performance of a double chamber microbial fuel cell. *Water Science and Technology*, *81*(7), 1336–1344. https://doi.org/10.2166/wst.2019.387

Valta, K., Kosanovic, T., Malamis, D., Moustakas, K., & Loizidou, M. (2015). Overview of water usage and wastewater management in the food and beverage industry. *Desalination and Water Treatment*, *53*(12), 3335–3347.

van Loosdrecht, M. C. M., & Brdjanovic, D. (2014). Anticipating the next century of wastewater treatment. *Science*, *344*(6191), 1452–1453. https://doi.org/10.1126/science.1255183

Venkataraman, A., Rosenbaum, M., Arends, J. B. A., Halitschke, R., & Angenent, L. T. (2010). Quorum sensing regulates electric current generation of Pseudomonas aeruginosa PA14 in bioelectrochemical systems. *Electrochemistry Communications*, *12*(3), 459–462. https://doi.org/10.1016/j.elecom.2010.01.019

Von Zuben, T. W., Moreira, D. E. B., Germscheidt, R. L., Yoshimura, R. G., Dorretto, D. S., de Araujo, A. B. S., Salles, A. G., & Bonacin, J. A. (2022). Is Hydrogen Indispensable for a Sustainable World? A Review of H2 Applications and Perspectives for the Next Years. *Journal of the Brazilian Chemical Society* (Vol. 33, Issue 8, pp. 824–843). Sociedade Brasileira de Quimica. https://doi.org/10.21577/0103-5053.20220026

Wagner, R. C., Regan, J. M., Oh, S. E., Zuo, Y., & Logan, B. E. (2009). Hydrogen and methane production from swine wastewater using microbial electrolysis cells. *Water Research*, *43*(5), 1480–1488. https://doi.org/10.1016/j.watres.2008.12.037

Walker, G. M., & Weatherley, L. R. (2001). COD removal from textile industry effluent: pilot plant studies. *Chemical Engineering Journal* (Vol. 84).

Wang, A., Liu, L., Sun, D., Ren, N., & Lee, D. J. (2010). Isolation of Fe(III)-reducing fermentative bacterium Bacteroides sp. W7 in the anode suspension of a microbial

electrolysis cell (MEC). *International Journal of Hydrogen Energy*, *35*(7), 3178–3182. https://doi.org/10.1016/j.ijhydene.2009.12.154

Wang, L., Long, F., Liang, D., Xiao, X., & Liu, H. (2021). Hydrogen production from lignocellulosic hydrolysate in an up-scaled microbial electrolysis cell with stacked bio-electrodes. *Bioresource Technology*, *320*. https://doi.org/10.1016/j.biortech.2020.124314

Wang, Y., Guo, W. Q., Xing, D. F., Chang, J. S., & Ren, N. Q. (2014). Hydrogen production using biocathode single-chamber microbial electrolysis cells fed by molasses wastewater at low temperature. *International Journal of Hydrogen Energy*, *39*(33), 19369–19375. https://doi.org/10.1016/j.ijhydene.2014.07.071

Watanabe, Y., Nagai, F., Morotomi, M., Sakon, H., & Tanaka, R. (2010). Bacteroides clarus sp. nov., Bacteroides fluxus sp. nov. and Bacteroides oleiciplenus sp. nov., isolated from human faeces. *International Journal of Systematic and Evolutionary Microbiology*, *60*(8), 1864–1869.

Weld, R. J., Glithero, N., & Pasco, N. (2011). Escherichia coli knock-out mutants with altered electron transfer activity in the Micredox® assay and in microbial fuel cells. *International Journal of Environmental Analytical Chemistry*, *91*(2), 138–149. https://doi.org/10.1080/03067311003778631

Wett, B., Buchauer, K., & Fimml, C. (2007). Energy self-sufficiency as a feasible concept for wastewater treatment systems. *IWA Leading Edge Technology Conference*, *21*, 21–24.

Wurster, R., & Wietschel, M. (2008). *HyWAyS-The European hydrogen roadmap*.

Xia, X., Cao, X. X., Liang, P., Huang, X., Yang, S. P., & Zhao, G. G. (2010). Electricity generation from glucose by a Klebsiella sp. in microbial fuel cells. *Applied Microbiology and Biotechnology*, *87*(1), 383–390. https://doi.org/10.1007/s00253-010-2604-5

Younas, M., Shafique, S., Hafeez, A., Javed, F., & Rehman, F. (2022). An Overview of Hydrogen Production: Current Status, Potential, and Challenges. *Fuel* (Vol. 316). Elsevier Ltd. https://doi.org/10.1016/j.fuel.2022.123317

Zhang, Y., Merrill, M. D., & Logan, B. E. (2010). The use and optimization of stainless steel mesh cathodes in microbial electrolysis cells. *International Journal of Hydrogen Energy*, *35*(21), 12020–12028. https://doi.org/10.1016/j.ijhydene.2010.08.064

Züttel, A., Remhof, A., Borgschulte, A., & Friedrichs, O. (2010). Hydrogen: the future energy carrier. *Philosophical Transactions of the Royal Society A: Mathematical, Physical and Engineering Sciences*, *368*(1923), 3329–3342.

List of Abbreviations

AD	Anaerobic digestion
AEM	Anion exchange membrane
ARB	Anode respiring bacteria
BES	Bioelectrochemical system
BMU	Biomethanation unit
BOD	Biological oxygen demand
CAS	Conventional activated sludge
CE	Coulombic Efficiency
CEM	Cation exchange membrane
COD	Chemical oxygen demand
COD_I	Inlet chemical oxygen demand
COD_O	Outlet chemical oxygen demand
COD_S	Soluble chemical oxygen demand
CV	Cyclic voltammetry
DNA	Deoxyribonucleic acid
E_C	Energy consumption
EE	Energy efficiency
emf	Electromotive force
E_P	Energy production
EPDM	Ethylene propylene diene monomer
GC	Gas chromatograph
HER	Hydrogen evolution reaction
HRAS	High-rate activated sludge
HRT	Hydraulic retention time
IEM	Ion exchange membrane
IWW	Industrial wastewater
KPI	Key performance indicator
L-MEC	Litre-scale microbial electrolysis cell
MDC	Microbial desalination cell
MEC	Microbial electrolysis cell
MES	Microbial electro-synthesis cell
MET	Microbial electrochemical technologies
M-MEC	m^3-scale microbial electrolysis cell
MFC	Microbial fuel cell
NE_P	Net energy production
Ni	Nickel
NPV	Net present value
OCV	Open-circuit voltage
OLR	Organic loading rate

ORR	Organic removal rate
PE	Population equivalent
PP	Polypropylene
PTFE	Polytetrafluoroethylene
PVC	Polyvinyl chloride
r_{CAT}	Cathodic recovery
r_E	Energy recovery
rRNA	Ribosomal ribonucleic acid
SHE	Standard hydrogen electrode
SS	Stainless-steel
SWW	Synthetic wastewater
TSS	Total suspended solids
UWW	Urban wastewater
UWW_A	Amended urban wastewater
VFA	Volatile fatty acid
VSS	Volatile suspended solids
WAS	Waste activated sludge
WWTP	Wastewater treatment plant
ΔG	Gibbs free energy
ΔH	Enthalpy
ΔS	Entropy
ΔV	Applied potential

List of Figures

Figure 1.1. Examples of current applications of bioelectrochemical systems (BES).

Figure 1.2. Extracellular electron transport mechanisms of exoelectrogens at the anode.

Figure 1.3. Diagram of a microbial fuel cell (MFC) for electricity production. CEM and AEM refers to cation and anion exchange membrane, respectively.

Figure 1.4. Diagram of a microbial electricity cell (MEC) for hydrogen production. CEM and AEM refers to cation and anion exchange membrane, respectively.

Figure 1.5. Number of articles related to microbial electrolysis cells (MECs) based on ScienceDirect database as of October 30th, 2023.

Figure 1.6. Diagram of the biomethane production process proposed in the LIFE+ NIMBUS project.

Figure 3.1. Top view flow diagram of the L-MEC pilot plant with nine cassette cells.

Figure 3.2. L-MEC pilot plant.

Figure 3.3. M-MEC pilot plant.

Figure 3.4. Scheme of the gas bag used for the gas quantification. $V_{CO2,a}$ refers to the well-known volume of CO_2 added; $V_{T,I}$ is the initial total gas volume in the bag; V_{r1} is the volume of gas injected in the GC in the first analysis; V_{r2} is the volume of gas injected in the GC in the second analysis; $X_{j,r1}$ and $X_{j,r2}$ refer to the molar fractions of compound j in the first and second analysis, respectively.

Figure 4.1. Graphical abstract.

Figure 4.2. Inlet (COD_I) and outlet (COD_O) COD, and total gas production over time at different fixed intensities during the synthetic wastewater period in continuous mode (Stage 1).

Figure 4.3. Average key performance indices, applied potential and total gas production at different fixed intensities during the continuous operation with synthetic wastewater. Standard deviations are shown in the figure.

Figure 4.4. Average current density and total gas production over time at different applied potentials during the urban wastewater period in continuous mode (Stage 2). $\Delta V < 0.8$ V are not shown in the figure. Shade indicates standard deviation of current density.

Figure 4.5. Average key performance indices, current density and total gas production at different applied potential during the continuous operation with urban wastewater. $\Delta V <$ 0.8 V are not shown in the figure. Standard deviations are shown in the figure.

Figure 4.6. Experimental profiles over time at different temperatures during the urban wastewater period in continuous mode (Stage 3). Dashed line indicates the change from raw to amended wastewater. Shade indicates standard deviation of current density.

Figure 4.7. Average current density and hydrogen production at different temperatures during the continuous operation with raw and amended urban wastewater. Experimental data are presented with standard deviation. Lines represent the model predictions (Equation 4.3).

Figure 4.8. Inlet (COD_I) and outlet (COD_O) COD, and removal trend over time at different HRTs during the urban wastewater period (Stage 4). Four periods with different HRT between 1.1 and 3.9 d were evaluated.

Figure 4.9. Average key performance indices, current density, and total gas production at different HRTs during the continuous operation with urban wastewater. Standard deviations are shown in the figure.

Figure 5.1. Graphical abstract.

Figure 5.2. Schematic representation of the cathode configurations tested.

Figure 5.3. Dissembled cassette-cell with a double-sheet Ni-foam cathode (NF_D).

Figure 5.4. Detail of the NF_D configuration (1: First Ni-foam sheet, 2: 3D-printed PP spacer, 3: Second Ni-foam sheet).

Figure 5.5. Detail of the 3D-printed separator.

Figure 5.6. Operational schedule of the MEC pilot plant.

Figure 5.7. Cyclic voltammetry (CV) of Ni-foam and SS-wool against counter electrode (Pt), and reference electrode ($Ag/AgCl_{(sat)}$).

Figure 5.8. Intensity profiles of each cassette during the start-up and batch operation. The grey dashed line indicates the start of a new batch.

Figure 5.9. Start-up and batch operation profiles. A) Average current densities (*j*) and specific hydrogen production rates of the single-sheet nickel-foam cells (NF_S) and the stainless-steel cell (SS). B) Anodic COD concentration, pH and coulombic efficiency (CE); Average cathodic recovery efficiencies (r_{CAT}) of the NF_S and SS cells. Shade indicates standard deviation of current density in the NF_S cells. The grey dashed line indicates the start of a new batch.

Figure 5.10. Start-up and batch operation profiles. A) Average current densities (*j*) and specific hydrogen production rates of the single-sheet nickel-foam cells (NF_S) and the stainless-steel cell (SS). B) Anodic COD concentration, pH and coulombic efficiency (CE); Average cathodic recovery efficiencies (r_{CAT}) of the NF_S and SS cells. Shade indicates standard deviation of current density in the NF_S cells. The grey dashed line indicates the start of a new batch.

Figure 5.11. Average current density (*j*) and specific hydrogen production over time in each configuration during the continuous operation with diluted industrial wastewater.

Figure 5.12. Intensity profiles of each cassette at different applied potentials (ΔV) during continuous operation with diluted industrial wastewater.

Figure 5.13. Key performance indices of the double-sheet nickel-foam MECs (NF_D), single-sheet nickel-foam MECs (NF_S) and the stainless-steel MEC (SS), at different applied potentials (ΔV) during continuous operation. A) Average current densities (*j*) and specific hydrogen production rates. B) Average energy production (EP), energy consumption (EC) and energy recovery efficiency (r_E).

Figure 5.14. Anodic bacterial communities at genus level based on cloned 16S rRNA gene sequence distribution for the double-sheet nickel foam (NF_D) and stainless-steel (SS) MECs after reactor decommissioning.

Figure 6.1. Graphical abstract.

Figure 6.2. Experimental set-up during the performance evaluation of a cassette with synthetic wastewater in the L-MEC.

Figure 6.3. Experimental set-up during the performance evaluation of three cassettes with urban wastewater in the M-MEC.

Figure 6.4. Experimental set-up during the performance evaluation of the M-MEC with ten cassettes with urban wastewater.

Figure 6.5. Comparison of the two cell configurations studied; Left (A) and right (B).

Figure 6.6. Dimensions of the anode frame (external frame).

Figure 6.7. Dimensions of the cathode frame (internal frame).

Figure 6.8. Exploded view of the M-MEC cassette prototype.

Figure 6.9. Layout of the M-MEC.

Figure 6.10. A) Location of the MEC pilot and the BMU in the wastewater treatment plant of El Prat de Llobregat (Barcelona, Spain). B) Detail of the MEC pilot plant location next to the primary settlers.

Figure 6.11. A) Shipping container located next to the primary settlers; B) Monitoring system and power sources; C) M-MEC; and D) Different cassette-type cells placed inside the reactor.

Figure 6.12. Current density (*j*), specific hydrogen production rate and applied potential (ΔV) over time during the preliminary evaluation of a cassette (Configuration A, 2.5 cm).

Figure 6.13. Key performance indices of the cassette at different applied potentials (ΔV). A) Current density (*j*), specific hydrogen production rate and estimated hydrogen leakages. B) Cathodic recovery (r_{CAT}), experimental energy recovery (r_E) and theoretical energy recovery (assuming r_{CAT} = 100 %). C) Energy production (EP) and energy consumption (EC).

Figure 6.14. Current density (*j*) and specific hydrogen production rate (H_2) during the preliminary evaluation of the cassettes with real wastewater. Dashed lines indicate the start and end time of the batch period.

Figure 6.15. A) Average temperature (T_{AV}) and online temperature (T) of the reactor. B) Inlet soluble COD concentration (COD_I), outlet soluble COD concentration (COD_O),

coulombic efficiency and soluble COD removal efficiency (COD removal). Dashed lines indicate the start and end time of the batch period.

Figure 6.16. Cumulative hydrogen production (H_2), cathodic recovery efficiency (r_{CAT}) and energy recovery efficiency (r_E) during the preliminary evaluation of the cassettes with real wastewater. Dashed lines indicate the start and end time of the batch period.

Figure 6.17. Current density (*j*) and volumetric hydrogen production rate (H_2) during the continuous operation of the M-MEC (10 cells) with real wastewater. (H_2(max)) refers to the estimated volumetric hydrogen production rate considering 15 cells yielding the maximum performance obtained. Dashed lines indicate the start and end time of the continuous operation at HRT = 2 d.

Figure 6.18. Continuous operation of the M-MEC (10 cells) with real wastewater. A) Temperature profile of the reactor. B) Inlet soluble COD concentration (COD_I), outlet soluble COD concentration (COD_O), coulombic efficiency (CE) and soluble COD removal efficiency (COD removal). Dashed lines indicate the start and end time of the continuous operation at an HRT of 2 d.

Figure 6.19. Cumulative hydrogen production (H_2), average cathodic recovery (r_{CAT}) and energy recovery (r_E) efficiency, during the continuous operation of the M-MEC. Dashed lines indicate the start and end time of the continuous operation at HRT = 2 d.

Figure 6.20. Comparison of the current density (*j*) and specific hydrogen production rate (H2), during the continuous operation of the M-MEC (10 cells) with real wastewater, between configuration A and B. Shade indicates standard deviation of current density. Dashed lines indicate the start and end time of the continuous operation at HRT = 2 d.

Figure 6.21. Profitability of the M-MEC pilot plant at different price ratios (PR) and different performance cases. Black dashed line indicates the PR yielded by the current price of electricity and the EU's hydrogen target price for 2030. Black dotted line indicates the PR yielded by the current prices of electricity and hydrogen.

Figure 6.22. Treatment cost of the M-MEC at different electricity prices, for different performance cases. CAS refers to the treatment cost of a reference conventional activated sludge.

Figure 6.23. Distribution of material costs among major components of a 1 m3 M-MEC pilot plant.

List of Tables

Table 4.1. Average characteristics of the different wastewaters treated.

Table 4.2. Key operational parameters of each experimental stage.

Table 4.3. Summary of the data reported with cassette-type MEC at pilot-scale for urban wastewater treatment.

Table 4.4. Comparison of conventional and high-rate activated sludge versus microbial electrolysis cell.

Table 5.1. Cathode configuration employed in each cassette MEC.

Table 5.2. Physicochemical properties of the raw and diluted industrial wastewater.

Table 5.3. Summary of the important results obtained during the batch tests.

Table 6.1. Average characteristics of the urban wastewater during Stage I and II.

Table 6.2. Design parameters of the L-MEC and the M-MEC.

Table 6.3. Body parts of a M-MEC cassette.

Table 6.4. Key design parameters of the L-MEC and M-MEC tanks.

Table 6.5. Summary of the most important results obtained during Stage I.

Table 6.6. Description of the different cases evaluated to assess profitability in the M-MEC. PR limit refers to the lowest price ratio threshold for a profitability of 1.

Table 6.7. Description of the different cases evaluated to assess the treatment cost in the M-MEC, kWh of electricity consumed per kg COD removed, kg of hydrogen produced per kg COD removed, and kWh of electricity produced per kg COD removed.

Table 6.8. NPV for a 20 year operational period of the M-MEC under different scenarios.

Curriculum Vitae

Óscar Guerrero Sodric

02/11/1995

Cerdanyola del Vallès, Barcelona, Spain

oscar.guerrero@uab.cat; oscar.guerrero1717@gmail.com

ORCID: 0000-0002-4022-6325

https://www.linkedin.com/in/oscar-guerrero-sodric/

EDUCATION

2020 - Ongoing	PhD Candidate in Environmental Science and Technology, entitled "Scaling-up and future perspectives of bioelectrochemical systems for wastewater treatment and hydrogen production" Universitat Autònoma de Barcelona, Spain
2018 - 2020	MS in Biological and Environmental Engineering. Final thesis entitled "Producció bioelectroquímica d'hidrogen a partir d'aigües residuals urbanes" Universitat Autònoma de Barcelona, Spain
2013 - 2018	Degree in Chemical Engineering. Final project entitled "Planta de producció de clorur de vinil" Universitat Autònoma de Barcelona, Spain

WORK EXPERIENCE

2021 - Ongoing	Research Support Technician at Universitat Autònoma de Barcelona
2020 - Ongoing	Assistant Professor at Universitat Autònoma de Barcelona
2019 - 2020	Project Engineer at CPQ Ingenieros
2017 - 2019	Chemical Engineer at Lubrizol

PARTICIPATION IN CONFERENCES AND SEMINARS

Guerrero-Sodric, O., Baeza, J., Guisasola, A., Comprehensive and long-term assessment of critical operational parameters of a pilot MEC for hydrogen production from urban wastewater. 5th European Meeting of the International Society for Microbial Electrochemistry and Technology (ISMET), Girona, Spain, September 2021.
Oral presentation.

Guerrero-Sodric, O., Baeza, J., Guisasola, A., Projecte LIFE+ NIMBUS: Demostració d'una planta de metanació biològica pel transport urbà sostenible. 1r Congrés BIT, Lleida, Spain, September 2022.
Oral presentation.

Guerrero-Sodric, O., Baeza, J., Guisasola, A., Enhancing hydrogen production from real wastewater in a 150 MEC pilot plant. 8th Global Conference of the International Society for Microbial Electrochemistry and Technology (ISMET), Crete, Greece, September 2022.
Oral presentation and poster.

Navarro, J., Cortada, M., Guerrero-Sodric, O., Baeza, J., **Guisasola, A.**, Computational fluid dynamics as a tool to understand and mitigate mass difussion issues in pilot-scale bioelectrochemical systems. 8th Global Conference of the International Society for Microbial Electrochemistry and Technology (ISMET), Crete, Greece, September 2022.
Oral presentation.

Guerrero-Sodric, O., Baeza, J., Guisasola, A., Producció d'hidrogen amb cel·les electrolítiques microbianes per a la biometanació. Jornada Impuls del Biogàs al Sector de l'Aigua, Manresa, Spain, March 2023.
Oral presentation.

Guerrero-Sodric, O., Baeza, J., Guisasola, A., Exploring the limits of hydrogen production by microbial electrochemical cells treating wastewater. 17th National Environmental Conference for Doctoral Students, Tsinghua, China, April 2023.
Oral presentation.

Guerrero-Sodric, O., Baeza, J., Guisasola, A., Exploring the limits of hydrogen production by microbial electrochemical cells treating wastewater. 15th Mediterranean Congress of Chemical Engineering, Barcelona, Spain, June 2023. Oral presentation.

Guerrero-Sodric, O., Baeza, J., Guisasola, A., Enhancing bioelectrochemical hydrogen production from industrial wastewater in a 150 L microbial electrolysis cell pilot plant. 6th IWA International Conference on eco-Technologies for Wastewater Treatment, Girona, Spain, June 2023.
Oral presentation.

Guerrero-Sodric, O., Baeza, J., **Guisasola, A.**, Long-term performance of a 1 m^3 pilot-MEC for hydrogen production in a real environment. 6th European Meeting of the International Society for Microbial Electrochemistry and Technology (ISMET), Wageningen, The Netherlands, September 2023.
Oral presentation.

Guisasola, A., Guerrero-Sodric, O., Baeza, J., Escalado de celdas microbianas de electrólisis para la producción de hidrógeno. Cátedra FACSA-FOVASA-UPV, Valencia, Spain, November 2023.
Oral presentation.

PUBLICATIONS

Guerrero-Sodric, O., Baeza, J., Guisasola, A., (2023) Exploring key operational factors for improving hydrogen production in a pilot-scale microbial electrolysis cell treating urban wastewater. Chemical Engineering Journal 469. https://doi.org/10.1016/j.cej.2023.144001

Guerrero-Sodric, O., Baeza, J., Guisasola, A., (2024) Enhancing bioelectrochemical hydrogen production from industrial wastewater using Ni-foam cathodes in a microbial electrolysis cell pilot plant. Water Research. Under revision.

Guerrero-Sodric, O., Baeza, J., Guisasola, A., Design, construction and operation of a 1 m^3 MEC pilot plant in a real wastewater treatment plant. In preparation.

LANGUAGES

Catalan	Mother tongue
Spanish	Mother tongue
English	Advanced
French	Basic